Università Degli Studi di Padova
Dipartimento di Scienze Biomediche

CORSO DI DOTTORATO DI RICERCA IN SCIENZE BIOMEDICHE

CICLO XXXII

Mitochondrial adaptation in parvalbumin knockout muscle fibers

Coordinatore: Ch.mo Prof. Paolo Bernardi

Supervisore: Ch.ma Prof.ssa Anna Raffaello

Co-Supervisori: Ch.mo Prof. Carlo Reggiani e Ch.mo Prof. Rosario Rizzuto

Ph.D. student: Gaia Butera

Table of contents

1. Summary

Calcium ions (Ca^{2+}) are highly versatile intracellular second messengers that regulate a plethora of cellular functions in both excitable and non-excitable cells [1], ranging from biological processes such as proliferation and control of aerobic metabolism to physiological mechanisms such as muscle contraction and synaptic plasticity during learning and memory [2].

Therefore, it is not surprising that cells show intricate and precise mechanisms to control cytosolic Ca^{2+} concentration ($[Ca^{2+}]_{cyt}$) [1,3]. Among these, mitochondria are recognized as crucial regulators of cellular Ca^{2+} homeostasis that ensure normal cellular functions [4,5]. Indeed, mitochondrial Ca^{2+} uptake shape the spatiotemporal patterns of intracellular Ca^{2+} by accumulating it in the very rapid time-scale of hundreds of milliseconds [6], reaching values up to 100 μM in some cell types [7]. However, excessive Ca^{2+} accumulation in mitochondria, a condition known as mitochondrial Ca^{2+} overload, has been long known to be a critical event in the bio-energetic crisis associated with cell death by necrosis [8,9].

Furthermore, one of the most important roles of mitochondrial Ca^{2+} uptake is the mitochondrial Ca^{2+}-dependent control of the rate of mitochondrial adenosine triphosphate (ATP) production, the main fuel for sustaining cellular functions [10,11]. This general picture is particularly relevant in skeletal muscle, a tissue where mitochondria produce most of the ATP required to sustain muscle contraction [10,12]. It is thus not surprising that skeletal muscle mitochondria display the highest mitochondrial Ca^{2+} transients, as demonstrated by the measurement of the MCU current by patch-clamp from IMM-derived mitoplasts from different tissues [13].

Moreover, pivotal findings have highlighted the role of mitochondria as key players in the dynamic regulation of crucial signalling pathways in skeletal muscle [14,15], involved not only in muscle contraction but also in skeletal muscle homeostasis [16,17]. However, whether skeletal muscle mitochondria

act also as a possible high capacity Ca^{2+} buffer remains a fundamental question on muscle physiology and diseases.

The major goal of my PhD project was to address the regulatory processes that modulate mitochondrial Ca^{2+} homeostasis in skeletal muscle and understand how $[Ca^{2+}]_{cyt}$ can affect mitochondrial Ca^{2+} uptake. To achieve these goals, we explored a specific condition where intra-fiber Ca^{2+} kinetics have been steadily altered by removing Parvalbumin (PV), one of the main cytosolic Ca^{2+} buffers in skeletal muscle [18,19]. To this end, as study tool, we used a PV knockout (KO) mouse model obtained from the laboratory of Prof. Beat Schwaller (Dept. of Medicine, University of Fribourg, Switzerland) [20].

PV plays an important role in skeletal muscle, acting as a temporary Ca^{2+} buffer (e.g. increasing the relaxation rate of fast twitch muscle contraction) [21]. To investigate the physiological role of PV in muscle fibers and in Ca^{2+} homeostasis, we investigated cytosolic and mitochondrial Ca^{2+} transients in PV KO mice compared. We observed that basal $[Ca^{2+}]_{cyt}$ was not affected in PV knockout fibers, but kinetics of Ca^{2+} transients and Ca^{2+} clearance were altered. In detail, consistently with the role of PV in buffering cytosolic Ca^{2+}, the time-to-peak and the half-relaxation time was increased in PV KO FDB fibers. Unexpectedly, however, under tetanic stimulation, PV KO FDB muscle fibers showed a decrease in $[Ca^{2+}]_{cyt}$. To explain this result we asked whether the lack of PV could induce rearrangements of one of the two main Ca^{2+} stores, the sarcoplasmic reticulum (SR) and mitochondria. SR Ca^{2+} measurements demonstrated that lack of PV increases SR Ca^{2+} release during stimulation. Therefore, we concluded that SR is not causative of the effect of PV removal on cytosolic Ca^{2+} transients. Consistently, we found no difference in the mRNA levels of RyR1, the main Ca^{2+} releasing channel in muscle, and on the expression of two different isoforms of SERCA in PV KO muscles compared to WT. Furthermore, no difference was detected in the expression of the two main SR Ca^{2+} buffers, Calsequestrin and Calreticulin. We then focused our attention on mitochondrial Ca^{2+} homeostasis. The data obtained demonstrated that the lack of PV induces an increase of

mitochondrial Ca^{2+} uptake and this is accompanied by the induction of the expression of mitochondrial calcium uniporter (MCU) complex components, the channel responsible for Ca^{2+} entry in mitochondria [4,5,22,23]. In addition, electron microscopy analysis demonstrated that the volume of PV KO mitochondria was doubled compared to WT with an increase of mitochondria associated to the Ca^{2+} release units (CRUs), suggesting a tight connection of PV expression with mitochondrial morphology and function in muscle cells. Furthermore, to further prove that mitochondria are responsible for cytosolic Ca^{2+} buffering in fibers lacking PV, we silenced MCU on WT and PV KO FDB fibers and we measured $[Ca^{2+}]_{cyt.}$. In WT animals, $[Ca^{2+}]_{cyt}$ was not affected by the absence of MCU, while MCU silencing in PV KO fibers resulted in a significant higher $[Ca^{2+}]_{cyt}$, reinforcing the hypothesis that, while in WT animals mitochondria do not significantly buffer $[Ca^{2+}]_{cyt}$, mitochondria of fibers lacking PV adapt to buffer $[Ca^{2+}]_{cyt}$ increases.

To investigate in-depth the effect of PV expression on mitochondrial Ca^{2+} uptake and to exclude any possible *in vivo* compensatory effects due to PV ablation during development, we performed acute PV silencing in adult WT FDB muscle fibers and we monitored cytosolic Ca^{2+} transients and mitochondrial Ca^{2+} uptake.

In basal resting condition and upon caffeine stimulation, PV silencing did not influence cytosolic Ca^{2+} transient. Indeed, no significant difference were detected between control (shLUC) fibers and PV silenced fibers (shPV). To verify whether, similarly to what observed in PV KO fibers, mitochondria could compensate for the lack of PV by increasing its buffering capacity, concomitantly with Ca^{2+} measurements, we treated fibers with the ionophore carbonyl cyanide m-chlorophenyl hydrazone (CCCP) and we measured $[Ca^{2+}]_{cyt.}$. CCCP abolishes mitochondrial Ca^{2+} uptake by dissipating the electrochemical potential across the inner mitochondrial membrane, which provides the driving force for Ca^{2+} import [24]. In this experimental condition, fibers silencing PV, treated with CCCP and stimulated with caffeine, showed an increase of $[Ca^{2+}]_{cyt}$ compared to control fibers, re-

enforcing the hypothesis that mitochondria of fibers lacking PV adapt to buffer cytosolic Ca^{2+} transient.

We next measured mitochondrial Ca^{2+} uptake in fibers silencing PV and control fibers. For this purpose, we co-transfected FDB fibers with shLUC as control and PV shRNA plasmids together with the mitochondrially targeted 4mtGCaMP6f probe. *Ex vivo* imaging experiments showed that, while the mitochondrial basal resting concentration is not affected by the lack of PV, a marked increase in caffeine-induced mitochondrial Ca^{2+} accumulation was detected in shPV-transfected fibers, confirming the data obtained in our KO model.

Moreover, since PV is one of the most downregulated "atrogenes", the genes commonly up- and down-regulated during both disuse and systemic types of atrophy [25,26] and that mitochondrial Ca^{2+} controls skeletal muscle trophism [17], the role of PV in the regulation of muscle mass was investigated through denervation experiments. In PV KO muscles, loss of muscle mass caused by denervation is reduced compared to WT fibers, demonstrating that the lack of PV can partially protect muscles from denervation-induced atrophy. Since the effect of PV ablation on denervated muscle was modest and the effect on innervated muscles was negligible, we decided to perform PV acute silencing and overexpression in adult WT tibialis anterior (TA) muscles and we monitored fiber size. We demonstrated that the acute modulation of PV protein controls skeletal muscle size. In detail, we observed an increase of fiber size in PV silenced muscles and coherently, PV overexpressing muscles displayed an atrophic phenotype. Since the regulation of muscle size involves a precise transcriptional program [26,27], we focused our attention on PGC-1α4, a splicing variant of the PGC-1α gene, that plays a key role in triggering muscle hypertrophy as adaptive response to exercise [28]. Intriguingly, we found an up-regulation of PGC-1α4 mRNA in PV KO skeletal muscles, suggesting the activation of this hypertrophic pathway. Of note, our data are in accordance with previous studies showing that mitochondrial Ca^{2+} positively regulates skeletal muscle mass by impinging also on PGC-1α4 pathway [17]. Our results show that the lack of PV in skeletal muscle leads

to morphological and functional adaptations of mitochondria. In particular, mitochondria of fibers lacking PV, either constitutively or transiently, adapt to take up more Ca^{2+} to control $[Ca^{2+}]_{cyt}$ increases. Furthermore, we demonstrated that the absence of PV partially counteracts denervation atrophy by triggering the expression of PGC-1α4. Our hypothesis is that PV ablation, leading to an increase of mitochondrial Ca^{2+} uptake, activates mitochondrial Ca^{2+}-dependent pathways to control skeletal muscle trophism.

2. Sommario

Lo ione calcio (Ca^{2+}) è uno dei più importanti secondi messaggeri intracellulari e riveste un ruolo fondamentale nella regolazione di un vasto spettro di funzioni cellulari che spaziano da processi biologici, come il controllo della proliferazione e del metabolismo aerobico, a meccanismi fisiologici, come la contrazione muscolare e la plasticità sinaptica durante l'apprendimento e la memoria [1,2,29]. I principali organelli intracellulari predisposti alla regolazione della concentrazione di Ca^{2+} citosolico ($[Ca^{2+}]_{cit}$) sono i mitocondri, che hanno la capacità di accumulare molto velocemente elevate concentrazioni di Ca^{2+} ($[Ca^{2+}]$) [4], fino a raggiungere anche livelli superiori a 100 μM in alcuni tipi cellulari [6]. Tuttavia, un eccessivo accumulo di Ca^{2+} all'interno del mitocondrio comporta una crisi energetica che induce alla morte cellulare per necrosi [8,9].

In condizioni fisiologiche, il Ca^{2+} mitocondriale regola il metabolismo cellulare promuovendo la formazione dell'adenosina trifosfato (ATP), la principale molecola energetica della cellula, necessaria per lo svolgimento di diverse funzioni [10,11]. Particolarmente importante è il ruolo dei mitocondri nell'omeostasi del muscolo scheletrico. A discapito di sostanze nutritive e ossigeno, infatti, i mitocondri controllano la produzione di ATP, necessaria per la contrazione muscolare [10,12]. Non sorprende dunque che i mitocondri presenti nel muscolo scheletrico mostrino il più alto transiente di Ca^{2+} mitocondriale, così come è stato dimostrato dalla misura della corrente dell'uniporto MCU, ottenuta tramite patch-clamp di mitoplasti derivati da diversi tessuti [13]. Recentemente, inoltre, è stato dimostrato che i mitocondri svolgono un ruolo chiave nella regolazione di diverse vie di segnale nel muscolo scheletrico [14,15], risultando dunque essenziali per l'omeostasi tissutale [16,17]. Tuttavia, ad oggi, rimane ancora aperta una domanda fondamentale nella fisiopatologia del muscolo scheletrico: comprendere se i mitocondri in questo tessuto fungano anche da buffer del Ca^{2+} citosolico.

L'obiettivo principale del mio progetto di Dottorato è stato quello di studiare i processi regolatori che modulano l'omeostasi del Ca^{2+} mitocondriale nel muscolo scheletrico e capire come la $[Ca^{2+}]_{cit}$ possa influenzare l'assorbimento del Ca^{2+}

mitocondriale. Per studiare questi aspetti ci siamo avvalsi dell'utilizzo di un modello animale ottenuto nel laboratorio del Prof. Beat Schwaller (Dipartimento di Medicina, Università di Friburgo) in Svizzera. Il modello di studio è stato un topo knockout (KO) per la parvalbumina (PV) uno dei principali buffer citosolici del Ca^{2+} nel muscolo scheletrico [20].

La PV, nelle fibre muscolari a contrazione rapida, lega il Ca^{2+} libero presente nel citoplasma agendo come un tampone temporaneo di Ca^{2+} ed influendo sulla loro velocità di rilassamento in seguito a contrazione [21]. Per studiare il ruolo fisiologico della PV nell'omeostasi del Ca^{2+}, abbiamo analizzato il transiente del calcio citosolico e la captazione del Ca^{2+} mitocondriale nei topi PV KO e in quelli WT. I dati ottenuti hanno dimostrato che la $[Ca^{2+}]_{cit}$ basale non è influenzata dall'assenza della PV, ma piuttosto è alterata la cinetica di contrazione delle fibre muscolari PV KO. Coerentemente al ruolo fisiologico espletato dalla PV, infatti, le fibre PV KO mostrano un ritardo nel raggiungimento del picco di contrazione ed un aumento del tempo necessario per il rilassamento della fibra. Inoltre, sotto stimolazione tetanica, nelle fibre muscolari PV KO è stata registrata un'inattesa diminuzione della $[Ca^{2+}]_{cit.}$ Per giustificare questo risultato ci siamo chiesti se l'assenza della PV potesse indurre delle modificazioni nel reticolo sarcoplasmatico (RS) e nei mitocondri, gli organelli principalmente coinvolti nell'omeostasi del Ca^{2+}.

Le misure dei transienti di Ca^{2+} nel RS dei topi PV KO hanno rilevato un aumento del Ca^{2+} rilasciato dopo stimolazione, dimostrando dunque che l'organello non è responsabile dell'effetto della rimozione della PV sul transiente di Ca^{2+} citosolico. Inoltre, l'espressione di alcune proteine specifiche del RS, principalmente coinvolte nell'omeostasi del Ca^{2+}, non ha mostrato differenze significative tra i topi PV KO e WT. Nel dettaglio, l'espressione dell'mRNA di RyR1, il principale canale di rilascio di Ca^{2+} nei muscoli, l'espressione delle due diverse isoforme di SERCA e dei principali tamponi per il Ca^{2+} del RS (Calsequestrina e Calreticulina) non hanno mostrato alcuna alterazione tra i topi PV KO ed i WT.

Abbiamo pertanto spostato la nostra attenzione sull'omeostasi del Ca^{2+} mitocondriale. I dati ottenuti finora hanno dimostrato che l'assenza di PV induce un

significativo aumento dell'accumulo di Ca^{2+} nei mitocondri ed un aumento dell'espressione di MCU, il canale direttamente coinvolto nell'assorbimento di Ca^{2+} nel mitocondrio [4,5,22,23]. A conferma della stretta correlazione tra l'espressione della PV e l'adattamento mitocondriale, l'analisi al microscopio elettronico ha mostrato un significativo aumento del volume dei mitocondri dei muscoli PV KO rispetto a quelli WT ed una loro differente redistribuzione nel tessuto muscolare. Infatti, il numero di mitocondri associati alle unità di rilascio di Ca^{2+} (CRU) è risultato essere più elevato nei muscoli PV KO rispetto a quelli WT. I risultati ottenuti, dunque, suggeriscono una stretta connessione tra l'espressione della PV e la morfologia e funzione mitocondriale.

Per confermare il ruolo dei mitocondri nel controllo della $[Ca^{2+}]_{cit}$ nelle fibre PV KO, abbiamo silenziato l'espressione del canale MCU nelle fibre muscolari del *flexor digitorum brevis* (FDB) dei topi WT e PV KO, misurando poi il transiente di Ca^{2+} citosolico. La $[Ca^{2+}]_{cit}$ nelle fibre WT, dopo stimolazione con caffeina, non è influenzata dall'assenza di MCU, mentre nelle fibre PV KO, abbiamo riscontrato un significativo aumento della $[Ca^{2+}]_{cit.}$ Tali esperimenti, pertanto, confermano l'ipotesi che i mitocondri delle fibre PV KO compensino la mancanza della PV tamponando l'aumento della $[Ca^{2+}]_{cit}$ durante stimolazione.

Per studiare più approfonditamente gli effetti dell'espressione della PV sull'assorbimento mitocondriale di Ca^{2+} e per escludere eventuali effetti compensatori del nostro modello animale durante lo sviluppo, dovuti dall'eliminazione della PV, abbiamo silenziato in maniera acuta l'espressione della PV in fibre muscolari FDB dei topi WT adulti ed abbiamo poi misurato i transienti del Ca^{2+} citosolico e mitocondriale. La $[Ca^{2+}]_{cit}$, sia in condizioni di riposo sia dopo somministrazione di caffeina non ha riportato alcun tipo di differenza tra le fibre di controllo (shLUC) e le fibre silenziate (shPV). Per verificare se, analogamente a quanto osservato nelle fibre PV KO, i mitocondri avessero subito meccanismi di compensazione per la mancanza di PV aumentando la loro capacità di buffer, abbiamo trattato le fibre con lo ionoforo carbonil cianuro m-clorofenil idrazone (CCCP) ed abbiamo misurato la $[Ca^{2+}]_{cit}$. Il CCCP impedisce l'assorbimento mitocondriale di Ca^{2+}, dissipando il potenziale elettrochimico della membrana mitocondriale interna, necessario per l'assorbimento del Ca^{2+} nel mitocondrio [24].

In questa condizione, le fibre shPV, trattate con CCCP e stimolate con caffeina, hanno mostrato un aumento della $[Ca^{2+}]_{cit}$ rispetto alle fibre di controllo, confermando che i mitocondri delle fibre prive di PV si adattano per tamponare più efficacemente il Ca^{2+} citosolico. Successivamente, abbiamo misurato nelle fibre shPV l'assorbimento del Ca^{2+} mitocondriale. A tale scopo, abbiamo co-trasfettato le fibre muscolari FDB di topi WT con il plasmide shLUC (controllo) o l'shRNA specifico per la PV, insieme alla sonda 4mtGCaMP6f per misurare la concentrazione di calcio mitocondriale ($[Ca^{2+}]_{mit}$). Gli esperimenti di imaging hanno mostrato che la $[Ca^{2+}]_{mit}$ basale non è influenzata dalla mancanza di PV, mentre, dopo stimolazione con caffeina, le fibre shPV mostrano un marcato aumento dell'accumulo mitocondriale di Ca^{2+}, confermando dunque i dati ottenuti nel nostro modello PV KO. È interessante notare, inoltre, che la PV è uno degli "atrogenes", geni la cui espressione varia in processi di atrofia muscolare causata sia da patologie sistemiche, come diabete e cachessia, sia da disuso, come l'inattività o la denervazione [25,26]. Pertanto, considerato che la PV è uno degli "atrogenes" e sapendo che il Ca^{2+} mitocondriale controlla positivamente il trofismo muscolare [17], abbiamo deciso di studiare il ruolo della PV nel controllo della massa muscolare tramite esperimenti di denervazione. Nei topi PV KO, si assiste ad una ridotta perdita di massa muscolare rispetto ai WT in seguito a denervazione, dimostrando dunque che la mancanza di PV protegge parzialmente i muscoli dall'atrofia muscolare. Tuttavia, poiché l'effetto dell'eliminazione della PV sui muscoli denervati è stato piuttosto moderato e il l'effetto sui muscoli controlaterali, innervati, è risultato trascurabile, abbiamo effettuato esperimenti di silenziamento e di overespressione della PV su muscoli tibiali anteriori (TA) di topi WT adulti, ed abbiamo poi monitorato i relativi cambiamenti nella dimensione delle fibre muscolari. Abbiamo dimostrato che la modulazione dell'espressione della PV controlla la dimensione del muscolo scheletrico. In particolare, abbiamo riscontrato un aumento delle dimensioni delle fibre in cui la PV è silenziata e, al contrario, le fibre over-esprimenti PV sono risultate atrofiche. Poiché la regolazione del trofismo muscolare attiva precisi programmi trascrizionali [26,27], ci siamo chiesti quale via di segnale potesse mediare l'effetto della PV sul trofismo muscolare. La nostra attenzione si è focalizzata su PGC-1α4, una variante di splicing del gene PGC-1α,

che svolge un ruolo chiave nell'ipertrofia muscolare come risposta adattativa all'esercizio [28]. L'analisi dell'espressione dell'mRNA di questo gene ha rivelato un aumento di PGC-1α4 nei muscoli PV KO, suggerendo l'attivazione di questa via di segnale. È interessante notare che i nostri dati sono concordi a quanto è stato riportato recentemente. Infatti, è stato dimostrato che il Ca^{2+} mitocondriale regola positivamente l'aumento della massa muscolare attivando PGC-1α4 [17].

Nel complesso, i nostri risultati dimostrano che l'assenza della PV nel muscolo scheletrico provoca adattamenti morfologici e funzionali dei mitocondri. In particolare, i mitocondri delle fibre PV KO, subiscono un meccanismo compensatorio per accumulare più Ca^{2+} al fine di limitare l'aumento eccessivo della $[Ca^{2+}]_{cit}$. Inoltre, abbiamo dimostrato che l'assenza di PV contrasta parzialmente l'atrofia dovuta a denervazione, inducendo l'espressione di PGC-1α4. La nostra ipotesi è che l'eliminazione della PV, portando ad un aumento dell'assorbimento mitocondriale di Ca^{2+}, attivi vie di segnale Ca^{2+}-dipendenti per controllare il trofismo del muscolo scheletrico, coerentemente a quanto è stato riportato nel nostro laboratorio.

3. Introduction

3.1 Calcium Homeostasis

The concept that Ca^{2+} ions are critical for many cellular functions dates back to the end of 1800 when Sidney Ringer noted that the presence of Ca^{2+} was necessary to the contraction of the heart [30]. In detail, he observed that saline solution prepared using tap water, which contained Ca^{2+}, supported the contraction of isolated frog hearts, whereas saline solution prepared using distilled water, which lacked Ca^{2+}, did not induce the same effect [30]. Nevertheless, this finding was taken into little consideration. Indeed, only in the late 1950s it was clearly demonstrated the correlation between Ca^{2+} and muscle contraction [31,32]. After these seminal observations, several studies led to the discovery of other biological processes controlled by Ca^{2+} signalling [33,34]. Nowadays, it is widely accepted the definition of Ca^{2+} as an almost universal intracellular messenger of fundamental importance that can modulate many different cellular functions, ranging from cell proliferation to cell death [35]. The ability of Ca^{2+} to play these pivotal roles results from a strict control of its concentration in space, time and amplitude [1,29]. The regulation of cytosolic Ca^{2+} concentration ($[Ca^{2+}]_{cyt}$) derives from the cooperation of two different sources of Ca^{2+} in the formation of $[Ca^{2+}]_{cyt}$ variation: the extracellular medium, a virtually unlimited reservoir with a $[Ca^{2+}]$ of ∼1 mM [4,9], and the intracellular stores with a $[Ca^{2+}] > 100$ μM, which allow rapid release of Ca^{2+} through store-resident channels [1]. The other requirement for the regulation of $[Ca^{2+}]_{cyt}$ is the existence of molecules that are able to generate and modulate $[Ca^{2+}]_{cyt}$ fluctuations, such as Ca^{2+} pumps, channels, Ca^{2+}-binding signalling molecules, enzymes, and buffering proteins [1,4]. In the plasma membrane, different channels regulate Ca^{2+} entry from the extracellular space. Among these, we distinguish the voltage-operated calcium channels (VOCCs), the receptor-operated calcium channels (ROCCs), the store-operated calcium channels (SOCCs), and the second messenger-operated calcium channels (SMOCs) that, according to the stimuli

evoking channel activation, allow Ca^{2+} entry through the plasma membrane [2,36]. Of note, the increase in $[Ca^{2+}]_{cyt}$ may be mediated also by Ca^{2+} release from intracellular compartments [1,4]. The most important intracellular store is the endoplasmic reticulum (ER) and its specialized counterpart in muscle cells, the sarcoplasmic reticulum (SR), where $[Ca^{2+}]$ can reach ~0.8 mM, depending on the cell type [37]. Ca^{2+} accumulation in the SR depends on the activity of sarco/endoplamic reticulum Ca^{2+} ATPase (SERCA) which resides in the ER/SR and that, at the expense of ATP hydrolysis, transfers Ca^{2+} from the cytosol to the organelle lumen [38,39]. Then, Ca^{2+} storage depends on the expression of low-affinity high capacity Ca^{2+} buffering proteins as Calsequestrin (CSQ) and Calreticulin (CARL) that are present in SR and in ER lumen, respectively [40,41]. Ultimately, Ca^{2+} release upon cell stimulation relies primarily on two intracellular Ca^{2+} channels localized on ER/SR membrane: the 1,4,5-trisphosphate (IP3) receptors (InsP3-R) and/or ryanodine receptors (RyR) [42]. When required, InsP3R or RYR channels mediates Ca^{2+} release in the cytosol to ensure specific cellular functions [36]. In detail, the agonist of IP3R is generated by the phospholipase C (PLC) enzymatic activity. This enzyme hydrolyses its substrate phosphatidylinositol 4,5-bisphosphate (PIP2) in diacylglycerol (DAG) and inositol 1,4,5-trisphosphate (InsP3) [43]. Subsequently, IP3 interacts with its receptors located in the ER inducing Ca^{2+} release into the cytosol [42]. Ca^{2+} itself regulates the InsP3Rs open probability, activating InsP3Rs at increasing $[Ca^{2+}]$ up to a specific $[Ca^{2+}]$ threshold, above which further increases in $[Ca^{2+}]$ act as inhibitory function [4]. RyRs channels are structurally and functionally analogous to InsP3Rs, although they have approximately twice the conductance and molecular mass of InsP3Rs [9,37,44]. Although Ca^{2+} is a major triggering ligand for RyRs, several other players modulate channel activity, such as the dihydropyridine receptor (DHPR; also known as L-type Ca^{2+} channel, CaV1.1/1.2), protein kinase A (PKA), calmodulin (CaM), Ca^{2+}/calmodulin-dependent protein kinase II (CaMKII), CSQ, and the FK506-binding protein (FKBP12) [44]. The increase of $[Ca^{2+}]_{cyt}$ induces the activation of many different Ca^{2+}-signalling pathways ranging from

proliferation, muscle contraction and cell metabolism [29]. To control and orchestrate the different processes activated by $[Ca^{2+}]_{cyt}$ increases ($[Ca^{2+}]$ reaches values of 2-3 μM during cell stimulation), cells have to maintain very low $[Ca^{2+}]_{cyt}$ [29]. This is obtained by Ca^{2+} extrusion to the extracellular space or by Ca^{2+} compartmentalization to intracellular stores. The activity of various pumps and exchangers allows intracellular $[Ca^{2+}]$ to return to its resting conditions (~100 nM) and ensures a tight control of Ca^{2+} signalling pathways [4,36]. ATPase pumps compartmentalize Ca^{2+} into the ER/SR stores via the activity of SERCAs or extrude Ca^{2+} in the extracellular space via plasma membrane Ca^{2+} ATPases (PMCA pumps) by exploiting ATP-derived energy [45,46]. A second mechanism utilizes the electrochemical gradient of Na^+ across the plasma membrane to provide the energy to transport Ca^{2+} ions to the extracellular space through the Na^+/Ca^{2+} (NCX) and Na^+/Ca^{2+}-K^+ exchangers (NCKX) [36]. Many studies, in addition, have highlighted a role in regulation of $[Ca^{2+}]_{cyt}$ also for other membrane-bound compartments such as the Golgi apparatus, endolysosomes, and mitochondria [4,37,47]. Among these organelles, mitochondria are nowadays recognized as potential regulators of cellular Ca^{2+} homeostasis since are able to accumulate large amount of Ca^{2+} (in some cell lines $[Ca^{2+}]_{mit}$ can reach values around 100 μM) in the very rapid time scale of hundred milliseconds [4,6]. Indeed, it is largely known that mitochondrial Ca^{2+} uptake regulates many different cellular processes, controlling the delicate balance between cell survival and cell death [4,5].

3.2 Ca^{2+} Buffer proteins

Intracellular Ca^{2+} modulates many aspects of physiological responses within a cell [3]. Therefore, it is not surprising, that cells need to be equipped with a complex machinery to control cytosolic Ca^{2+} signals in a specific localization and in a time-dependent manner [1,3]. To perform this precise regulation, cells rely on different cellular components that include, in addition to the above discussed Ca^{2+} channels and exchangers, Ca^{2+} buffer proteins [48]. The class of Ca^{2+} buffers refers to the large family of Ca^{2+} binding proteins that

are important modulators of intracellular Ca^{2+} dynamics in different cells types and compartments, and can therefore influence Ca^{2+} signalling response of the cells upon stimulation [3,21]. The term Ca^{2+} buffer is applied only to a small subset of Ca^{2+} binding proteins of the EF-hand family, including parvalbumin, calbindin-D28k and calbidin-D9k and calretinin [48]. In general, an EF-hand domain consists of 29 – 30 amino acids structurally organised as an α-helix, followed by a highly conserved stretch of 12 amino acids involved in chelating the Ca^{2+} ion and a second α-helix oriented approximately perpendicular to the first one [49]. The conserved stretch of 12 amino acids contains usually a series of negatively charged residues (such as Glu, Asp) and/or backbone carbonyl groups providing the site for Ca^{2+} binding [19]. The first Ca^{2+} buffer of the EF-hand family was discovered more than 50 years ago and was named parvalbumin (PV), based on its small size (parvus = small) and its albumin-like solubility [50]. In the PV protein structure, α-helices are referred as A, B, C, D, E and F helices starting from the N-terminus of the protein. Among the three domains present in parvalbumin (AB, CD and EF domains), only two can bind Ca^{2+} (CD and EF). The C-terminal domain (EF domain) is the best defined and has been used to characterize the canonical EF-hand Ca^{2+} binding motif [19]. The structural motif of EF- domain may be represented by the right hand, where the index finger represents the E-helix, the bent middle finger represents the Ca^{2+}-binding loop, and the thumb the F-helix (Figure 1 and [48]).

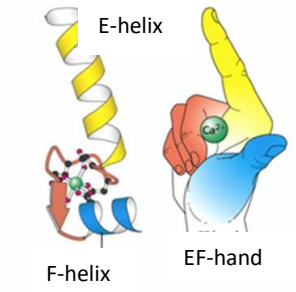

Figure 1. Schematic representation of EF-hand motif (Adapted from Grisar T, Lakaye B, de Nijs L, et al. Jasper's Basic Mechanisms of the Epilepsies, 4th edition, 2012).

Left panel: representation of the three-dimensional structure of an EF-hand domain that consists of an α-helix (E-helix), followed by a highly conserved stretch of 12 amino acids involved in chelating the Ca^{2+} ion and, a second α-helix (F-helix) oriented approximately perpendicular to the E-helix. Right panel: Representation of the EF-hand motif as the right hand. The index finger represents the E-helix, the bent fingers stands for the 12 amino acids of the canonical Ca^{2+} binding loop, and the thumb represents the F-helix.

When buffer molecules bind Ca^{2+} their molecular structures undergo small Ca^{2+}-dependant conformational changes, mostly confined to the loop region [21,48]. Moreover, Nuclear Magnetic Resonance (NMR) relaxation studies on the typical Ca^{2+} buffer PV, revealed the protein structure to be relatively rigid [51], and Ca^{2+} binding induces only relatively small conformational modifications. Thus, the predominant function of PV and, more in general, of Ca^{2+} buffers, is the control and/or the modulation of intracellular Ca^{2+} signals. Indeed, Ca^{2+} buffers stabilize Ca^{2+} concentration by binding Ca^{2+} ions in specific cell compartments and then releasing them back in the cytosol to affect transient increases of $[Ca^{2+}]_{cyt}$ [21].

How Ca^{2+} buffers modulate and affect intracellular Ca^{2+} signals depends on several parameters that include: (i) the intracellular concentration of a given Ca^{2+} buffer; (ii) the affinity for Ca^{2+} and other ions; (iii) the kinetics of Ca^{2+}-binding and Ca^{2+}-release and (iv) the mobility of Ca^{2+} buffer inside the cytosol [21].

The difficulty in obtaining a reliable value for Ca^{2+} buffer concentration is strictly linked to the fact that only specific subset of cells expresses Ca^{2+} buffers proteins [21]. The concentration of PV, for example, is approximately 1 mM in mouse fast-twitch muscle while it is lower in other type of muscle fibers and highly correlated with their speed of muscle relaxation [52]. PV is also differently expressed within different neurons subpopulation, reaching value of 80 μM in mouse Purkinje cells [53], 150 μM in mouse cerebellar interneurons [54] and 120 μM in rat Purkinje cells [55]. The amount of endogenous Ca^{2+} buffer in a cell is essential for shaping $[Ca^{2+}]_{cyt}$ rises [48]. In this respect, Ca^{2+} buffers are crucial in limiting the spreading of Ca^{2+} to prevent Ca^{2+}-overload and vicious Ca^{2+}cycle [21].

Metal binding affinity is a key property of buffers molecules and it is defined as the intrinsic cation affinity and selectivity of EF-hand domains [21]. Indeed, due to their selectively affinity for Ca^{2+} and Mg^{2+} ions, two different type of EF-hand binding sites are discernible: the Ca^{2+} specific sites, that display high affinity for Ca^{2+} and significantly lower affinity for Mg^{2+} and

the mixed Ca^{2+}/Mg^{2+} sites that show high affinity for Ca^{2+} binding and a moderate affinity for Mg^{2+} in a competitive manner [21]. Strictly connected to the Metal-binding affinity is the Metal-binding kinetics that, among Ca^{2+} buffer proprieties, mostly affects the cellular Ca^{2+} homeostasis. Indeed, Ca^{2+} binding and release kinetics proprieties of a given EF hands protein, strongly affect the spatiotemporal aspect of Ca^{2+}signals. This is particularly true for excitable cells in which $[Ca^{2+}]_{cyt}$ transients are short, lasting for tens milliseconds to several hundred milliseconds [48]. In resting cells, when cytosolic free $[Ca^{2+}]$ is below 0.1 mM and free $[Mg^{2+}]$ is around 1 M, cytosolic Ca^{2+} buffers are mostly in their "Ca^{2+}-free" conformation and Ca^{2+}/Mg^{2+} sites are to a large degree occupied by Mg^{2+}. Following a rise in $[Ca^{2+}]_{cyt,}$ Ca^{2+} buffers proteins will dissociate from Mg^{2+} and bind Ca^{2+} modulating the spatiotemporal aspects of Ca^{2+} signals [56]. The kinetics of Ca^{2+} binding therefore is determined by the slow of Mg^{2+}-off rate form the binding site.

Another important parameter for Ca^{2+} buffers proteins is the diffusion coefficient (*D*) that is defined as the mobility of a given protein in aqueous solution [21]. This property is approximately proportional to the hydrodynamic radius of the molecule (i.e. proportional to the relative molecular mass) [21]. PV, it is freely mobile molecules in Purkinje cells but its value of *D* can vary considerately in the different compartments of the cell such as in axons, soma and nuclei [57]. This is probably due to the different cytoplasmic properties such as viscosity, tortuosity and density of the medium in the different compartments [21].

3.2.1 Parvalbumin

Parvalbumin (PV) has been identified more than 50 years ago and described as the first Ca^{2+}-binding protein of the EF-hand family [50]. The protein was isolated from a carp muscle and its X-ray analysis allowed the elucidation of the structure of the EF-hand domain [58]. However, as mentioned above, PV is a remarkable exception in the family of EF-hand proteins since is one of the few proteins with three EF-hand sites: AB, CD and EF domains. Among

these three domains only CD and EF bind Ca^{2+} while the third AB domain, is necessary for the stability of PV [19,59,60]. In detail, the CD- and EF-hands form a functional pair domain with Ca^{2+}/Mg^{2+} mixed sites that bind Ca^{2+} with high affinity but also Mg^{2+} with a moderate affinity, in a competitive manner [19,48]. Consequently, in the cytoplasm of a cell in resting conditions (e.g. in fast-twitch muscle fibers and neurons, where PV is largely expressed), in which it is reported an intracellular Mg^{2+} concentrations of 0.5–1 mM [61], the mixed Ca^{2+}/Mg^{2+} sites of PV are occupied largely by Mg^{2+}. When $[Ca^{2+}]_{cyt}$ increases during a cell stimulation, the binding sites need to dissociate Mg^{2+} before Ca^{2+} binding can occur [19]. Due to this propriety, PV is considered to be a "slow" buffer since the rate of Ca^{2+} binding is determined by the rather slow Mg^{2+} dissociation-rate (Figure 2 and [62]).

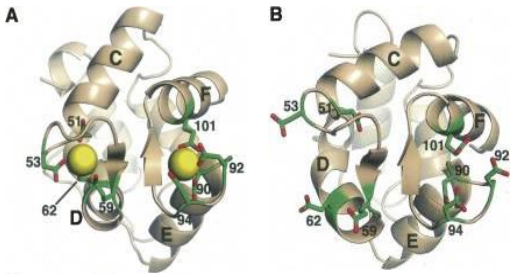

Figure 2. Rat α-PV structure in Ca^{2+}-bound (A) and Ca^{2+}-free (B) state (Adapted from Henzl, M. T., & Tanner, J. J. Protein Sci. 2008; 431–438).

Parvalbumin (PV) is small EF-hand protein involved in cytosolic Ca^{2+}-buffering. Its tertiary structure includes six α-helical segments (A–F) organized into two domains—the N-terminal AB domain and the CD-EF domain. The two metal ion-binding sites, the CD and EF sites are related by an approximate twofold symmetry axis and are physically linked by a short fragment of antiparallel β structure. The figure shows the CD and EF binding pockets in the Ca^{2+}-loaded (panel A) and unbounded (panel B) state of rat α-PV.

PV family includes α and β isoforms that, despite the 49% of sequence identity [63], exhibit distinct divalent ion-binding affinities [64,65]. Mammals express prevalently the α isoform (α-PV), the canonical cytosolic Ca^{2+}-buffer [66], while the β isoform (in humans and rodents named oncomodulin (OM)) is secreted by activated macrophages and functions as a potent nerve growth factor for retinal ganglion cells [67]. Although principally expressed in GABAergic interneurons, α-PV is also present at excitatory nerve terminal in the auditory brainstem, in fast twitch muscle

fibers, in parathyroid glands and in distal convolutes tubule in nephrons and it is mainly involved in modulating the spatiotemporal aspects of Ca^{2+} transients [21,68]. The role of PV as important Ca^{2+} signals modulator has been largely investigated in neurons. Indeed, already in 1993 Chard and co-authors exanimated the ability of PV to modulate the increase in intracellular free [Ca^{2+}] produced by brief depolarizations in rat dorsal root ganglion neurons [62]. The study reported that, in neurons, PV reduces the peak of Ca^{2+} increase and increases a fast component in Ca^{2+} decay. The role of PV as potent Ca^{2+} sensor modulator has been studied also in others excitable cells such as in skeletal muscle fibers. Simulation studies indicated that the exchange of Ca^{2+} for Mg^{2+} on PV binding sites can occur with sufficient rapidity to contribute to the relaxation of frog skeletal muscle fibers [20,69], a prediction that then has been confirmed experimentally [70]. Indeed, PV reaches millimolar ranges in fast twitch muscle and its expression is correlated with the speed of muscle relaxation [56,71]. In muscle fibers in relaxed state, Ca^{2+} is stored in the SR and PV is in "Ca^{2+}-free" conformation, binding Mg^{2+}. During cell stimulation, the action potential promotes Ca^{2+} release from the SR, inducing a transient increase of Ca^{2+} concentration in myoplasm that leads to the activation of the contractile apparatus and to the binding of Ca^{2+} to cytosolic buffering system [72]. Following dissociation of Mg^{2+}, PV removes Ca^{2+} from the sarcoplasm inducing myofibers relaxation and the returning to the relaxed state [52]. Constantly active Ca^{2+} pump SERCA on the SR membranes removes Ca^{2+} ions from the cytosol and accumulating them again in the SR lumen [52,73,74]. Ca^{2+} dissociates from PV and Mg^{2+} is then rebounded [71]. However, understanding the physiological role of PV in mammal skeletal muscle fibers has been challenging. Since more than 30 years ago, PV has been predicted to promote relaxation in fast-contracting skeletal muscle, but a major problem in the debate for the role of PV in mammals muscle relaxation, has been the slow rate of Mg^{2+} dissociation from this protein [75]. Indeed, it has been presumed that Ca^{2+} was transported into SR via SERCA before PV could contribute to cytosolic Ca^{2+} buffering [52]. Later studies on the dissociation rate of Mg^{2+}

from PV were performed at more physiological temperatures for mammals (30°C) than that documented for the frog and fish in the 0–20°C range [76]. These results lead to directly observe a significantly higher dissociation rate of Mg^{2+} which is sufficiently rapid for PV to act as a Ca^{2+} acceptor during contractions [20,52,77].

Müntener *et al* reported the first *in vivo* study that addressed the function of PV in rodent model [78]. The authors demonstrated that PV overexpression in the rat slow-twitch muscle soleus, significantly increases the speed of relaxation, without affecting its contraction [78]. Other evidences were reported in 1999, when the first knockout mouse for PV (PV KO) was generated in Schwaller laboratory [20]. The comparison between parvalbumin-deficient muscles and the corresponding WT parvalbumin-containing muscles, has demonstrated the specific contribution of PV in accelerating the rate of relaxation of fast mouse muscles [20]. In detail, it was observed that in the absence of PV, the decay of $[Ca^{2+}]_{cyt}$ in PV KO fast twitch muscle fibers was slower, thus leading to a prolongation of the time required to reach the peak twitch tension and to an extension of the half-relaxation time [20]. This result demonstrated that, in the absence of PV, myofibers loose the fast mechanism to reduce sarcoplasmic $[Ca^{2+}]$. Recently, is has also been reported that both in fast-twitch muscle and as well as in cell model C2C12 myotubes, the down regulation of PV leads to an increase of mitochondrial fractional volume and an increase of Peroxisome proliferator-activated receptor γ co-activator 1α (PGC-1α) expression, which is considered as a master regulator of mitochondrial biogenesis [79,80]. The increased mitochondrial volume might partially compensate the loss of PV in controlling Ca^{2+} homeostasis in skeletal muscle fibers to prevent or restrict the spreading of Ca^{2+} signals [56].

3.3. Mitochondria

3.3.1 Mitochondria general framework

Mitochondria are dynamic organelles that represent the primary energy-generating system in most eukaryotic cells, in which the oxidative phosphorylation produces the majority of cellular ATP [11,81]. Besides this essential role in energy metabolism, mitochondria play important functions as a regulators and decoders of Ca^{2+} signals [4]. Indeed, mitochondria participate in many aspects of cell homeostasis ranging from the control of lipid metabolism, reactive oxygen species (ROS) production to cell death regulation [4,82,83]. In addition, mitochondria have been also proposed as dynamic cytosolic Ca^{2+} buffering system in many cellular type [5].

Mitochondria are separated from the cytoplasm by the outer and the inner mitochondrial membrane (OMM and IMM, respectively). The OMM is permeable to solutes that are smaller than 5 kDa, and thus also to Ca^{2+}, thanks to the abundant expression of voltage-dependent anion channels (VDACs), whose permeability is controlled by ATP and other regulatory factors [84]. By contrast, the IMM is a tight diffusion barrier to all ions and molecules that can bypass it by specific channels and membrane transporter proteins which are selective for a particular ion and molecule [4].

As mentioned above, the most important task of mitochondria is the regulated production of ATP production by oxidative phosphorylation. During the oxidation of nutrients such as glucose, amino acids or fatty acids, reduced metabolites with low reduction potentials, such as NADH or succinate, are produced in the mitochondrial matrix [11,81]. These reduced metabolites provide electrons to the respiratory chain, several IMM membrane protein complexes that contain redox centres with progressively higher reduction potential, until the final electron acceptor that is O_2 [85,86]. In the 60s, Peter Mitchell clarified the process by which this electron transfer is coupled to ATP synthesis in oxidative phosphorylation proposing for the first time an indirect mechanism named “chemiosmotic theory” [87]. The free-energy obtained by the reactions performed by the respiratory complexes is used to

pump protons from the mitochondrial matrix to the intermembrane space (IMS), to create a transmembrane potential (ΔΨm) of about -180 mV. The energy stored by this electrochemical potential is then subsequently used by F0-F1ATP synthase to produce ATP [87,88].

3.3.2 Mitochondrial Ca^{2+} as regulators of cellular metabolism

Preceding the enouncement of the chemiosmotic theory, two seminal papers described for the first time that energized mitochondria could accumulate large amount of Ca^{2+} [89,90]. In the following years, when the majority of scientists in the field accepted the chemiosmotic model, the properties of mitochondrial Ca^{2+} uptake became clear. In detail, the ΔΨm generated across the IMM by the translocation of protons across the IMM, led to the concept of an energetically favourable Ca^{2+} uptake mechanism [91,92]. The generation of an internal negative electrochemical gradient by the mitochondrial respiratory chain, indeed, provides the thermodynamic basis for cation accumulation into the organelle matrix [92], mediated by the mitochondrial Ca^{2+} uniporter (MCU), a channel that allows the rapid Ca^{2+} accumulation into the matrix [4]. However, further characterizations of the channel properties of MCU demonstrated that, despite the high selectivity for Ca^{2+} measured by direct patch-clamp of mitoplasts [13], the apparent mitochondrial affinity for Ca^{2+} was very low at physiological [Ca^{2+}] [93]. Therefore, since cytosolic [Ca^{2+}] is about 10-100 nM in resting conditions and reaches the values of 2-3 μM only during cell stimulation, for many years the role of mitochondria in controlling cytosolic Ca^{2+} homeostasis was considered marginal and involved mainly in pathological conditions [9,23]. The situation reversed when tools to perform reliable measurement of [Ca^{2+}] in intact living cells were developed [94]. These probes revealed that, while mitochondrial Ca^{2+} concentration ($[Ca^{2+}]_{mit}$) in basal resting condition is low, comparable to the cytosolic one (10-100 nM), upon cell stimulation, mitochondria are able to rapidly and efficiently accumulate large amount of Ca^{2+} that in some cells can reach 100 μM [7]. The apparent discrepancy between the low affinity of mitochondrial Ca^{2+} uptake and the prompt

response of mitochondria to [Ca^{2+}] increases, was solved by the demonstration that mitochondria are located in close proximity to the Ca^{2+} channels of ER/SR [95,96]. Thus, the quasi-synaptic junctions with the ER/SR membranes and mitochondria allow the organelle to directly sense local high [Ca^{2+}] compatible with the low affinity of the MCU [94]. Ca^{2+} taken up by mitochondria then is rapidly extruded preventing mitochondrial Ca^{2+} overload or vicious Ca^{2+} cycling across the mitochondrial membrane [95]. The Ca^{2+} efflux from the mitochondrial matrix in excitable-cells is mediated by the recently identified mitochondrial Na^+/Ca^{2+} exchanger (NCLX) [97,98]. Ca^{2+} extrusion is powered by the electrochemical gradient for Na^+ entry into the mitochondrial matrix from the cytosol, thus the energy available to NCLX for mitochondrial Ca^{2+} efflux depends on the concentrations of Na^+ in the cytosol ($[Na^+]_i$) and matrix ($[Na^+]_m$), on $\Delta\Psi_m$ and also on the stoichiometry of NCLX [99]. In non-excitable cells (e.g., liver cells) Ca^{2+} efflux is also mediated by a H^+/Ca^{2+} exchanger of unknown molecular identity [100,101] These evidences sustained the general idea that mitochondria could actively and rapidly change their [Ca^{2+}] and contribute to cellular homeostasis [102]. The physiological relevance of mitochondrial Ca^{2+} accumulation started to be elucidated when it was demonstrated that mitochondrial Ca^{2+} regulates three key enzymes of mitochondrial metabolism: ketoglutarate dehydrogenase, isocitrate dehydrogenase, and pyruvate dehydrogenase phosphatase 1 (PDP1). In addition, Ca^{2+} pulses also stimulate the adenine nucleotide transporter and complex V (mitochondrial F0-F1 ATP synthase) [81,103], using the proton gradient to upregulate ATP production. Finally, Ca^{2+} activates α-glycerolphosphate dehydrogenase, a component of the glycerol phosphate shuttle, that supplies NAD^+ for glycolysis [9,81]. Altogether these processes ensure prompt stimulation of aerobic metabolism in stimulated cells in parallel with the activation of ATP-consuming processes in the cytosol [4].

3.3.4 Mitochondrial Ca^{2+} as a regulator of cell death

The interest in the process of mitochondrial Ca^{2+} homeostasis dramatically increased when it became clear that cell death is causally linked to mitochondrial Ca^{2+} loading. Mitochondrial matrix Ca^{2+}, together with other causal factors, most notably oxidative stress, high phosphate concentrations, and low adenine nucleotide concentration, represents an essential permissive factor for opening of the mitochondrial permeability transition pore (mPTP), a high conductance channel whose opening enables the release of pro-apoptotic mitochondrial components [104,105]. This event triggers the so-called mitochondrial permeability transition (PT) that is characterized by a dramatic increase in the IMM permeability to any ions and solutes with molecular mass up to 1500 Da [105,106]. The consequent dissipation of the mitochondrial $\Delta\Psi m$ leads to membrane depolarization and mitochondrial swelling, increased mitochondrial ROS species generation and cytochrome c releases [8,9]. The increased cytosolic Ca^{2+} then triggers a massive exit of cytochrome c from all mitochondria in the cell activating caspase and nuclease enzymes that finalize the apoptotic process [105,107,108].

3.3.5 Mitochondria as cytosolic Ca^{2+} buffers

In addition to the metabolic functions, mitochondrial Ca^{2+} accumulation was shown to have also an important role in shaping the spatiotemporal pattern of cytosolic Ca^{2+} rises [4,109,110]. Mitochondria are highly sophisticated "modifiable" buffers that vary their activity in different phases and functional states of the cell. Therefore, their number, shape, distribution [111] and, most likely, their responsiveness to Ca^{2+} [112] are controlled by converging signalling pathways. The heterogeneity of mitochondrial morphology and function within the cell are well documented in several cell models. For instance, mitochondria of pancreatic acinar cells show different subpopulations of mitochondria, particularly around the acinar granule region where they are able to prevent the spread of the $[Ca^{2+}]_{cyt}$ from the apical (secretory) region [4,113]. Similarly, in neurons, mitochondria appear to be

located in specific sites contributing to the accumulation of large amount of Ca^{2+} in defined subcellular domains and thus affecting neurotransmitter release [114]. Moreover, it has been largely documented that mitochondria recruitment to neuronal soma, synapses and dendritic spines is crucial for the regulation of nerve activity and any change in the positioning of mitochondria to subcellular domains affects neuron physiology and might contribute to the pathogenesis of neurodegeneration [115,116]. Overall, the emerging picture defines mitochondria as efficient Ca^{2+} buffers that shape cytosolic $[Ca^{2+}]_{cyt}$ by either regulating the kinetic properties of Ca^{2+} channels or by preventing Ca^{2+} diffusion [4].

3.4 MCU complex

The study of the physiological role of mitochondrial Ca^{2+} uptake was severely limited by the lack of the molecular identity of the MCU. The channel was characterized only in 2011 by two different groups [117,118], marking a turning point in the study of the pathophysiological roles of mitochondrial Ca^{2+} uptake. MCU is a Ca^{2+} channel of 40 KDa located in the IMM that consists of two transmembrane domains spanning the IMM [102]. Soon, after its discovery, it was clear that the MCU was part of a macromolecular complex since it lacks classical Ca^{2+}-binding domains and the loop region that faces the IMS appears to be too small to contain regulatory elements [5]. This was confirmed by blue native gel separation experiments of purified mitochondria that display a high-molecular-weight complex containing MCU with an apparent molecular weight of about 450 kDa, suggesting that many other proteins are part of the channel, forming a complex known as MCU complex [22,119,120]. Indeed, is nowadays known that the MCU complex is composed by various proteins that include MCUb, the Essential MCU Regulator (EMRE) and MICUs family (MICU1, MICU2 and MICU3) that regulate the amount of Ca^{2+} taken up by mitochondria.

3.4.1 Pore forming subunits

EMRE ("essential MCU regulator") is a 10 kDa metazoan-specific protein with a single transmembrane domain that spans the IMM with a highly acidic carboxyl terminus [121]. It has been proposed that EMRE is essential for MCU activity, since its silencing abolish mitochondrial Ca^{2+}uptake [121], although experiments in the planar lipid bilayer demonstrated that mouse MCU alone is sufficient to give rise to Ca^{2+} currents [118]. As for the function, EMRE appears fundamental in mediating the interaction between MCU and the regulatory subunits as MICU1 and MICU2 [121].However, it has also been observed that MICU1 is sufficient to induce MCU channel activity [119]. Interestingly, in yeast, which does not show mitochondrial Ca^{2+} uptake, human MCU is able to act as a functional channel and assemble in a functional channel only when EMRE is present [122]. Thus, these observations suggest that EMRE is essential to assemble a functional MCU channel in metazoan organisms [78]. Of note, very recently, it was shown that the acidic C-terminal domain operates as a matrix Ca^{2+}sensor that regulates the MCU activity [123]. Therefore, in this model, EMRE acts, together with MICU1, as a regulatory complex able to sense [Ca^{2+}]. Nevertheless, these data are in opposition to another report, which proposes a structural role of EMRE and a different topology across the IMM, incompatible with the suggested matrix-Ca^{2+} sensor of the acidic C-terminal domain [124]. Future studies will clarify the role of EMRE in the MCU channel activity.

MCUb is a MCU isoform that share 50% sequence similarity with MCU and it is conserved in most vertebrates but absent in other organisms in which MCU is present like plants, some protozoans (kinetoplastids), Nematoda, and Arthropoda [125]. MCUb possesses two transmembrane domains separated by a short loop similar in structure with MCU [125]. Despite the sequence similarity with MCU in the transmembrane domains, MCUb displays altered Ca^{2+} permeation, given to two conserved amino acid substitutions in close proximity of the conserved DIME motif, that reduces the conductivity of the channel. Specifically, as has been recently demonstrated [125], in the MCUb

sequence the Arg 251 and Glu 256 residues are mutated in tryptophan and valine, respectively (R251W and E256V) [125] These substitutions, as mentioned, drastically reduce conductivity of the channel reducing mitochondrial Ca^{2+} uptake [125]. Coherently, it was shown that MCUb overexpression in Hela cells dramatically reduces mitochondrial Ca^{2+} uptake evoked by agonist stimulation and that MCUb oligomers, reconstituted in planar lipid bilayers, reduces the amplitude of Ca^{2+} transients [125]. Moreover, reconstituting MCU together with MCUb in planar lipid bilayers demonstrated that the inclusion of MCUb in the MCU oligomer completely inhibited Ca^{2+} permeation through the MCU [125]. Interestingly, MCU and MCUb expression profile differs among tissues, possibly contributing to the spatiotemporal control of mitochondrial Ca^{2+} uptake in different tissues [125]. Consistently, tissues characterized by low mitochondrial Ca^{2+} transients, such as the heart, exhibit a low MCU/MCUb ratio, while others tissues, such as skeletal muscle that present a higher mitochondrial Ca^{2+} uptake ability, display a higher ratio [125].

3.4.2 Regulatory subunits

One of the key features of mitochondrial Ca^{2+} uptake is its sigmoidal response to $[Ca^{2+}]_{cyt}$ [4]. At resting $[Ca^{2+}]_{cyt}$, mitochondrial Ca^{2+} uptake is inhibited, despite the huge driving force for Ca^{2+} accumulation [4], in order to prevent matrix Ca^{2+} overload and the dissipation of the $\Delta\Psi m$. On the contrary, at higher $[Ca^{2+}]_{cyt}$, when cells are stimulated, mitochondrial Ca^{2+} uptake has to rapidly increase in order to guarantee mitochondria prompt response to cell stimulation [4,5]. This property is regulated by a highly sophisticated gatekeeping mechanism that include both negative modulators, acting at low $[Ca^{2+}]_{cyt}$, and activators able to induce mitochondrial response. For this property are responsible the MICU (mitochondrial calcium uptake) family members composed by MICU1, MICU2,and MICU3 [126]. All of these regulators are localized in the IMS, display EF-hand Ca^{2+}-binding domains in their protein sequence and interact with MCU.

MICU1 is a 54 kDa protein that was identified as the first member of MICUs family even before the identification of MCU [127]. Already in 2010 MICU1 was defined as a critical modulator of mitochondrial Ca^{2+} uptake since its silencing is sufficient to abolish mitochondrial Ca^{2+} entry in intact and permeabilized cell [127]. Interestingly, it was then shown that MICU1 silencing is sufficient to induce mitochondrial Ca^{2+} overload, suggesting therefore that MICU1 could play a gatekeeping role in preventing mitochondrial Ca^{2+} uptake at low $[Ca^{2+}]_{cyt}$ [128]. In addition, it has been demonstrated that MICU1 acts also as cooperative activator of MCU, thus ensuring the increase in the MCU Ca^{2+} conductivity during cell stimulation [129]. The relevance of MICU1 in the regulation of mitochondrial Ca^{2+} uptake was also demonstrated in human patients in which loss of function mutation in MICU1 gene cause myopathy and learning difficulties due to mitochondrial Ca^{2+} overload [130].

The discovery of MICU1 was soon followed by the identification of MICU1 paralog, MICU2 (Mitochondrial Calcium Uptake protein 2) [120], that helped to clarify the mechanism responsible for the sigmoidal response of the MCU to extra-mitochondrial $[Ca^{2+}]$. MICU2 was demonstrated to act as the genuine gatekeeper of the MCU at low $[Ca^{2+}]_{cyt}$ [119] and when cytosolic $[Ca^{2+}]$ increases, Ca^{2+}-dependent MICU2 inhibition and MICU1 activation guarantees the prompt response of rapid mitochondrial Ca^{2+} accumulation. MICU2 protein stability depends on that of MICU1 [119,120,131] since MICU1 silencing experiments induces MICU2 protein degradation. Notably, MICU1 and MICU2 have been shown to form an obligate heterodimer through the formation of a disulphide bond [119].

Recently, an alternative splice variant of MICU1, named MICU1.1, was identified and characterized [15]. MICU1.1 expression varies greatly among tissues; indeed, it is present only in skeletal muscle and in lower levels are found in the brain, suggesting tissue-specific functions. MICU1.1 is characterized by the addition of a micro-exon coding for four amino acids (EFWQ) far from the EF-hand domains, which modifies the Ca^{2+} binding properties of the protein. In detail, MICU1.1 can bind Ca^{2+}one order of

magnitude more effective than MICU1 and, when it heterodimerizes with MICU2, activates MCU current at lower [Ca^{2+}] than MICU1-MICU2 heterodimers [15]. It was hypothesized that the inclusion of this splice variant in the MCU complex could represent an important mechanism in excitable tissues [15]. Indeed the prevalent expression of MICU1.1 in skeletal muscle, allows a prompter response of mitochondrial metabolism to [Ca^{2+}] ensuring a sustained ATP formation, necessary for muscle contraction [15].

MICU3, unlike MICU1 and MICU2 that present an ubiquitous and correlated expression pattern among tissues, is expressed only in the central nervous system (CNS) and, at low levels, in skeletal muscle [132]. Recently, it was shown that MICU3 forms heterodimers only with MICU1 but not with itself or MICU2 and acts as a highly potent activator of MCU, with no gatekeeping function [133].

Representative image of MCU complex components is showed in Figure 3

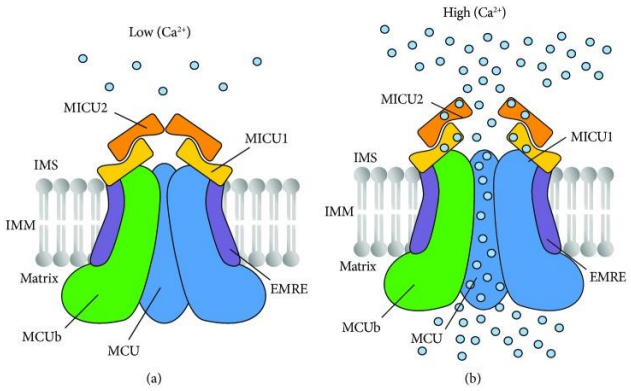

Figure 3. Schematic representation of the mitochondrial Ca^{2+} uniporter (MCU) complex. (Adapted from Feno, Simona et al. Oxid Med Cell Longev. 2019).

MCU is a macromolecular complex composed by pore-forming (MCU, MCUb and EMRE) and regulatory (MICU1 and MICU2) subunits. The regulatory subunits are responsible for the sigmoidal response to extra mitochondrial [Ca^{2+}]. In basal resting condition (left panel) MICU1-MICU2 heterodimers act as gatekeeper of the channel, thus avoiding a massive energy dissipation and the induction of cell death. Increases in [Ca^{2+}] during cell stimulation (right panel) abolish the inhibitory function of the MICU1-MICU2 heterodimers and stimulate MCU opening, ensuring a mitochondrial prompt response to the needs of a stimulated cells.

3.5 Role of MCU in skeletal muscle homeostasis

Concomitantly with the elucidation of the molecular identity and function of the MCU complex, a number of studies have been conducted to better understand the pathophysiological role of mitochondrial Ca^{2+} uptake. Genetic ablation of MCU complex indeed, helped to clarify the function of mitochondrial Ca^{2+} transport in different tissue.

The first work on MCU knockout mice showed a very surprising result. Given the central role of mitochondrial Ca^{2+} in metabolic regulation, these mice were expected to die during embryogenesis. Nonetheless, in 2013 Finkel and co-workers generated a MCU knockout mouse characterized by a very mild phenotype with only a modest defect in skeletal muscle [14]. In detail, in muscle mitochondria of MCU KO mice, stimulation of O_2 consumption by Ca^{2+}, is suppressed, although basal matrix Ca^{2+} levels were reduced of about the 75% [14]. In addition, consistent with the role for the calcium-sensitive phosphatase PDP1 regulating PDH phosphorylation, lower levels of matrix calcium in the MCU KO mice led to markedly increased levels of PDH phosphorylation and thus its inhibition [14]. Importantly, since mitochondrial Ca^{2+} stimulate ATP production that is necessary for muscle function, MCU KO mice showed also an impairment in the exercise capacity and a significant decrease in the muscular strength [14]. However, it should be noted that Finkel and co-workers obtained viable mice only in an outbred strain composed by a mix of C57/BL6 and CD1 backgrounds. In addition, the birth ratio of the homozygous MCU KO mice was lower than expected. Two different mouse model, then confirmed the embryonic lethality of MCU in inbred strain [134,135].

To exclude any possible *in vivo* compensatory effects in response to MCU ablation during development, in 2015, MCU acute silencing and overexpression in neonatal and adult mice have been performed [17]. Interestingly, overexpression of MCU by adenoassociated virus (AAVs) infection induces dramatic skeletal muscle hypertrophy while, coherently,

MCU silencing causes muscle atrophy both during post-natal growth and in adulthood [17]. In addition, MCU overexpression protects muscles from the loss of muscle mass that occurs during denervation-induced atrophy in mouse muscles, indicating a potential therapeutic role of MCU modulation in muscle atrophy [17]. IGF1-AKT/PKB-mediated pathway, that is known to control muscle growth, is induced by MCU and thus by mitochondrial Ca^{2+}. Furthermore, the modulation of MCU expression induces the expression of another gene: the peroxisome proliferator-activated receptor gamma coactivator 1-alpha 4 (PGC-1α4), a PGC-1α isoform that is not involved in mitochondrial biogenesis and whose overexpression has been shown to induce muscle hypertrophy [28].

Recently, it has been also reported that MCU controls muscle substrate preference for energy production by impinging on the activity level of PDH [16]. In the absence of MCU indeed, pyruvate to acetyl-CoA conversion slows down limiting the TCA supply and thus rewiring cell metabolism [16]. The decrease in muscle glucose oxidation translates into increased glycolysis, increased in glycogen storage, and lactate production. The aberrant glucose utilization signals to the liver and the adipose tissue, which in turn mobilize nutrient depots and lipid catabolism in order to partially compensates this defect [16]. Therefore, the observed impairment in muscle performance of skeletal muscle MCU KO mice, are probably mainly due to reduced glucose oxidation consequent to inhibition of PDH and thus TCA cycle activity. Of note, this metabolic effect is accompanied also by fiber-type remodelling toward faster MHCs [16].

Moreover, as mentioned above, it has also been demonstrated that skeletal muscle mitochondria has a peculiar MCU complex composition containing an alternative splice isoform of MICU1, named MICU1.1 [15]. This muscle-specific isoform, by binding Ca^{2+} with higher affinity, confers myofiber mitochondria sustained Ca^{2+} uptake and ATP production that are required for muscle contraction [15]. Altogether, these finding clearly demonstrate the importance of mitochondrial Ca^{2+} signalling in skeletal muscle pathophysiology.

3.6 Mitochondria in skeletal muscle

Skeletal muscle is a dynamic organ characterized by an incredible ability to rapidly increase its rate of energy consumption to sustain activity. In this tissue, ATP demand increases ~100 times during rapid muscle contraction. Such high demand of ATP cannot be accomplished by the finite amount ATP normally stored inside the skeletal muscle (~20–25 mmol/kg dry muscle) [136]. Therefore, during contraction, there is an essential requirement for rapid and sustained ATP production, a role fulfilled primarily by mitochondria [137]. As such, skeletal muscle cells are densely populated with these organelles that occupy 5-10% of muscle fiber volume [72,138,139] and control the rate of ATP synthesis to sustain muscle contraction [11,81]. In skeletal muscle, different type of mitochondria population according to diverse subcellular localization co-exist. Adult skeletal muscle fibers present three distinct subpopulations with differing morphology and biochemical properties [140]. Below the sarcolemmal membrane, proximal to the capillary and nuclei and organized as dense clusters, reside the subsarcolemmal (SS) mitochondria, which are important in providing ATP for membrane active transport as well as for gene transcription [141]. The second subpopulation is covering the myonuclei as a continuation of SS population [141,142] and are identified as perinuclear mitochondria. The third subgroup are placed between the myofibrils, adjacent to the Z-line of the sarcomere and are termed intermyofibrillar (IMF) mitochondria. These mitochondria play a prominent role in providing ATP to the contractile filaments within muscle to facilitate contraction [143]. IMF mitochondria indeed, are located in direct contact with the transverse tubules and specifically close to Ca^{2+} release units of the sarcoplasmic reticulum (CRUs), the site of Ca^{2+} release during excitation-contraction coupling [143]. This localization favour fast ATP delivery to support Ca^{2+} transport into SR and to capture Ca^{2+} from high microdomains near the releasing site [138,144,145]. SS and IMF mitochondria are the most studied population. They show a distinct

morphological properties in electron microscopy analysis: SS mitochondria appear more punctate, whereas IMF mitochondria are much more elongated as they extend between the myofibrils [146]. These morphologies however are not static despite the constraints imposed by the surrounding myofibrils. Picard *et al*. have demonstrated that functionally competent mitochondria are maintained by continuous remodelling depending on the cellular metabolic demands [146]. The morphological plasticity of mitochondria is controlled by tightly regulated processes that are coordinated to influence mitochondrial homeostasis. Mitochondria remodelling, is a common feature in all the cell type, and it is achieved by the breakdown of damaged components or even whole mitochondria [147–149] and by replacing them with functional ones [150,151]. The re-shaping processes involve: fusion and fission, mitochondria motility, cristae re-shaping and the interaction with other organelles, such as the endoplasmic reticulum [147,152]. In detail, the fusion of smaller organelles allows the sharing of mitochondrial material and facilitates the expansion of the "mitochondrial reticulum". The proteins mainly involved in mitochondrial fusion include mitofusin 1/2 (Mfn1 and Mfn2), which anchor adjacent OMMs, and optical atrophy 1/2 (Opa1 and Opa2), which play a similar role in IMM fusion [141,147]. Conversely, fission is required to break the organelle into smaller fragments that represents an important step in removing dysfunctional mitochondria from the mitochondrial pool. In a manner similar to Mfn2, the fission protein dynamin-related protein 1 (Drp1), that resides on the OMM, works in conjunction with mitochondrial fission factor (Mff) and fission protein 1 (Fis1) to wrap around and constrict the mitochondria to promote organelle separation [147,149] (Figure 4).

The alterations in mitochondrial morphology and function are more evident in skeletal muscle tissue, where mitochondria respond to the acute stress of exercise [153]. In detail, the cellular response to exercise involves the initiation of internal signalling cascades that provoke an altered gene expression response which lead to augmented mitochondria fusion and biogenesis [153,154] and also the simultaneous activation of mitochondrial

autophagy (i.e. mitophagy), with the purpose of increasing organelle turnover to maintain a healthy mitochondrial pool [155,156]. Interestingly, impaired mitochondrial fusion and a consequent unbalanced in the mitochondrial-turnover, prevents excitation-contraction Ca^{2+} signalling in muscle fibers, suggesting that the integrity of mitochondrial communication is necessary to maintain not only the energy homeostasis of the muscle fiber but also its contractile function [141,147].

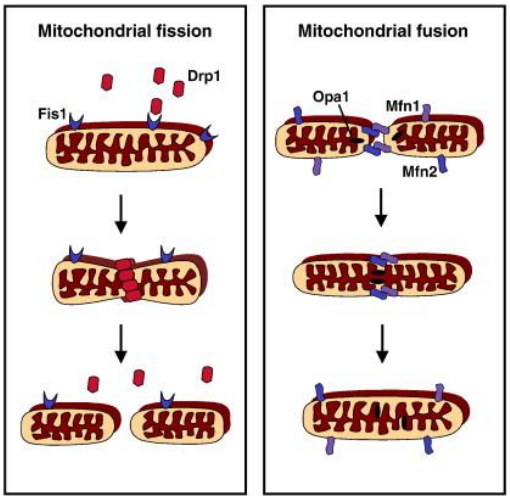

Figure 4. Mitochondrial fission and fusion (Adapted from Sheridan, Clare and Martin, Seamus J. Mitochondrion, Volume 10, issue 6 2010, pages 640-648).

Mitochondrial fission (left panel) is a mechanism that segregates dysfunctional or damaged components of the mitochondrial network allowing their removal via mitophagy. The process is driven by Drp1, a GTPase dynamin-related protein which is recruited to the OMM and oligomerizes to form active GTP-dependent mitochondrial fission sites. In some species as in yeast and human, translocation of Drp1 is facilitated by its receptor, Fis1, which is tethered to the mitochondrial outer membrane. Drp1, in constriction sites, forms multimeric spirals around mitochondria further constricting mitochondrial tubules leading to mitochondrial fission
Fusion process (right panel) is driven by Mfn1 and Mfn2 located on the OMM. Interactions between these protein tethers two adjacent mitochondria together and mitofusin proteins then mediate mitochondrial outer membrane fusion. Opa1, a dynamin-related protein, then mediates IMM fusion.

Under steady-state conditions, the mitochondrial removal process is balanced by an equal rate of biogenesis, such that mitochondrial content within the cell remains unchanged. Therefore, it is not surprising that disequilibrium or imbalance between mitochondrial proliferation and degradation processes, is strictly associated to the onset and progression of several pathological conditions in humans, including neurodegenerative diseases, myopathies and other age-associated disorders [111]. The correct functions of mitochondria

in the context of energy production, cellular quality control and integration of cell death/survival pathways hence place these organelles at the centre of signalling pathways that regulate myocyte homeostasis [136,157].

3.7 Signalling pathways that control skeletal muscle mass

Skeletal muscle has the incredible ability to rapidly adapt to a wide range of metabolic and mechanical physiological and pathological stimuli. [158]. Quantitative alterations in myofibrillar protein levels finally lead to changes in fiber size [27,159]. In detail, an increase in protein synthesis leading to fiber size growth is known as muscle hypertrophy, that occurs during development and in response to exercise or mechanical overload or anabolic hormonal stimulation (testosterone or β2-adrenergic agonists) [159–161]. Conversely, in aging, in starvation and in several disease states as cancer, diabetes, loss of neural input (denervation, motor neuron disease) and on catabolic hormonal stimulation (corticosteroids), protein degradation prevails leading to a muscle atrophy [158,161,162]. Reprogramming of gene expression has been recognized to be involved in muscle adaptation in response to these various kinds of stimuli [163,164]. The application of gene expression profiling has provided a powerful tool to elucidate the molecular pathways underlying such tissue remodelling [165]. The comparison of several systemic and disuse types of atrophy such as fasting, diabetes, cancer cachexia, uremia and denervation, identified a set of 120 genes defined as “atrogenes” which were commonly induced or suppressed in all the analysed models [25,26]. Of note, one of the most downregulated atrogenes is PV [25,26].

Muscle hypertrophy occurs when the overall rates of protein synthesis exceed the rates of protein degradation [166]. One of the best-characterized muscle growth-promoting pathway is the IGF1-AKT/PKB pathway which controls both protein synthesis, via the kinases mammalian target of rapamycin (mTOR) and glycogen synthase kinase 3β (GSK3β), and protein degradation,

via the transcription factors of the FoxO family [167]. In detail, AKT activates mTOR thus promoting the activation of S6 kinase and blocking the inhibition of 4E-BP1 (eukaryotic initiation factor 4E-binding protein 1) on eIF4E (eukaryotic translation initiation factor 4E), thus leading to protein synthesis [168]. Moreover, inhibition of GSK3β, results in the stimulation of protein synthesis, since GSK3β blocks protein translation initiated by eIF2B (eukaryotic translation initiation factor 2B) [169]. AKT is also able to suppress catabolic pathways by phosphorylating and thus repressing the transcription factors of the FoxO family [167,170,171]. FoxO factors are required for the transcriptional regulation of the ubiquitin ligases atrogin-1 and muscle ring finger 1 (MuRF1), two ubiquitin-ligases involved in the muscle atrophy [25,26]. FoxO factors are also required for the transcriptional regulation of the microtubule-associated protein 1 light chain 3 (LC3), which together with BCL2/adenovirus E1B interacting protein 3 (BNIP3), is essential for the activation of the autophagy-lysosome pathway [172]. AKT-dependent phosphorylation of FoxOs therefore inhibits the two major systems of protein breakdown in skeletal muscle, the ubiquitin-proteasomal and autophagic/lysosomal pathways.

Recently, Spiegelman and co-workers demonstrated that also PGC-1α4 is involved in the control of muscle mass [28]. PGC-1α4, is a splicing form of PGC-1α and it is abundantly expressed in skeletal muscle where it appears to play a role in the adaptive response to exercise, particularly in the setting of resistance training [28]. This protein does not regulate the same set of oxidative genes induced by PGC-1α but, rather, it activates the expression of IGF-1 while concomitantly suppressing myostatin pathway, an inhibitor of muscle cell differentiation and growth [173]. Of note, it has been recently demonstrated that mitochondrial Ca^{2+} uptake positively regulates myofiber size in physiological conditions and counteracts pathological loss of muscle mass by impinging on PGC-1α4 and AKT anabolic pathways [17]

.

4. Aim

Skeletal muscle is a dynamic organ characterized by a remarkable ability to rapidly increase its rate of energy production to sustain activity [174]. In this regard, mitochondria play a crucial role in muscle metabolism, since they control the rate of ATP production. Indeed, it is well established that mitochondrial Ca^{2+} accumulation stimulates three different Ca^{2+}-sensitive dehydrogenases that are key rate-controlling enzymes in the tricarboxylic acid cycle to avoid a quick exhaustion of ATP during contraction [11,81]. The identification of the molecular identity of the mitochondrial calcium uniporter (MCU), the highly selective channel responsible for Ca^{2+} accumulation by mitochondria, and its associated regulators, has allowed to characterize the physiological roles of mitochondrial calcium uptake in skeletal muscle homeostasis. Indeed, recently, it has been demonstrated that the regulation of MCU-mediated mitochondrial Ca^{2+} uptake is not only involved in the control of the rate of ATP production, but it also controls skeletal muscle trophism [17] and whole body metabolism [16].

These findings increased the interest in characterizing the role of mitochondrial Ca^{2+} in skeletal muscle homeostasis. Although the role of mitochondrial Ca^{2+} uptake in energy production in skeletal muscle is undisputed [11,81] and the important role of mitochondrial Ca^{2+} uptake in muscle homeostasis have been recently demonstrated [16,17], the function of the other key properties of mitochondrial Ca^{2+} uptake in skeletal muscle tissue requires further researches. In particular, elucidating how mitochondrial Ca^{2+} uptake regulates skeletal muscle homeostasis and understanding whether, in physiological condition, muscle mitochondria are able to actively buffer $[Ca^{2+}]_{cyt}$, are still matters of debate.

In this regard, the focus of my PhD research was to investigate the regulatory processes that modulate mitochondrial Ca^{2+} signalling in skeletal muscle and understand how $[Ca^{2+}]_{cyt}$ affects mitochondrial Ca^{2+} uptake in skeletal muscle. For this purpose, we examined a specific condition where intra-fiber Ca^{2+} kinetics have been steadily altered by removing parvalbumin (PV), the main cytosolic Ca^{2+} buffer [48].

PV is mainly express in fast-twitch muscle fibers and its absence influences the response of cell upon stimulation [20,175]. To this end, as study tool, we used the PV knockout (KO) mouse model obtained from the laboratory of Prof. Beat Schwaller (Dept. of Medicine, University of Fribourg, Switzerland). We demonstrated that mitochondria of fibers lacking PV adapt to store and take up more Ca^{2+} by increasing their Ca^{2+} buffering capacity. This is mediated by an upregulation of the expression of MCU complex components and an increase of mitochondria number and volume. These results suggest a possible mitochondrial compensatory mechanism to prevent and restrict the spreading of cytosolic Ca^{2+} signals in skeletal muscle fibers.

Furthermore, since it has recently been demonstrated that increases of mitochondrial Ca^{2+} positively regulates skeletal muscle mass [17], we asked whether the absence of PV might also control muscle trophism by activating mitochondrial Ca^{2+}-dependent pathways to control skeletal muscle trophism. We observed that the absence of PV partially counteracts denervation-induced atrophy, triggering the expression of PGC1α4, a splicing variant of the master regulator of mitochondrial biogenesis PGC1α, that has been recently demonstrated to control the hypertrophic growth of muscle upon exercise [28].

Future studies will investigate the pivotal role of mitochondria as integration points of different cytosolic Ca^{2+} signals and will consequently clarify how mitochondria could decode these different stimuli in biological responses.

5. Results

5.1 Cytosolic Ca^{2+} transients in PV KO animal model

To investigate the effect of PV ablation on muscle fibers, we studied the effect of its removal on Ca^{2+} homeostasis of the main subcellular domains, starting from the measurement of $[Ca^{2+}]_{cyt}$. We performed this analysis on *flexor digitorum brevis* (FDB) isolated muscle fibers from WT and from the total constitutive PV knockout mouse (PV KO), obtained from the laboratory of Professor Beat Schwaller (Dept. of Medicine, University of Fribourg, Switzerland) [20]. We analysed both single twitch and tetanic contractions.

5.1.1 Single twitch electrical stimulation

To mimic the physiological response of innervated muscles, we measured sarcoplasmic Ca^{2+} transients upon single electrical stimulation of 0.5 Hz that induces a physiological depolarization of the fiber and the release of Ca^{2+} from the SR. As observed also by Schwaller [20], $[Ca^{2+}]_{cyt}$ in resting conditions and upon single electrical pulse did not show any difference in WT and PV KO muscle fibers (Figure 5A and Figure 5B).

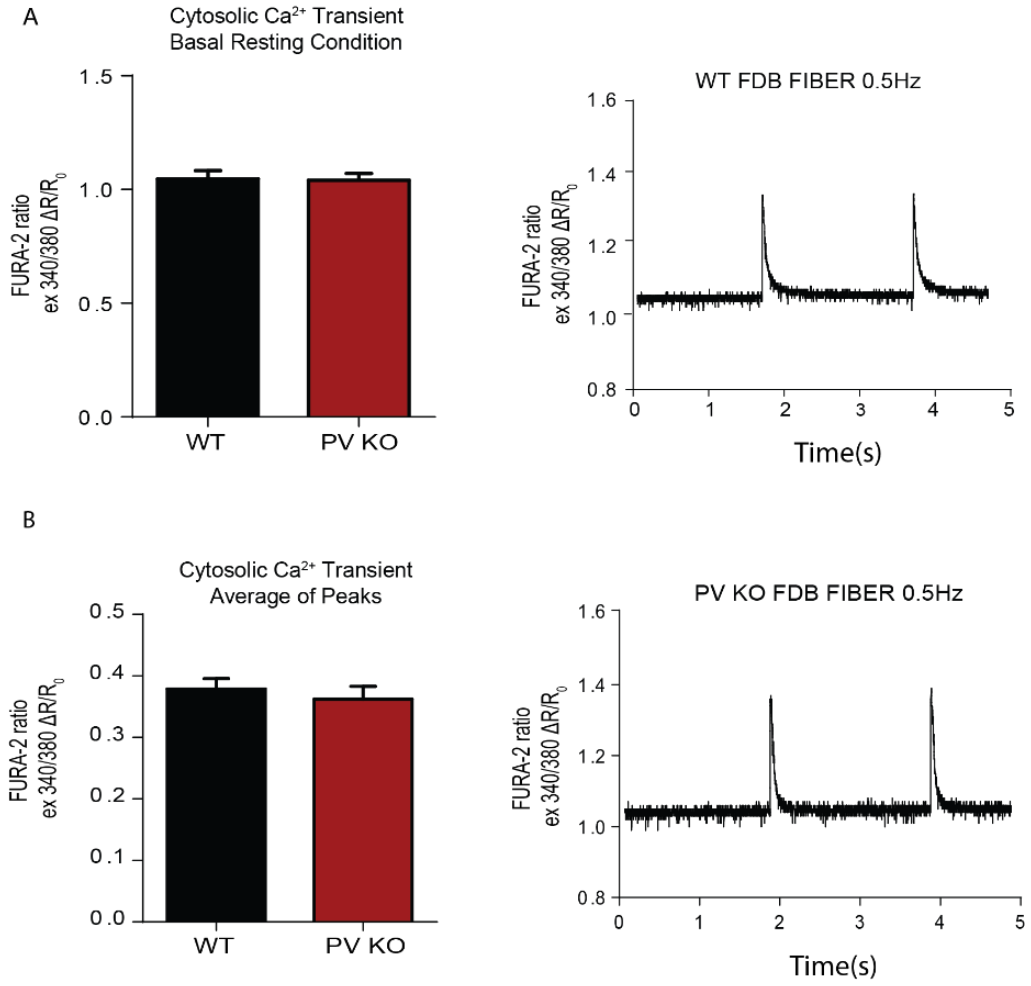

Figure 5. Cytosolic Ca^{2+} transients upon single twitch stimulation in single isolated FDB muscle fibers of WT and PV KO mice.

A) Resting sarcoplasmic Ca^{2+} levels in WT and PV KO single isolated FDB fibers, evaluated through ratiometric imaging (Ex 340/380) using the Ca^{2+}indicator Fura-2 AM dye. In this experiment, images were acquired every 200 milliseconds. The bar diagram (left panel) shows the mean basal resting value ± SD. n ≥ 38. On the right, representative traces of the experiment. For data analysis, parametric Student t tests (two-tailed, unpaired) was used. Three independent experiments were performed
B) Sarcoplasmic Ca^{2+} transient measurements in the same conditions as in (A) in single isolated FDB fibers from WT and KO muscles. Fibers were stimulated with a single electrical pulse of 0.5 Hz for 20 seconds. The bar diagram (left panel) shows the mean peak ± SD. n ≥ 38. On the right, representative trace of the experiment. For data analysis, parametric Student t tests (two-tailed, unpaired) was used. Three independent experiments were performed.

Consistently with the data reported by Schwaller [20], kinetics of Ca^{2+} transients and Ca^{2+} clearance were altered in PV KO animal model. Indeed, consistently with the physiological role of PV in buffering cytosolic Ca^{2+}, the time-to-peak and the half-relaxation time was increased in PV KO fibers compared to the WT (Figure 6A and 6B).

The prolongation of the time required for muscle contraction in PV KO fibers, reflects the maintenance of the muscles active state. Indeed, PV has been described as a dynamic and diffusible Ca^{2+} buffer that facilitates Ca^{2+} diffusion between myofibrils and Ca^{2+} reuptake to the SR through the Ca^{2+}-ATPase of the sarcoplasmic reticulum (SERCA) [20,78,176]. Thus, as previously shown [20], PV-deficient muscles loose a fast mechanism to reduce $[Ca^{2+}]_{cyt}$, remaining in the active state for a longer time.

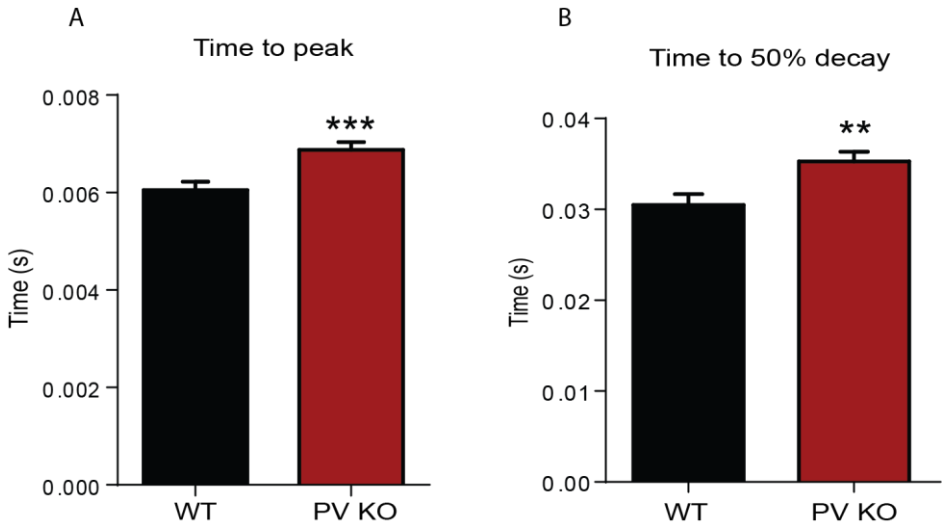

Figure 6. Kinetics of cytosolic Ca^{2+} transients upon single twitch stimulation in single isolated FDB fibers of WT and PV KO mice.

A) Time to reach the peak of the twitch tension after a single 0.5 Hz stimulation of single isolated WT and PV KO fibers. The bar diagram represents the mean ± SD. n ≥ 38. For data analysis, parametric Student t tests (two-tailed, unpaired) was used. *** $p < 0.001$. Three independent experiments were performed.
B) Half-time of the decay of the cytosolic Ca^{2+} transients in single isolated FDB fibers of WT and PV KO fibers stimulated as in (A). The bar diagram represents the mean of the time required to obtain the half-relaxation ± SD. n ≥ 38. For data analysis, parametric Student t tests (two-tailed, unpaired) was used. ** $p < 0.01$. Three independent experiments were performed.

5.1.2 Tetanic electrical stimulation

Next, we investigated cytosolic Ca^{2+} transients during a tetanic contraction. For this purpose, we stimulated single isolated FDB fibers with a 2 seconds stimulation train at 60 Hz that has been shown to induce a partially fused tetanic contraction in isolated FDB mouse fibers [177,178]. Unexpectedly, PV KO fibers were unable to sustain high levels of cytosolic Ca^{2+} during a tetanus as WT fibers (Figures 7A and 7B).

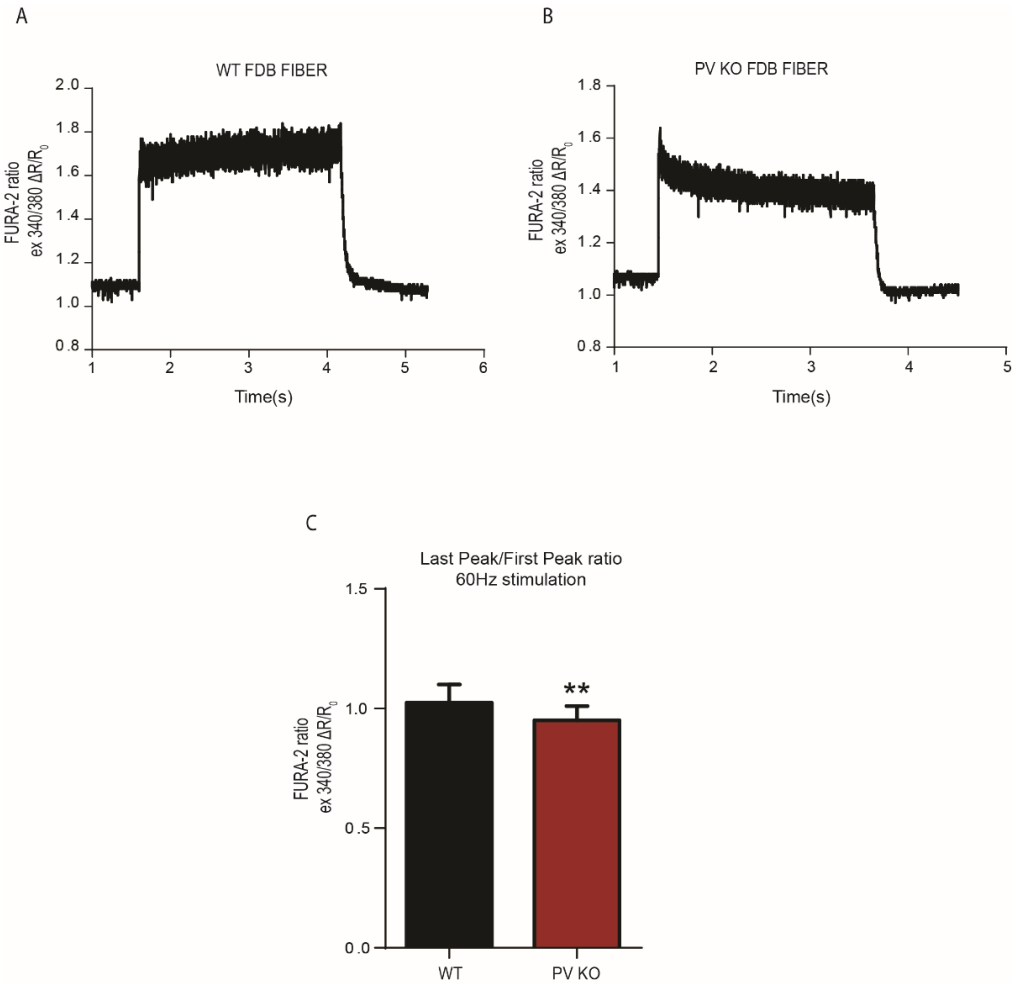

Figure 7. Cytosolic Ca^{2+} transient evoked upon tetanic stimulation on single isolated FDB muscle fibers of WT and PV KO mice.

A) and B) Representative traces of cytosolic Ca^{2+} transients of WT (A) and PV KO (B) measured with the Ca^{2+} indicator Fura-2 AM dye. Tetanic stimulation was induced by means of a 60 Hz train for 2 seconds
C) Ratio of $[Ca^{2+}]_{cyt}$ values reordered after the beginning and before the end of the tetanic stimulus (last peak/first peak) in WT and PV KO single isolated FDB fibers, stimulated as in (A). Cytosolic Ca^{2+} levels evaluated through ratiometric imaging (Ex 340/380) using the Ca^{2+} indicator Fura-2 AM dye. The bar diagram represents the mean ± SD. n ≥ 15. For data analysis, parametric Student t tests (two tailed, unpaired) was used. ** $p < 0.01$. Three independent experiments were performed.

It is known that during a tetanic train of stimuli, a large quantity Ca^{2+} enters the sarcoplasm through repeated releases from the SR, although the amplitude of the subsequent releases progressively decreases [74,179]. In order to sustain tension for more than one second, it is necessary to saturate cytosolic Ca^{2+} binding proteins [70]. Therefore, fibers lacking PV should have revealed an increase of $[Ca^{2+}]_{cyt}$ after the tetanic stimulation, since it represents the main buffer in fast twitch skeletal muscle. Unexpectedly, as shown by the ratio between the cytosolic Ca^{2+} transients measured after the beginning and before the end of the tetanic stimulation in Figure 7C, PV KO muscle fibers present a significant decrease of $[Ca^{2+}]_{cyt}$ upon electrical stimulation, thus failing to maintain a prolonged tetanic tension. We hypothesize that the functional impact of PV ablation on cytosolic Ca^{2+} transient could derive from molecular or functional adaptations.

5.2 Mitochondrial calcium handling in PV KO muscle fibers

Among the intracellular organelles, mitochondria are recognized as crucial regulators of cellular Ca^{2+} homeostasis [1,180]. Indeed, mitochondrial Ca^{2+} has been associated not only with the regulation of energy metabolism through oxidative phosphorylation, but also with the modulation of cytosolic Ca^{2+} signals [4,5]. We thus asked whether the unexpected result on cytosolic Ca^{2+} transients in fibers lacking PV (Figure 7) could be due to adaptation of mitochondria. We analysed mitochondrial calcium uptake on single isolated FDB fibers in response to both electrical stimulation and addition of caffeine. Both treatments are known to induce the release of Ca^{2+} from the SR of fibers *in vitro* [17,179,181,182]. We first analysed mitochondrial Ca^{2+} transients in single isolated FDB fibers stimulated with caffeine (10 mM), that has been shown to induce Ca^{2+} release from the SR in single isolated FDB fibers [17]. The intra-mitochondrial free Ca^{2+} concentration ($[Ca^{2+}]_{mt}$) was analysed both in resting conditions and during contractile activity, using a ratiometric GFP-based Ca^{2+} probe targeted to mitochondria, 4mtGCaMP6f [183]. We transfected adult FDB mouse muscles of PV KO and WT animals with 4mtGCaMP6f plasmid, as previously reported [15], and one week later myofibers were isolated and analysed. No difference were detected in mitochondrial basal concentrations in resting condition (Figure 8A), while mitochondrial Ca^{2+} uptake, during caffeine-induced Ca^{2+} release, was significantly higher in PV KO muscle

fibers compared to control fibers (Figure 8B and 8C), suggesting that in these animals, mitochondria change their properties when the main cytosolic buffer is removed.

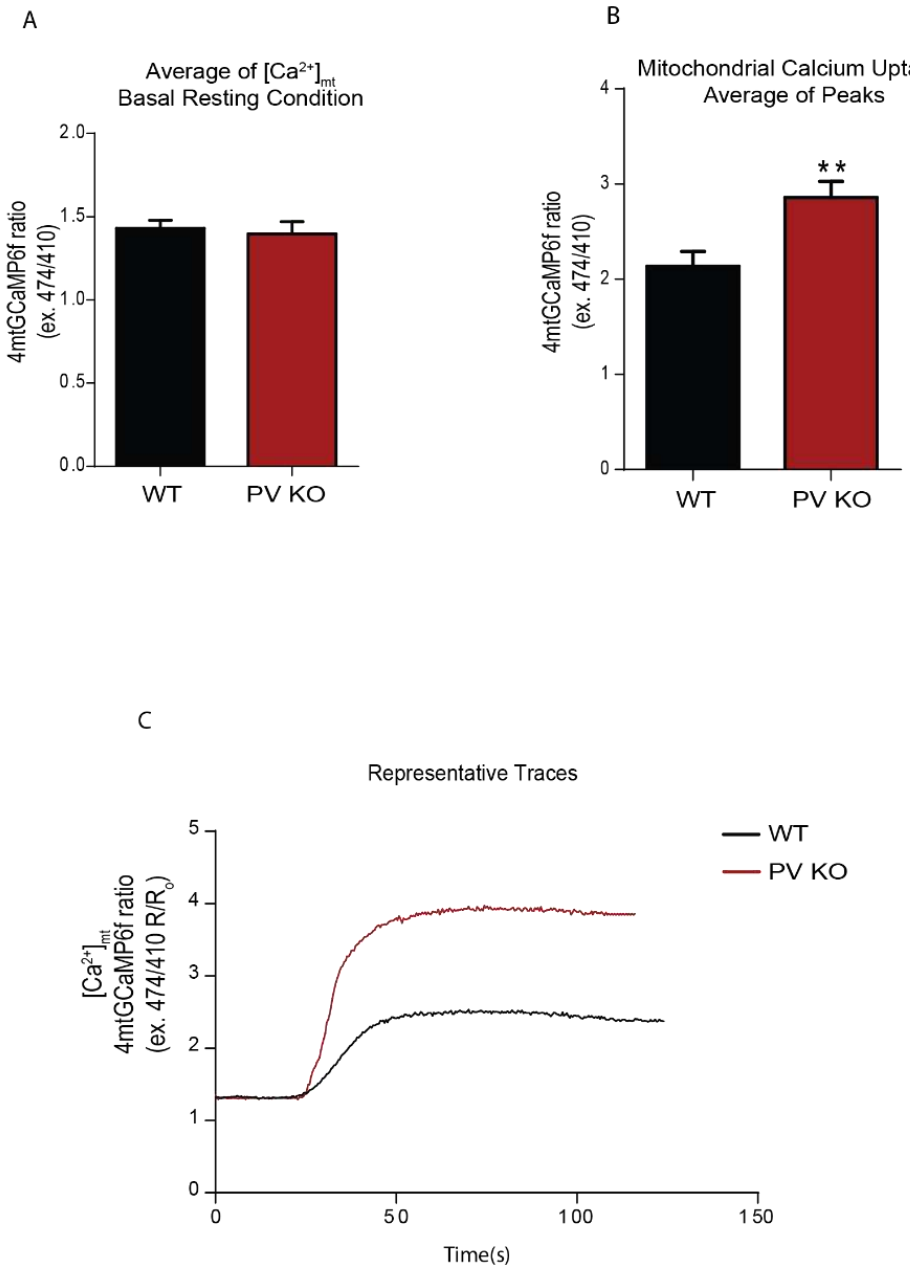

Figure 8. Mitochondrial [Ca^{2+}] in basal resting condition and upon stimulation with caffeine in single isolated FDB fibers of WT and PV KO mice.

FDB muscle fibers of WT and PV KO mice were electroporated with a plasmid encoding 4mtGCaMP6f. Seven days later, single FDB fibers were isolated and cultured. SR Ca^{2+} release was induced with caffeine (10 mM). Three independent experiments were performed.
A) Resting mitochondrial Ca^{2+} levels. The bar diagram represents the mean ± SD. n ≥ 23. For data analysis, parametric Student t tests (two tailed, unpaired) was used
B) Mitochondrial Ca^{2+} concentration during caffeine stimulation. The bar diagram represents the mean ± SD. n ≥ 23. For data analysis, parametric Student t tests (two tailed, unpaired) was used. ** $p < 0.001$.
C) Representative traces of the experiment as in (B).

We then wanted to confirm these data with a more physiological stimulus. For this purpose, fibers from WT and PV KO mice were stimulated by an electrical stimulation of 60 Hz for 2 seconds, in order to mimic a more physiological contraction [177]. No difference was found between WT and PV KO muscle fibers in resting conditions (Figure 9A), while, upon electrical stimulation, a significantly greater increase of $[Ca^{2+}]_{mt}$ in PV KO fibers was detected compared to WT (Figures 9B and 9C).

Since the lack of PV in our KO model does not induce a significant increase of cytosolic Ca^{2+} transient (Figure 5A and 5B) and that it causes a major increase of mitochondrial Ca^{2+} uptake (Figure 8B and Figure 9B) we hypothesized that mitochondria, in this condition, undergo an adaptive response to buffer sarcoplasmic Ca^{2+} increase when PV buffer is removed. Indeed, it is recognized in many cell types, that mitochondria can regulate $[Ca^{2+}]_{cyt}$ by taking up cytosolic Ca^{2+} and store it transiently in the matrix [4,184].

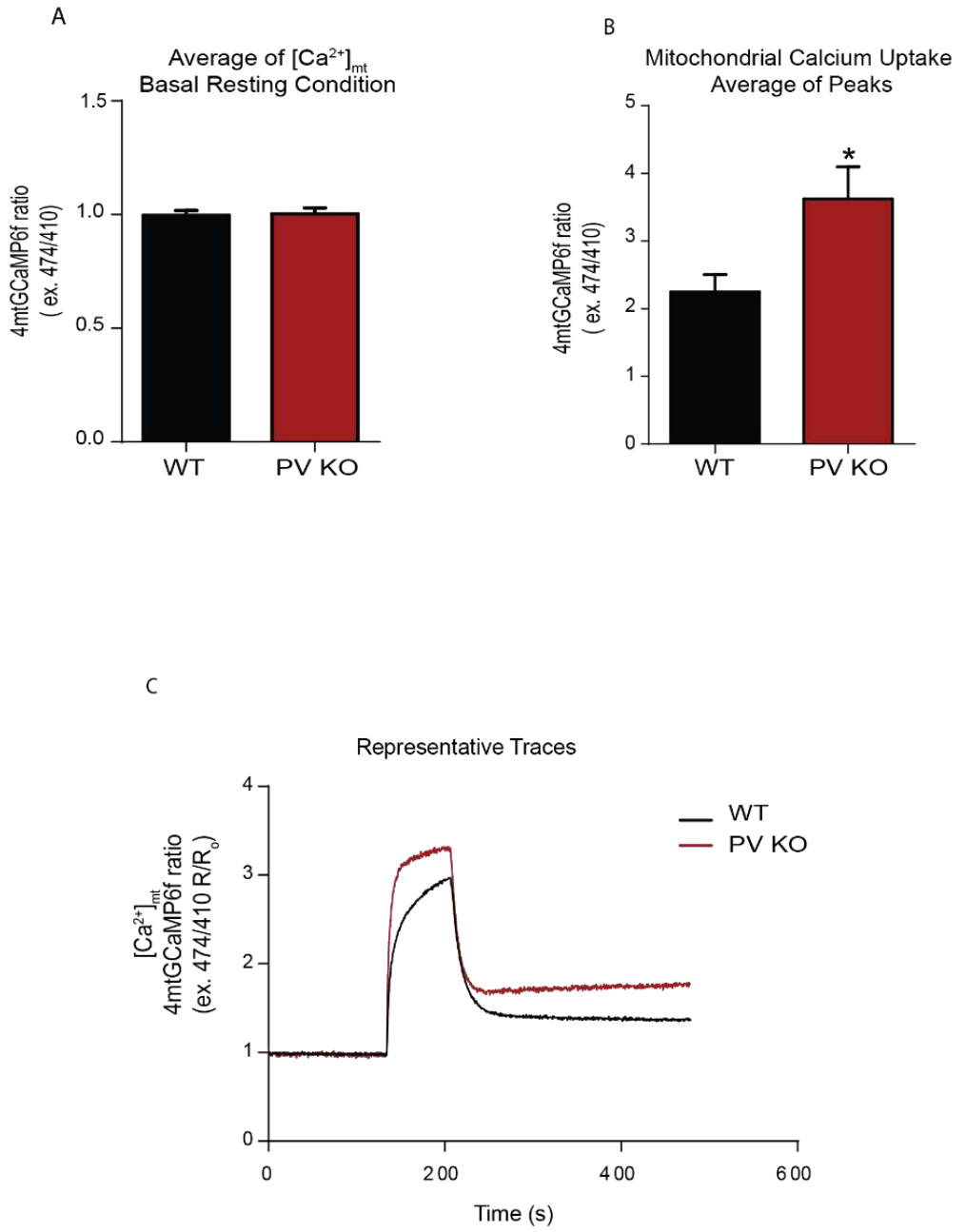

Figure 9. Mitochondrial [Ca^{2+}] in basal resting condition and upon tetanic stimulation on single isolated FDB fibers of WT and PV KO mice.

FDB muscle fibers of WT and PV KO mice were electroporated with a plasmid encoding 4mtGCaMP6f. Seven days later, single FDB fibers were isolated and cultured. Tetanic stimulation was induced by means of a 60 Hz train for 2 seconds. Three independent experiments were performed.
A) Resting mitochondrial Ca^{2+} levels. The bar diagram represents the mean ± SD. n ≥ 17. For data analysis, parametric Student t tests (two tailed, unpaired) was used.
B) Mitochondrial Ca^{2+} concentration during tetanic stimulation. The bar diagram represents the mean ± SD. n ≥ 17. For data analysis, parametric Student t tests (two tailed, unpaired) was used.* $p < 0.05$.
C) Representative traces of the experiment as in (B).

5.3 Effects of the acute modulation of PV expression on cytosolic and mitochondrial calcium transients

To exclude any possible *in vivo* compensatory effects due to PV ablation during development on our knockout model, we performed PV acute silencing and overexpression in adult WT FDB muscle fibers and we monitored cytosolic Ca^{2+} transients and mitochondrial Ca^{2+} uptake.

PV acute silencing in adult FDB of WT mice was achieved by the use of short hairpin RNA targeted to PV and expressing mCherry red fluorescent protein (shPV-mCherry). mCherry protein was helpful to visualize *in vivo* transfected fibers. For the overexpression experiments, PV coding sequence was tagged with a Flag-tag and linked to a self-cleaving P2A peptide to the mCherry fluorescent protein. The 2A self-cleaving peptide (2A), mediating a ribosome-skipping event [185,186], regulates the simultaneous expression and cleavage of multiple gene targets from a single mRNA sequence [185,187]. This method allow the co-expression of our gene of interest, PV, along with the reporter, the fluorescence gene mCherry [188]. Thus, any cells that are positive for the fluorescent protein should also be expressing the gene since they are both derived from the same transcript.

5.3.1 PV silencing

To silence PV, we designed and tested three different plasmids carrying three different shRNA sequences against PV. To test the efficiency of silencing, HeLa cells were co-transfected with the three different shRNA sequences and PV-Flag-P2A-mCherry plasmid, since HeLa cells do not express PV. HeLa cells were harvested 48 hours after transfection and total proteins were extracted and subjected to Western blotting analysis with α-Flag and α-Tubulin antibodies, to detect endogenous PV and to normalize for loading, respectively (Figure 10A and 10B). The plasmid carrying shPV3 was chosen for our subsequent experiments since it provided the best silencing efficiency.

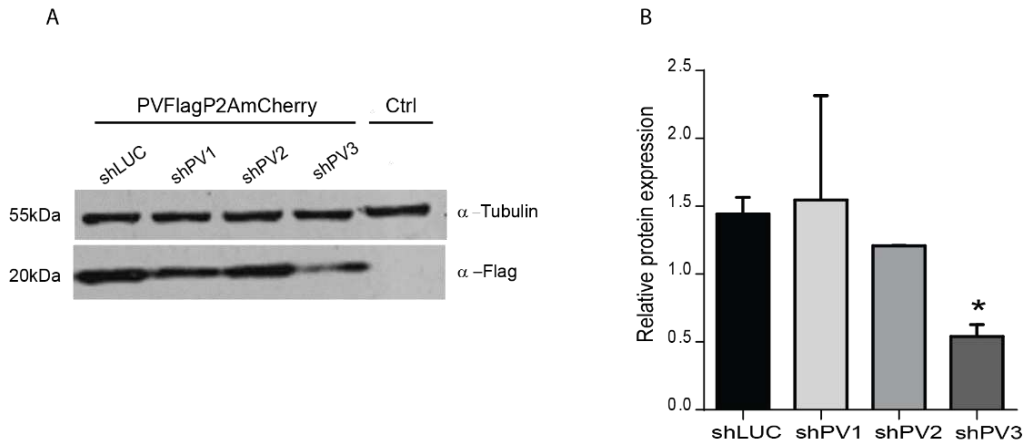

Figure 10. Efficacy of PV silencing in *vitro*

A) HeLa cells were transfected with three different shRNA plasmids (shPV1-3) or non-targeting shRNA (shLUC) together with PV-Flag-P2A-mCherry plasmid. 48 hours after transfection, cells were collected, and protein extracts were subjected to Western blotting with the α-Flag antibody to detect PV and α-Tubulin as loading control. Three independent experiments were performed.
B) Quantification of the level of PV expression obtained as in (A) normalized for the expression of Tubulin. The bar diagram represents the mean ± SD. n =3. For statistical analysis, one way ANOVA with post hoc Dunnett's multiple comparison test was used. * $p < 0.05$

The selected shRNA was then electroporated *in vivo* in FDB muscles of 3 months old WT CD1 mice. Mice were transfected with either non targeting shRNA (shLUC) or shPV and one week or two weeks later FDB muscles were collected and silencing efficiency was tested by RT-qPCR. The data confirmed that also *in vivo* the shRNA against PV can efficiently reduce its mRNA level (Figure 11).

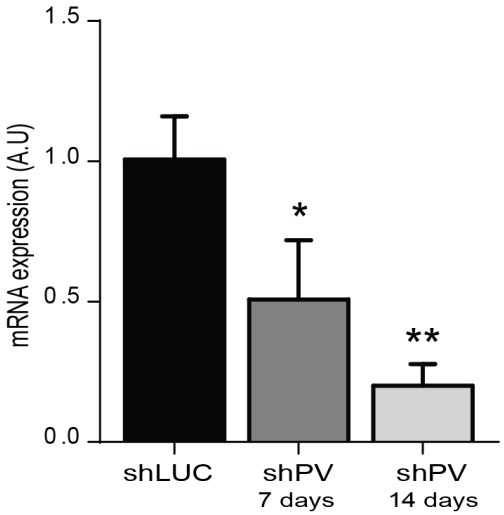

Figure 11. Evaluation of PV silencing efficiency in *vivo* by RT-qPCR.

FDB muscle of six CD1 male mice (3 months old) were electroporated with either shLUC control plasmid or with shPV. Bar diagram represents the expression levels of PV normalized to shLUC and presented as means ± S.D. (n = 3 per condition). Expression levels were normalized for POL2. For statistical analysis, one way ANOVA with post hoc Dunnett's multiple comparisons test was performed. * $p < 0.05$.

5.3.2 Cytosolic calcium levels in PV silenced muscle fibers

We first determined free $[Ca^{2+}]_{cyt}$ with the fluorescent indicator Fura-2 AM dye in fibers where PV was acutely silenced. No significant difference were observed in $[Ca^{2+}]_{cyt}$ between shLUC control fibers and in PV silenced fibers (shPV), both in basal resting condition and upon caffeine stimulation (Figure 12A and 12B).

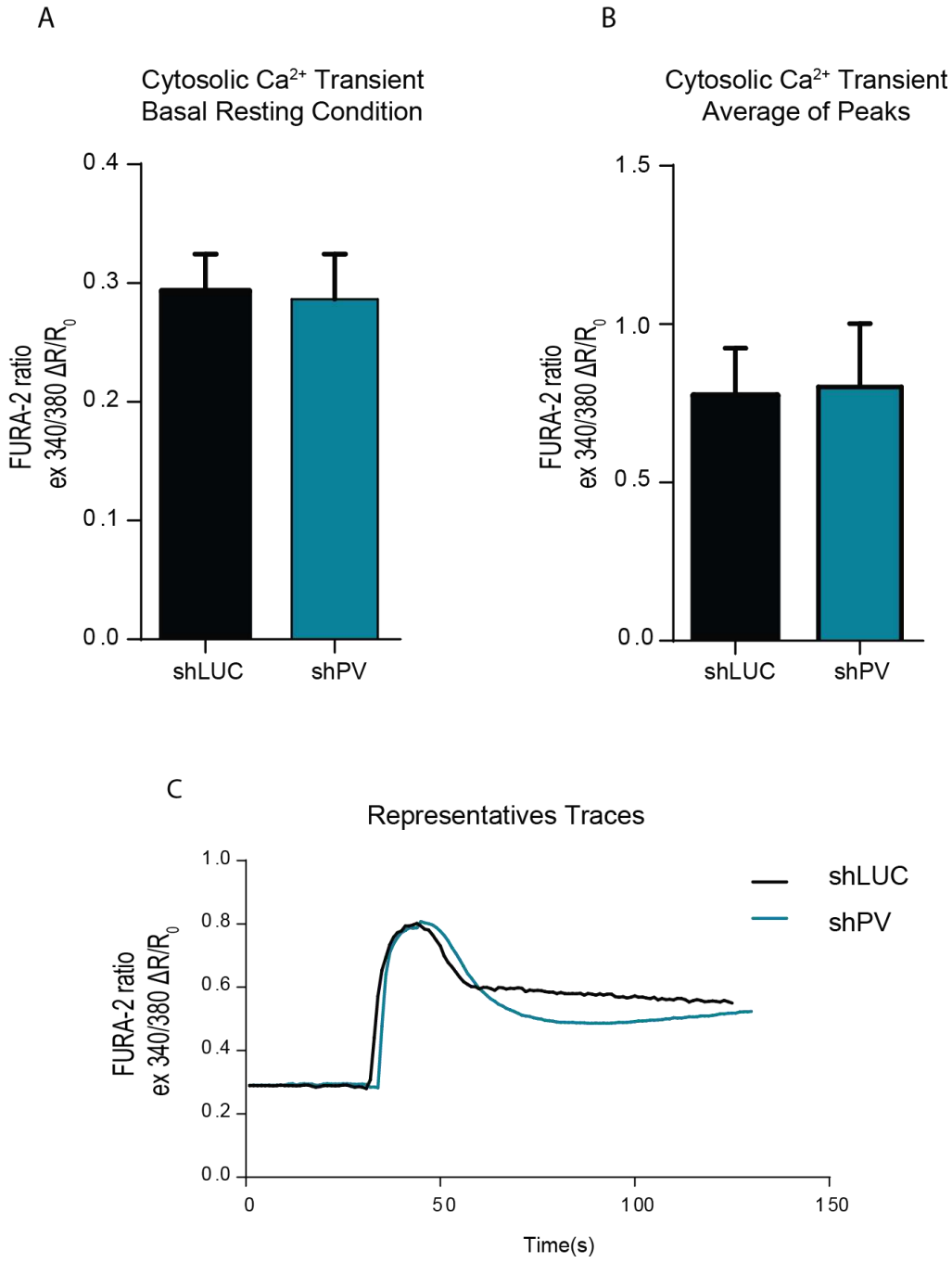

Figure 12. Cytosolic calcium levels in PV silenced single isolated FDB myofibers.

FDB muscle fibers of 2-3 months old CD1 male mice (n = 6) were electroporated with either shLUC or shPV. Seven days later, single FDB fibers were isolated and cultured. For cytosolic Ca^{2+} measurements fibers were loaded with Fura-2 AM dye.
A) Resting cytosolic Ca^{2+} levels evaluated through ratiometric imaging (Ex 340/380) using the Ca^{2+} indicator Fura-2 AM dye. The bar diagram represents the mean ± SD. n ≥ 43. For data analysis, parametric Student t tests (two tailed, unpaired) was used.
B) Cytosolic Ca^{2+} concentration during stimulation evoked by caffeine treatment (10 mM). Cytosolic Ca^{2+} transient was measured in the same conditions as in (A). The bar diagram represents the mean ± SD. n ≥ 43. For data analysis, parametric Student t tests (two tailed, unpaired) was used.
C) Representative traces of the experiment as in (B).

5.3.3 Mitochondrial calcium uptake in PV silenced muscle fibers

Our results demonstrated that PV ablation induces a significant increase of mitochondrial Ca^{2+} uptake in PV KO myofibers (Figure 8 and Figure9) suggesting that, in this specific condition, mitochondria could adapt to compensate for the lack of PV by increasing their buffering capacity. Therefore, we asked whether, similarly to what observed in PV KO fibers, also the acute silencing of PV could induce the same response mechanism in mitochondria. To verify this hypothesis, we decided to analyse mitochondrial Ca^{2+} uptake in PV silenced muscle fibers by co-transfecting FDB myofibers of adult WT CD1 mice with the shPV plasmid together with the Ca^{2+} probe targeted to mitochondria, 4mtGCaMP6f. *Ex vivo* imaging experiments showed that, while the basal $[Ca^{2+}]_{mt}$ is not affected by the removal of PV (Figure 13A) a marked increase of caffeine-induced transients, was detected in shPV-transfected fibers (Figure 13B and 13C). This data confirm what observed in our PV KO model (Figure 8 and Figure 9).

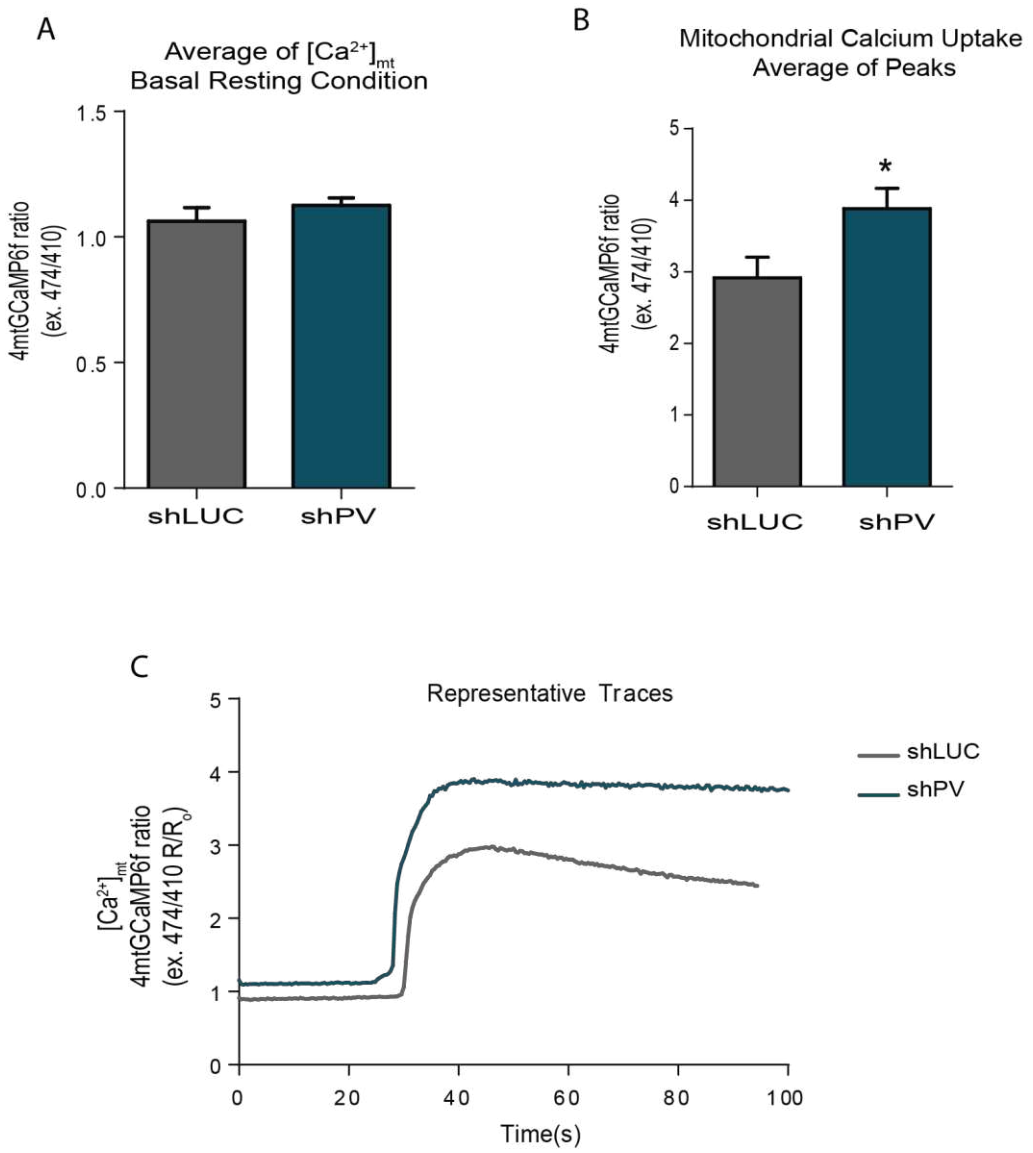

Figure 13. Mitochondrial [Ca^{2+}] in basal resting condition and upon caffeine stimulation on single isolated FDB fibers silencing PV.

FDB muscle fibers of 3 months old CD1 male mice (n = 3) were electroporated with a plasmid encoding for 4mtGCaMP6f together with either shLUC or shPV. Seven days later, single FDB fibers were isolated and cultured.

A) Resting mitochondrial Ca^{2+} levels. The bar diagram represents the mean ± SD. n ≥ 18. For data analysis, parametric Student t tests (two tailed, unpaired) was used

B) Mitochondrial Ca^{2+} uptake was stimulated by caffeine treatment (10 mM). The bar diagram represents the mean ± SD. n ≥ 18. For data analysis, parametric Student t tests (two tailed, unpaired) was used. * $p < 0.05$.

C) Representative traces of the experiment as in (B).

5.3.4 Cytosolic calcium levels in PV silenced muscle fibers treated with CCCP

The data obtained on mitochondrial [Ca^{2+}] on PV silenced fibers, confirmed the potential role of mitochondria as responsible buffer of cytosolic [Ca^{2+}] increases. We hypothesised that, during fiber stimulation, mitochondria could compensate for the lack of the main cytosolic Ca^{2+} buffer, by increasing their buffering capacity to prevent and restrict the spreading of cytosolic Ca^{2+} signals in skeletal muscle fibers. This hypothesis could explain the lack of changes in cytosolic [Ca^{2+}] in PV silenced fibers (Figure 12).

To verify this hypothesis, concomitantly with cytosolic Ca^{2+} measurements, we treated the fibers with the ionophore carbonilcyanide m-chlorophenylhydrazone (CCCP) and we measured $[Ca^{2+}]_{cyt}$. CCCP abolishes mitochondrial Ca^{2+} uptake by dissipating the electrochemical potential across the IMM, which provides the driving force for Ca^{2+} import [24,86]. Therefore, addition of CCCP (10 μM) during caffeine stimulation promptly prevents mitochondrial Ca^{2+} accumulation. In this experimental condition, FDB muscle fibers transfected with shPV and treated with CCCP, showed increased $[Ca^{2+}]_{cyt}$ compared to control fibers, re-enforcing the hypothesis that mitochondria of fibers lacking PV both constitutively and transiently, adapt to buffer cytosolic Ca^{2+} transient (Figure 14B and 14C).

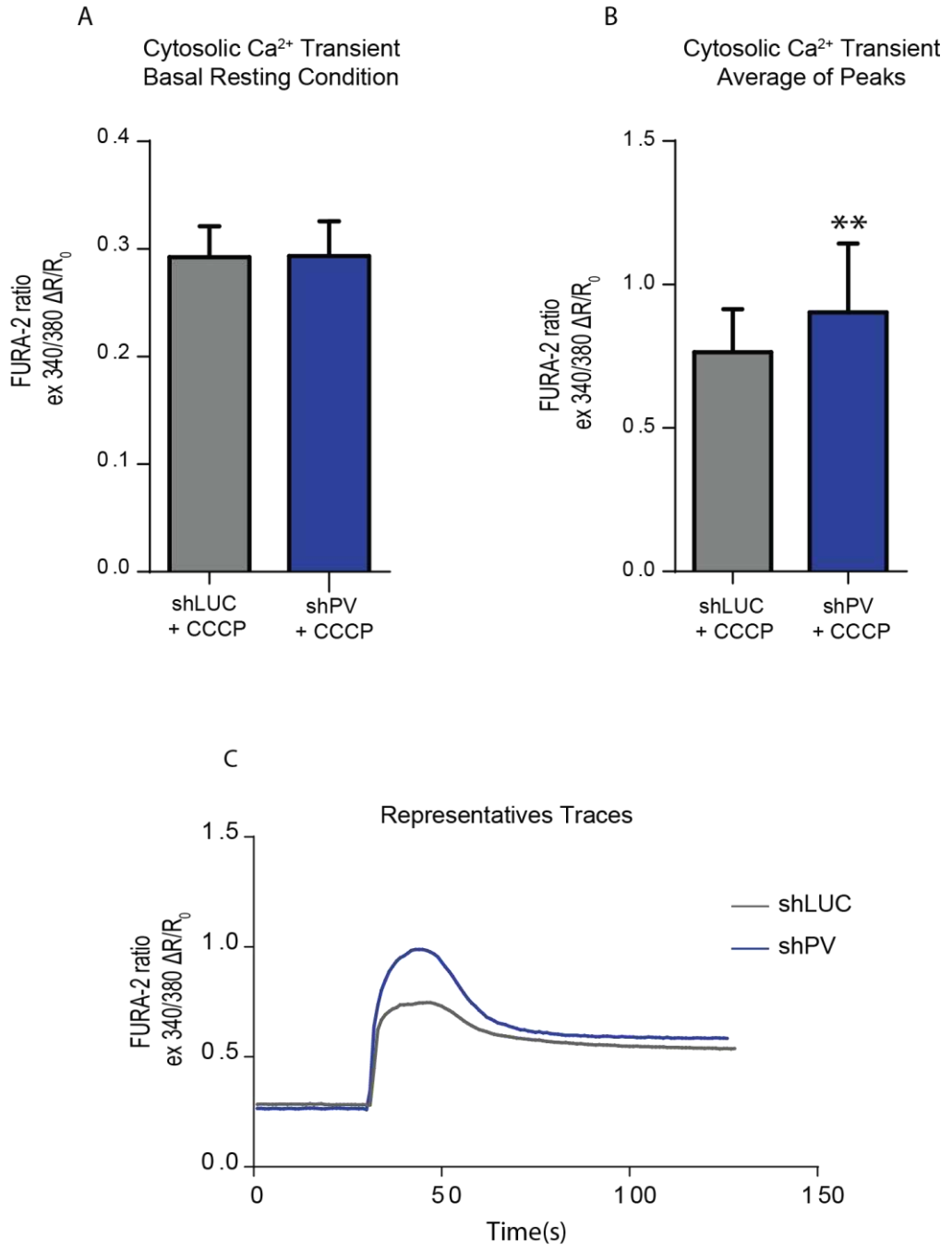

Figure 14. Cytosolic Ca^{2+} transients in PV silenced single isolated FDB myofibers in basal resting condition and upon stimulation with caffeine and CCCP.

FDB muscle fibers of 2-3 months old CD1 male mice (n = 6) were electroporated with either shLUC or shPV. Seven days later, single FDB fibers were isolated and cultured. For cytosolic Ca^{2+} measurements fibers were loaded with Fura-2 AM dye.
A) Resting cytosolic Ca^{2+} levels evaluated through ratiometric imaging (Ex 340/380) using the Ca^{2+} indicator Fura-2 dye. The bar diagram represents the mean ± SD. n ≥ 29. For data analysis, parametric Student t tests (two tailed, unpaired) was used.
B) Cytosolic Ca^{2+} concentration during stimulation evoked by caffeine (10 mM) and CCCP (10 µM) treatment. Cytosolic Ca^{2+} transient was measured as in (A). The bar diagram represents the mean ± SD. n ≥ 29. For data analysis, parametric Student t tests (two tailed, unpaired) was used ** $p < 0.001$.
C) Representative traces of the experiment as in (B).

5.3.5 Mitochondrial calcium uptake in PV overexpressing muscle fibers

We then analysed the effects of PV acute overexpression on mitochondrial Ca^{2+} uptake. FDB mouse muscles of adult 2-3 months old WT CD1 mice were electroporated with 4mtGCaMP6f probe in combination with a plasmid encoding mCherry (Ctrl, empty vector) or mCherry linked to PV sequence (PV-P2A-mCherry). One week later, we analysed $[Ca^{2+}]_{mt}$ by real time imaging experiments in the transfected (red) single isolated fibers stimulated with caffeine. The results obtained are coherent with those performed in the KO model and in the PV silencing fibers. Indeed, PV overexpression has a profound effect on mitochondrial Ca^{2+} handling, causing a significant decrease of mitochondrial calcium uptake after caffeine stimulation without affecting resting $[Ca^{2+}]_{mt}$ (Figure 15A and 15B).

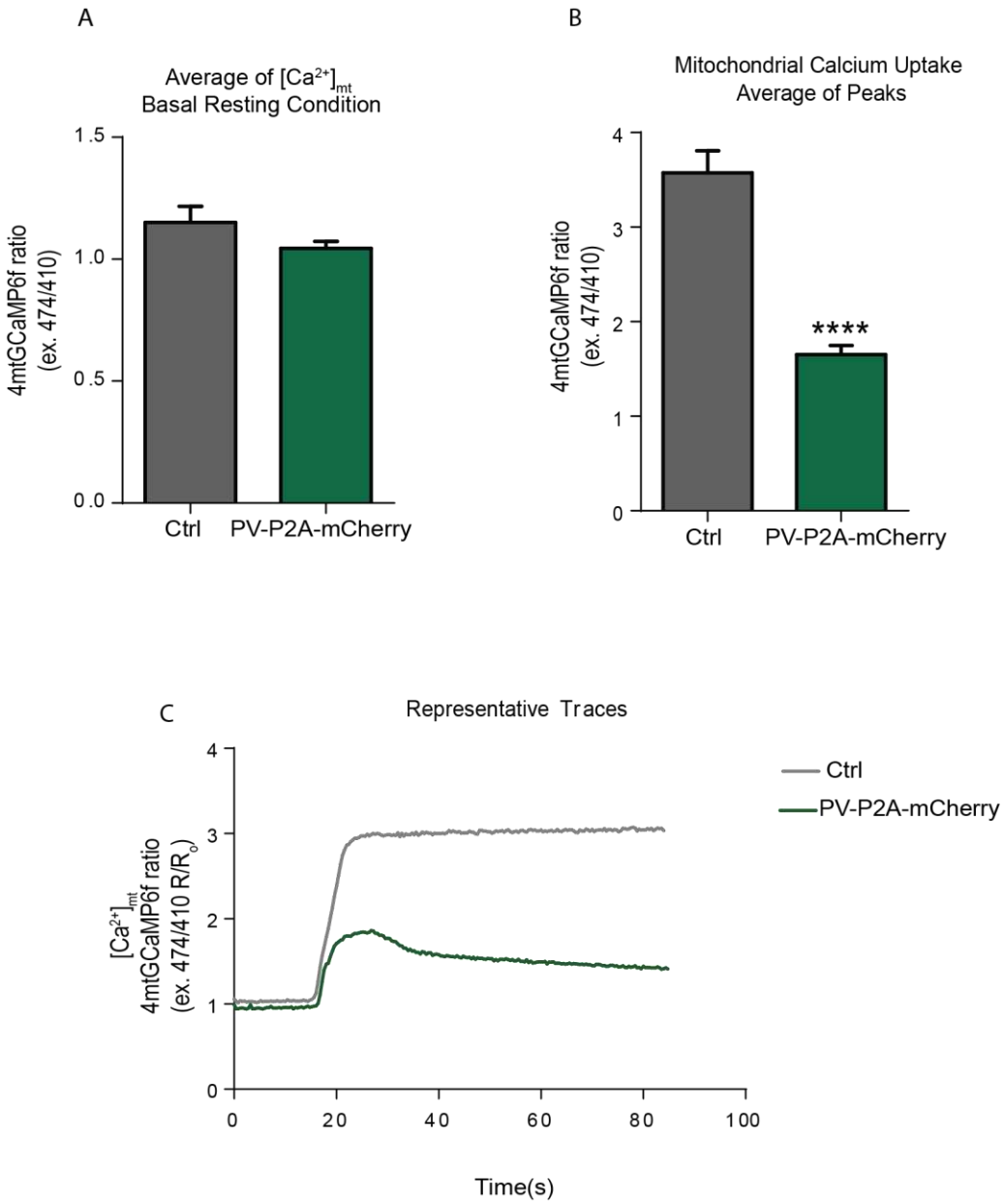

Figure 15. Mitochondrial [Ca^{2+}] in basal resting condition and upon caffein stimulation on single isolated FDB fibers overexpressing PV.

FDB muscle fibers of 2-3 months old CD1 male mice (n = 4) were electroporated with a plasmid encoding for 4mtGCaMP6f together with a plasmid encoding mCherry (Ctrl) or mCherry- linked to PV (PV-P2A-mCherry). Seven days later, FDB muscle fibers were isolated and cultured. Four independent experiments were performed.

A) Resting mitochondrial Ca^{2+} levels. The bar diagram represents the mean ± SD. n ≥ 21 fibers. For data analysis, parametric Student t tests (two tailed, unpaired) was used.

B) Mitochondrial Ca^{2+} uptake was stimulated by caffeine (10 mM). Bar diagram represents the mean of values recorded ± SD, n ≥ 21. For data analysis, parametric Student t tests (two tailed, unpaired) was used. *** $p < 0.0001$.

C) Representative traces of the experiment as in (B).

5.3.6 Cytosolic calcium levels in PV overexpressing muscle fibers

Cytosolic Ca^{2+} transient on WT FDB fibers overepressing PV exhibited a significant decrease of $[Ca^{2+}]_{cyt}$ both in basal condition (Figure 16A) and upon caffeine stimulation (Figure 16B), suggesting that the overexpressed PV is able to buffer the endogenous free $[Ca^{2+}]_{cyt}$ (Figure 16A) and Ca^{2+} released from SR following caffeine stimulation (Figure 16B). Our hypothesis is that, the overexpressed PV is able to promptly buffer much of the Ca^{2+} released from the SR, thus affecting cytosolic $[Ca^{2+}]$ transients and also mitochondrial Ca^{2+} uptake (Figure 15B).

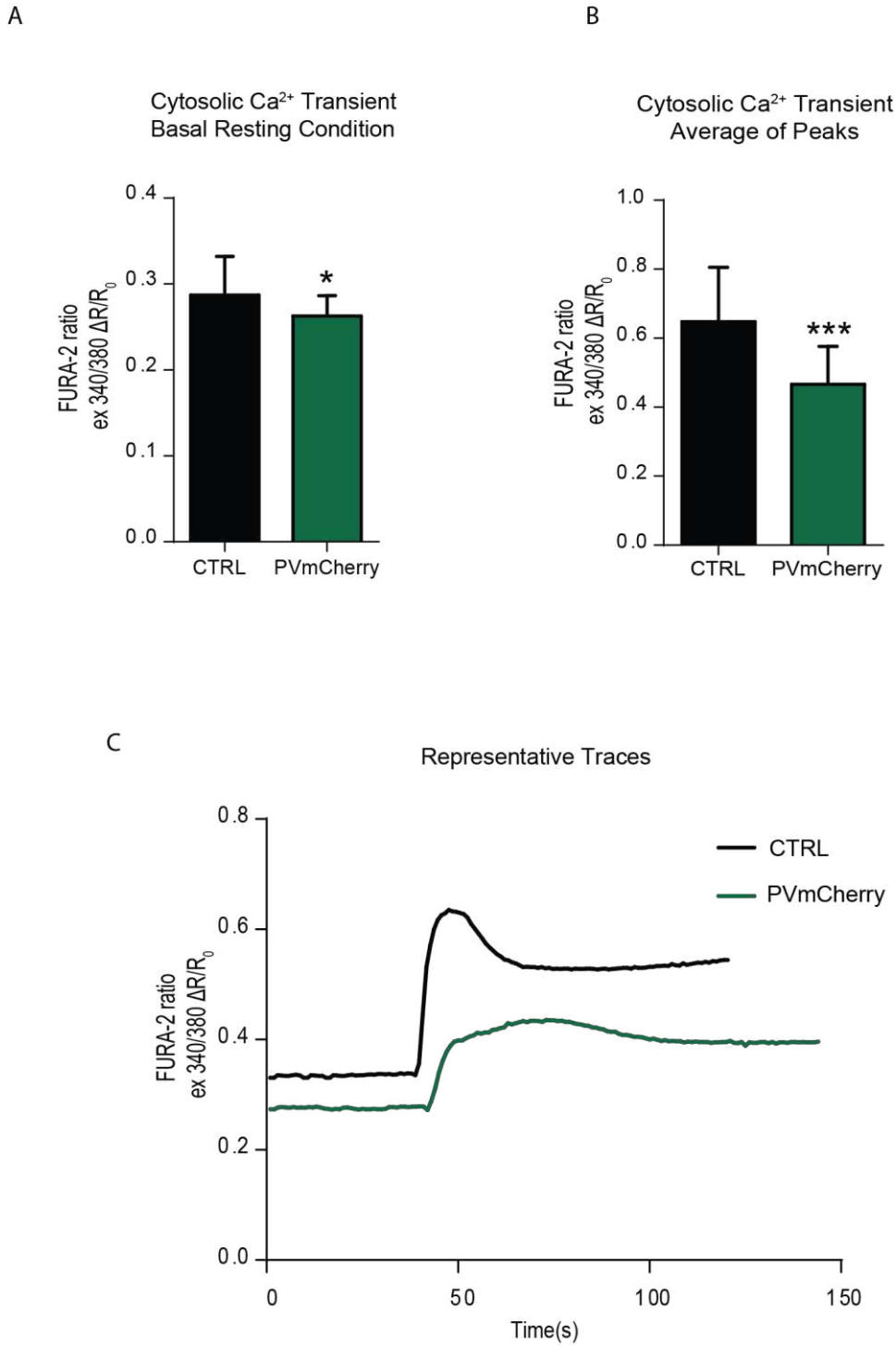

Figure 16. Cytosolic [Ca^{2+}] in basal resting condition and upon caffein stimulation on single isolated FDB fibers overexpressing PV.

FDB muscle fibers of 2-3 months old CD1 male mice (n = 4) were electroporated with a plasmid encoding either mCherry (Ctrl) or PV-P2A-mCherry plasmid. Seven days after the electroporation FDB muscle were isolated and cultured. For cytosolic Ca^{2+} measurements fibers were loaded with Fura-2 AM dye. Four independent experiments were performed.

A) Resting sarcoplasmic Ca^{2+} levels in WT and PV KO single isolated FDB muscle fibers. $[Ca^{2+}]_{cyt}$ was evaluated through ratiometric imaging (Ex 340/380) using the Ca^{2+} indicator Fura-2 AM dye. The bar diagram shows the mean basal resting value ± SD, n ≥ 28. For data analysis, parametric two-tailed unpaired Student t tests was used. * $p < 0.05$.

B) FDB fibers were stimulated with caffeine treatment (10 mM) and sarcoplasmic Ca^{2+} transient was measured in the same conditions as in (A). The bar diagram shows the mean peak ± SD, n ≥ 28. For statistical analysis non-parametric Student t-test (two-tailed, unpaired) was performed. *** $p < 0.0001$.

C) Representative traces of the experiment as in (B).

5.4 SR Ca^{2+} homeostasis and SR Ca^{2+} handling protein analysis in PV KO animal model

To fully understand Ca^{2+} homeostasis in skeletal muscle fibers of PV KO animals during contraction, Ca^{2+} transients have been investigated also in the SR, the main Ca^{2+} store in skeletal muscle, that might, similarly to mitochondria, adapt to the lack of PV. For this purpose, we investigated the effects of PV ablation on SR using a recently developed genetically targeted FRET-based fluorescent probe (D4ER), characterized by lower Ca^{2+} affinity, suitable for the measurement of the levels of $[Ca^{2+}]$ in the ER lumen and characterized by a high dynamic range for monitoring Ca^{2+} variations within the ER ($[Ca^{2+}]_{SR}$) [189,190]. This probe was electroporated in FDB muscles of PV KO and WT mice and 7 days later fibers were enzymatically dissociated. $[Ca^{2+}]_{SR}$ was measured at resting conditions and during a 2 seconds train of tetanic stimulation at 60 Hz. $[Ca^{2+}]_{SR}$ was evaluated from the single excitation dual emission (YFP/CFP) intensity ratio after correction for background fluorescence and SR Ca^{2+} depletion was measured by the change in the YFP/CFP ratio after the 2 seconds of 60 Hz stimulation. Whereas SR free $[Ca^{2+}]$ measured during resting condition was indistinguishable in fibers lacking PV from the WT value (Figure 17A), the ablation of PV resulted in changes in intraluminal Ca^{2+} during electrical stimulation (Figure 17B and 17C). In detail, during electrical stimulation, WT fibers showed minor changes in $[Ca^{2+}]_{SR}$, whereas in PV KO fibers, a large drop in $[Ca^{2+}]_{SR}$ was measured (Figure 17C). The overall reduction in $[Ca^{2+}]_{SR}$ during the train of stimuli was quantified by the drop of the YFP/CFP ratio after the train of stimuli and expressed as a percentage of Ca^{2+} depletion in comparison to the basal $[Ca^{2+}]_{SR}$ (Figure 16B). We concluded that SR of PV KO muscle fibers therefore, release more Ca^{2+} than that of WT myofibers.

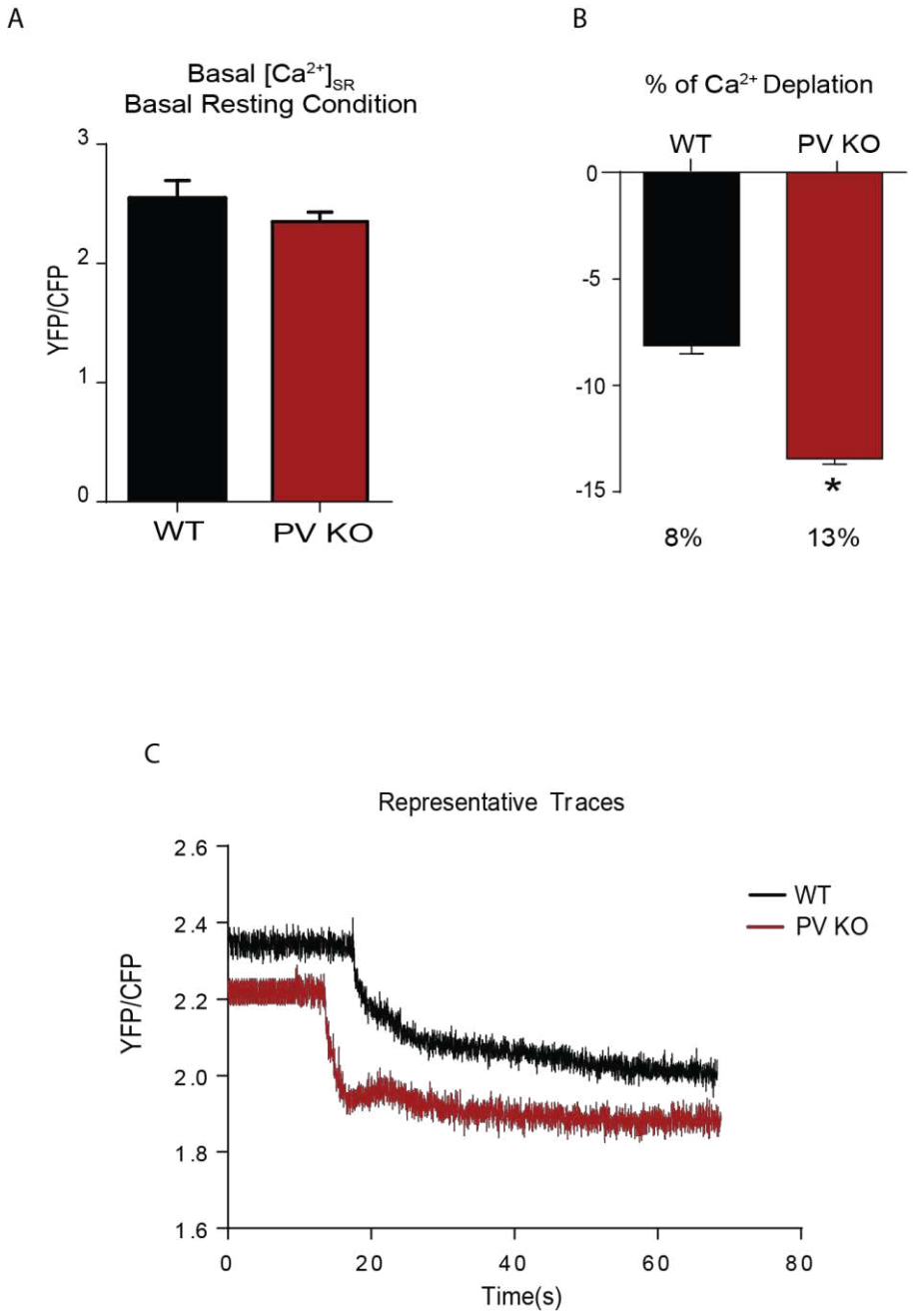

Figure 17. SR [Ca^{2+}] in basal resting condition and upon tetanic stimulation on FDB fibers of WT and PV KO mice.

FRET-based fluorescent probe (D4ER) was electroporated in FDB muscle of 3 months old PV KO and WT mice Seven days later, single FDB fibers were isolated and cultured. Tetanic stimulation was induced by means of a 60Hz train for 2 seconds. SR free calcium concentrations were calculated from the single excitation, dual emission (YFP/CFP) intensity ratio after correction for background fluorescence. Three independent experiments were performed.
A) Resting SR Ca^{2+} levels of WT and PV KO fibers. The bar diagram shows the mean basal resting value ± SD, n ≥ 15. For statistical analysis non-parametric Student t-test (two-tailed, unpaired) was performed.
B) SR Ca^{2+} depletion 2 seconds after the tetanic stimulation. The bar diagram shows the percentage of SR Ca^{2+} depletion ± SD, n ≥ 15. For statistical analysis non-parametric Student t-test (two-tailed, unpaired) was performed. * $p < 0.05$.
C) Representative traces of SR Ca^{2+} dynamics as in (B).

Since we found this difference in SR Ca^{2+} release, we asked whether the proteins involved in SR Ca^{2+} homeostasis and SR Ca^{2+} buffer could be altered by the absence of PV. Therefore, RT-qPCR was performed to detect putative changes on the mRNA levels of RyR1 channel, the main Ca^{2+} releasing channel in muscle [44], and of skeletal muscle SERCA in TA muscles of WT and PV KO mice. Regarding SERCA, two isoforms of Ca^{2+}-ATPase are encoded by two distinct genes in skeletal muscle [191,192]. The products of these genes, SERCA1a and SERCA2a, are found in fast- and slow-twitch adult skeletal muscles, respectively [45]. In addition, we checked the expression levels for STIM1 (stromal interaction molecule 1) and ORAI1 (calcium release-activated calcium channel protein 1) gene expression. These two proteins are responsible of store-operated Ca^{2+} (SOCE) [193], STIM1 is an ER Ca^{2+} sensor [194], that activates Ca^{2+}-selective ORAI1 channels in the plasma membrane [195]. In addition, in our RT-qPCR analysis, we included the expression level of the main SR Ca^{2+} buffers Calsequestrin (CLSQ1) and Calreticulin (CLRT) [40,41], in order to verify whether the lack of PV could induce an adaptation on other Ca^{2+} buffers. For all the genes analysed, no significant difference was detected between WT and PV KO (Figure 18A) demonstrating that SR proteins involved in Ca^{2+} homeostasis are not directly affected by the lack of PV. We also performed WB analysis of CLSQ1, RyR and IP3R receptors (Figures 18B, 18D and 18F). No significant difference in protein levels were detected between WT and KO animals (Figure 18C, 18E and 18G), further confirming that the expression of proteins involved in Ca^{2+} homeostasis in the SR are not affected by PV deficiency.

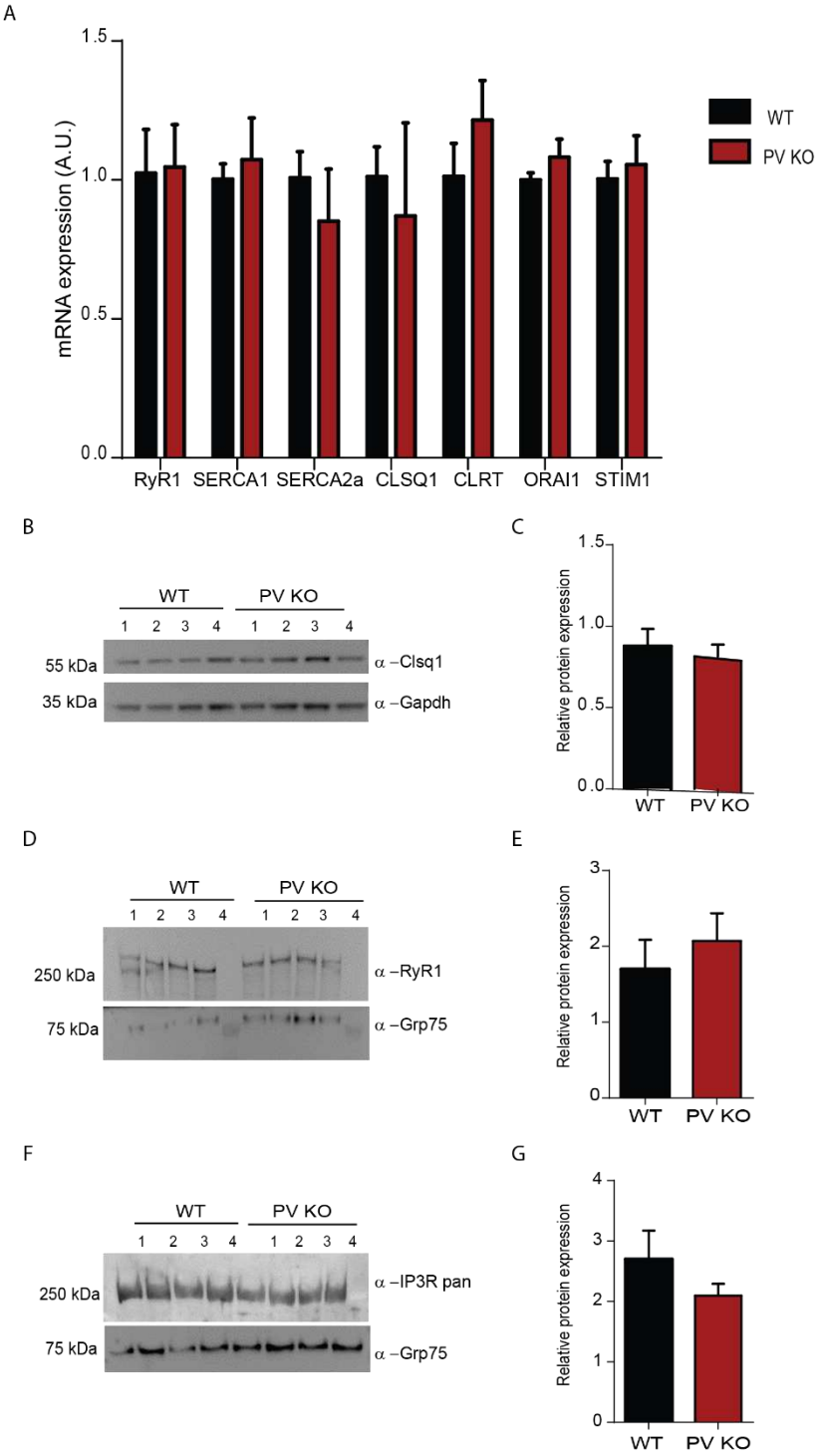

Figure 18. Proteins involved in SR Ca^{2+} homeostasis are not affected by the lack of PV.

A) Relative expression levels of the indicated genes in TA muscles of 3 months old WT and PV KO mice, normalized to GAPDH and presented as mean ± SD, (n = 4 mice per genotype). For statistical analysis, parametric Student t test (two-tailed, unpaired) was performed.
B), **D)** and **F)** Representative western blot of WT and PV KO TA muscles (n = 4) in the same conditions as in (A) and blotted with α-Calsequestrin1 (B), α-RyR1 (D) and α-IP3R (F) antibodies. Where indicated, α-Gadph and α-Grp75 were used as loading controls.
C) Quantification of the level of Calsq expression obtained as in (B) normalized for the expression of Gadph. The bar diagram represents the mean ± SD. n = 4.
E) Quantification of the level of RyR1 expression obtained as in (D) normalized for the expression of Grp75. The bar diagram represents the mean ± SD. n = 4.
G) Quantification of the level of IP3R expression obtained as in (F) normalized for the expression of Grp75. The bar diagram represents the mean ± SD. n = 4. For statistical analysis non-parametric Student t-test (two-tailed, unpaired) was performed.

5.5 PV ablation affects the expression of the mitochondrial calcium uniporter complex components

As already mentioned, PV in skeletal muscle is a key player in intracellular Ca^{2+}-buffering and has profound effect on the spatiotemporal kinetics of cytosolic Ca^{2+} transients [20,176,196]. Similarly, mitochondria, in many cell types, have been described as high capacity organelles that can sequester and store large amount of Ca^{2+} contributing to the cellular Ca^{2+} homeostasis [4,197]. Ca^{2+} entry in mitochondria occurs through a sophisticated channel called mitochondrial calcium uniporter (MCU) complex [4].

In PV KO mice, lack of PV causes an increase in mitochondrial Ca^{2+} uptake, suggesting that mitochondria are likely involved to prevent and restricts the increase of $[Ca^{2+}]_{cyt}$ due to PV ablation. Thus, in skeletal muscles of PV KO model, mitochondria exert the role of cytosolic Ca^{2+} buffering. One hypothesis that could explain the increase of mitochondrial Ca^{2+} uptake is the increase in the expression levels of the components of the MCU complex in PV KO muscles. To verify this hypothesis, we performed RT-qPCR to analyse the mRNA expression of the MCU complex components in WT and PV KO TA muscles

In PV KO TA muscles, the pore forming subunit MCU and the regulatory subunits MICU1, MICU1.1 and MICU2 were significantly upregulated compared to WT (Figure 19). This data can explain the increase in mitochondrial Ca^{2+} uptake in this animal model.

In addition, between PV KO and WT, no statistical difference was detected in the expression of mitochondrial markers as COX IV and TOM 20 (Figure 19), suggesting a precise transcriptional program, induced by the lack of PV, and leading to the increase in mitochondrial Ca^{2+} carrying capacity.

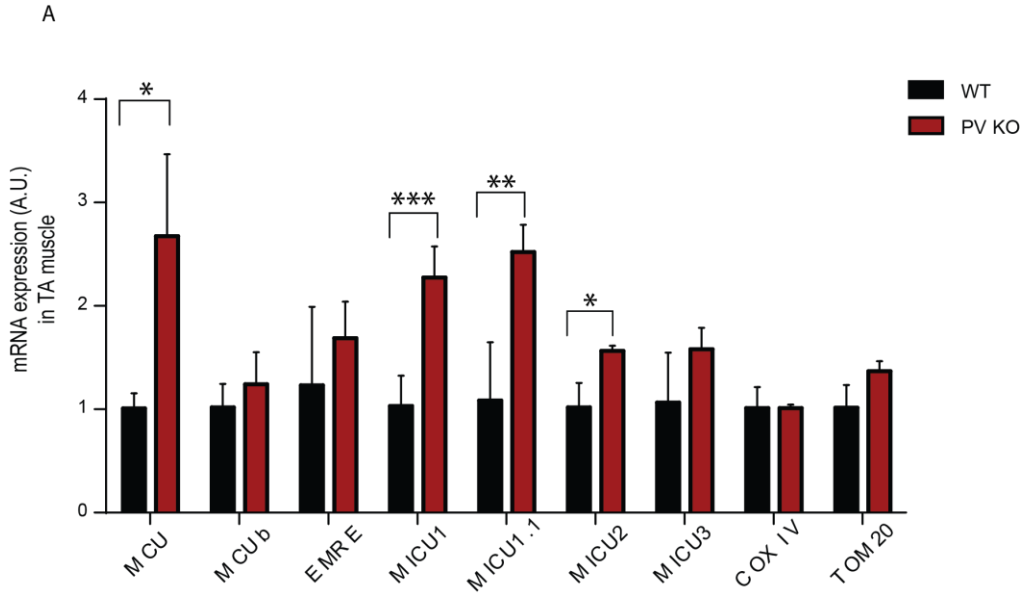

Figure 19. Lack of PV induces the expression of genes coding for the MCU complex.

TA muscles of 3 months old WT and PV KO mice were harvested and frozen in liquid nitrogen-cooled isopentane. Total mRNA was extracted and subjected to RT-qPCR. The expression of genes coding for MCU complex components was assessed and normalized to POL2. The bar diagram represents the genes expression levels normalized to WT and presented as means ± SD. n = 3 muscles per group. For statistical analysis, parametric Student t test (two-tailed, unpaired) was performed. * $p < 0.05$, ** $p < 0.01$, *** $p \leq 0.001$.

5.6 Parvalbumin ablation alters mitochondrial morphology and number

The data obtained so far picture a complex crosstalk between PV expression levels and mitochondrial function.

Since we observed that PV ablation induces a significant increase of mitochondrial Ca^{2+} uptake and of the expression of the MCU complex components, we asked whether the lack of PV could affect also the morphology of mitochondria in skeletal muscle. Thus, Prof. Feliciano Protasi and Dr. Simona Boncompagni performed mitochondrial distribution and morphology analysis on transversal and longitudinal sections of *extensor digitorum longus* (EDL) muscles of WT and PV KO mice, by transmission electron microscopy (TEM).

Quantification of TEM images revealed a strong alteration of mitochondrial ultrastructure in PV KO muscles, indicating that the lack of PV strongly affects mitochondrial morphology and redistribution. In detail, in longitudinal sections of WT EDL fibers (Figure 20A), mitochondria are mostly round-shaped and almost exclusively positioned at the I band on both sides of the Z-lines (small black arrows

in Figure 20A). In contrast, mitochondria of PV KO appear more variable in shape and often longitudinally oriented between myofibrils (Figure 20C), suggesting a different redistribution of the organelle in the muscular tissue. Consistently, the incidence of mitochondria placed at the A bands of the sarcomere is markedly increased in PV KO EDL fibers, both as in number per fiber area and percentage of total mitochondria (see Table 1). Furthermore, as already observed by Schwaller [196], the relative fiber volume occupied by mitochondria was also significantly increased in PV KO EDL fibers (Figure 20D) compared to WT EDL fibers (Figure 20B), suggesting that PV ablation leads to a marked alteration of mitochondria ultrastructure. Interestingly, the frequency of mitochondria profiles associated with the Calcium Release Units (CRUs), the sites of Ca^{2+} release during excitation contraction coupling [143], was higher in PV KO fibers.

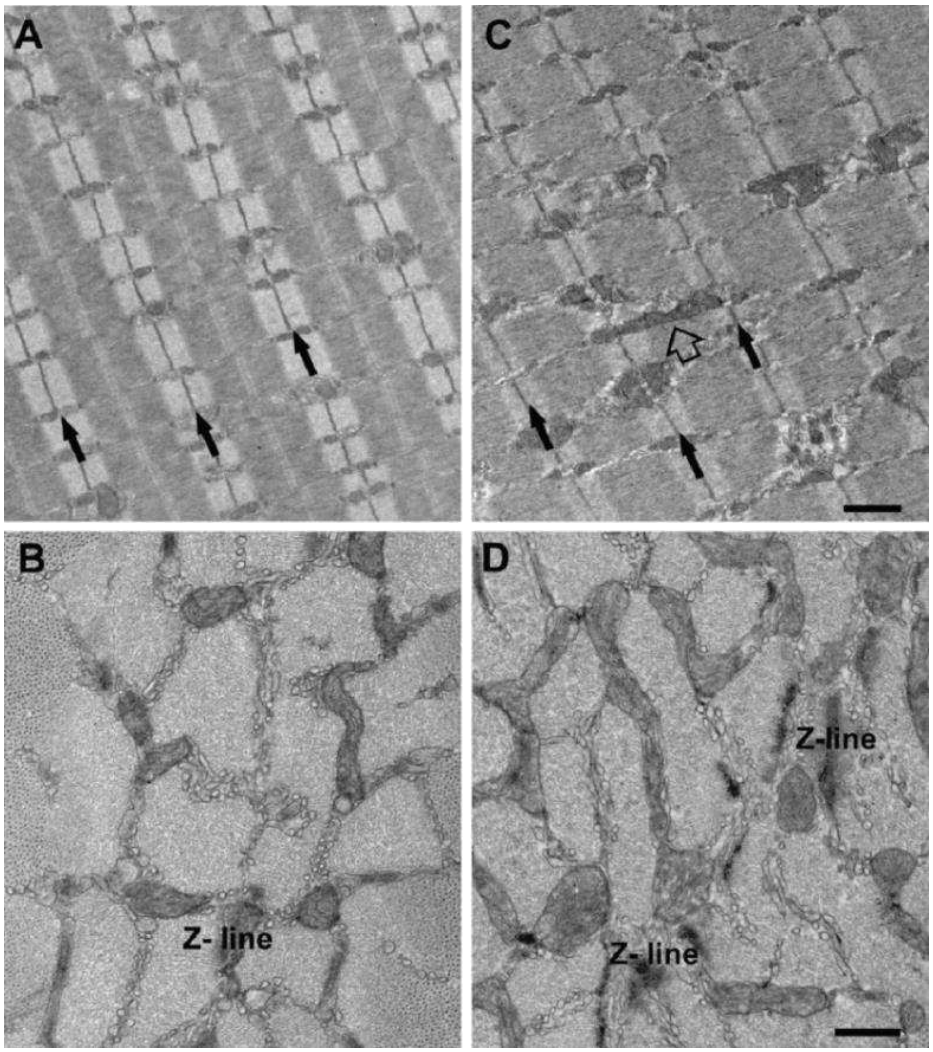

Figure 20. PV ablation alters mitochondrial volume and mitochondrial distribution.

Representative longitudinal and transversal EM images of mitochondrial distribution and morphology in adult EDL fiber from WT **(A and B)** and PV KO mice **(C and D).**
Representative longitudinal sections of EDL fibers from adult WT (A) and PV KO (C) mice: small black arrows point to mitochondria placed at the I band of the sarcomere, in proximity of Z lines, whereas the empty arrow points to a longitudinally oriented mitochondrion.
Distribution of mitochondria in cross sections of EDL fibers from WT (B) and PV KO (D) mice.
Scale bars: A and C, 1 μm; B and D, 0.5 μm.n = 2 WT; n = 3 PV-KO.

	A	B	C	D	E
	Mitochondria volume/ Total volume (%)	**No. of Mitochondria /100 μm²**	**Size of apparently normal mitochondria (nm² x 10³)**	**No. of Mitochondria at A band /100 μm² (%)**	**No. of Mitochondrion /CRU pairs / 100 μm²**
WT	4.2 ± 0.3	35.9 ± 1.5	62.2 ± 0.2	0.1 ± 0.1 (0.2)	32.7 ± 1.5
PV KO	5.6 ± 0.2*	45.7 ± 1.4*	74.5 ± 2.2*	1.1 ± 0.2 (2.5)*	39.3 ± 1.2*

Table I. Quantitative analyses of mitochondria of WT and PV KO mice.

In PV KO mice, mitochondria volume (column A), their number and size (columns B and C), and the percentage of mitochondria misplaced at the A band (column D) are all increased compared to WT.
In detail:
Column A) Relative fiber volume occupied by mitochondria;
Column B) Number of mitochondria/fiber area;
Column C) Size of apparently normal mitochondria;
Column D) Incidence of mitochondria placed in improper position at the A bands;
Column E) Quantitative analysis of mitochondria placed in proximity of Calcium Release Units (CRUs) as frequency of mitochondria profiles closely associated with CRUs.
Data are shown as mean ± SEM. For statistical analysis parametric Student t test was performed.
* $p < 0.01$. Sample size: 20 fibers from 2 WT mice, 30 fibers from 3 PV-KO mice; 5 micrographs/fiber.

5.7 Parvalbumin ablation alters mitochondrial biogenesis

Since PV KO fibers display this significant alteration of mitochondrial volume density, number and morphology, we investigated whether the signalling pathways involved in mitochondrial biogenesis were also involved. Mitochondrial biogenesis can be defined as the growth and division of pre-existing mitochondria [150,198], which depends on mitochondrial DNA replication and on the synthesis/ import and incorporation of lipids and proteins into the organelles structure [151]. All these processes must be tightly coupled and regulated in order to meet the tissue requirements.

The peroxisome proliferator-activated receptor gamma co-activator (PGC-1α) is a master regulator of mitochondrial biogenesis in mammals [151], and this gene is highly expressed, along with its homologous PGC-1β, in skeletal muscle and in other tissues characterised by high oxidative capacity [154,199]. We investigated the expression of PGC-1α and its positive regulator, the deacetylase SIRT1 [150] in TA muscles of WT and KO mice. Interestingly, both PGC-1α and SIRT1 mRNA expression was induced in TA of PV KO mice (Figure 21), suggesting a possible increase of mitochondrial biogenesis in PV KO muscle tissue, in line with findings of Schwaller and co-workers [79].

Therefore, the increase of the expression levels of SIRT1 and PGC-1α might contribute to the increase in mitochondrial number and volume in PV KO muscles.

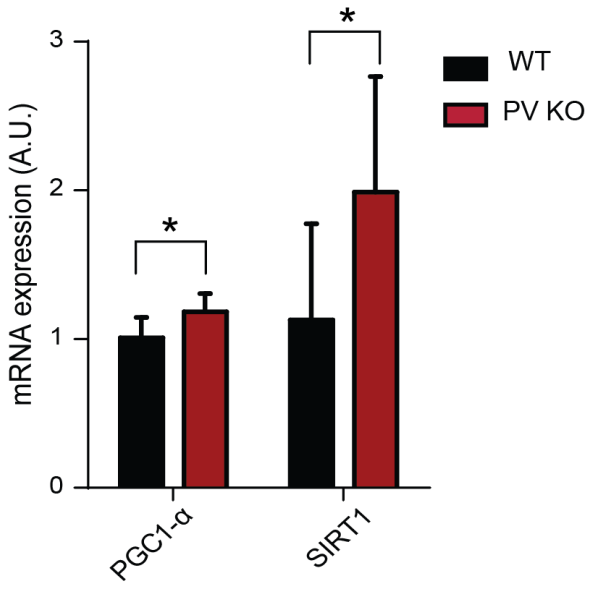

Figure 21. PV ablation induces the expression of genes controlling in mitochondrial biogenesis.

TA muscles of 3 months old WT and PV KO mice were harvested and frozen in liquid nitrogen-cooled isopentane. Total mRNA was extracted and subjected to RT-qPCR. PGC-1α and SIRT1 relative mRNA expression was assessed. Expression levels were normalized for GAPDH. The bar diagram represents the genes expression levels normalized to WT and presented as means ± SD. For statistical analysis non-parametric Student t-test (two-tailed, unpaired) was performed. n = 6 muscles per group. * $p < 0.05$.

5.8 Parvalbumin ablation alters mitochondrial dynamics

Strictly connected to mitochondrial biogenesis is mitochondria dynamics. The morphological plasticity of mitochondria is controlled by tightly regulated processes related to fusion and fission, which are coordinated to influence mitochondrial homeostasis [111].

In general, mitochondrial fission process plays a central role in fractionating dysfunctional mitochondria, allowing their removal and thus minimizing widespread detrimental effects [148]. In skeletal muscle, it was shown that increases in mitochondrial fragmentation contribute to muscle loss and that the inhibition of organelle fission could protect from muscle atrophy [200]. Mitochondrial fusion, is the mechanism by which mitochondria fuse together to equilibrate matrix metabolites and mitochondrial membrane component with intact mtDNA copies [155]. Moreover, fusion between healthy and damaged mitochondria allows to dilute the damaged material into the healthy network, avoiding the accumulation of dysfunctional mitochondria and maintaining their overall functions [201]. Mitochondrial fusion is particularly relevant in skeletal

muscle since it induces the extension of the mitochondrial network to increase energy efficiency and increase ATP production [147,202]. The proteins involved in fusion and fission processes are well characterized and include proteins of both the IMM and the OMM. GTPase dynamin-related protein (OPA1) and Mitofusin 2 (MFN2) are necessary to initiate the fusion of two mitochondria [203], while for mitochondrial fission, dynamin-related protein DRP1 and Fission 1 (FIS1) are indispensable to mediate the fission events, leading to the segregation of mitochondria [149,204].

To investigate whether mitochondrial dynamics is also influenced by PV and to understand whether the increase of mitochondrial volume is also the result of an alteration in fusion/fission processes, we performed RT-qPCR on TA muscle of WT and PV KO mice of genes involved in mitochondrial dynamics. In KO tissues, OPA1 and MFN2, were found to be up-regulated (Figure 22), while no significant difference was detected in the mRNA expression levels of DRP1 and FIS1 (Figure 22), suggesting that PV could influence the morphology of mitochondria in muscle fibers inducing both mitochondrial biogenesis and mitochondrial fusion.

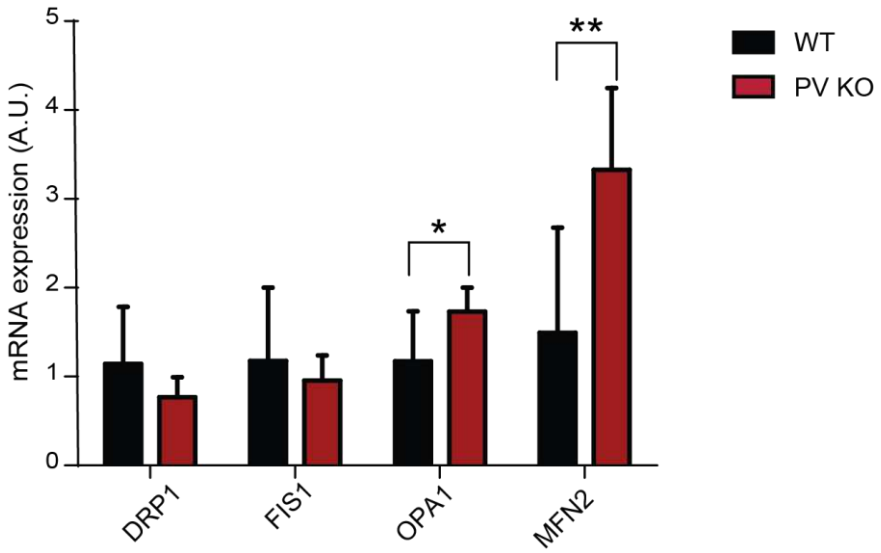

Figure 22. PV ablation modulates the expression of genes implicated in mitochondrial fusion.

TA muscle of 3 months old WT and PV KO mouse lines were used. TA muscles were harvested for analysis and total mRNA was extracted. The mRNA expression levels of genes involved in mitochondrial dynamics was measured by RT-qPCR. mRNA expression levels were normalized for GAPDH.
The bar diagram represents the gene expression levels normalized to WT and presented as means ± SD. n = 6 muscles per group. For statistical analysis non-parametric Student t-test (two-tailed, unpaired) was performed. * $p < 0.05$, ** $p < 0.01$.

5.9 Mitochondria act as dynamic Ca^{2+} buffers in PV KO muscle fibers

To further prove that, in the PV KO model, mitochondrial adapt to buffer cytosolic Ca^{2+} increases through MCU, we performed MCU silencing experiments and we measured $[Ca^{2+}]_{cyt}$ evoked by caffeine treatment. In detail, FDB muscles of WT and PV KO animals were transfected *in vivo* with plasmids encoding either control shRNA (shLUC) or shRNA designed to specifically silence MCU (shMCU), as already performed [17]. One week later, fibers were dissected, loaded with Fura-2 AM dye and $[Ca^{2+}]_{cyt}$ measurements were performed on basal resting conditions and upon caffeine stimulation. As reported in Figure 23A, in resting conditions, PV KO and WT MCU-silenced fibers did not show any significant difference on basal $[Ca^{2+}]_{cyt}$ compared to controls fibers (shLUC WT and shLUC KO). Upon caffeine stimulation (10 mM), $[Ca^{2+}]_{cyt}$ was not affected by the absence of MCU in WT fibers, while, MCU silencing in PV KO fibers, resulted in a significant higher $[Ca^{2+}]_{cyt}$ (Figure 23B). The data obtained so far demonstrated that in WT muscles, mitochondria do not buffer $[Ca^{2+}]_{cyt}$ increases and reinforce the hypothesis that the lack of PV induces a profound mitochondrial adaptation to prevent $[Ca^{2+}]_{cyt}$ increases.

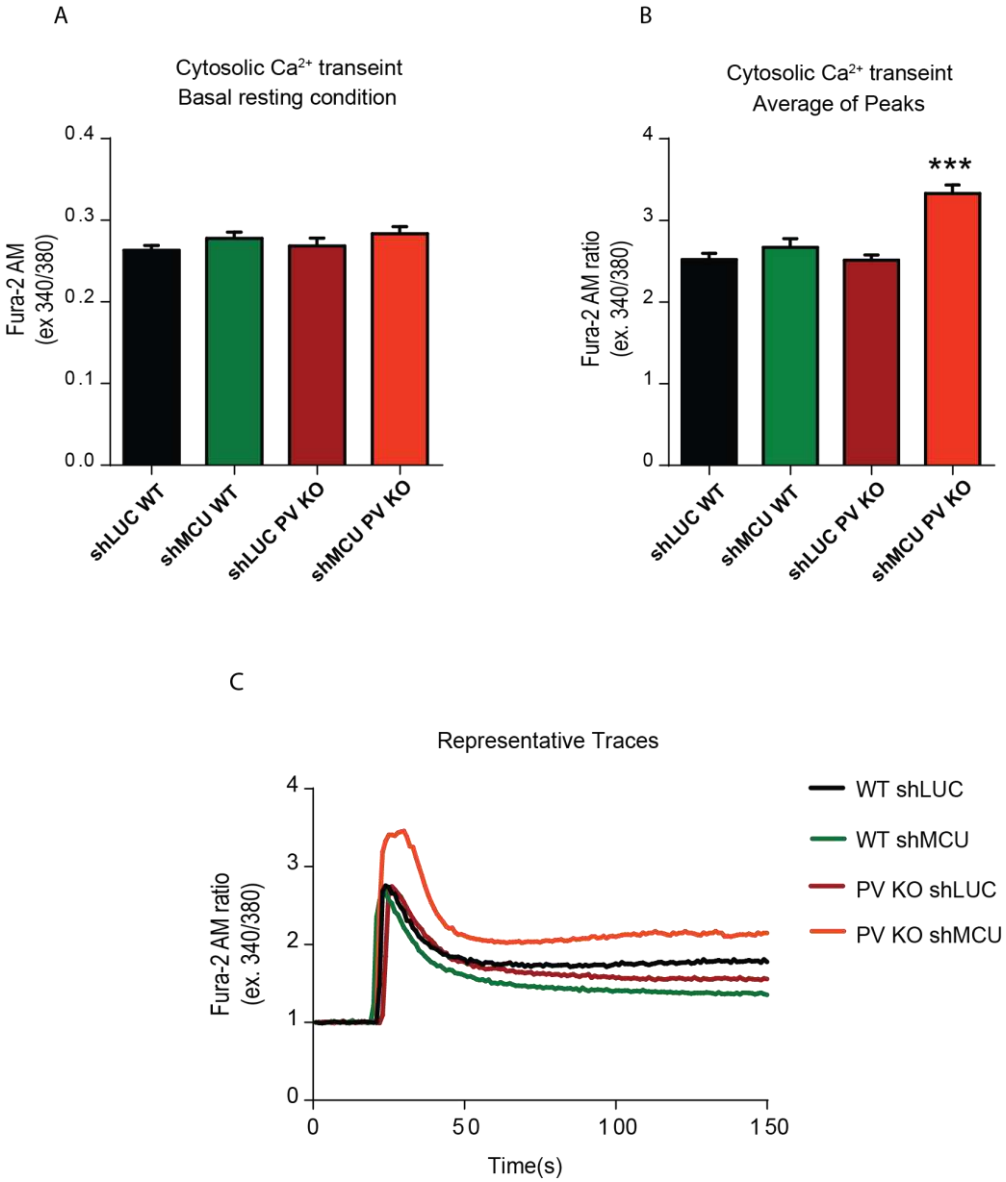

Figure 23. Cytosolic [Ca^{2+}] in basal resting conditions and upon caffeine stimulation on WT and PV KO FDB muscle fibers silencing MCU.

FDB muscle fibers of 3 months old WT and PV KO mice (n = 8) were electroporated with either shLUC (control) or shMCU. Seven days later FDB muscle fibers were isolated, cultured and loaded with Fura-2 AM dye Ca^{2+}indicator. Five independent experiments were performed.
A) Resting sarcoplasmic Ca^{2+} levels in WT and PV KO controls or MCU silencing fibers, evaluated through ratiometric imaging (Ex 340/380) using the Ca^{2+} indicator Fura-2 AM dye. The bar diagram shows the mean basal resting value ± SD, n ≥ 20.
B) Fibers were stimulated with caffeine (10 mM) and sarcoplasmic Ca^{2+} transients were measured in the same conditions as in (A). The bar diagram shows the mean peak ± SD. n ≥ 20. For data analysis, two-way ANOVA was used with post hoc Bonferroni's multiple comparison test for each sample. *** $p < 0.0001$.
C) Representative traces of the experiment as in (B).

5.10 Lack of PV does not induce fiber type switching

We demonstrated that PV deficiency induces an increase of mitochondrial fractional volume in fast twitch muscle (Figure 20), a common feature of slow type fibers, characterized by low ATPase activity, high oxidative and low glycolytic capacity and relatively resistance to fatigue [80,205]. Furthermore, in Schwaller laboratory, quantitative analysis of mitochondrial proteins as COX I, COX Vb and F1-ATPase subunit β revealed that PV KO mitochondria of fast twitch muscles resembled that of slow twitch ones [80,196]. To characterize in depth PV KO fast fibers, we asked whether PV removal could also induce fiber type switching in terms of myosin isoforms. Therefore, to evaluate fiber type composition of TA muscle sections from WT and PV KO animals, we performed immunocytochemistry assay using specific antibodies to discriminate between type I, IIA, and IIB fibers (Figure 24A and 24B). No evident alterations of skeletal muscle fiber-type composition were detected in KO mice compared to WT muscles. Indeed, TA muscles, a type IIB-rich muscle, had equal number of type I, IIA, IIB and IIX fibers in PV KO and WT mice (Figure 24C).

Consistent with this, as already mentioned in the previous paragraphs, the expression of genes normally enriched in oxidative fibers as SERCA2a [192] and of other Ca^{2+} buffers as Calsequestrin, that is mainly express in fast twitch muscle fibers [40], were comparable between TA muscle from WT and PV KO mice (Figures 18A and 18B), further confirming that fiber-type specific components are not affected by the absence of PV.

To investigate deeply the differences between WT and KO in muscle fibers mass, we measured also the cross-sectional area (CSA) for each fiber type subgroup (Figure 24D). No differences were detected in fiber size between WT and KO in TA muscle sections, further indicating that lack of PV does not induce fiber type switching.

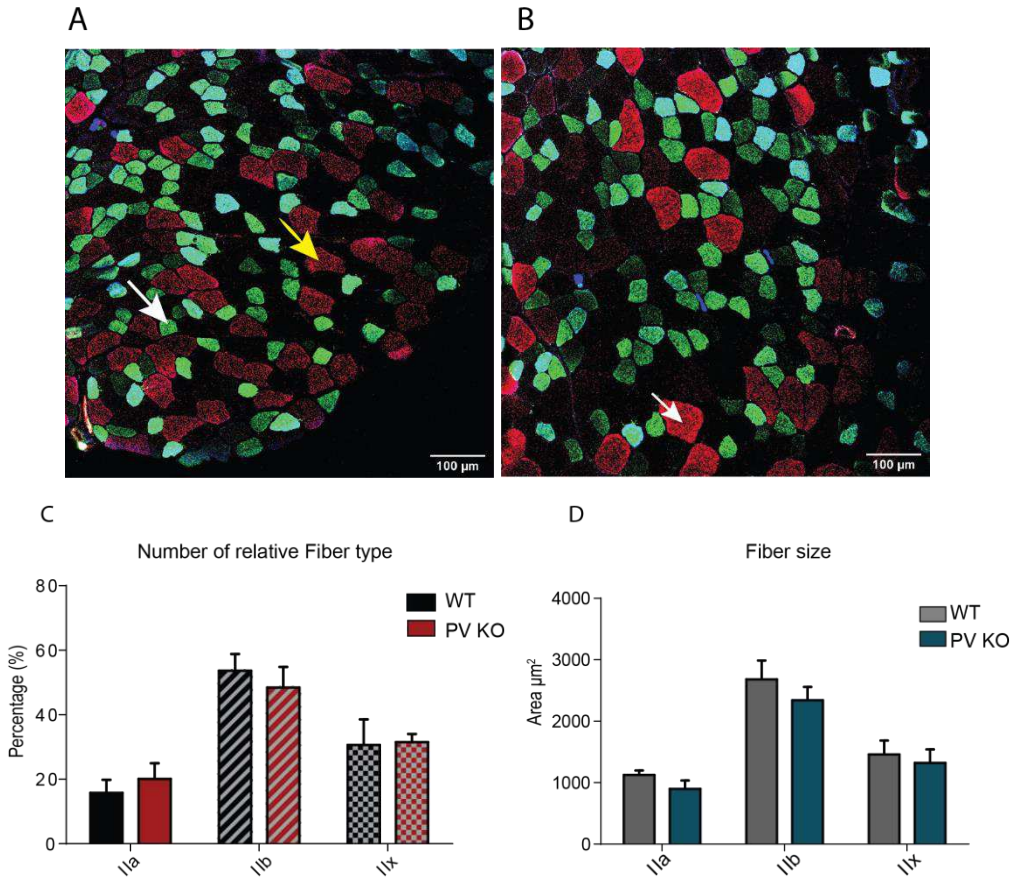

Figure 24. PV ablation does not alter fiber type composition.

A) Representative image of 20 µm thick cryosections of WT and PV KO TA muscles. Scale bar 100 µm. α-SC-71, α-BF-F3 and α-BAD5 primary antibodies were used to label type IIA (green, white arrow), type IIB (red, yellow arrow) and type I (not detected) types of myosin, respectively. The unstained fibers correspond to type IIX myosin, typical of fast twitch muscles.
B) Quantitative analysis of fiber type composition in WT and PV KO TA muscles. n = 4 muscles per group, n of fibers per group ≥ 300.
C) Average fiber area of the three different fiber type group. Data are presented as mean ± SD. For statistical analysis parametric Student t-test (two-tailed, unpaired) was performed.

5.11 Lack of PV leads to an increase in muscle performance

The classic view of mitochondria as the "powerhouse of the cell" could not be more appropriate in the case of skeletal muscle, since, in this tissue, mitochondrial Ca^{2+} controls the rate of ATP synthesis by oxidative phosphorylation that is essential for muscle contraction [11,81]. Considering the huge alteration in mitochondrial morphology and Ca^{2+} handling capacity of PV KO muscles, we asked whether PV ablation could affects also exercise performance.

To answer to this question, we decided to compare maximal running distance of PV KO and WT mice. Exhaustion exercise performance was evaluated by a single bout of treadmill run test on 10% of uphill, that involves concentric muscle contraction and increases the muscle workload for the animals, leading to a faster exhaustion [206]. We observed that PV deletion in KO mice caused a significant increase in running performance compared to WT animals (Figure 25), indicating the beneficial effects of PV ablation on running capacity. We can hypothesize that lack of PV, and the related increase in mitochondrial volume, increases fatigue resistance and enhance the ability to sustain muscle activity for prolonged periods.

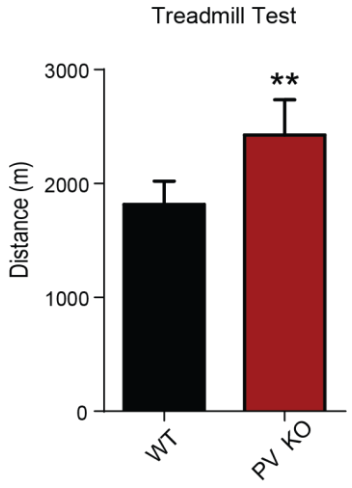

Figure 25. Lack of PV improves muscle performance.

Five young mice per genotype (2 months old) were trained on a treadmill chamber until exhaustion. Exercise was performed by subjecting mice to a forced run on 10% of uphill on a treadmill device. Briefly, mice were first left to adapt to the treadmill with a speed of 17 cm/sec that was increased of 2 cm/sec every 10 minutes until mice were unable to run. Once mice were unable to run for 5 seconds consecutively, they were removed from the treadmill and total running distance of each animal was recorded. Data are presented as mean of total running distance ± SD. For statistical analysis parametric Student t test (two-tailed, unpaired) was performed. **$p < 0.001$.

5.12 PV and the regulation of fiber size

Skeletal muscle mass shows an enormous plasticity to adapt to different stimuli according to physiological and pathological conditions [158,159]. An increase in muscle mass and fiber size, defined as muscle growth or hypertrophy, occurs during development and in response to mechanical overload [27,158], while a decrease in muscle mass and fiber size, defined as muscle atrophy, is a consequence of several systemic and disuse conditions such as aging, cancer, diabetes, loss of neural input or catabolic hormonal stimulation [27,159].

The great plasticity of skeletal muscle tissue is due to several mechanisms that regulate the balance between protein synthesis and protein degradation within the muscle fiber [159,166]. This mechanism involves a precise transcriptional program of a set of genes that are commonly up- or down-regulated in atrophying skeletal muscle. These common genes, termed “atrogenes”, are co-ordinately induced or suppressed in muscle during both systemic and disuse types of muscle wasting and are thought to regulate the loss of muscle components [25,26]. One of the most downregulated genes in both systemic and disuse types of atrophy is PV [25,26]. We thus decided to study the role of this buffer protein in the regulation of muscle mass.

We first confirmed the microarray data found in literature [25,26] by performing denervation experiment on 3-month-old WT CD1 mice. A small section of the sciatic nerve was excised in one limb and the contralateral non-denervated hind limb served as internal control in the analyses, which were carried out 3 and 14 days after nerve cut. We checked both PV mRNA and protein levels (Figure 26A-C). We observed a decrease of both mRNA (Figure 26A) and protein levels (Figure 26B and 26C) of PV both 3 and 14 days post denervation, thus confirming the microarray data [25,26].

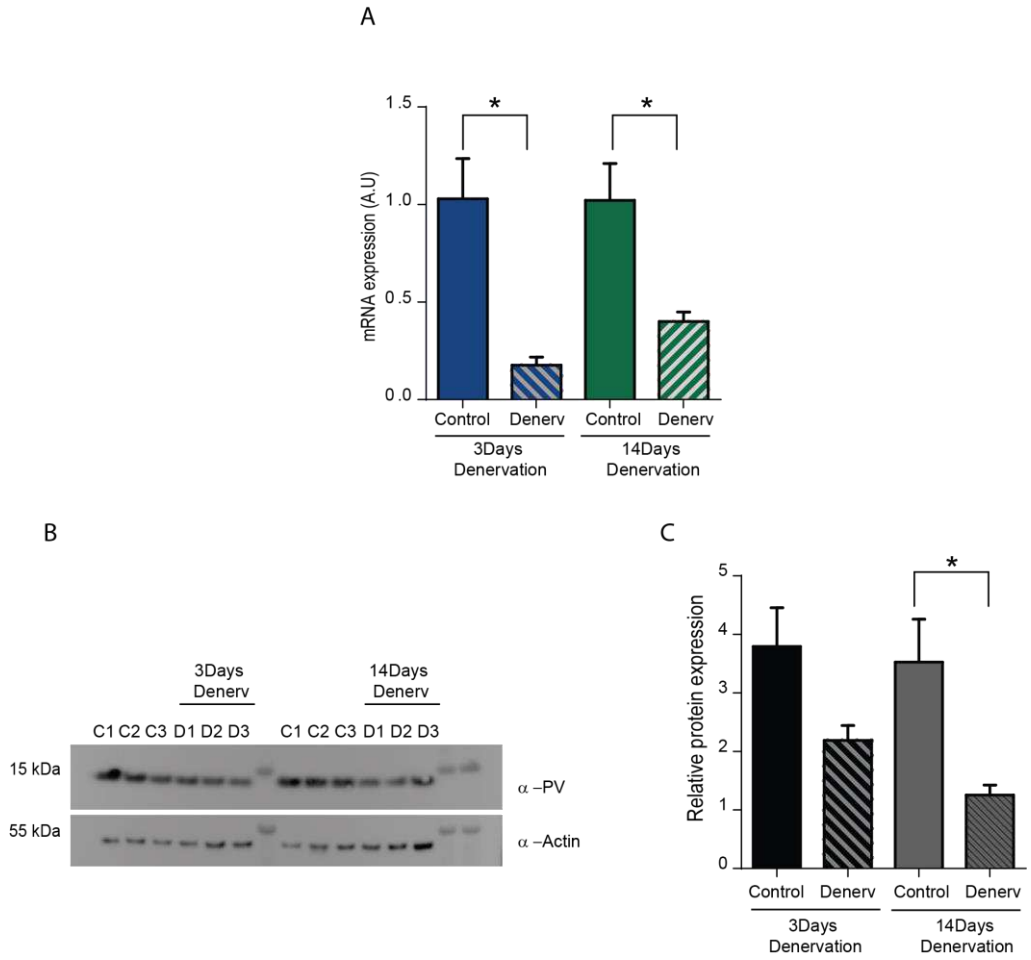

Figure 26. PV expression level decreases after denervation.

Denervation was performed of 3-month-old CD1 mice by sciatic nerve excision. Contralateral non-denervated hind limb served as internal control in subsequent analyses, which were carried out 3 and 14 days after the cut of the nerve. TA muscles at the indicated time points were collected and WB and RT-qPCR analysis were performed.

A) Evaluation of the mRNA expression levels of PV obtained through RT-qPCR analysis. The bar diagram represents PV gene expression levels normalized to contralateral hind limb and presented as means ± SD. n =3 muscles per group. For statistical analysis non-parametric Student t-test was performed (two- tailed, unpaired). * $p < 0.005$.

B) Representative WB on denervated and contralateral TA. PV protein level was detected 3 and 14 days after denervation. α-Actin antibody was used as loading control. n = 3 per condition.

C) Quantification of the levels of PV protein obtained as in (B) and normalized for actin. The bar diagram represents the mean ± SD. For data analysis, parametric Student t-test was used. n = 3 muscles per condition. * $p < 0.05$.

In order to investigate whether PV plays a direct role in skeletal muscle trophism, we decided to perform denervation experiments of PV KO mice and to analyse fiber size 3, 7, or 14 days after the cut of the nerve.

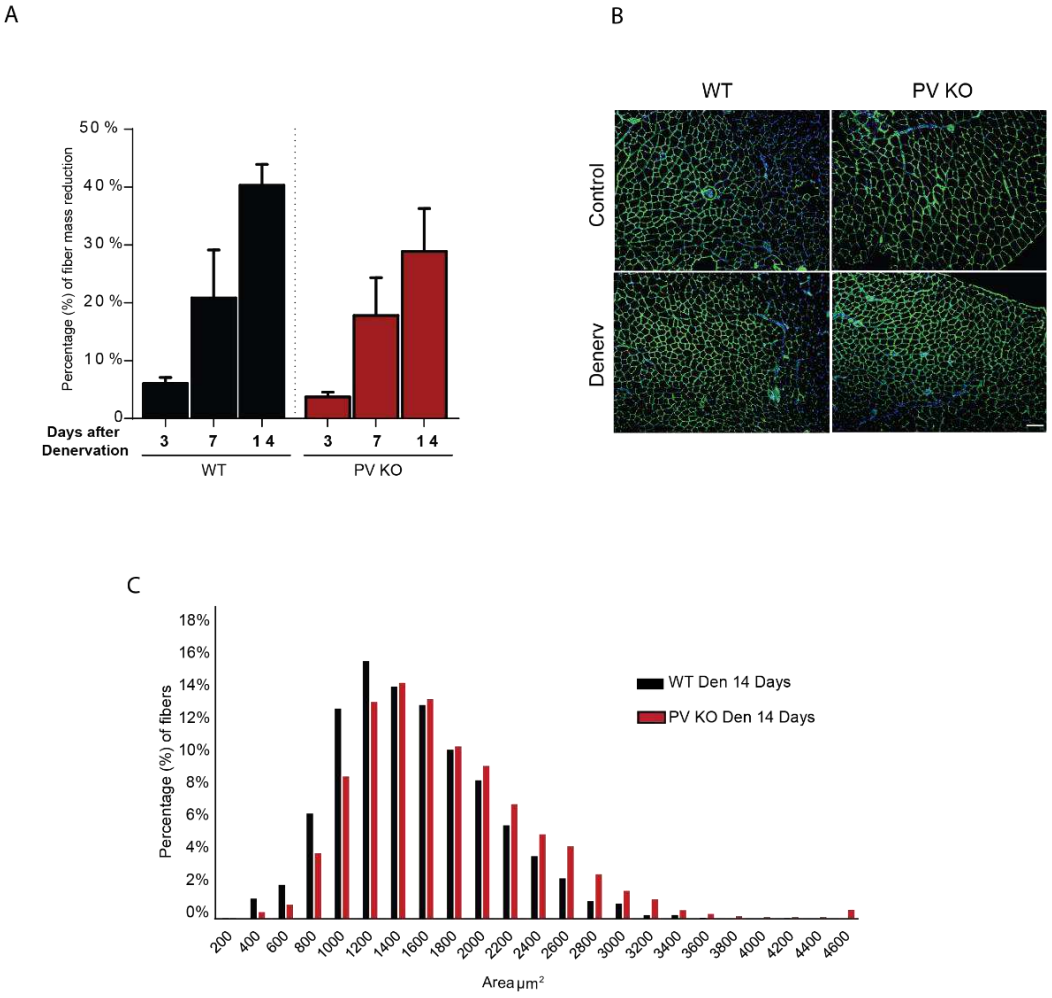

Figure27. PV absence partially protects muscles from the loss of mass induced by denervation.

Denervation experiment was performed on TA muscles of 3 months old WT and PV KO mice (n = 3 WT and n = 3 PV KO for each time point). The sciatic nerve was excised and contralateral non-denervated hind limb was used as internal control in the subsequent analyses that were carried out 3, 7 and 14 days after the cut of the nerve.
A) The bar diagram represents the percentage (%) of CSA reduction of WT and PV KO muscles 3, 7 and 14 days after denervation compared to the contralateral hindlimb ± SD.
B) Representative image of muscle transversal sections of contralateral and denervated WT and PV KO TA muscles. α-laminin primary antibody was used to mark the sarcolemma. Scale bar 100 µm.
C) Size-frequency histograms of CSA of WT and PV KO mice myofibers after 14 days of denervation.

As expected, denervation induced a progressive muscle loss of WT TA muscle mass: in WT muscles the percentage of muscle loss at 3, 7 and 14 days after denervation was 6%, 23% and 40%, respectively (Figure 27A, black bars). In the absence of PV, denervation-induced atrophy was reduced by only 3%, 17% and

27% at 3, 7 and 14 days after denervation, respectively (Figure 27A, red bars). Interestingly, no significant difference was found in fiber size of controlateral PV KO and WT muscles. Representative sections are shown in Figure 27B. Therefore, PV ablation shows a trend of partial protection from denervation-induced muscle atrophy, as also demonstrated by the shift to the right of the size-frequency distribution of CSA of PV KO fibers denervated for 14 days compared to denervated WT fibers (Figure 27C). However, since the effect of PV ablation on denervated muscle appeared rather modest and no effect of PV ablation was observed on contralateral muscles, we decided to either acutely silence or overexpress PV in adult WT mice by plasmid electroporation and we evaluated CSA, in order to exclude also any developmental adaptation of PV loss.

5.12.1 PV acute silencing increases muscle size

We electroporated TA muscles of WT CD1 mice with plasmids encoding either control shRNA (shLUC) or shPV expressing mCherry red fluorescent protein. After 7 days of transfection, we performed immunostaining assay to detect transfected fibers and to perform cross-sectional area (CSA) analysis.

To reduce variability between mice, we used as control for CSA evaluation the non-transfected fibers of the same muscle transfected with shPV. Since the silencing plasmids encode also for mCherry, we first assessed whether its expression alone has no effect on fiber size.

We thus electroporated shLUC non-targeting plasmid and we compared the CSA of the transfected fibers with that of the non-transfected ones (Ctrl) in the same muscle. We detected high transfection efficiency with no overt muscle damage, we observed no significant difference between the shLUC positive fibers and the non-

transfected ones, concluding therefore that the injection the mCherry fluorescent protein plasmid does not affect fiber size *per se* (Figure 28A).

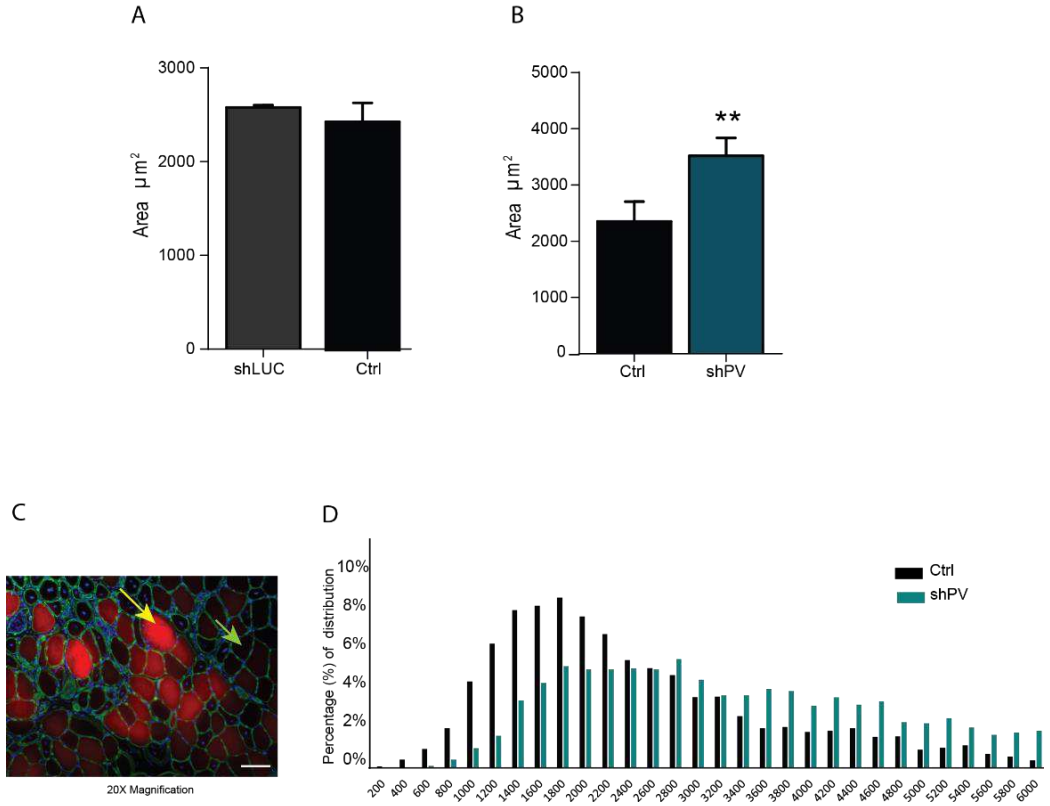

Figure 28. PV acute silencing *in vivo* increases fiber size.

TA muscle of 3-month-old CD1 were electroporated with shRNA for PV or shLUC. Seven days later, TA muscles were collected, and immunofluorescence analysis was performed on 20 µm transversal cryosections using α-laminin antibody to mark the sarcolemma.
A) CSA of fibers transfected with shLUC were compared to non-transfected fibers of hind limb electroporated with shPV. The bar diagram represents the mean CSA ± SD. For data analysis, parametric Student t-test (two-tailed, unpaired) was used. n = 3 muscles per condition.
B) CSA of fluorescent fibers transfected with shPV were compared to non-transfected fibers in the same muscle. The bar diagram represents the mean CSA ± SD. For data analysis, parametric Student t-test (two-tailed, unpaired) was used. n = 3 muscles. ** $p \leq 0.01$.
C) Representative immunoflourescence analysis. The yellow arrow indicates the positive, fluorescent fibers for shPV, the green arrow indicates the non-transfected fibers defined as Ctrl in the plotted data in figure 28B. α-laminin primary antibody was used to mark the sarcolemma.
D) Size-frequency histograms of cross-sectional area for transfected (shPV) and non-transfected (Ctrl) myofibers.

Next, we assessed CSA one week after the intramuscular injection of shPV (Figure 28B). Intriguingly, fibers positive for shPV (Figure 28C, yellow arrow) were larger than the non-transfected fibers (Figure 28C, green arrow) by 35% (Figure 28B). Furthermore, PV acute silencing causes a clear shift to the right of the size-frequency histogram (Figure 28D).

5.12.2 PV overexpression decreases myofibers size

Overexpression of PV gave coherent results. TA muscles of CD1 WT mice were electroporated with either PV-P2A-mCherry or mCherry plasmids. One week later, immunohistochemistry analysis of transversal section of the isolated muscles were performed. The evaluation of CSA on transfected fibers showed a significant reduction of fiber size in PV overexpressing fibers compared to control, suggesting that PV overexpression is sufficient to induce muscle atrophy (Figure 29A). The reduction of myofiber size in PV overexpressing fibers was more than 20%, and frequency distribution of CSA of fibers overexpressing PV was shifted toward smaller sizes compared to control myofibers (Figure 29C).

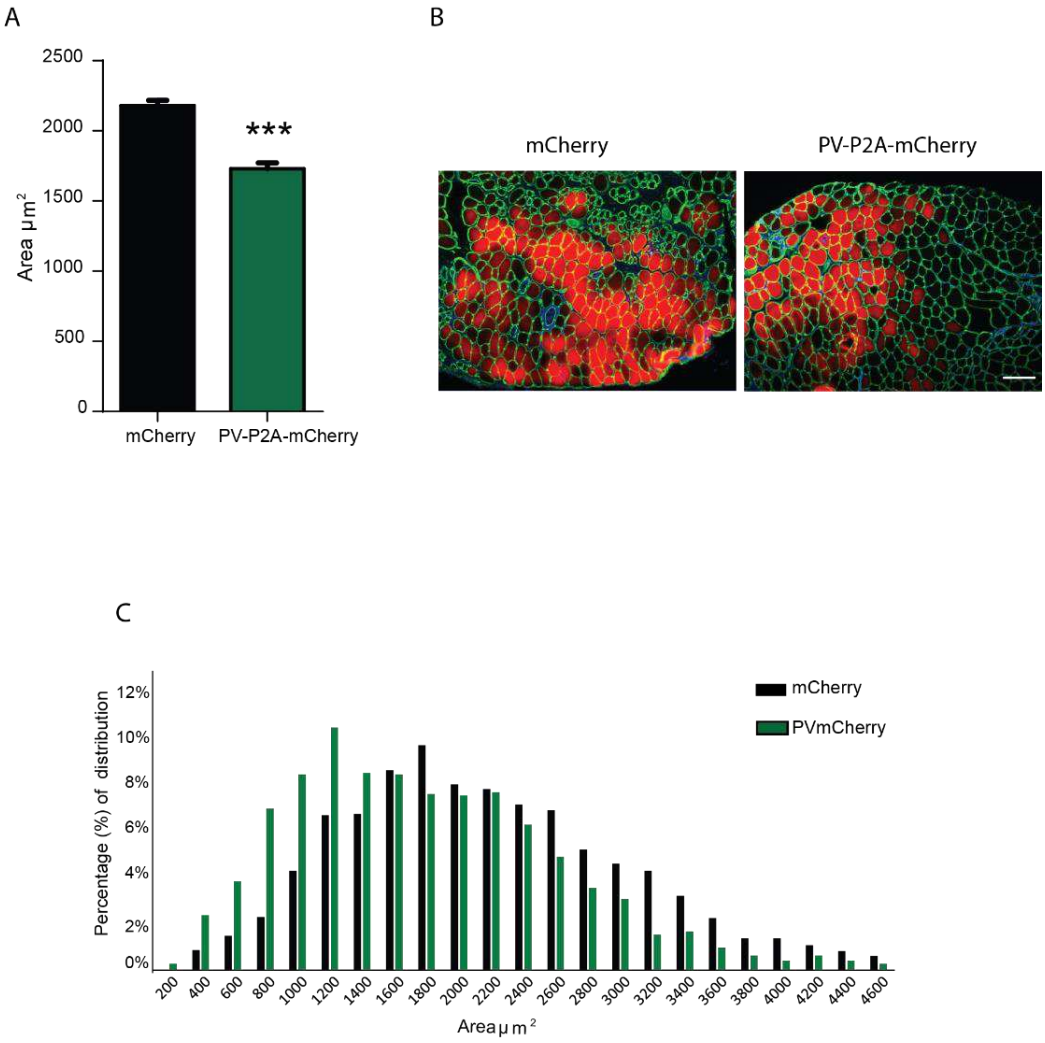

Figure 29. PV acute silencing *in vivo* increase fiber size.

TA muscles of 3 months old CD1 mice were electroporated with either PV-P2A-mCherry or empty plasmid (mCherry). Seven days later the electroporated muscles were collected and immunofluorescence analysis was performed on 20 µm transversal cryosections using α-Laminin antibody to mark fiber sarcolemma.

A) CSA measurements of fluorescent fibers positive for mCherry empty vector were compared to PV overexpressing fibers. The bar diagram represents the mean CSA ± SD. For data analysis, parametric Student t-test (two-tailed, unpaired) was performed. n= 4 muscles per condition. *** $p < 0.0001$.

B) Representative images of muscle sections of mCherry fluorescent fibers and of PV overexpressing fibers (right panel). α-Laminin primary antibody was used to mask the sarcolemma.

C) Size-frequency histograms of CSA of control fibers (mCherry) and PV overexpressing myofibers. Scale bar 100 µm.

5.13 Signalling pathways controlling skeletal muscle mass by PV

As already mentioned, muscle mass is controlled by a precise balance between *de novo* protein synthesis and degradation of pre-existing proteins [159]. The molecular pathways controlling these two processes are tightly regulated. Regarding the hypertrophy process, a major signalling pathway, that positively controls protein synthesis, is the IGF1-AKT/PKB pathway [168]. AKT promotes skeletal muscle growth and simultaneously blocks protein degradation, thus preventing the induction of Atrogin-1 and Murf-1, the two main ubiquitin ligases involved in the atrophy process [170,171]. Since we observed a partial protection in denervation-induced atrophy in our PV KO model and based on the effect of acute silencing of PV in fiber size, we decided to investigate the effect of PV ablation on the activation of the IGF1-AKT/PKB pathway. No significant differences were detected in the phosphorylation levels of the different components of the AKT pathway in PV KO compared to WT mice TA muscles 14 days after denervation (Figure 30A and 30B).

Recently, PGC-1α4, a splice variant of PGC-1α, was discovered as an important player in the control of muscle mass [28]. This isoform, that does not induce mitochondrial biogenesis as PGC-1α, is abundantly expressed in skeletal muscle and appears to play a key role in triggering muscle hypertrophy as adaptive response to exercise [28].

Of note, it has been recently demonstrated that increases of mitochondrial Ca^{2+} positively regulates skeletal muscle mass by increasing PGC-1α4 expression [17]. We performed RT-qPCR measurement of PGC-1α4 expression levels on TA muscles from WT and PV KO mice. Interestingly, we observed a significant induction of PGC-1α4 expression in PV KO muscles (Figure 30C).

We hypothesize that PV ablation, leading to an increase of mitochondrial Ca^{2+} uptake, activates mitochondria Ca^{2+}-dependent pathways controlling muscle trophism.

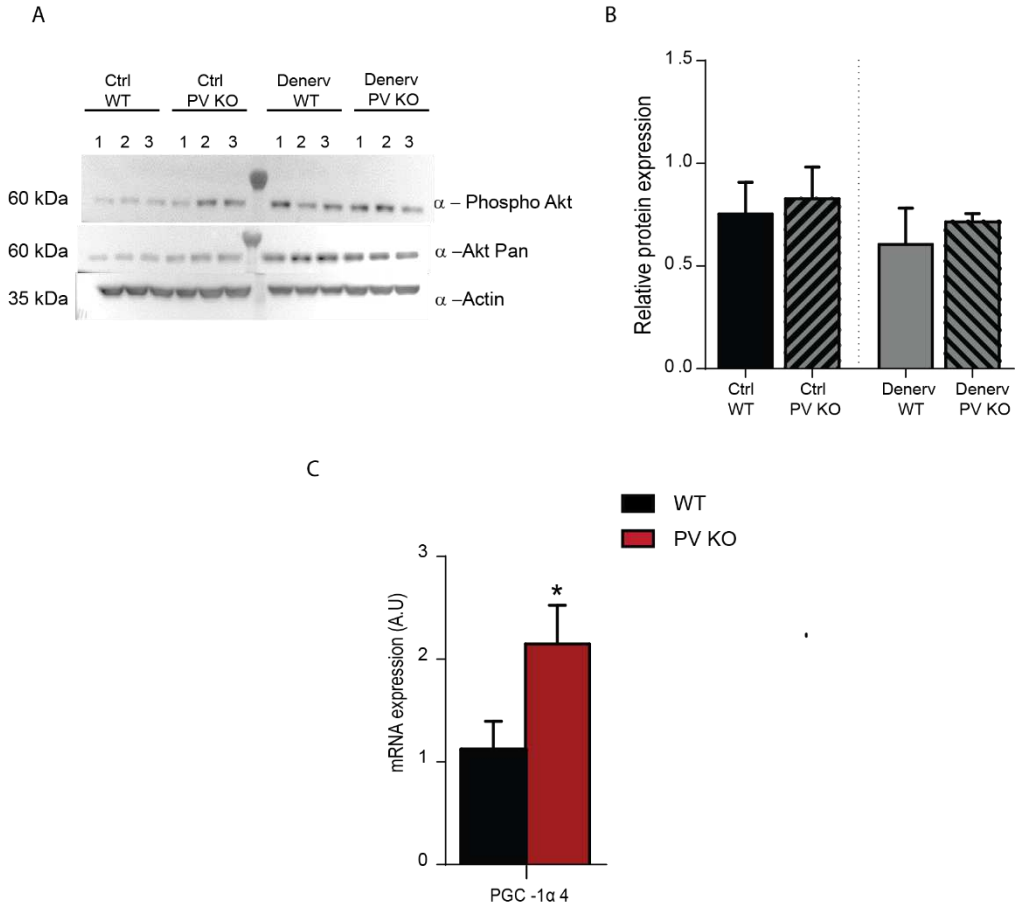

Figure 30. Lack of PV induces the expression of PGC-1α4.

A) Representative image of WB of controlateral and denervated TA muscles from WT and PV NO mice 14 days after denervation. TA protein muscles extracts of WT and PV KO mice were probed with α-pAkt (Ser473) and α-Akt pan antibodies. α-Actin was used as protein loading control. n = 3 muscles per conditions.
B) Quantification of the levels of phospho Akt protein obtained as in (A) and normalized for Akt protein levels. The bar diagram represents the mean ± SD. For data analysis, two-way ANOVA was used with post hoc Bonferroni's multiple comparison test for each sample.
C) Total mRNA of WT and PV KO was extracted form TA muscles and subjected to RT-qPCR. The mRNA expression of PGC-1α4 was assessed and normalized to POL2 expression level. The bar diagram represents PGC-1α4 expression levels normalized to WT and presented as means ± SD. n = 4 muscles per group, * $p \leq 0.05$.

6. Discussion

Ca^{2+} is one of the most crucial intracellular second messengers that plays a central role in cellular signalling [35]. Ca^{2+} is involved in various cellular functions, ranging from biological processes, such as the control of aerobic metabolism, to physiological mechanisms, such as muscle contraction [29]. Cells can decode Ca^{2+} signals based on the properties of the intracellular changes in Ca^{2+} concentration as amplitude, duration, frequency and localization [1,2], and generate outputs as diverse as proliferation or cell death [29].

To control the specificity of the activated functions, cells have evolved complex and sophisticated mechanisms to decode frequency-encoded Ca^{2+} signals [1,2]. To perform such a precise regulation, cells rely on the co-ordinated activity of Ca^{2+} channels, Ca^{2+} pumps, exchangers and Ca^{2+}-buffering proteins as compartmentalisation in organelles. The latter allow highly coordinated and transient modifications of intracellular Ca^{2+} concentrations [207–209].

It is largely known that the endoplasmic reticulum (ER) or its specialized counterpart in striated muscles, the sarcoplasmic reticulum (SR), is the largest Ca^{2+} store in the cell. In detail, while the cytosolic Ca^{2+} concentration ($[Ca^{2+}]_{cyt}$) at rest is about 100 nM, ER/SR free $[Ca^{2+}]$ can reach 1 mM, depending on the cell type [6]. Upon stimulation, Ca^{2+} is released from the ER/SR, which in turn stimulates Ca^{2+} influx from the plasma membrane, leading to the $[Ca^{2+}]_{cyt}$ increases [2,210].

Furthermore, many functions have been ascribed to Ca^{2+} accumulation by mitochondria [4]. Of note, mitochondria were the first organelles shown to be capable of taking up Ca^{2+} even before the chemiosmotic theory of mitochondrial Ca^{2+} accumulation [4,211]. Indeed, it is well established that increases in mitochondrial Ca^{2+} activates three different Ca^{2+}-dependent dehydrogenases of the TCA cycle, thus promoting ATP synthesis necessary for the correct energy state of the cell [81,212].

In this regard, mitochondrial Ca^{2+} uptake is of special physiological interest in skeletal muscle where the high energy cost of contractile activity requires large (even 100 fold) and fast variations of aerobic ATP production [10,39,136]. Hence,

in this tissue, mitochondria control the rate of ATP production necessary for muscle contraction.

Moreover, it has been recently demonstrated that mitochondrial Ca^{2+} uptake controls muscle trophism [5]. Indeed, increases of mitochondrial Ca^{2+} uptake triggers muscle hypertrophy and, coherently, the block of mitochondrial Ca^{2+} uptake induces atrophy [5].

However, even if the role of mitochondrial Ca^{2+} in energy production and in the regulation of trophism in skeletal muscle is clear [11,81], whether, in physiological conditions, muscle mitochondria are able to actively buffer $[Ca^{2+}]_{cyt}$ is still matter of debate.

In this regard, the focus of my PhD research was to understand how changes in $[Ca^{2+}]_{cyt}$ affects mitochondrial Ca^{2+} uptake in skeletal muscle. For this purpose, we examined a specific condition where intra-fiber Ca^{2+} kinetics have been steadily altered by removing PV, the main cytosolic Ca^{2+} buffer in skeletal muscle [56].

PV is one of the members of the EF-hand Ca^{2+} -binding family of proteins [66]. This buffer is mainly expressed in fast twitch muscle fibers where, acting as a soluble cytoplasmic Ca^{2+} buffer, it induces a rapid decrease in $[Ca^{2+}]_{cyt}$, participating in the temporal regulation of Ca^{2+} homeostasis [20,52,176]. Indeed, it has been demonstrated that in skeletal muscle fibers, PV facilitates Ca^{2+} translocation between the sarcoplasm and the Ca^{2+}-ATPase (SERCA) of the SR, thus contributing to muscle relaxation [52,69,213].

We chose the PV KO mice model since it represents a good study tool to investigate the Ca^{2+} buffering capacity of mitochondria. Indeed, it has been demonstrated that PV ablation leads to changes in intra-fiber Ca^{2+} kinetics by modifying the temporal and as well as the spatial properties of Ca^{2+} transients during muscle contraction [20,69,176].

The first data on the effects of PV ablation on cytosolic Ca^{2+} transients dates back to the end of 1990 when Schwaller and co-workers analysed $[Ca^{2+}]_{cyt}$ in extensor digitorum longus (EDL) fast-twitch muscles of PV KO [20]. This experiment showed that the decay of $[Ca^{2+}]_{cyt}$ after a single pulse of electrical stimulation was slower compared to WT fibers, leading to a prolongation of the time required to reach the peak of twitch tension [20]. Furthermore, an extension of the half-

relaxation time was also observed [20], thus confirming the physiological role of PV in shaping $[Ca^{2+}]_{cyt}$. Interestingly, no difference was found in the amplitude of Ca^{2+} transients between PV KO and WT muscle fibers [20].

We first decided to confirm this data by measuring cytosolic Ca^{2+} transients using Fura-2 AM in isolated FDB muscle fibers from age-matched WT and PV KO mice.

In Schwaller laboratory, for cytosolic Ca^{2+} measurements Indo 1-AM was used as Ca^{2+} indicator [20]. Indo-1 dye is similar to Fura-2. Indeed, both are aminopolycarboxylic acids that bind intracellular Ca^{2+} acting as Ca^{2+} sensors and both allow ratiometric measurements [214]. At low concentrations of the indicator, the use of either the 340/380 nm excitation ratio for Fura-2 or the 405/490 nm excitation ratio for Indo-1, enables accurate measurements of $[Ca^{2+}]_{cyt}$. However, the main advantage of Fura-2 is that this dye shows lower Ca^{2+} binding affinity (K_d Ca^{2+} 0.14 μM), thus decreasing the Ca^{2+} buffering effects of the indicator.

To mimic the physiological response of innervated muscles, isolated muscle fibers were stimulated with a single electrical pulse of 0.5 Hz that induces a physiological depolarization of the fiber. As already demonstrated by Schwaller and co-workers [20], $[Ca^{2+}]_{cyt}$ was not affected in PV knockout fibers both under basal resting conditions and upon electric stimulation (Figure 5) but, upon stimulation, the kinetic of Ca^{2+} increase and Ca^{2+} clearance were altered (Figure 6). Consistently with the physiological role of PV in buffering cytosolic Ca^{2+}, the time-to-peak and the half-relaxation time were increased in PV KO fibers compared to WT. In physiological conditions, during a single twitch, Ca^{2+} released from the SR induces a transient increase of Ca^{2+} concentration in the sarcoplasm, leading to the activation of the contractile apparatus. Constantly active Ca^{2+} pump SERCA on the SR membranes, removes Ca^{2+} ions from the cytosol and accumulate them in the SR lumen [52,73,74]. Then, Ca^{2+} dissociates from PV and the Ca^{2+} buffer returns in its "Ca^{2+}-free conformation" [71]. Therefore, the prolongation of the time required to contract and relax in PV KO fibers reflects the prolongation of the myofibers in the active state since PV-deficient muscles loose the fast mechanism to reduce $[Ca^{2+}]_{cyt}$ [26].

Next, we analysed cytosolic Ca^{2+} transients in WT and PV KO muscle fibers under tetanic stimulation (60Hz). Indeed, it is known that during a tetanic train of stimuli, a large quantity Ca^{2+} enters the sarcoplasm through repeated releases from the SR, although the amplitude of the subsequent releases progressively decreases [74,179]. To sustain fiber tension for more than one second, it is necessary to saturate cytosolic Ca^{2+} binding proteins during the contractile cycle [70]. Fibers lacking PV should have revealed an increase of $[Ca^{2+}]_{cyt}$ after the tetanic stimulation, since the protein represents the main buffer in fast twitch skeletal muscle. Unexpectedly, PV KO FDB muscle fibers showed a significant decrease of cytosolic $[Ca^{2+}]$ after tetanic stimulation (Figure 7). To explain this result, we asked whether the lack of PV could induce rearrangements of one of the two main Ca^{2+} stores, the sarcoplasmic reticulum (SR) and mitochondria. First, we focused our attention on mitochondria that are recognized as crucial regulators of cellular Ca^{2+} homeostasis [1,180]. Indeed, as mentioned above, in many cell types, mitochondrial Ca^{2+} has been associated not only with the regulation of energy metabolism through oxidative phosphorylation but also with the modulation of cytosolic Ca^{2+} signals [4,5]. We thus asked whether the unexpected decrease of cytosolic Ca^{2+} transients in fibers lacking PV (Figure 7) could be due to an adaptive mechanism exerted by mitochondria. To analyse this aspect, we measured mitochondrial Ca^{2+} uptake on single isolated FDB fibers of WT and PV KO in response to both electrical stimulation and addition of caffeine that induces the release of Ca^{2+} from the SR [17,179,181,182]. No difference was detected in mitochondrial concentrations in resting conditions, while mitochondrial Ca^{2+} uptake was significantly higher in PV KO muscle fibers compared to control fibers (Figure 8 and Figure 9). Therefore, since the lack of PV in our KO model does not induce a significant increase of cytosolic Ca^{2+} transients (Figure 5A) and that it causes a major increase of mitochondrial Ca^{2+} uptake (Figures 8 and 9), we hypothesized that mitochondria, in this specific condition, might buffer sarcoplasmic Ca^{2+} increase due to the absence of PV, thus acting as high capacity fixed buffers.

PV acute silencing and overexpression experiments in muscle fibers confirmed this hypothesis. In detail, to investigate in-depth the effect of PV expression on mitochondrial Ca^{2+} uptake and to exclude any possible *in vivo* compensatory effects

due to PV ablation during development in our knockout model, we performed PV silencing and overexpression on FDB of adult WT mice, and we monitored cytosolic Ca^{2+} transients and mitochondrial Ca^{2+} uptake.

In basal condition and upon caffeine stimulation, PV silencing did not influence cytosolic Ca^{2+} transient (Figure 12), while mitochondrial Ca^{2+} measurements in fibers where PV was silenced, confirmed what observed in our PV KO model. Indeed, while the basal $[Ca^{2+}]_{mt}$ was not affected by PV silencing (Figure 13A), a marked increase of caffeine-induced transients was detected in shPV-transfected fibers (Figure 13B). To further prove that mitochondria, in our KO model, are responsible for buffering $[Ca^{2+}]_{cyt}$ increases, we measured cytosolic Ca^{2+} transients treating the fibers with CCCP (the ionophore carbonilcyanide m-chlorophenylhydrazone) that abolishes mitochondrial Ca^{2+} uptake [24]. FDB muscle fibers, transfected with shPV and treated with CCCP, showed increased $[Ca^{2+}]_{cyt}$ compared to control fibers, re-enforcing the hypothesis that mitochondria of fibers lacking PV, both constitutively and transiently, adapt to buffer cytosolic Ca^{2+} transients (Figure 14).

The analysis of mitochondrial Ca^{2+} uptake in PV overexpressing fibers gave coherent results. Indeed, PV overexpression had a profound effect on mitochondrial Ca^{2+} uptake, causing a significant decrease of mitochondrial calcium uptake after caffeine treatment without affecting resting $[Ca^{2+}]_{mt}$ (Figure 15), while cytosolic Ca^{2+} transients in PV overexpressing fibers showed a significant decrease of $[Ca^{2+}]_{cyt}$ both in basal conditions and upon caffeine stimulation (Figure 16).

Overall, our results demonstrated that the effect of mitochondria on $[Ca^{2+}]_{cyt}$ is strictly correlated to PV expression and that mitochondria compensate for the lack of the main cytosolic buffer by preventing and restricting the spreading of Ca^{2+} signals due to the lack of PV.

In the sarcoplasm, the magnitude and kinetics of elevation and decay of $[Ca^{2+}]_{cyt}$ depend also from SR Ca^{2+} release [215]. To fully understand Ca^{2+} homeostasis in skeletal muscle fibers of PV KO animals, Ca^{2+} transients have been investigated also in the SR, the main Ca^{2+} store in skeletal muscle, that could, similarly to mitochondria, adapt to the lack of PV. Whereas SR free Ca^{2+} concentrations

[$[Ca^{2+}]_{SR}$] measured during resting conditions was indistinguishable in fibers lacking PV from the WT ones, the ablation of PV resulted in changes in intraluminal Ca^{2+} during electrical stimulation (Figure 17). Indeed, during electrical stimulation, a large drop in $[Ca^{2+}]_{SR}$ was measured in PV KO fibers, meaning that the SR of PV KO muscle fibers releases more Ca^{2+} than WT myofibers. Therefore, it can be excluded that the slowing of the relaxation phase reported for PV deficient muscles ([20] and our data) is due to changes in the Ca^{2+} release rate by the SR. A further confirmation also comes from the analysis of the SERCA activity, performed by Schwaller and co-workers [176]. Indeed, no significant difference was found in the activity of SERCA between WT and PV KO muscles [20,176]. Consistently, we found no difference in the mRNA levels of RyR1, the main Ca^{2+} releasing channel in muscle and in the expression of two different isoforms of SERCA (SERCA1 and SERCA2a). Moreover, since we observed an increased release of Ca^{2+} from the SR of PV KO fibers compared to WT, we analysed the expression levels of STIM1 and ORAI1, the two proteins responsible of store operated Ca^{2+} entry (SOCE), the mechanism that allows Ca^{2+} entry into the cytosol from the extracellular space [216,217]. Surprisingly, no difference was detected in mRNA expression levels between PV KO and WT (Figure 18). Furthermore, no difference was also detected on the expression of the two main SR Ca^{2+} buffers, Calsequestrin (CLSQ1) and Calreticulin (CLRT) (Figure 18), further confirming that the expression of proteins involved in Ca^{2+} homeostasis in the SR are not affected by PV deficiency.

Based on our findings, strongly suggesting that PV induces a compensatory response of mitochondrial Ca^{2+} uptake, we performed RT-qPCR to analyse the mRNA expression of the components of the MCU complex, the channel responsible for Ca^{2+} entry in mitochondria [4,5,22,23]. In PV KO TA muscles, the pore forming subunit MCU and the regulatory subunits MICU1, MICU1.1 and MICU2, but not that of other mitochondrial proteins not involved in Ca^{2+} homeostasis, were significantly upregulated compared to WT (Figure 19). This data suggest the activation of a precise transcriptional program, induced by the lack of PV, leading to the increase in mitochondrial Ca^{2+} carrying capacity (Figure 19).

To further prove that, in our PV KO model, mitochondria adapt to buffer cytosolic Ca^{2+} increases through an upregulation of the MCU complex components

expression, we performed MCU silencing experiments and we measured $[Ca^{2+}]_{cyt}$ evoked by caffeine treatment (Figure 23). While basal $[Ca^{2+}]_{cyt}$ was not affected by the absence of MCU both in WT and PV KO animals, MCU silencing in PV KO fibers resulted in a significant higher cytosolic Ca^{2+} accumulation upon stimulation (Figure 23). These results reinforce the hypothesis that, while in WT animals mitochondria do not significantly buffer $[Ca^{2+}]_{cyt}$, lack of PV induces compensatory effect on mitochondrial handling capacity.

Since we observed this complex crosstalk between PV expression levels and mitochondrial function, we asked whether PV ablation could also affect the morphology of mitochondria in skeletal muscle. Therefore, mitochondrial distribution and morphology on transversal and longitudinal sections of EDL muscles of WT and PV KO mice was performed using electron microscopy analysis (Figure 20). Quantification of TEM images revealed a strong alteration of mitochondrial ultrastructure in PV KO muscles, indicating that the lack of PV strongly affects mitochondrial morphology and distribution (Figure 20). In detail, mitochondria of PV KO appear more variable in shape and often longitudinally oriented between myofibrils compared to WT (Figure 20), suggesting a different distribution of the organelle in the muscular tissue. Consistently, the incidence of mitochondria placed at the A bands of the sarcomere is markedly increased in PV KO EDL fibers, both as in number per fiber area and percentage of total mitochondria (Figure 20 and Table I). Furthermore, as already observed by Schwaller and co-workers [196], the relative fiber volume occupied by mitochondria was also significantly increased in PV KO EDL fibers (Figure 20). In addition, the frequency of mitochondria profiles associated with the Calcium Release Units (CRUs), the sites of Ca^{2+} release during excitation contraction coupling [143], was higher in PV KO fibers.

It is interesting to note that the correlation between PV expression and mitochondria content and volume is not restricted to fast twitch muscle but has been shown in cerebellar Purkinje cells [218]. Indeed, Schwaller and co-workers demonstrated that in the GABAergic neurons of PV KO mice, the relative mitochondrial mass is increased by 40% and that mitochondria are located selectively to a peripheral region of 1.5 µm underneath the plasma membrane [18,218]. These mitochondria

have been proposed to act as “firewall” to prevent e restrict the spreading of Ca^{2+} signals from the plasma membrane to the nucleus, similarly to what observed in pancreatic acinar cells [113]. Intriguingly, other *in vivo* and *in vitro* studies have confirmed the regulation of PV expression and mitochondria volume. Indeed, in transgenic mice overexpressing PV in all neurons [219,220], in C2C12 myotubes [221] and in Madin-Darby canine kidney (MDCK) epithelial cells overexpressing PV [68], mitochondrial volume is reduced to nearly 40% compared to the WT samples. This strongly indicates that the regulation of PV and mitochondrial volume is strictly correlated.

We then asked which signaling pathways could be involved in the observed changes in mitochondrial volume and number. We first focused our attention on the expression of the peroxisome proliferator-activated receptor gamma co-activator (PGC-1α) and its positive regulator, the deacetylase SIRT1. PGC-1α is a crucial factor coordinating the activation of genes implicated in mitochondria biogenesis and fiber-type specificity [154]. In myotubes, SIRT1 is the main deacetylase of PGC-1α that positively regulates genes involved in fatty acid metabolism and in mitochondrial respiration [222]. Interestingly, in line with findings of Schwaller and co-workers [79], both PGC-1α and SIRT1 mRNA expression is induced in TA of PV KO mice, suggesting an increase of mitochondrial biogenesis in PV KO muscle tissue (Figure 21). The increase of PGC-1α expression level might justify the increase in mitochondrial number and volume in PV KO muscles.

In line with our findings, it has been demonstrated that in canine kidney cells (MDCK cells) overexpressing PV, mitochondrial mass is decreased by 40% compared to control and that increased PV expression resulted in lower PGC-1α transcript levels, suggesting that PV mediates changes in mitochondrial biogenesis impinging on the PGC-1 α pathway.[68,221]

In the future, we will analyse the activation of Ca^{2+}-dependent pathways in the regulation of mitochondrial biogenesis. Particular attention will be given to $Ca^{2+/}$calmodulin kinase α that is known to affect SIRT1 expression whose expression is increased in TA of PV KO muscles and on $Ca^{2+/}$calmodulin kinase II (CaMKII) that was found also up-regulated in TA of PV KO mice [79].

Since PV KO fibers display significant alteration of mitochondrial morphology, we investigated whether the signalling pathways involved in mitochondrial dynamics were also involved. Indeed, mitochondrial fusion and fission processes contribute to regulate mitochondrial volume density, controlling mitochondrial structural integrity [152,223]. Moreover, emerging evidences demonstrated that in skeletal muscle, functionally competent mitochondria are maintained by continuous organelle remodelling achieved by the breakdown of damaged components or even whole mitochondria accompanied by mitochondrial biogenesis [147,202]. To investigate whether mitochondrial dynamics is also influenced by PV ablation and to understand whether the observed increase of mitochondrial volume is also the result of an alteration in fusion/fission processes, we performed RT-qPCR on TA muscle of WT and PV KO mice of the genes involved in mitochondrial dynamics (Figure 22). In PV KO tissues, OPA1 and MFN2, were found to be up-regulated, while no significant difference was detected in the mRNA expression levels of DRP1 and FIS1 (Figure 22), suggesting that PV could influence the morphology of mitochondria in muscle fibers by inducing both mitochondrial biogenesis and mitochondrial fusion.

As discussed above, we observed that the time-to-peak and the half-relaxation time was increased in PV KO FDB fibers (Figures 6A and 6B) and that the volume of PV KO mitochondria was doubled compared to WT (Figure 20). Since these features are typically common of slow type fibers [205], we asked whether PV removal could also induce fiber type switching. To evaluate fiber composition of TA muscle sections from WT and PV KO animals, we performed immunocytochemistry assay using specific antibodies to discriminate between type I, IIA, and IIB fibers (Figure 24). Interestingly, no changes in fiber-type composition were detected in KO mice compared to WT muscles (Figure 24). Moreover, the mRNA levels of CALSQ1 and the expression of the slow isoform of SERCA, SERCA2a, did not change in PV KO muscles compared to WT (Figure 18), clearly demonstrating that signalling pathways linked to fiber specific isoforms are not regulated by PV.

Considering the evident alteration in mitochondrial morphology and Ca^{2+} handling capacity of PV KO muscles, we next evaluated muscle performance. The *in vivo*

analysis of the distance run on a treadmill during a single bout of uphill strenuous exercise, showed a significant increase in running performance of PV KO mice compared to WT (Figure 25). We hypothesize that lack of PV, by inducing an increase in mitochondrial volume and enhancing the mitochondrial handling capacity, could lead to an increase in muscle fatigue resistance in order to sustain muscle activity for prolonged periods (Figure 25). In agreement with our data, quantitative analysis of the mitochondrial proteins COX I, COX Vb and the F1-ATPase subunit β were found up-regulated in PV KO TA muscles by Schwaller and his collaborators [80]. These data suggest that, even if there are no changes in fiber type composition in PV KO muscles, PV KO mitochondria of fast twitch muscles resemble that of slow twitch fibers [80], characterized by low ATPase activity, high oxidative and low glycolytic capacity and increased resistance to fatigue [205].

Moreover, since ATP and phosphocreatine concentration are different between fast- and slow-twitch muscles [224,225], Schwaller and co-workers analysed also the ATP content in a resting muscle tissue [80]. They observed that the ATP levels in PV KO TA muscles were significantly lower than in WT TA [80], a common feature of slow-twitch muscle fibers [205,224]. Thus, these data suggest that PV ablation leads to a clear morphological and functional adaptation of mitochondria in skeletal muscle fibers.

Moreover, PV is one of the most downregulated “atrogenes”, the genes commonly up- and down-regulated during both disuse and systemic types of atrophy [25,26]. Considering that PV ablation induces a compensatory mechanism by increasing mitochondrial Ca^{2+} and that, as recently demonstrated, mitochondrial Ca^{2+} positively controls skeletal muscle trophism [17], we decided to study the role of PV on the regulation of muscle mass through denervation experiments. We chose this model since denervation induces a dramatic and fast decrease in muscle mass [41]. We collected the muscles after 3, 7 and 14 days after the cut of the nerve and we measured fiber size. Interestingly, upon denervation, PV KO muscles loose less muscle mass then WT muscles (Figure 23). Denervation for 14 days induced a 40% reduction of TA mean fiber size in WT animals. Notably, in the absence of PV, denervation-induced atrophy was reduced by only the 27%. (Figure 27).

These data were also confirmed by PV acute transfection experiments of adult muscles. Indeed, since the effect of PV ablation on denervated muscles was rather modest and the effect on innervated muscles was negligible, we either acutely silenced or overexpressed PV in adult WT mice by plasmid electroporation to exclude any developmental adaptation to the lack of PV. Interestingly, acute PV silencing leads to muscle hypertrophy (Figure 28) and, consistently, PV overexpression *in vivo* was sufficient to induce atrophy (Figure 29).

Overall, these data indicate that PV expression controls also muscle trophism. We next wondered what was the mechanism exerted by PV in the regulation of fiber size. We first checked the IGF1-AKT/PKB pathway, a major signalling pathway that positively controls protein synthesis and the hypertrophic growth of muscle [159,226]. We performed western blot analysis on denervated muscles of PV and WT mice on the total and the phosphorylated forms of some components of this pathway, but no significant differences were detected in PV KO animals compared to WT (Figure 30A and 30B).

We then focused our attention on PGC-1α4, an isoform of the transcriptional regulator of mitochondrial biogenesis PGC-1α, that was recently shown to induce muscle hypertrophy as adaptive response to exercise [28]. Analysis of the mRNA expression of PGC-1α4 on TA muscles of PV KO and WT TA (Figure 30C), demonstrated that PV ablation is sufficient to induce PGC-1α4 expression, suggesting the activation of this hypertrophic pathway. Our data are coherent with previous studies showing that mitochondrial Ca^{2+} positively regulates skeletal muscle mass by impinging on PGC-1α4 pathway [17]. Our hypothesis is that PV ablation, leading to an increase of mitochondrial Ca^{2+} uptake, activates mitochondrial Ca^{2+}-dependent pathways to control skeletal muscle trophism and to counteract denervation-induced atrophy. Future experiments will clarify at molecular levels how PV knockdown determine these effects on skeletal muscle homeostasis.

It is well established that impaired mitochondrial Ca^{2+} uptake is a typical feature of many skeletal muscle myopathies and neuromuscular diseases. Indeed, defective intracellular Ca^{2+} signalling is associated with degeneration of skeletal muscle cells

in aging [227,228] and in the pathogenesis of many muscular dystrophies [229–233]. In this context, it is fundamental to understand whether alterations in mitochondrial Ca^{2+}-buffering capacity contribute to muscle dysfunction under pathophysiological conditions. Through analysis of the PV KO model, it shall be possible to understand how mitochondria decode different stimuli in biological responses. By clarifying the role of mitochondria as integration points of different cytosolic Ca^{2+} signals, we believe that our research might be an important contribution for uncovering the molecular basis of chronic muscular diseases.

7. Materials and Methods

7.1 Legend of Abbreviation

bp = base pair;

BCA = Bicinchoninic acid assay;

BSA = albumin bovine serum;

BTS= myosin inhibitor

Ca^{2+} = calcium ions;

$CaCl_2$ = calcium chloride;

°C = centigrade;

CCCP = Carbonyl cyanide m-chlorophenyl hydrazine;

cDNA = complementary to DNA;

Ctrl= control;

DAPI = 4,6-diaminidino-2-phenylindole

DMEM = media for cell culture;

DMSO = Dimethyl sulfoxide, polar aprotic solvent;

dNTP = Deoxynucleotide tri-phosphate

DTT = Dithiothreitol

EDL = extensor digitorum longus;

FBS = foetal bovine serum;

FDB= Flexor digitorum brevis;

g = grams;

GFP= Green fluorescent protein;

HBS = Hepes buffer saline;

HCl = hydrochloric acid;

HEPES = 4-(2-hydroxyethyl)-1-piperazineethanesulfonic acid;

Hr: hour;

Hz = Hertz;

kb = kilobase;

KCl = potassium chloride;

KH_2PO_4 = potassium phosphate;

KO = knockout;

M = molar;

m = metres;

min = minutes;

ml = milliliters;

Mg^{2+}= Magnesium ions;

ms = milli seconds;

N = normal;

NaCaCo = Sodium cacodylate;

NaCl= Sodium chloride;

nm = nanometers;

o.n. = over night;

PCR = polymerase chain reaction;

RNA = ribonucleic acid

RT-qPCR = reverse transcriptase-polymerase chain reaction;

rpm = revolutions per minute;

RT = room temperature;

SDS = sodium dodecyl sulfate;

sec = seconds;

TA = tibialis anterior;

TEM = Transmission electron microscopy

PFA = paraformaldehyde;

PV = parvalbumin;SD = standard deviation;

SEM = standard error of the mean;

shRNA = short hairpin RNA;

SOC = Super Optimal broth with Catabolite repression;

µl = microliters;

WT = wild type.

7.2 Animals

In all experiments, adult C57/BL6J WT and PV KO male mice obtained in C57/BL6J strain were used. PV KO mice were generated in Schwaller laboratory

and disruption of the parvalbumin (PV) gene was obtained by homologous recombination [20].

PV KO mice were crossed with C57/BL6 WT mice. Crossing of the heterozygous animals yielded homozygous mice and WT littermates. The frequency of homozygous animals was not statistically different from the expected Mendelian transmission of autosomal gene. This therefore suggests that deletion of the functional PV gene is neither lethal to embryos nor significantly affects embryonic development. The three different genotypes (WT, PV KO and Heterozygous) were characterized by genotyping procedure with the following primers:

PV_FW: GCTGAGCTGTGCGCTGA

PV_REV: GGCTCCTATCGCCTTCTTGA

PGK-REV: CCGGTGGATGTGGAATGTGT

In vivo experiments were performed in accordance with the Italian law D. L.vo n.26/2014.

7.3 In vivo DNA transfection of mouse skeletal muscle

7.3.1 FDB muscle electroporation

Adult C57/BL6J, CD1 WT or PV KO male mice were used in all experiments. First, the animals were anesthetized with intraperitoneal injection of Zoletil - Sedaxilan mixture (an anaesthetic agent and a sedative agent respectively, 15mg/g i.p.). Hyaluronidase solution (2mg/mL) (Sigma) was injected under the hind limb footpads. After 30 minutes, 20 μg of plasmid DNA was injected with the same procedure of the hyaluronidase. After 10 min, one gold-plated acupuncture needle was placed under the skin at the level of the heel, and a second one at the base of the toes. The electrodes are oriented parallel to each other and perpendicular to the long axis of the foot. The electrodes were connected to the BTX porator (Harvard apparatus). The muscles were electroporated by applying 20 pulses, 20 ms each, 1

s of interval to yield an electric field of 100 V. Isolation of single fibers was carried out 7 days later.

7.3.2 TA muscles electroporation

Adult male CD1 mice were used in all experiments. First, animals were anesthetized with intraperitoneal injection of Zoletil - Sedaxilan mixture (15mg/g i.p.). 40 μg of plasmid DNA was injected along the TA muscle length externally. Gel G008 ECO & IPL, a transparent ultrasound gel, was then spread on the hind limb. Electric pulses were then applied by two stainless steel electrodes that were placed on each side of the hind limb (5 pulses, 200 ms each of 110 Volts) using a BTX porator (Harvard apparatus). Animals were allowed to recover for 7 days. Next, TA muscles were harvested and frozen in liquid nitrogen-cooled isopentane.

7.4 Denervation procedure

Right hind limbs of 3 months old CD1 mice or 3 months old WT and PV KO mice, were denervated cutting unilaterally the sciatic nerve. Animals were anesthetized by an intraperitoneal injection of Zoletil –Sedaxilan mixture (15mg/g i.p.) and then a small portion of sciatic nerve was chirurgical excised. The contralateral non-denervated hind limb served as an internal control in subsequent analyses, which were carried out 3, 7, or 14 days after the operation. This procedure does not affect the animal ability to ambulate. At the time point indicated, TA muscles were dissected from the denervated hind limbs, frozen in liquid nitrogen and stored at –80°C. The muscles were utilized for cryo-cross sectional area measurements, gene expression studies (see RNA extraction and RT-qPCR) and for protein analysis (see Western Blots procedures).

7.5 Mouse exercise studies

For muscle performance test, 2-month old mice were acclimated and trained on a 10% uphill LE8700 treadmill (Harvard apparatus) the day before the experiment. Mice of both genotype WT and PV KO, ran for 5 min at 8 m/min. The day after, mice were subjected to a single bout of running starting at the speed of 10 m/min.

Forty minutes later, the treadmill speed was increased at a rate of 1 m/min every 10 min for a total of 30 min, and then increased at the rate of m/min every 5 min until mice were exhausted. Exhaustion was defined as the point at which mice spent more than 5 sec on the electric shock grid without attempting to resume running. Total running time and total running distance were recorded for each mouse.

7.6 TEM Analysis

7.6.1 Preparation and analysis of samples for electron microscopy (EM)

EDL muscles were dissected, fixed at room temperature with 3.5% glutaraldehyde in 0.1 M NaCaCo buffer (pH 7.4), and kept at 4 °C in fixative until further use. Small bundles of fixed muscles were then post-fixed, embedded, stained and block, and sectioned as previously described [234]. For EM, ultrathin sections (~50 nm) were examined with a Morgagni Series 268D electron microscope (FEI Company, Brno, Czech Republic), equipped with Megaview III digital camera (Olympus Soft Imaging Solutions, Munster, Germany) and Soft Imaging System at 60 kV.

7.6.2 Quantitative analyses by EM

- Number of mitochondria and mitochondria-CRUs pairs/area were evaluated in micrographs taken from longitudinal sections at 14.000X of magnification and reported as average number/100μm^2 ([143] for additional detail). In each EM image, the mitochondrial positioning was also determined with respect to the I and A bands. If an individual mitochondrion extended from one I band to another, it was counted in both. In each sample, 10 fibers were analysed, and in each fiber 5 micrographs were randomly collected from non-overlapping regions.
- Mitochondrial volume was determined using the stereology point-counting technique [235,236] in micrographs taken from transversal sections at 8.900X of magnification. Briefly, after superimposing an orthogonal array of dots at a spacing of 0.20 μm to the electron micrographs, the ratio between the number of dots falling within mitochondrial profiles and the total number of dots covering the whole image was used to calculate the relative fiber volume occupied by mitochondria. In

each sample, 13-25 fibers were analysed. In each fiber 2 micrographs were randomly collected from non-overlapping regions.

- The average area of mitochondria was measured in 5 micrographs randomly collected from non –overlapping regions, as for the analysis of number of mitochondria. Soft Imaging System (Munster, Germany) provided with the electron microscope was used for analysis. Only mitochondria that were entirely visualized in the micrograph were measured. A total of 112 (WT) to 192 (PV KO) mitochondria areas were measured in each specimen and reported as average area (in $nm^2 \times 10^3$) ± SEM.

- Statistical analysis. Mean and SEM were determined using Microcal Origin 6.0 (Microcal Software, Inc.). Statistically significant differences between the control and PV KO groups were determined by the Student's t test (Microcal Origin 6.0; Microcal Software, Inc.) or by a Chi-squared test (Microsoft Office Excel 2007; Microsoft Corporation). Values of $p < 0.01$ were considered significant.

7.7 RNA extraction, reverse transcription, and quantitative realtime PCR (RT-qPCR)

Total RNA from TA EDL Soleus or FDB muscles was extracted trough mechanical tissue homogenization in TRIZOL reagent (Thermo Fisher Scientific), following manufacturer instructions. The RNA was quantified with Nanodrop (Thermo Fisher Scientific) and 1 µg, for each sample, and 500 ng of RNA, for each cellular sample, was retro-transcribed with the cDNA synthesis kit SuperScript II (Thermo Fisher Scientific), following manufacturer instructions. Oligo $(dT)_{12-18}$ primer (Thermo Fisher Scientific) was used as primer for first stand cDNA synthesis with reverse transcriptase together with dNTPs (Thermo Fisher Scientific), following manufacturer instructions. The obtained cDNA was analysed by RT-qPCR using the IQ5 thermocycler and SYBR green chemistry (Bio Rad), following manufacturer instructions. The primers were designed and analysed with Primer 3 and their efficiency was between 95 and 100%. The housekeeping genes as GAPDH, GRP75 or POL2 were used for cDNA normalization in cDNA samples derived from TA muscles of WT and PV KO animals. For quantification, expression levels were calculated by using the 2-ΔΔCT Method [237]. Primers for

RT-qPCR were used at the final concentration of 20 μM and the sequences are reported in the table below:

Gene	Forward	Reverse
CALRETICULIN	5'- AGGCTCCTTGGAGGATGATT-3'	5'- TCCCACTCTCCATCCATCTC-3'
CALSEQUESTRIN 1	5'- GAGCCTATGACCATCCCAGA- 3'	5'- GTCGGGGTTCTCAGTGTTGT-3'
COX IV	5'-CTACTTCGGTGTGCCTTGA-3'	5'-ACATCAGGCAAGGGGTAGTC-3'
DRP1	5'-GTTCCACGCCAACAGAATAC-3'	5'-CCTAACCCCCTGAATGAAGT-3'
EMRE	5'-GGACTCTGGGCTCTTGTCAC-3'	5'-AGAACTTCGCTGCTCTGCTT-3'
FIS1	5'- AAGTATGTGCGAGGGCTGT-3'	5'-TGCCTACCAGTCCATCTTTC-3'
GAPDH	5'-CACCATCTTCCAGGAGCGAG-3'	5'-CCTT T ATGGTGGTGAAGAC-3'
MCU	5'- AAAGGAGCCAAAAAGTCACG-3'	5'- AACGGCGTGAGTTACAAACA-3'
MCUb	5'-CTGGCTTACTTGGTGGGTGT-3'	5'-CGCTGCGATTTCTTGTGGAA-3'
MICU1	5'- AAGGCAGCATCTTCTACAGCC-3	5'- CCTGCTCAAACTCCTCCATGT-3'
MICU1.1	5'-CTTTGATGGAAAGGAGTTCTGGC-3'	5'-CCTCCATGTCTACCTCTCCGT-3'
MICU2	5'- TGGAGCACGACGGAGAGTAT-3'	5'- GCCAGCTTCTTGACCAGTGT-3'
MICU3	5'-CGACCTTCAAATCCTGCCTG-3'	5'-TCTGCGTGCTCTGACCTTAC-3'
MITOFUSIN 2	5'-ATGTTACCACGGAGCTGGAC-3'	5'-AACTGCTTCTCCGTCTGCAT-3'
OPA1	5'-ATACTGGGATCTGCTGTTGG-3'	5'-AAGTCAGGCACAATCCACTT-3'
ORAI1	5'- AAGCCGCGCCAAGCTCAAAG-3'	5'-GGTGGGTAGTCATGGTCTGTGTCCAG-3'
PGC-1α	5'- CGCTGCTCTTGAGAATGGAT-3'	5'- CGCAAGCTTCTCTGAGCTTC-3'
PGC-1α4	5'- TCACACCAAACCCACAGAAA-3'	5'- CTGGAAGATATGGCACAT -3'
POL2	5'-CGACGACTTTGATGACGTTG-3'	5'-GCTCACCAGATGGGAGAATC-3'
PV	5'-GATAGGAGCCTTTGCTGCTG-3'	5'-GCCAGAAGCGTCTTTGTTTC-3'
RYR2	5'-GGTCTGATTATTGATGCTTTTGGGG-3'	5'-TGGTCTCCATGTCTTCCTTCACTTG-3'
SERCA1	5'-GGCCTCATGTCAGCTACCATCAGC-3'	5'-TCGGGGGCCTCAAAGACCTC-3'
SERCA2a	5'-ATGGGGCTCCAACGAATTGC-3	5'-GCCAAAACGAAAGATATACATGCTGC-3'
SIRT1	5'-TTTTAAGGCTGTTGGTTCCAG-3'	5'-TACCTCAGCACCGTGGAATA-3'
STIM 1	5'-GGTGATGTGGATGTGGAAGAAAGTG-3	5'-ACAGGTCCTCCACGCTGATAAGC-3'
TOM 20	5'-CTGACAAATGCCATTGCTGT-3'	5'-CACATCATCTTCAGCCAAGC-3'

7.8 Western blotting and Antibodies

To monitor protein levels, frozen muscles were pulverized by means of Qiagen Tissue Lyser and protein extracts were prepared in a lysis buffer. This buffer contains 50 mM Tris pH 7.5, 150 mM NaCl, 5 mM $MgCl_2$, 1 mM DTT, 10% glycerol, 2% SDS, 1% Triton X-100, Roche Complete Protease Inhibitor Cocktail, 1 mM PMSF, 1 mM $NaVO_3$, 5 mM NaF and 3 mM β-glycerophosphate. 40 μg of total proteins were loaded, according to BCA quantification. Proteins were separated by SDS-PAGE electrophoresis, in commercial 4-12% acrylamide gels (Thermo Fisher Scientific) and transferred onto nitrocellulose membranes (Thermo Fisher Scientific) by semi-dry or wet electrophoretic transfer. Blots were blocked for 1 hr at RT with 5% non-fat dry milk (Bio-Rad) in TBS-tween buffer (0.5 M Tris, 1.5 M NaCl, 0.01% Tween) and incubated at 4°C with the primary antibodies. Secondary antibodies were incubated 1 hr at RT. The following antibodies were used: α-phosphoAKT (1:1000, Cell Signaling), α-Akt Pan (1:1000, Cell Signaling) α-Actin (1:10000, Santa Cruz), α-Calsequestrin1 (1:1000 Invitrogen), α-IP3R pan I/II/III (1:2000, Santa Cruz), α-GRP75 (1:5000, Santa Cruz), α-PV (1:10000, Abcam), α-RyR1 (1:2000, Invitrogen).
Secondary HRP-conjugated antibodies were purchased from Bio-Rad and used at 1:5000 dilution.

7.9 Fiber size measurements

20 μm-thick muscle cryo-sections of TA muscles from CD1 mice or from denervated and contralateral hind limbs of WT and PV KO animals were fixed in 4% PFA for 20 min. Next, the slides were quenched with 50 mM NH_4Cl in PBS and blocked in PBS containing 0.5% BSA for 20 min, as already described [17]. Sections were then incubated with α-laminin primary antibody (Sigma-Aldrich) at the dilution of 1:100 in PBS with 0,5% BSA o.n. at 4° C to label the sarcolemma of muscle fibers. Muscle cryosections were washed 3 times with PBS. The sections were then incubated for 1 hr at r.t. with an α-rabbit Alexa Fluor 488-conjugated secondary antibody (Thermo Fisher Scientific) at the dilution of 1:500 in PBS with 0.5% BSA. Nuclei were identified by Hoechst 33342 (Sigma-Aldrich). Tissue sections were then mounted with aqueous mounting media Mowiol (Sigma

Aldrich). CSA was manually measured by using ImageJ software. More than 1000 fibers were measured for each muscle.

7.10 Single myofibers culture

For real-time imaging, FDB fibers were isolated 7 days after *in vivo* transfection. Muscles were digested in collagenase A (4 mg/ml) (Roche) dissolved in Tyrode's salt solution (pH 7.4) (Sigma-Aldrich), containing 10% FBS (Thermo Fisher Scientific). Single fibers were isolated, plated on laminin-coated glass coverslips and cultured in DMEM with HEPES (Thermo Fisher Scientific), supplemented with 10% FBS, containing penicillin (100 U/ml), streptomycin (100 µg/ml). Fibers were maintained in culture at 37°C with 5% CO^2.

7.11 Real time imaging of mitochondrial Ca^{2+} in FDB fibers

FDB muscles were electroporated with a plasmid encoding 4mtGCaMP6f [15,118,125,183]. The probe is composed by GFP circularly permutated protein in which the amino and the carboxyl portions had been interchanged and reconnected by calmodulin (CaM) and the M13 domain of the myosin light chain kinase [183]. This allows that, at low [Ca^{2+}] the circularly permuted GFP exits in a poorly fluorescent state that increases after CaM Ca^{2+} binding and protein structural shift [183]. This fluorescent protein presents an isosbestic point (410 nm) in the excitation spectrum of the fluorescent protein, where emission is not Ca^{2+}-dependent [183]. We exploited this property to normalize the traces for the probe expression. Therefore, the ratio between the excited fluorescence at 470 nm and 410 nm wavelengths is proportional to $[Ca^{2+}]_{mt}$ but independent of the probe expression.

After single fibers isolation, real time imaging was performed. During the experiments, myofibers were maintained in Krebs-Ringer modified buffer (135 mM NaCl, 5 mM KCl, 1 mM $MgCl_2$, 20 mM HEPES, 1 mM $MgSO_4$,0.4 mM KH_2PO_4, 1 mM $CaCl_2$, 5.5 mM glucose, pH 7.4) at r.t., in presence of 75 µM N-benzyl-P-toluenesulfonamide (BTS, Sigma-Aldrich) to avoid fiber contraction. 10 mM caffeine (Sigma-Aldrich) was added to elicit Ca^{2+} release from the intracellular

stores. Experiments were performed on a Zeiss Axiovert 200 microscope equipped with a 40×/1.3 N.A. PlanFluor objective.

Excitation was performed with a DeltaRAM V high-speed monochromator (Photon Technology International) equipped with aW xenon arc lamp. Images were captured with a high-sensitivity Evolve 512 Delta EMCCD (Photometrics). The system is controlled by MetaMorph 7.5 (Molecular Devices) and was assembled by Crisel Instruments.

Exposure time was set to 50 ms and acquisition was performed at binning 1 with 200 of EM gain. Image analysis was performed with Fiji distribution of the ImageJ software [238]. Data are expressed as F/F_0 where F_0 is the mean intensity at the beginning of the experiments.

To study mitochondrial calcium uptake under physiological condition, fibers were electrically stimulated with trains at high frequency (60 Hz, 2 sec). Master-8 pulsing stimulator (A.M.P.I, Jerusalem, Israel) was used to induce electrical stimulations and the Master-8 software was used to control stimulation parameters (number of pulses per train, pulse duration and interval time) in accordance with experiments. To induce tetanic stimulation (60 Hz) the following parameters were set: number of pulses (M) 120, pulse duration (D): 5 ms, interval time (I): 5 ms.

7.12 FRET-based SR Ca^{2+} measurement

To evaluate SR Ca^{2+} content and dynamics, we took advantage of the SR-targeted Cameleon D4ER [189]. This sensor locates in the SR thanks to the signal sequence of human calreticulin fused to CFP (Cyan Fluorescent protein donor), whilst SR retention sequence is attached to the C-terminus of citrine, a Yellow Fluorescent Protein (YFP), that has been chosen as acceptor. The two chromophores are linked through calmodulin (CaM) and a peptide ligand derived from skeletal muscle light chain kinase (M13). Ca^{2+} binds to M13 and enable CaM to wrap around the M13 peptide shortening the distances between chromophores and thus enhancing FRET efficacy. The fluorescence YFP/CFP ratio depends on Ca^{2+} concentration [189,239].

To evaluate SR Ca^{2+} dynamics, fibers were electrically stimulated with a pulse of 60Hz. For FRET-based measurements, two images were collected simultaneously:

a direct CFP image and a FRET image (YFP emission upon CFP excitation). Images were acquired on a Nikon Eclipse Ti inverted microscope equipped with a 40x/1.3 N.A.S Fluor objective. Excitation was performed with an OptoScan monochromator (Cairn Research), equipped with a 150W Xenon Arc lamp. Images were captured with a sCMOS Zyla 4.2plus camera (Andor). The microscope is endowed with a motorized dichroic turret. Dual-pass dichroic mirror, which allows at least two wavelengths to pass selectively; beam splitter, composed of emission filters HQ 480/40 M (for ECFP) and HQ 535/30 M (for YFP variants), allows the simultaneous collection of at least two (dual-view) emission wavelengths. Filter and dichroic used were from Cairn Research (Cairn Research Graveney Road, Faversham, UK) and a microscopy filter cube was used with pre-installed fluorescent filters. Exposure time of image capture was 250 ms without interval.
The system is controlled by NIS-Elements (Nikon) a software that allows monitoring of the experiment progress in real time.
Quantification of FRET measurements was performed using ImageJ software. TIFF files were imported into ImageJ and analysed. The background signal was subtracted and a FRET ratio image was obtained by calculating background-subtracted acceptor (YFP) intensities divided by background-subtracted donor (CFP) intensities (YFP/CFP), which directly correlates to the level of Ca^{2+} present in SR. Electrically induced release of calcium from the SR was achieved by electrical stimulation trains at high frequency (60 Hz, 2 sec), as described in 7.11.

7.13 Cytosolic Ca^{2+} measurements

Fibers were dissected and loaded with 2 μM Fura-2/AM (Thermo Fisher Scientific) diluted in Krebs-Ringer modified buffer (described above) containing 0.02% pluronic acid for 20 min at 37°C and then washed with Krebs-Ringer modified buffer in presence of 75 μM N-benzyl-P-toluenesulfonamide (BTS, Sigma-Aldrich) to avoid the fiber contraction. 10 mM caffeine (Sigma-Aldrich) was added to elicit Ca^{2+} release from intracellular stores. In the indicated experiments, CCCP (10 μM) was co-administered with caffeine. This molecule abolishes mitochondrial Ca^{2+} uptake by collapsing the mitochondrial proton gradient and thus by dissipating the electrochemical potential across the inner membrane, which provides the driving

force for mitochondrial Ca^{2+} import. Experiments were performed on a Zeiss Axiovert 200 microscope equipped with a 40×/1.3 N.A. PlanFluor objective. Excitation was performed with a DeltaRAM V high-speed monochromator (Photon Technology International) equipped with a 75 W xenon arc lamp. Images were captured with a high-sensitivity Evolve 512 Delta EMCCD (Photometrics). The system is controlled by MetaMorph 7.5 (Molecular Devices) and was assembled by Crisel Instruments. Images were collected by alternatively exciting the fluorophore at 340 and 380 nm and fluorescence emission recorded through a 515/30 nm band-pass filter (Semrock). Exposure time was set to 50 ms. Acquisition was performed at binning 1 with 200 of EM gain. Image analysis was performed with Fiji distribution of the ImageJ software. Images were background subtracted. Changes in fluorescence (340/380 nm ratio) were expressed as R/R0, where R is the ratio at time t and R0 is the ratio at the beginning of the experiment.
To study Ca^{2+} release under physiological condition of contractile activity, fibers were electrically stimulated with trains of pulses at 0.5 H (0.5 Hz, 20 sec) or stimulated with trains at higher frequency (60 Hz, 2 sec), as described in 7.11.

7.14 Immunofluorescence analysis

For fiber type measurements, 20 μm thick cryosections were blocked in M.O.M. working solution (Vector Laboratories), following manufacturer instructions. Sections were then incubated with primary antibody α-SC-71 (Hybridoma bank) 1:100 in 0.5% BSA in PBS to label the type IIA myosins for 1 hr at 37°C and washed 3 times in PBS. Alexa Fluor 488 conjugated secondary antibody (Life Technologies) was used. Then, sections were incubated with primary antibody α-BF-F3 (Hybridoma bank) 1:100 in 0.5% BSA in PBS to label the type IIB myosins for 1 hr at 37°C and washed 3 times in PBS. Alexa Fluor 555 conjugated secondary antibody (Life Technologies) was used. Finally, sections were then incubated with primary antibody α-BAD5 (Hybridoma bank) 1:100 in 0.5% BSA in PBS to label the type I myosins for 1 hr at 37°C and washed 3 times in PBS. Alexa Fluor 647 conjugated secondary antibody (Thermo Fisher Scientific) was used. Sections then were mounted with the glycerol-based (antifade) mounting media ProLongs (Thermo Fisher Scientific) that prevents photo-bleaching and preserves the signals

of fluorescently labelled target molecules for long-term storage and analysis. Fiber type analyses were performed with the Fiji distribution of ImageJ

7.15 Confocal microscopy

Samples were imaged using a confocal microscope (Leica TCS SP5, Leica microsystems, Germany), equipped with 40X 1.4NA and 63X, 1.4NA oil immersion objectives. The microscope is equipped with four different laser lines for excitation (405 nm, 488 nm, 561 nm and 633 nm) and three tenable emission filters. Images were digitally acquired and stored in a PC station, and analysis was performed using the image analysis software ImageJ.

7.16 Cell culture and transfection

Hela cells were cultured in DMEM (Thermo Fisher Scientific) supplemented with FBS (Thermo Fisher Scientific) containing penicillin (100 U/ml) and streptomycin (100 μg/ml). Cells were transfected with a standard Ca^{2+} phosphate procedure, as previously performed [240]. Briefly, the solution containing the desired amount of DNA and 250 mM $CaCl_2$ was added quickly to an equal volume of HBS. The solution was added directly to the cell; 8-16 hours later, cells were washed on PBS until the excess of precipitate was completely removed. Experiments were carried out 24-36 hr after transfection. Empty vectors (mCherry, Ctrl) were used as control in all overexpression experiment and a non-targeting shRNA (shLUC) was used as control in the silencing experiments.

7.17 shRNA and constructs.

Three potential targeting sites on PV cDNA sequence were selected by the absence of BLAST matches, absence of overlap with a region of SNP and absence of multiple binding target within the gene. We used as control a shRNA that targets the luciferase gene (shLUC). The plasmid containing the shLUC and shPV expresses also mCherry fluorescent protein under the control of CMV promoter. The red fluorescent protein was used visualize the shRNA efficacy of transfection in *vitro* in HeLa cells and to visualize the transfected fibers in *vivo.*

The selected functional shRNA for PV was as follows:

shRNA_PV

Fw:

5'GATCG**AGAACCCGGATGAGGTGAAGA**TTCAAGAGA**TCTTCACCTCATCCGGGTTCT**TTTTTT G 3'

Rv:

3'AATTCAAAAAAGAACCCGGATGAGGTGAAGATCTCTTGAATCTTCACCTCATCCGGGTTCTC 5'

The expression of multiple polypeptides from a single mRNA is made possible by inclusion of a short viral 2A self-cleaving peptide coding sequence. The 2A peptide is a short peptide sequence that mediates a ribosome-skipping event and yields generation of multiple separate peptide products from one mRNA [185][186]. This novel method allows to co-express the gene of interest along with a reporter, such as a fluorescence gene or a resistance gene [187]. Thus, this plasmids ensure that any cells that are positive for the fluorescent protein should also be expressing the gene since they are both derived from the same transcript.

For **PV overexpression** in muscle fibers, pmCherry-P2A-N1 was obtained from pmCherry-N1 (Clonotech) by cloning in frame the P2A sequence (GSGATNFSLLKQAGDVEENPGP) to the N-end of mCherry.

Fw:

5'GATCCAGGTTCCGGCGCAACAAACTTCTCTCTGCTGAAACAAGCCGGAGATGTCGAAGAGAA TCCTGGACCG 3'

Rv:

5'GGCCCGGTCCAGGATTCTCTTCGACATCTCCGGCTTGTTTCAGCAGAGAGAAGTTTGTTGCGC CGGAACCTG 3'

The aligned oligos were cloned into BamHI and AgeI sites of pmCherry in frame with mCherry coding sequence.

For cloning PV-Flag in pmCherry-P2A:

Parvalbumin-Flag

Fw: 5' AATTTGGATCCGCCACCATGTCGATGACAGACGTGCT 3'

Rev:

3'CCACTCTGGTGGCTGAAAGCGATTACAAGGATGACGACGATAAGTAACTCGAGAATTT 5

Rc:

5' AAATTCTCGAGTTACTTATCGTCGTCATCCTTGTAATCGCTTTCAGCCACCAGAGTGG 3'

The PCR fragment were cloned into XhoI and BamHI sites in pmCherry-P2A-N1. Thanks to the P2A self-cleaving peptide between PV coding sequence and mCherry, PV overexpressing fibers displays mCherry fluorescence in the cytoplasm, as previously reported [187]. In mitochondrial Ca^{2+} handling experiments, FDB muscle fibers were co-transfected with the plasmid expressing PV and the mitochondrial Ca^{2+} probe. Only fibers positive for both 4mtGCaMP6f and mCherry were analysed.

7.18 Statistical analysis

All in *vitro* experiments were replicated at least three times and at least three animals for each condition were used for in *vivo* analyses. For data analysis, Excel® and GraphPad Prism® were used. Statistical data are presented as mean ± SD, unless otherwise specified. Depending on the experiments, a parametric Student's t test (two-tailed, unpaired), one way ANOVA with Dunnett's or Turkey's multiple comparison test and two-way ANOVA with Bonferroni post hoc test were applied. $p < 0.05$ was considered significant.

8. References

[1] M.J. Berridge, M.D. Bootman, H.L. Roderick, Calcium signalling: Dynamics, homeostasis and remodelling, Nat. Rev. Mol. Cell Biol. 4 (2003) 517–529. doi:10.1038/nrm1155.

[2] M.D. Bootman, T.J. Collins, C.M. Peppiatt, L.S. Prothero, L. MacKenzie, P. De Smet, M. Travers, S.C. Tovey, J.T. Seo, M.J. Berridge, F. Ciccolini, P. Lipp, Calcium signalling - An overview, Semin. Cell Dev. Biol. 12 (2001) 3–10. doi:10.1006/scdb.2000.0211.

[3] B. Schwaller, The Regulation of a Cell's Ca2+ Signaling Toolkit: The Ca2+ Homeostasome, in: Springer, Dordrecht, 2012: pp. 1–25. doi:10.1007/978-94-007-2888-2_1.

[4] R. Rizzuto, D. De Stefani, A. Raffaello, C. Mammucari, Mitochondria as sensors and regulators of calcium signalling., Nat. Rev. Mol. Cell Biol. 13 (2012) 566–78. doi:10.1038/nrm3412.

[5] C. Mammucari, A. Raffaello, D. Vecellio Reane, G. Gherardi, A. De Mario, R. Rizzuto, Mitochondrial calcium uptake in organ physiology: from molecular mechanism to animal models, Pflügers Arch. - Eur. J. Physiol. (2018) 1165–1179. doi:10.1007/s00424-018-2123-2.

[6] E. Carafoli, The fateful encounter of mitochondria with calcium: How did it happen?, Biochim. Biophys. Acta - Bioenerg. 1797 (2010) 595–606. doi:10.1016/J.BBABIO.2010.03.024.

[7] M. Montero, M.T. Alonso, E. Carnicero, I. Cuchillo-Ibáñez, A. Albillos, A.G. García, J. García-Sancho, J. Alvarez, Chromaffin-cell stimulation triggers fast millimolar mitochondrial Ca2+ transients that modulate secretion, Nat. Cell Biol. 2 (2000) 57–61. doi:10.1038/35000001.

[8] A. Rasola, P. Bernardi, Mitochondrial permeability transition in Ca 2+-dependent apoptosis and necrosis, Cell Calcium. 50 (2011) 222–233. doi:10.1016/j.ceca.2011.04.007.

[9] S. Feno, G. Butera, D. Vecellio Reane, R. Rizzuto, A. Raffaello, Crosstalk between Calcium and ROS in Pathophysiological Conditions, Oxid. Med. Cell. Longev. 2019 (2019) 1–18. doi:10.1155/2019/9324018.

[10] B. Glancy, W.T. Willis, D.J. Chess, R.S. Balaban, Effect of calcium on the oxidative phosphorylation cascade in skeletal muscle mitochondria., Biochemistry. 52 (2013) 2793–809. doi:10.1021/bi3015983.

[11] E.J. Griffiths, G.A. Rutter, Mitochondrial calcium as a key regulator of mitochondrial ATP production in mammalian cells, Biochim. Biophys. Acta - Bioenerg. 1787 (2009) 1324–1333. doi:10.1016/J.BBABIO.2009.01.019.

[12] A.R. Díaz-Vegas, A. Cordova, D. Valladares, P. Llanos, C. Hidalgo, G. Gherardi, D. De Stefani, C. Mammucari, R. Rizzuto, A. Contreras-Ferrat, E. Jaimovich, Mitochondrial Calcium Increase Induced by RyR1 and IP3R Channel Activation After Membrane Depolarization Regulates Skeletal Muscle Metabolism., Front. Physiol. 9 (2018) 791. doi:10.3389/fphys.2018.00791.

[13] F. Fieni, S.B. Lee, Y.N. Jan, Y. Kirichok, Activity of the mitochondrial calcium uniporter varies greatly between tissues., Nat. Commun. 3 (2012) 1317. doi:10.1038/ncomms2325.

[14] X. Pan, J. Liu, T. Nguyen, C. Liu, J. Sun, Y. Teng, M.M. Fergusson, I.I. Rovira, M. Allen, D.A. Springer, A.M. Aponte, M. Gucek, R.S. Balaban, E. Murphy, T. Finkel, The physiological role of mitochondrial calcium revealed by mice lacking the mitochondrial calcium uniporter., Nat. Cell Biol. 15 (2013) 1464–72. doi:10.1038/ncb2868.

[15] D. Vecellio Reane, F. Vallese, V. Checchetto, L. Acquasaliente, G. Butera, V. De Filippis, I. Szabò, G. Zanotti, R. Rizzuto, A. Raffaello, A MICU1 Splice Variant Confers High Sensitivity to the Mitochondrial Ca2+ Uptake Machinery of Skeletal Muscle, Mol. Cell. 64 (2016) 760–773. doi:10.1016/j.molcel.2016.10.001.

[16] G. Gherardi, L. Nogara, S. Ciciliot, G.P. Fadini, B. Blaauw, P. Braghetta, P. Bonaldo, D. De Stefani, R. Rizzuto, C. Mammucari, Loss of mitochondrial

calcium uniporter rewires skeletal muscle metabolism and substrate preference, Cell Death Differ. 26 (2019) 362–381. doi:10.1038/s41418-018-0191-7.

[17] C. Mammucari, G. Gherardi, I. Zamparo, A. Raffaello, S. Boncompagni, F. Chemello, S. Cagnin, A. Braga, S. Zanin, G. Pallafacchina, L. Zentilin, M. Sandri, D. DeStefani, F. Protasi, G. Lanfranchi, R. Rizzuto, D. De Stefani, F. Protasi, G. Lanfranchi, R. Rizzuto, D. De Stefani, F. Protasi, G. Lanfranchi, R. Rizzuto, D. De Stefani, F. Protasi, G. Lanfranchi, R. Rizzuto, D. De Stefani, F. Protasi, G. Lanfranchi, R. Rizzuto, The mitochondrial calcium uniporter controls skeletal muscle trophism in vivo., 2015. doi:10.1016/j.celrep.2015.01.056.

[18] B. Schwaller, M. Meyer, S. Schiffmann, "New" functions for "old" proteins: The role of the calcium-binding proteins calbindin D-28k, calretinin and parvalbumin, in cerebellar physiology. Studies with knockout mice, The Cerebellum. 1 (2002) 241–258. doi:10.1080/147342202320883551.

[19] B. Schwaller, The continuing disappearance of "pure" Ca2+ buffers, Cell. Mol. Life Sci. 66 (2009) 275–300. doi:10.1007/s00018-008-8564-6.

[20] B. Schwaller, J. Dick, G. Dhoot, S. Carroll, G. Vrbova, P. Nicotera, D. Pette, A. Wyss, H. Bluethmann, W. Hunziker, M.R. Celio, Prolonged contraction-relaxation cycle of fast-twitch muscles in parvalbumin knockout mice, Am. J. Physiol. Physiol. 276 (1999) C395–C403. doi:10.1152/ajpcell.1999.276.2.C395.

[21] B. Schwaller, Cytosolic Ca2+ Buffers, Cold Spring Harb. Perspect. Biol. 2 (2010) a004051–a004051. doi:10.1101/cshperspect.a004051.

[22] D. De Stefani, M. Patron, R. Rizzuto, Structure and function of the mitochondrial calcium uniporter complex, Biochim. Biophys. Acta - Mol. Cell Res. 1853 (2014) 2006–2011. doi:10.1016/j.bbamcr.2015.04.008.

[23] C. Mammucari, A. Raffaello, D. Vecellio Reane, R. Rizzuto, D. Vecellio-Reane, R. Rizzuto, Molecular structure and pathophysiological roles of the Mitochondrial Calcium Uniporter, Biochim. Biophys. Acta - Mol. Cell Res.

1863 (2015) 2457–2464. doi:10.1016/j.bbamcr.2016.03.006.

[24] S. Vaur, P. Sartor, L. Dufy-Barbe, Calcium Store Depletion Induced by Mitochondrial Uncoupling in Prostatic Cells, 2000.

[25] J.M. Sacheck, J.-P.K. Hyatt, A. Raffaello, R.T. Jagoe, R.R. Roy, V.R. Edgerton, S.H. Lecker, A.L. Goldberg, Rapid disuse and denervation atrophy involve transcriptional changes similar to those of muscle wasting during systemic diseases, FASEB J. 21 (2006) 140–155. doi:10.1096/fj.06-6604com.

[26] S.H. Lecker, Multiple types of skeletal muscle atrophy involve a common program of changes in gene expression, FASEB J. 18 (2004) 39–51. doi:10.1096/fj.03-0610com.

[27] M. a Egerman, D.J. Glass, Signaling pathways controlling skeletal muscle mass., Crit. Rev. Biochem. Mol. Biol. 49 (2014) 59–68. doi:10.3109/10409238.2013.857291.

[28] J.L. Ruas, J.P. White, R.R. Rao, S. Kleiner, K.T. Brannan, B.C. Harrison, N.P. Greene, J. Wu, J.L. Estall, B.A. Irving, I.R. Lanza, K.A. Rasbach, M. Okutsu, K.S. Nair, Z. Yan, L.A. Leinwand, B.M. Spiegelman, A PGC-1α Isoform Induced by Resistance Training Regulates Skeletal Muscle Hypertrophy, Cell. 151 (2012) 1319–1331. doi:10.1016/j.cell.2012.10.050.

[29] M.J. Berridge, P. Lipp, M.D. Bootman, The Versatility and universality of calcium signalling, 1 (2000).

[30] S. Ringer, A further Contribution regarding the influence of the different Constituents of the Blood on the Contraction of the Heart, J. Physiol. 4 (1883) 29–42. doi:10.1113/jphysiol.1883.sp000120.

[31] L. V. Heilbrunn, F.J. Wiercinski, The action of various cations on muscle protoplasm, J. Cell. Comp. Physiol. 29 (1947) 15–32. doi:10.1002/jcp.1030290103.

[32] A. Weber, On the role of calcium in the activity of adenosine 5’-triphosphate hydrolysis by actomyosin., J. Biol. Chem. 234 (1959) 2764–9.

http://www.ncbi.nlm.nih.gov/pubmed/13843278.

[33] E.B. Ridgway, C.C. Ashley, Calcium transients in single muscle fibers, Biochem. Biophys. Res. Commun. 29 (1967) 229–234. doi:10.1016/0006-291X(67)90592-X.

[34] S. Ebashi, M. Endo, I. Otsuki, Control of muscle contraction., Q. Rev. Biophys. 2 (1969) 351–84. http://www.ncbi.nlm.nih.gov/pubmed/4935801.

[35] M.D. Bootman, K. Rietdorf, H. Hardy, Y. Dautova, E. Corps, C. Pierro, E. Stapleton, E. Kang, D. Proudfoot, Calcium Signalling and Regulation of Cell Function, ELS. (2012). doi:10.1002/9780470015902.a0001265.pub3.

[36] D.E. Clapham, Calcium Signaling, Cell. 131 (2007) 1047–1058. doi:10.1016/j.cell.2007.11.028.

[37] A. Raffaello, C. Mammucari, G. Gherardi, R. Rizzuto, Calcium at the Center of Cell Signaling: Interplay between Endoplasmic Reticulum, Mitochondria, and Lysosomes, Trends Biochem. Sci. 41 (2016) 1035–1049. doi:10.1016/j.tibs.2016.09.001.

[38] S. Winegrad, Intracellular Calcium Movements of Frog Skeletal Muscle during Recovery from Tetanus, J. Gen. Physiol. 51 (1968) 65–83. doi:10.1085/jgp.51.1.65.

[39] S.M. Baylor, S. Hollingworth, Intracellular calcium movements during excitation–contraction coupling in mammalian slow-twitch and fast-twitch muscle fibers, J. Gen. Physiol. 139 (2012) 261–272. doi:10.1085/jgp.201210773.

[40] P. Novák, T. Soukup, Calsequestrin Distribution, Structure and Function, Its Role in Normal and Pathological Situations and the Effect of Thyroid Hormones, Physiol. Acad. Sci. Czech Republic, v. v. I. 60 (2011) 439–452.

[41] M. Michalak, E.F. Corbett, N. Mesaeli, K. Nakamura, M. Opas, Calreticulin: one protein, one gene, many functions., Biochem. J. 344 Pt 2 (1999) 281–92. http://www.ncbi.nlm.nih.gov/pubmed/10567207.

[42] M.J. Berridge, Inositol trisphosphate and calcium signalling., Nature. 361 (1993) 315–325. doi:10.1038/361315a0.

[43] M. Schmidt, P.A. Oude Weernink, F. vom Dorp, M.B. Stope, K.H. Jakobs, Mammalian phospholipase C, Adv. Mol. Cell Biol. 33 (2003) 431–450. doi:10.1016/S1569-2558(03)33021-8.

[44] J.T. Lanner, D.K. Georgiou, A.D. Joshi, S.L. Hamilton, Ryanodine Receptors: Structure, Expression, Molecular Details, and Function in Calcium Release, Cold Spring Harb. Perspect. Biol. 2 (2010) a003996. doi:10.1101/CSHPERSPECT.A003996.

[45] J. Lytton, M. Westlin, S.E. Burk, G.E. Shull, D.H. MacLennan, Functional comparisons between isoforms of the sarcoplasmic or endoplasmic reticulum family of calcium pumps., J. Biol. Chem. 267 (1992) 14483–9. http://www.ncbi.nlm.nih.gov/pubmed/1385815.

[46] A. Herchuelz, A. Kamagate, H. Ximenes, F. Van Eylen, Role of Na/Ca exchange and the plasma membrane Ca2+-ATPase in β cell function and death, Ann. N. Y. Acad. Sci. 1099 (2007) 456–467. doi:10.1196/annals.1387.048.

[47] P. Pinton, T. Pozzan, R. Rizzuto, The Golgi apparatus is an inositol 1,4,5-trisphosphate-sensitive Ca2+ store, with functional properties distinct from those of the endoplasmic reticulum, EMBO J. 17 (1998) 5298–5308. doi:10.1093/emboj/17.18.5298.

[48] B. Schwaller, Cytosolic Ca $^{2+}$ Buffers Are Inherently Ca $^{2+}$ Signal Modulators, Cold Spring Harb. Perspect. Biol. (2019) a035543. doi:10.1101/cshperspect.a035543.

[49] M.R. Nelson, E. Thulin, P.A. Fagan, S. Forsén, W.J. Chazin, The EF-hand domain: a globally cooperative structural unit., Protein Sci. 11 (2002) 198–205. doi:10.1110/ps.33302.

[50] J.G. Henrotte, A Crystalline Constituent from Myogen of Carp Muscles, Nature. 169 (1952) 968–969. doi:10.1038/169968b0.

[51] C. Baldellon, J.-R. Alattia, M.-P. Strub, T. Pauls, M.W. Berchtold, A. Cavé, A. Padilla, ^{15} N NMR Relaxation Studies of Calcium-Loaded Parvalbumin Show Tight Dynamics Compared to Those of Other EF-Hand Proteins †, Biochemistry. 37 (1998) 9964–9975. doi:10.1021/bi980334p.

[52] C.W. Heizmann, M.W. Berchtold, A.M. Rowlerson, Correlation of parvalbumin concentration with relaxation speed in mammalian muscles., Proc. Natl. Acad. Sci. 79 (1982) 7243–7247. doi:10.1073/pnas.79.23.7243.

[53] H. Schmidt, K.M. Stiefel, P. Racay, B. Schwaller, J. Eilers, Mutational analysis of dendritic Ca2+ kinetics in rodent Purkinje cells: role of parvalbumin and calbindin D28k, J. Physiol. 551 (2003) 13–32. doi:10.1113/jphysiol.2002.035824.

[54] T. Collin, M. Chat, M.G. Lucas, H. Moreno, P. Racay, B. Schwaller, A. Marty, I. Llano, Developmental Changes in Parvalbumin Regulate Presynaptic Ca2+ Signaling, J. Neurosci. 25 (2005) 96–107. doi:10.1523/JNEUROSCI.3748-04.2005.

[55] C.M. Hackney, S. Mahendrasingam, A. Penn, R. Fettiplace, The Concentrations of Calcium Buffering Proteins in Mammalian Cochlear Hair Cells, J. Neurosci. 25 (2005) 7867–7875. doi:10.1523/JNEUROSCI.1196-05.2005.

[56] B. Schwaller, The use of transgenic mouse models to reveal the functions of Ca 2 + buffer proteins in excitable cells, Biochim. Biophys. Acta - Gen. Subj. 1820 (2012) 1294–1303. doi:10.1016/j.bbagen.2011.11.008.

[57] H. Schmidt, O. Arendt, E.B. Brown, B. Schwaller, J. Eilers, Parvalbumin is freely mobile in axons, somata and nuclei of cerebellar Purkinje neurones, J. Neurochem. 100 (2007) 727–735. doi:10.1111/j.1471-4159.2006.04231.x.

[58] R.H. Kretsinger, C.E. Nockolds, Carp muscle calcium-binding protein. II. Structure determination and general description., J. Biol. Chem. 248 (1973) 3313–26. http://www.ncbi.nlm.nih.gov/pubmed/4700463.

[59] J.A. Cox, I. Durussel, D.J. Scott, M.W. Berchtold, Remodeling of the AB

site of rat parvalbumin and oncomodulin into a canonical EF-hand, Eur. J. Biochem. 264 (1999) 790–799. doi:10.1046/j.1432-1327.1999.00650.x.

[60] M.T. Henzl, Solution structure of Ca 2 + -free rat a -parvalbumin, (2008) 431–438. doi:10.1110/ps.073318308.1973.

[61] Y. Li-Smerin, E.S. Levitan, J.W. Johnson, Free intracellular Mg(2+) concentration and inhibition of NMDA responses in cultured rat neurons., J. Physiol. 533 (2001) 729–43. doi:10.1111/j.1469-7793.2001.t01-1-00729.x.

[62] P.S. Chard, D. Bleakman, S. Christakos, C.S. Fullmer, R.J. Miller, Calcium buffering properties of calbindin D28k and parvalbumin in rat sensory neurones., J. Physiol. 472 (1993) 341–357. doi:10.1016/j.aquatox.2011.05.003.

[63] M.W. Berchtold, A.R. Means, The Ca2+-binding protein parvalbumin: molecular cloning and developmental regulation of mRNA abundance., Proc. Natl. Acad. Sci. U. S. A. 82 (1985) 1414–8. doi:10.1073/pnas.82.5.1414.

[64] M. Goodman, J.-F. Pechère, The Evolution of Muscular Parvalbumins Investigated by the Maximum Parsimony Method, J. Mol. Evol. 9 (1977) 131–58. http://www.ncbi.nlm.nih.gov/pubmed/864720.

[65] J.A. Cox, M. Milos, J.P. MacManus, Calcium- and magnesium-binding properties of oncomodulin. Direct binding studies and microcalorimetry., J. Biol. Chem. 265 (1990) 6633–7. http://www.ncbi.nlm.nih.gov/pubmed/2108959.

[66] U.G. Fohr, B.R. Weber, M. Muntener, W. Staudenmann, G.J. Hughes, S. Frutiger, D. Banville, B.W. Schafer, C.W. Heizmann, Human alpha and beta parvalbumins. Structure and tissue-specific expression, Eur J Biochem. 215 (1993) 719–727.

[67] Y. Yin, M.T. Henzl, B. Lorber, T. Nakazawa, T.T. Thomas, F. Jiang, R. Langer, L.I. Benowitz, Oncomodulin is a macrophage-derived signal for axon regeneration in retinal ganglion cells., Nat. Neurosci. 9 (2006) 843–52.

doi:10.1038/nn1701.

[68] T. Henzi, B. Schwaller, Antagonistic regulation of parvalbumin expression and mitochondrial calcium handling capacity in renal epithelial cells, PLoS One. 10 (2015) 1–19. doi:https://doi.org/10.1371/journal.pone.0142005.

[69] J.M. Gillis, D. Thomason, J. Lefèvre, R.H. Kretsinger, Parvalbumins and muscle relaxation: a computer simulation study., J. Muscle Res. Cell Motil. 3 (1982) 377–98. http://www.ncbi.nlm.nih.gov/pubmed/7183710.

[70] T.T. Hou, J.D. Johnson, J.A. Rall, Parvalbumin content and Ca2+ and Mg2+ dissociation rates correlated with changes in relaxation rate of frog muscle fibres., J. Physiol. 441 (1991) 285–304. doi:10.1113/jphysiol.1991.sp018752.

[71] C.W. Heizmann, Parvalbumin, an intracellular calcium-binding protein; distribution, properties and possible roles in mammalian cells, Birkhäuser-Verlag, 1984. doi:10.1007/BF01946439.

[72] J.C. Calderón, P. Bolaños, C. Caputo, The excitation–contraction coupling mechanism in skeletal muscle, Biophys. Rev. 6 (2014) 133–160. doi:10.1007/s12551-013-0135-x.

[73] J.R. Moore, S.G. Campbell, W. Lehman, Structural determinants of muscle thin filament cooperativity, Arch. Biochem. Biophys. 594 (2016) 8–17. doi:10.1016/j.abb.2016.02.016.

[74] S.M. Baylor, S. Hollingworth, Sarcoplasmic reticulum calcium release compared in slow-twitch and fast-twitch fibres of mouse muscle., J. Physiol. 551 (2003) 125–38. doi:10.1113/jphysiol.2003.041608.

[75] J. Haiech, J. Derancourt, J.F. Pechere, J.G. Demaille, Magnesium and calcium binding to parvalbumins: evidence for differences between parvalbumins and an explanation of their relaxing function, Biochemistry. 18 (1979) 2752–2758. doi:10.1021/bi00580a010.

[76] T.T. Hou, J.D. Johnson, J.A. Rall, Effect of temperature on relaxation rate and Ca2+, Mg2+ dissociation rates from parvalbumin of frog muscle fibres.,

J. Physiol. 449 (1992) 399–410. doi:10.1113/jphysiol.1992.sp019092.

[77] Y. Jiang, J.D. Johnson, J.A. Rall, Parvalbumin relaxes frog skeletal muscle when sarcoplasmic reticulum Ca(2+)-ATPase is inhibited, Am. J. Physiol. Physiol. 270 (1996) C411–C417. doi:10.1152/ajpcell.1996.270.2.C411.

[78] M. Müntener, L. Käser, J. Weber, M.W. Berchtold, Increase of skeletal muscle relaxation speed by direct injection of parvalbumin cDNA., Proc. Natl. Acad. Sci. U. S. A. 92 (1995) 6504. doi:10.1073/PNAS.92.14.6504.

[79] S. Ducreux, P. Gregory, B. Schwaller, Inverse Regulation of the Cytosolic Ca2+ Buffer Parvalbumin and Mitochondrial Volume in Muscle Cells via SIRT1/PGC-1α Axis, PLoS One. 7 (2012). doi:10.1371/journal.pone.0044837.

[80] P. Racay, P. Gregory, B. Schwaller, Parvalbumin deficiency in fast-twitch muscles leads to increased “slow-twitch type” mitochondria, but does not affect the expression of fiber specific proteins, FEBS J. 273 (2006) 96–108. doi:10.1111/j.1742-4658.2005.05046.x.

[81] A.I. Tarasov, E.J. Griffiths, G.A. Rutter, Regulation of ATP production by mitochondrial Ca2+, Cell Calcium. 52 (2012) 28–35. doi:10.1016/j.ceca.2012.03.003.

[82] A. Nickel, M. Kohlhaas, C. Maack, Mitochondrial reactive oxygen species production and elimination, J. Mol. Cell. Cardiol. 73 (2014) 26–33. doi:10.1016/j.yjmcc.2014.03.011.

[83] G. Hajnóczky, L.D. Robb-Gaspers, M.B. Seitz, A.P. Thomas, Decoding of cytosolic calcium oscillations in the mitochondria, Cell. 82 (1995) 415–424. doi:10.1016/0092-8674(95)90430-1.

[84] M. Colombini, The VDAC channel: Molecular basis for selectivity, Biochim. Biophys. Acta - Mol. Cell Res. 1863 (2016) 2498–2502. doi:10.1016/J.BBAMCR.2016.01.019.

[85] B.C. Marreiros, F. Calisto, P.J. Castro, A.M. Duarte, F. V. Sena, A.F. Silva, F.M. Sousa, M. Teixeira, P.N. Refojo, M.M. Pereira, Exploring membrane

respiratory chains, Biochim. Biophys. Acta - Bioenerg. 1857 (2016) 1039–1067. doi:10.1016/j.bbabio.2016.03.028.

[86] D.F. Babcock, J. Herrington, P.C. Goodwin, Y.B. Park, B. Hille, Mitochondrial Participation in the Intracellular Ca $^{2+}$ Network, J. Cell Biol. 136 (1997) 833–844. doi:10.1083/jcb.136.4.833.

[87] P. Mitchell, Coupling of phosphorylation to electron and hydrogen transfer by a chemi-osmotic type of mechanism, Nature. 191 (1961) 144–148. doi:10.1038/191144a0.

[88] P. Mitchell, Chemiosmotic Coupling in Oxidative and Photosynhetic Phosphorylation (“First Book”, 1966) - 1, Bio. Rev. 41 (1966) 445–502. doi:10.1111/j.1469-185X.1966.tb01501.x.

[89] H.F. Deluca, G.W. Engstrom, Calcium uptake by rat kidney mitochondria., Proc. Natl. Acad. Sci. U. S. A. 47 (1961) 1744–50. doi:10.1073/pnas.47.11.1744.

[90] F.D. Vasington, J. V Murphy, Ca++ Uptake by Rat Kidnev Mitochondria and Its Dependence J on Respiration and Phosphorylation*, 1962. http://www.jbc.org/.

[91] P. Mitchell, J. Moyle, Respiration-driven proton translocation in rat liver mitochondria., Biochem. J. 105 (1967) 1147–62. http://www.pubmedcentral.nih.gov/articlerender.fcgi?artid=1198436&tool=pmcentrez&rendertype=abstract.

[92] H. Rottenberg, A. Scarpa, Calcium uptake and membrane potential in mitochondria, Biochemistry. 13 (1974) 4811–4817. doi:10.1021/bi00720a020.

[93] Y. Kirichok, G. Krapivinsky, D.E. Clapham, The mitochondrial calcium uniporter is a highly selective ion channel., Nature. 427 (2004) 360–4. doi:10.1038/nature02246.

[94] R. Rizzuto, A.W.M. Simpson, M. Brini, T. Pozzan, Rapid changes of mitochondrial Ca2+ revealed by sepcifically targeted recombinant aequorin,

Nature. 355 (1992) 542–5. doi:10.1038/355542a0.

[95] R. Rizzuto, P. Pinton, W. Carrington, F.S. Fay, K.E. Fogarty, L.M. Lifshitz, R.A. Tuft, T. Pozzan, Close contacts with the endoplasmic reticulum as determinants of mitochondrial Ca2+ responses., Science. 280 (1998) 1763–6. doi:10.1126/science.280.5370.1763.

[96] G. Csordás, A.P. Thomas, G. Hajnóczky, Quasi-synaptic calcium signal transmission between endoplasmic reticulum and mitochondria, EMBO J. 18 (1999) 96–108. doi:10.1093/emboj/18.1.96.

[97] R. Palty, W.F. Silverman, M. Hershfinkel, T. Caporale, S.L. Sensi, J. Parnis, C. Nolte, D. Fishman, V. Shoshan-Barmatz, S. Herrmann, D. Khananshvili, I. Sekler, NCLX is an essential component of mitochondrial Na+/Ca2+ exchange, Proc. Natl. Acad. Sci. 107 (2010) 436–441. doi:10.1073/pnas.0908099107.

[98] R. Palty, M. Hershfinkel, I. Sekler, Molecular Identity and Functional Properties of the Mitochondrial Na ⁺ / Ca 2 ⁺, 287 (2012) 31650–31657. doi:10.1074/jbc.R112.355867.

[99] L. Boyman, G.S.B. Williams, D. Khananshvili, I. Sekler, W.J. Lederer, NCLX: the mitochondrial sodium calcium exchanger., J. Mol. Cell. Cardiol. 59 (2013) 205–13. doi:10.1016/j.yjmcc.2013.03.012.

[100] U. De Marchi, J. Santo-Domingo, C. Castelbou, I. Sekler, A. Wiederkehr, N. Demaurex, NCLX protein, but not LETM1, mediates mitochondrial Ca2+ extrusion, thereby limiting Ca2+-induced NAD(P)H production and modulating matrix redox state., J. Biol. Chem. 289 (2014) 20377–85. doi:10.1074/jbc.M113.540898.

[101] D. Jiang, L. Zhao, D.E. Clapham, Genome-wide RNAi screen identifies Letm1 as a mitochondrial Ca2+/H+ antiporter., Science. 326 (2009) 144–7. doi:10.1126/science.1175145.

[102] M. Patron, A. Raffaello, V. Granatiero, A. Tosatto, G. Merli, D. De Stefani, L. Wright, G. Pallafacchina, A. Terrin, C. Mammucari, R. Rizzuto, The

Mitochondrial Calcium Uniporter (MCU): Molecular Identity and Physiological Roles, J. Biol. Chem. 288 (2013) 10750–10758. doi:10.1074/jbc.R112.420752.

[103] M. Kohlhaas, A.G. Nickel, C. Maack, Mitochondrial energetics and calcium coupling in the heart, J. Physiol. 595 (2017) 3753–3763. doi:10.1113/JP273609.

[104] F. Di Lisa, P. Bernardi, A CaPful of mechanisms regulating the mitochondrial permeability transition, J. Mol. Cell. Cardiol. 46 (2009) 775–780. doi:https://doi.org/10.1016/j.yjmcc.2009.03.006.

[105] V. Giorgio, L. Guo, C. Bassot, V. Petronilli, P. Bernardi, Calcium and regulation of the mitochondrial permeability transition, Cell Calcium. 70 (2018) 56–63. doi:10.1016/j.ceca.2017.05.004.

[106] T.E. Gunter, D.I. Yule, K.K. Gunter, R.A. Eliseev, J.D. Salter, Calcium and mitochondria, FEBS Lett. 567 (2004) 96–102. doi:10.1016/j.febslet.2004.03.071.

[107] V. Giorgio, V. Burchell, M. Schiavone, C. Bassot, G. Minervini, V. Petronilli, F. Argenton, M. Forte, S. Tosatto, G. Lippe, P. Bernardi, Ca^{2+} binding to F-ATP synthase β subunit triggers the mitochondrial permeability transition, EMBO Rep. 18 (2017) 1065–1076. doi:10.15252/embr.201643354.

[108] V. Giorgio, S. von Stockum, M. Antoniel, A. Fabbro, F. Fogolari, M. Forte, G.D. Glick, V. Petronilli, M. Zoratti, I. Szabo, G. Lippe, P. Bernardi, Dimers of mitochondrial ATP synthase form the permeability transition pore, Proc. Natl. Acad. Sci. 110 (2013) 5887–5892. doi:10.1073/pnas.1217823110.

[109] E. Boitier, R. Rea, M.R. Duchen, Mitochondria Exert a Negative Feedback on the Propagation of Intracellular Ca^{2+} Waves in Rat Cortical Astrocytes, J. Cell Biol. 145 (1999) 795–808. doi:10.1083/jcb.145.4.795.

[110] G. Hajnóczky, R. Hager, A.P. Thomas, Mitochondria Suppress Local Feedback Activation of Inositol 1,4,5-Trisphosphate Receptors by Ca^{2+}, J.

Biol. Chem. 274 (1999) 14157–14162. doi:10.1074/jbc.274.20.14157.

[111] S. Herzig, J.-C. Martinou, Mitochondrial dynamics: to be in good shape to survive., Curr. Mol. Med. 8 (2008) 131–7. http://www.ncbi.nlm.nih.gov/pubmed/18336293.

[112] J.B. Hoek, J.L. Farber, A.P. Thomas, X. Wang, Calcium ion-dependent signalling and mitochondrial dysfunction: mitochondrial calcium uptake during hormonal stimulation in intact liver cells and its implication for the mitochondrial permeability transition., Biochim. Biophys. Acta. 1271 (1995) 93–102. doi:10.1016/0925-4439(95)00015-v.

[113] H. Tinel, J.M. Cancela, H. Mogami, J. V. Gerasimenko, O. V. Gerasimenko, A. V. Tepikin, O.H. Petersen, Active mitochondria surrounding the pancreatic acinar granule region prevent spreading of inositol trisphosphate-evoked local cytosolic Ca2+ signals, EMBO J. 18 (1999) 4999–5008. doi:10.1093/emboj/18.18.4999.

[114] B. Billups, I.D. Forsythe, Presynaptic mitochondrial calcium sequestration influences transmission at mammalian central synapses., J. Neurosci. 22 (2002) 5840–7. doi:20026597.

[115] Z.-H. Sheng, Q. Cai, Mitochondrial transport in neurons: impact on synaptic homeostasis and neurodegeneration, Nat. Rev. Neurosci. 13 (2012) 77–93. doi:10.1038/nrn3156.

[116] T. Calì, D. Ottolini, M. Brini, Mitochondrial Ca2+and neurodegeneration, Cell Calcium. 52 (2012) 73–85. doi:10.1016/j.ceca.2012.04.015.

[117] J.M. Baughman, F. Perocchi, H.S. Girgis, M. Plovanich, C.A. Belcher-Timme, Y. Sancak, X.R. Bao, L. Strittmatter, O. Goldberger, R.L. Bogorad, V. Koteliansky, V.K. Mootha, Integrative genomics identifies MCU as an essential component of the mitochondrial calcium uniporter., Nature. 476 (2011). doi:10.1038/nature10234.

[118] D. De Stefani, A. Raffaello, E. Teardo, I. Szabò, R. Rizzuto, A forty-kilodalton protein of the inner membrane is the mitochondrial calcium

uniporter., Nature. 476 (2011) 336–40. doi:10.1038/nature10230.

[119] M. Patron, V. Checchetto, A. Raffaello, E. Teardo, D. Vecellio Reane, M. Mantoan, V. Granatiero, I. Szabò, D. De Stefani, R. Rizzuto, MICU1 and MICU2 finely tune the mitochondrial Ca2+ uniporter by exerting opposite effects on MCU activity., Mol. Cell. 53 (2014) 726–37. doi:10.1016/j.molcel.2014.01.013.

[120] M. Plovanich, R.L. Bogorad, Y. Sancak, K.J. Kamer, L. Strittmatter, A.A. Li, H.S. Girgis, S. Kuchimanchi, J. De Groot, L. Speciner, N. Taneja, J. OShea, V. Koteliansky, V.K. Mootha, MICU2, a Paralog of MICU1, Resides within the Mitochondrial Uniporter Complex to Regulate Calcium Handling, PLoS One. 8 (2013). doi:10.1371/journal.pone.0055785.

[121] Y. Sancak, A.L. Markhard, T. Kitami, E. Kovács-Bogdán, J. Kamer, N.D. Udeshi, S.A. Carr, D. Chaudhuri, D.E. Clapham, A.A. Li, S.E. Calvo, O. Goldberger, V.K. Mootha, K.J. Kamer, N.D. Udeshi, S.A. Carr, D. Chaudhuri, D.E. Clapham, A.A. Li, S.E. Calvo, O. Goldberger, V.K. Mootha, EMRE is an essential component of the mitochondrial calcium uniporter complex Yasemin, Science. 342 (2014) 1379–1382. doi:10.1126/science.1242993.EMRE.

[122] E. Kovacs-Bogdan, Y. Sancak, K.J. Kamer, M. Plovanich, A. Jambhekar, R.J. Huber, M.A. Myre, M.D. Blower, V.K. Mootha, Reconstitution of the mitochondrial calcium uniporter in yeast, Proc. Natl. Acad. Sci. 111 (2014) 8985–8990. doi:10.1073/pnas.1400514111.

[123] H. Vais, K. Mallilankaraman, D.O.D. Mak, H. Hoff, R. Payne, J.E. Tanis, J.K. Foskett, EMRE Is a Matrix Ca2+Sensor that Governs Gatekeeping of the Mitochondrial Ca2+Uniporter, Cell Rep. 14 (2016) 403–410. doi:10.1016/j.celrep.2015.12.054.

[124] T. Yamamoto, R. Yamagoshi, K. Harada, M. Kawano, N. Minami, Y. Ido, K. Kuwahara, A. Fujita, M. Ozono, A. Watanabe, A. Yamada, H. Terada, Y. Shinohara, Analysis of the structure and function of EMRE in a yeast expression system, Biochim. Biophys. Acta - Bioenerg. 1857 (2016) 831–

839. doi:10.1016/j.bbabio.2016.03.019.

[125] A. Raffaello, D. De Stefani, D. Sabbadin, E. Teardo, G. Merli, A. Picard, V. Checchetto, S. Moro, I. Szabò, R. Rizzuto, The mitochondrial calcium uniporter is a multimer that can include a dominant-negative pore-forming subunit., EMBO J. 32 (2013) 2362–76. doi:10.1038/emboj.2013.157.

[126] K.J. Kamer, V.K. Mootha, The molecular era of the mitochondrial calcium uniporter., Nat. Rev. Mol. Cell Biol. 16 (2015) 545–53. doi:10.1038/nrm4039.

[127] F. Perocchi, V.M. Gohil, H.S. Girgis, X.R. Bao, J.E. McCombs, A.E. Palmer, V.K. Mootha, MICU1 encodes a mitochondrial EF hand protein required for Ca2+uptake, Nature. 467 (2010) 291–296. doi:10.1038/nature09358.

[128] K. Mallilankaraman, P. Doonan, C. Cárdenas, C. Harish, M. Muller, R. Miller, N.E. Hoffman, J. Molgó, M.J. Birnbaum, B. Rothberg, D.D. Mak, J.K. Foskett, M. Madesh, MICU1 is an Essential Gatekeeper for MCU-Mediated Mitochondrial Ca2+ Uptake That Regulates Cell Survival, 151 (2013) 630–644. doi:10.1016/j.cell.2012.10.011.MICU1.

[129] G. Csordás, T. Golenár, E.L. Seifert, K.J. Kamer, Y. Sancak, F. Perocchi, C. Moffat, D. Weaver, S. de la Fuente Perez, R. Bogorad, V. Koteliansky, J. Adijanto, V.K. Mootha, G. Hajnóczky, MICU1 controls both the threshold and cooperative activation of the mitochondrial Ca^{2+} uniporter., Cell Metab. 17 (2013) 976–87. doi:10.1016/j.cmet.2013.04.020.

[130] C. V Logan, G. Szabadkai, J.A. Sharpe, D.A. Parry, S. Torelli, A.-M. Childs, M. Kriek, R. Phadke, C.A. Johnson, N.Y. Roberts, D.T. Bonthron, K.A. Pysden, T. Whyte, I. Munteanu, A.R. Foley, G. Wheway, K. Szymanska, S. Natarajan, Z.A. Abdelhamed, J.E. Morgan, H. Roper, G.W.E. Santen, E.H. Niks, W.L. van der Pol, D. Lindhout, A. Raffaello, D. De Stefani, J.T. den Dunnen, Y. Sun, I. Ginjaar, C.A. Sewry, M. Hurles, R. Rizzuto, M.R. Duchen, F. Muntoni, E. Sheridan, E. Sheridan, Loss-of-function mutations in MICU1 cause a brain and muscle disorder linked to primary alterations in mitochondrial calcium signaling, Nat. Genet. 46 (2013) 188–193.

doi:10.1038/ng.2851.

[131] K.J. Kamer, V.K. Mootha, MICU1 and MICU2 play nonredundant roles in the regulation of the mitochondrial calcium uniporter., EMBO Rep. 15 (2014) 299–307. doi:10.1002/embr.201337946.

[132] M. Paillard, G. Csordás, G. Szanda, T. Golenár, V. Debattisti, A. Bartok, N. Wang, C. Moffat, E.L. Seifert, A. Spät, G. Hajnóczky, Tissue-Specific Mitochondrial Decoding of Cytoplasmic Ca2+ Signals Is Controlled by the Stoichiometry of MICU1/2 and MCU, Cell Rep. 18 (2017) 2291–2300. doi:10.1016/j.celrep.2017.02.032.

[133] M. Patron, V. Granatiero, J. Espino, MICU3 is a tissue-speci fi c enhancer of mitochondrial calcium uptake, Cell Death Differ. (2018). doi:10.1038/s41418-018-0113-8.

[134] M.E. Dickinson, A.M. Flenniken, X. Ji, L. Teboul, M.D. Wong, J.K. White, T.F. Meehan, W.J. Weninger, H. Westerberg, H. Adissu, C.N. Baker, L. Bower, J.M. Brown, L.B. Caddle, F. Chiani, D. Clary, J. Cleak, M.J. Daly, J.M. Denegre, B. Doe, M.E. Dolan, S.M. Edie, H. Fuchs, V. Gailus-Durner, A. Galli, A. Gambadoro, J. Gallegos, S. Guo, N.R. Horner, C.-W. Hsu, S.J. Johnson, S. Kalaga, L.C. Keith, L. Lanoue, T.N. Lawson, M. Lek, M. Mark, S. Marschall, J. Mason, M.L. McElwee, S. Newbigging, L.M.J. Nutter, K.A. Peterson, R. Ramirez-Solis, D.J. Rowland, E. Ryder, K.E. Samocha, J.R. Seavitt, M. Selloum, Z. Szoke-Kovacs, M. Tamura, A.G. Trainor, I. Tudose, S. Wakana, J. Warren, O. Wendling, D.B. West, L. Wong, A. Yoshiki, W. Wurst, D.G. MacArthur, G.P. Tocchini-Valentini, X. Gao, P. Flicek, A. Bradley, W.C. Skarnes, M.J. Justice, H.E. Parkinson, M. Moore, S. Wells, R.E. Braun, K.L. Svenson, M.H. de Angelis, Y. Herault, T. Mohun, A.-M. Mallon, R.M. Henkelman, S.D.M. Brown, D.J. Adams, K.C.K. Lloyd, C. McKerlie, A.L. Beaudet, M. Bućan, S.A. Murray, S.D.M. Brown, D.J. Adams, K.C.K. Lloyd, C. McKerlie, A.L. Beaudet, M. Bućan, S.A. Murray, High-throughput discovery of novel developmental phenotypes, Nature. 537 (2016) 508–514. doi:10.1038/nature19356.

[135] T.S. Luongo, J.P. Lambert, A. Yuan, X. Zhang, P. Gross, J. Song, S. Shanmughapriya, E. Gao, M. Jain, S.R. Houser, W.J. Koch, J.Y. Cheung, M. Madesh, J.W. Elrod, The Mitochondrial Calcium Uniporter Matches Energetic Supply with Cardiac Workload during Stress and Modulates Permeability Transition, Cell Rep. 12 (2015) 23–34. doi:10.1016/j.celrep.2015.06.017.

[136] C. Porter, B.T. Wall, Skeletal muscle mitochondrial function: is it quality or quantity that makes the difference in insulin resistance?, J. Physiol. 590 (2012) 5935–6. doi:10.1113/jphysiol.2012.241083.

[137] J. Zhou, K. Dhakal, J. Yi, Mitochondrial Ca(2+) uptake in skeletal muscle health and disease., Sci. China. Life Sci. 59 (2016) 770–6. doi:10.1007/s11427-016-5089-3.

[138] A.E. Rossi, S. Boncompagni, L. Wei, F. Protasi, R.T. Dirksen, Differential impact of mitochondrial positioning on mitochondrial Ca $^{2+}$ uptake and Ca $^{2+}$ spark suppression in skeletal muscle, Am. J. Physiol. Physiol. 301 (2011) C1128–C1139. doi:10.1152/ajpcell.00194.2011.

[139] C.K.E. Bleck, Y. Kim, T.B. Willingham, B. Glancy, Subcellular connectomic analyses of energy networks in striated muscle, Nat. Commun. 9 (2018) 5111. doi:10.1038/s41467-018-07676-y.

[140] A. Díaz-Vegas, V. Eisner, E. Jaimovich, Skeletal muscle excitation-metabolism coupling., Arch. Biochem. Biophys. 664 (2019) 89–94. doi:10.1016/j.abb.2019.01.037.

[141] V. Eisner, G. Lenaers, G. Hajnóczky, Mitochondrial fusion is frequent in skeletal muscle and supports excitation-contraction coupling., J. Cell Biol. 205 (2014) 179–95. doi:10.1083/jcb.201312066.

[142] B. Glancy, L.M. Hartnell, D. Malide, Z.-X. Yu, C.A. Combs, P.S. Connelly, S. Subramaniam, R.S. Balaban, Mitochondrial reticulum for cellular energy distribution in muscle., Nature. 523 (2015) 617–20. doi:10.1038/nature14614.

[143] S. Boncompagni, A.E. Rossi, M. Micaroni, G. V. Beznoussenko, R.S. Polishchuk, R.T. Dirksen, F. Protasi, Mitochondria Are Linked to Calcium Stores in Striated Muscle by Developmentally Regulated Tethering Structures, Mol. Biol. Cell. 20 (2009) 1058–1067. doi:10.1091/mbc.e08-07-0783.

[144] R. Rizzuto, T. Pozzan, Microdomains of Intracellular Ca 2+ : Molecular Determinants and Functional Consequences, Physiol. Rev. 86 (2006) 369–408. doi:10.1152/physrev.00004.2005.

[145] I. Drago, D. De Stefani, R. Rizzuto, T. Pozzan, Mitochondrial Ca2+ uptake contributes to buffering cytoplasmic Ca2+ peaks in cardiomyocytes., Proc. Natl. Acad. Sci. U. S. A. 109 (2012) 12986–91. doi:10.1073/pnas.1210718109.

[146] M. Picard, K. White, D.M. Turnbull, Mitochondrial morphology, topology, and membrane interactions in skeletal muscle: a quantitative three-dimensional electron microscopy study., J. Appl. Physiol. 114 (2013) 161–71. doi:10.1152/japplphysiol.01096.2012.

[147] V. Romanello, M. Sandri, Mitochondrial Quality Control and Muscle Mass Maintenance., Front. Physiol. 6 (2015) 422. doi:10.3389/fphys.2015.00422.

[148] B. Westermann, Bioenergetic role of mitochondrial fusion and fission, Biochim. Biophys. Acta - Bioenerg. 1817 (2012) 1833–1838. doi:10.1016/j.bbabio.2012.02.033.

[149] M. Karbowski, R.J. Youle, Dynamics of mitochondrial morphology in healthy cells and during apoptosis, Cell Death Differ. 10 (2003) 870–880. doi:10.1038/sj.cdd.4401260.

[150] F.R. Jornayvaz, G.I. Shulman, Regulation of mitochondrial biogenesis., Essays Biochem. 47 (2010) 69–84. doi:10.1042/bse0470069.

[151] Z. Wu, P. Puigserver, U. Andersson, C. Zhang, G. Adelmant, V. Mootha, A. Troy, S. Cinti, B. Lowell, R.C. Scarpulla, B.M. Spiegelman, Mechanisms Controlling Mitochondrial Biogenesis and Respiration through the

Thermogenic Coactivator PGC-1, Cell. 98 (1999) 115–124. doi:10.1016/S0092-8674(00)80611-X.

[152] B. Westermann, Mitochondrial fusion and fission in cell life and death., Nat. Rev. Mol. Cell Biol. 11 (2010) 872–84. doi:10.1038/nrm3013.

[153] E. Barbieri, D. Agostini, E. Polidori, L. Potenza, M. Guescini, F. Lucertini, G. Annibalini, L. Stocchi, M. De Santi, V. Stocchi, The pleiotropic effect of physical exercise on mitochondrial dynamics in aging skeletal muscle., Oxid. Med. Cell. Longev. 2015 (2015) 917085. doi:10.1155/2015/917085.

[154] G. Kou, Z. Li, C. Wu, Y. Liu, Y. Hu, L. Guo, X. Xu, Z. Zhou, Citrus Tangeretin Improves Skeletal Muscle Mitochondrial Biogenesis via Activating the AMPK-PGC1-α Pathway In Vitro and In Vivo: A Possible Mechanism for Its Beneficial Effect on Physical Performance, J. Agric. Food Chem. 66 (2018) 11917–11925. doi:10.1021/acs.jafc.8b04124.

[155] G. Twig, O.S. Shirihai, The Interplay Between Mitochondrial Dynamics and Mitophagy, Antioxid. Redox Signal. 14 (2011) 1939–1951. doi:10.1089/ars.2010.3779.

[156] D.A. Kubli, Å.B. Gustafsson, Mitochondria and mitophagy: the yin and yang of cell death control., Circ. Res. 111 (2012) 1208–21. doi:10.1161/CIRCRESAHA.112.265819.

[157] M. Kelly-Worden, E. Thomas, Mitochondrial Dysfunction in Duchenne Muscular Dystrophy, Open J. Endocr. Metab. Dis. 4 (2014) 211–218. doi:10.4236/ojemd.2014.48020.

[158] B. Blaauw, S. Schiaffino, C. Reggiani, Mechanisms modulating skeletal muscle phenotype, Compr. Physiol. 3 (2013) 1645–1687. doi:10.1002/cphy.c130009.

[159] S. Schiaffino, K.A. Dyar, S. Ciciliot, B. Blaauw, M. Sandri, Mechanisms regulating skeletal muscle growth and atrophy., FEBS J. 280 (2013) 4294–314. doi:10.1111/febs.12253.

[160] C. McGlory, S.M. Phillips, Exercise and the Regulation of Skeletal Muscle

Hypertrophy, in: Prog. Mol. Biol. Transl. Sci., 2015: pp. 153–173. doi:10.1016/bs.pmbts.2015.06.018.

[161] M. Sandri, Signaling in Muscle Atrophy and Hypertrophy, Physiology. 23 (2008) 160–170. doi:10.1152/physiol.00041.2007.

[162] C. Reggiani, G. Te Kronnie, Muscle plasticity and high throughput gene expression studies., J. Muscle Res. Cell Motil. 25 (2004) 231–4. http://www.ncbi.nlm.nih.gov/pubmed/15467387.

[163] D. Pette, R.S. Staron, Mammalian skeletal muscle fiber type transitions., Int. Rev. Cytol. 170 (1997) 143–223. http://www.ncbi.nlm.nih.gov/pubmed/9002237.

[164] M. Flück, H. Hoppeler, Molecular basis of skeletal muscle plasticity-from gene to form and function, in: Rev. Physiol. Biochem. Pharmacol., Springer Berlin Heidelberg, Berlin, Heidelberg, 2003: pp. 159–216. doi:10.1007/s10254-002-0004-7.

[165] M. Flück, C. Däpp, S. Schmutz, E. Wit, H. Hoppeler, Transcriptional profiling of tissue plasticity: role of shifts in gene expression and technical limitations, J. Appl. Physiol. 99 (2005) 397–413. doi:10.1152/japplphysiol.00050.2005.

[166] A.L. Goldberg, Protein turnover in skeletal muscle. I. Protein catabolism during work-induced hypertrophy and growth induced with growth hormone., J. Biol. Chem. 244 (1969) 3217–22. http://www.ncbi.nlm.nih.gov/pubmed/5792657.

[167] S. Schiaffino, C. Mammucari, Regulation of skeletal muscle growth by the IGF1-Akt/PKB pathway: insights from genetic models., Skelet. Muscle. 1 (2011) 4. doi:10.1186/2044-5040-1-4.

[168] C. Rommel, S.C. Bodine, B.A. Clarke, R. Rossman, L. Nunez, T.N. Stitt, G.D. Yancopoulos, D.J. Glass, Mediation of IGF-1-induced skeletal myotube hypertrophy by PI(3)K/Akt/mTOR and PI(3)K/Akt/GSK3 pathways, Nat. Cell Biol. 3 (2001) 1009–1013. doi:10.1038/ncb1101-1009.

[169] S.C. Bodine, T.N. Stitt, M. Gonzalez, W.O. Kline, G.L. Stover, R. Bauerlein, E. Zlotchenko, A. Scrimgeour, J.C. Lawrence, D.J. Glass, G.D. Yancopoulos, Akt/mTOR pathway is a crucial regulator of skeletal muscle hypertrophy and can prevent muscle atrophy in vivo, Nat. Cell Biol. 3 (2001) 1014–1019. doi:10.1038/ncb1101-1014.

[170] M. Sandri, C. Sandri, A. Gilbert, C. Skurk, E. Calabria, A. Picard, K. Walsh, S. Schiaffino, S.H. Lecker, A.L. Goldberg, Foxo transcription factors induce the atrophy-related ubiquitin ligase atrogin-1 and cause skeletal muscle atrophy, Cell. 117 (2004) 399–412. doi:10.1016/S0092-8674(04)00400-3.

[171] T.N. Stitt, D. Drujan, B.A. Clarke, F. Panaro, Y. Timofeyva, W.O. Kline, M. Gonzalez, G.D. Yancopoulos, D.J. Glass, The IGF-1/PI3K/Akt pathway prevents expression of muscle atrophy-induced ubiquitin ligases by inhibiting FOXO transcription factors., Mol. Cell. 14 (2004) 395–403. http://www.ncbi.nlm.nih.gov/pubmed/15125842.

[172] C. Mammucari, G. Milan, V. Romanello, E. Masiero, R. Rudolf, P. Del Piccolo, S.J. Burden, R. Di Lisi, C. Sandri, J. Zhao, A.L. Goldberg, S. Schiaffino, M. Sandri, FoxO3 controls autophagy in skeletal muscle in vivo., Cell Metab. 6 (2007) 458–71. doi:10.1016/j.cmet.2007.11.001.

[173] M. Thomas, B. Langley, C. Berry, M. Sharma, S. Kirk, J. Bass, R. Kambadur, Myostatin, a negative regulator of muscle growth, functions by inhibiting myoblast proliferation., J. Biol. Chem. 275 (2000) 40235–43. doi:10.1074/jbc.M004356200.

[174] D.A. Hood, I. Irrcher, V. Ljubicic, A.-M. Joseph, Coordination of metabolic plasticity in skeletal muscle., J. Exp. Biol. 209 (2006) 2265–75. doi:10.1242/jeb.02182.

[175] B. Schwaller, I. V. Tetko, P. Tandon, D.C. Silveira, M. Vreugdenhil, T. Henzi, M.C. Potier, M.R. Celio, A.E.P. Villa, Parvalbumin deficiency affects network properties resulting in increased susceptibility to epileptic seizures, Mol. Cell. Neurosci. 25 (2004) 650–663. doi:10.1016/j.mcn.2003.12.006.

[176] J.M. Raymackers, P. Gailly, M. Colson-Van Schoor, D. Pette, B. Schwaller,

W. Hunziker, M.R. Celio, J.M. Gillis, Tetanus relaxation of fast skeletal muscles of the mouse made parvalbumin deficient by gene inactivation, J. Physiol. 527 (2000) 355–364. doi:10.1111/j.1469-7793.2000.00355.x.

[177] K.K. Pedersen, O.B. Nielsen, K. Overgaard, Effects of high-frequency stimulation and doublets on dynamic contractions in rat soleus muscle exposed to normal and high extracellular [K(+)]., Physiol. Rep. 1 (2013) e00026. doi:10.1002/phy2.26.

[178] C. Paolini, M. Quarta, L. D'Onofrio, C. Reggiani, F. Protasi, Differential Effect of Calsequestrin Ablation on Structure and Function of Fast and Slow Skeletal Muscle Fibers, J. Biomed. Biotechnol. 2011 (2011) 1–10. doi:10.1155/2011/634075.

[179] G.S. Posterino, G.D. Lamb, Effect of sarcoplasmic reticulum Ca2+ content on action potential-induced Ca2+ release in rat skeletal muscle fibres., J. Physiol. 551 (2003) 219–37. doi:10.1113/jphysiol.2003.040022.

[180] M. Murgia, R. Rizzuto, Molecular diversity and pleiotropic role of the mitochondrial calcium uniporter., Cell Calcium. 58 (2015) 11–7. doi:10.1016/j.ceca.2014.11.001.

[181] H. Kong, P.P. Jones, A. Koop, L. Zhang, H.J. Duff, S.R.W. Chen, Caffeine induces Ca2+ release by reducing the threshold for luminal Ca2+ activation of the ryanodine receptor., Biochem. J. 414 (2008) 441–52. doi:10.1042/BJ20080489.

[182] K. V. Olorunshola, L.N. Achie, Caffeine Alters Skeletal Muscle Contraction by Opening of Calcium Ion Channels, Curr. Res. J. Biol. Sci. 3 (2011) 521–525.

[183] T.-W. Chen, T.J. Wardill, Y. Sun, S.R. Pulver, S.L. Renninger, A. Baohan, E.R. Schreiter, R.A. Kerr, M.B. Orger, V. Jayaraman, L.L. Looger, K. Svoboda, D.S. Kim, Ultrasensitive fluorescent proteins for imaging neuronal activity., Nature. 499 (2013) 295–300. doi:10.1038/nature12354.

[184] G. Szabadkai, M.R. Duchen, Mitochondria: The Hub of Cellular Ca $^{2+}$

Signaling, Physiology. 23 (2008) 84–94. doi:10.1152/physiol.00046.2007.

[185] R.W. Daniels, A.J. Rossano, G.T. Macleod, B. Ganetzky, Expression of multiple transgenes from a single construct using viral 2A peptides in Drosophila., PLoS One. 9 (2014) e100637. doi:10.1371/journal.pone.0100637.

[186] V.A. Doronina, C. Wu, P. de Felipe, M.S. Sachs, M.D. Ryan, J.D. Brown, Site-specific release of nascent chains from ribosomes at a sense codon., Mol. Cell. Biol. 28 (2008) 4227–39. doi:10.1128/MCB.00421-08.

[187] J.H. Kim, S.R. Lee, L.H. Li, H.J. Park, J.H. Park, K.Y. Lee, M.K. Kim, B.A. Shin, S.Y. Choi, High cleavage efficiency of a 2A peptide derived from porcine teschovirus-1 in human cell lines, zebrafish and mice, PLoS One. 6 (2011) 1–8. doi:10.1371/journal.pone.0018556.

[188] Z. Liu, O. Chen, J.B.J. Wall, M. Zheng, Y. Zhou, L. Wang, H. Ruth Vaseghi, L. Qian, J. Liu, Systematic comparison of 2A peptides for cloning multi-genes in a polycistronic vector., Sci. Rep. 7 (2017) 2193. doi:10.1038/s41598-017-02460-2.

[189] E. Greotti, A. Wong, T. Pozzan, D. Pendin, P. Pizzo, Characterization of the ER-Targeted Low Affinity Ca(2+) Probe D4ER., Sensors (Basel). 16 (2016). doi:10.3390/s16091419.

[190] L. Galla, P. Pizzo, E. Greotti, Exploiting Cameleon Probes to Investigate Organelles Ca2+ Handling, in: A. Raffaello, D. Vecellio Reane (Eds.), Calcium Signal. Methods Protoc., Humana, New York, NY, 2019: pp. 15–30. doi:10.1007/978-1-4939-9018-4_2.

[191] S. Gehlert, W. Bloch, F. Suhr, Ca2+-Dependent Regulations and Signaling in Skeletal Muscle: From Electro-Mechanical Coupling to Adaptation, Int. J. Mol. Sci. 16 (2015) 1066. doi:10.3390/IJMS16011066.

[192] K.-M. Zhang, P. Hu, S.-W. Wang, L.D. Wright, A.S. Wechsler, J.A. Spratt, F.N. Briggs, Fast- and slow-twitch isoforms (SERCA1 and SERCA2a) of sarcoplasmic reticulum Ca-ATPase are expressed simultaneously in

chronically stimulated muscle fibers, Pflgers Arch. Eur. J. Physiol. Arch. Eur. J. Physiol. 433 (1997) 766–772. doi:10.1007/s004240050343.

[193] Z. Pan, M. Brotto, J. Ma, Store-operated Ca2+ entry in muscle physiology and diseases, BMB Rep. 47 (2014) 69. doi:10.5483/BMBREP.2014.47.2.015.

[194] J. Liou, M.L. Kim, W. Do Heo, J.T. Jones, J.W. Myers, J.E. Ferrell, T. Meyer, STIM Is a Ca2+ Sensor Essential for Ca2+-Store-Depletion-Triggered Ca2+ Influx, Curr. Biol. 15 (2005) 1235–1241. doi:10.1016/j.cub.2005.05.055.

[195] S. Feske, Y. Gwack, M. Prakriya, S. Srikanth, S.-H. Puppel, B. Tanasa, P.G. Hogan, R.S. Lewis, M. Daly, A. Rao, A mutation in Orai1 causes immune deficiency by abrogating CRAC channel function, Nature. 441 (2006) 179–185. doi:10.1038/nature04702.

[196] G. Chen, S. Carroll, P. Racay, J. Dick, D. Pette, I. Traub, G. Vrbova, P. Eggli, M. Celio, B. Schwaller, Deficiency in parvalbumin increases fatigue resistance in fast-twitch muscle and upregulates mitochondria, Am J Physiol Cell Physiol. 281 (2001) C114-122. http://ajpcell.physiology.org/content/281/1/C114.

[197] T. Pozzan, P. Magalhães, R. Rizzuto, The comeback of mitochondria to calcium signalling, Cell Calcium. 28 (2000) 279–283. doi:10.1054/ceca.2000.0166.

[198] E. Nisoli, E. Clementi, S. Moncada, M.O. Carruba, Mitochondrial biogenesis as a cellular signaling framework, Biochem. Pharmacol. 67 (2004) 1–15. doi:10.1016/J.BCP.2003.10.015.

[199] H. Esterbauer, H. Oberkofler, F. Krempler, W. Patsch, Human Peroxisome Proliferator Activated Receptor Gamma Coactivator 1 (PPARGC1) Gene: cDNA Sequence, Genomic Organization, Chromosomal Localization, and Tissue Expression, Genomics. 62 (1999) 98–102. doi:10.1006/geno.1999.5977.

[200] V. Romanello, E. Guadagnin, L. Gomes, I. Roder, C. Sandri, Y. Petersen, G. Milan, E. Masiero, P. Del Piccolo, M. Foretz, L. Scorrano, R. Rudolf, M. Sandri, Mitochondrial fission and remodelling contributes to muscle atrophy, EMBO J. 29 (2010) 1774–1785. doi:10.1038/emboj.2010.60.

[201] G. Twig, A. Elorza, A.J.A. Molina, H. Mohamed, J.D. Wikstrom, G. Walzer, L. Stiles, S.E. Haigh, S. Katz, G. Las, J. Alroy, M. Wu, B.F. Py, J. Yuan, J.T. Deeney, B.E. Corkey, O.S. Shirihai, Fission and selective fusion govern mitochondrial segregation and elimination by autophagy, EMBO J. 27 (2008) 433–446. doi:10.1038/sj.emboj.7601963.

[202] B.N. VanderVeen, D.K. Fix, J.A. Carson, Disrupted Skeletal Muscle Mitochondrial Dynamics, Mitophagy, and Biogenesis during Cancer Cachexia: A Role for Inflammation, Oxid. Med. Cell. Longev. 2017 (2017) 1–13. doi:10.1155/2017/3292087.

[203] M. Rojo, F. Legros, D. Chateau, A. Lombès, Membrane topology and mitochondrial targeting of mitofusins, ubiquitous mammalian homologs of the transmembrane GTPase Fzo., J. Cell Sci. 115 (2002) 1663–74. http://www.ncbi.nlm.nih.gov/pubmed/11950885.

[204] C.S. Palmer, K.D. Elgass, R.G. Parton, L.D. Osellame, D. Stojanovski, M.T. Ryan, Adaptor Proteins MiD49 and MiD51 Can Act Independently of Mff and Fis1 in Drp1 Recruitment and Are Specific for Mitochondrial Fission, J. Biol. Chem. 288 (2013) 27584–27593. doi:10.1074/jbc.M113.479873.

[205] S. Schiaffino, C. Reggiani, Fiber Types in Mammalian Skeletal Muscles, Physiol. Rev. 91 (2011) 1447–1531. doi:10.1152/physrev.00031.2010.

[206] B. Castro, S. Kuang, Evaluation of Muscle Performance in Mice by Treadmill Exhaustion Test and Whole-limb Grip Strength Assay., Bio-Protocol. 7 (2017). doi:10.21769/BioProtoc.2237.

[207] E. Carafoli, L. Santella, D. Branca, M. Brini, Generation, Control, and Processing of Cellular Calcium Signals, Crit. Rev. Biochem. Mol. Biol. 36 (2001) 107–260. doi:10.1080/20014091074183.

[208] M. Brini, Ca2+ signalling in mitochondria: mechanism and role in physiology and pathology, Cell Calcium. 34 (2003) 399–405. doi:10.1016/S0143-4160(03)00145-3.

[209] M.R. Duchen, Contributions of mitochondria to animal physiology: from homeostatic sensor to calcium signalling and cell death., J. Physiol. 516 (Pt 1) (1999) 1–17. doi:10.1111/j.1469-7793.1999.001aa.x.

[210] D.E. Clapham, Review Calcium Signaling, (2007) 1047–1058. doi:10.1016/j.cell.2007.11.028.

[211] E. Carafoli, M. Crompton, The regulation of intracellular calcium by mitochondria., Ann. N. Y. Acad. Sci. 307 (1978) 269–284. doi:10.1111/j.1749-6632.1978.tb41957.x.

[212] B. Korzeniewski, Regulation of ATP supply during muscle contraction: theoretical studies., Biochem. J. 330 (Pt 3 (1998) 1189–95. http://www.pubmedcentral.nih.gov/articlerender.fcgi?artid=1219260&tool=pmcentrez&rendertype=abstract.

[213] M. Montener, L. Kasert, J. Webert, M.W. Berchtoldu, M. Müntener, L. Käser, J. Weber, M.W. Berchtold, No Title, National Academy of Sciences, 1995. doi:10.1073/PNAS.92.14.6504.

[214] R.M. Paredes, J.C. Etzler, L.T. Watts, W. Zheng, J.D. Lechleiter, Chemical calcium indicators., Methods. 46 (2008) 143–51. doi:10.1016/j.ymeth.2008.09.025.

[215] O. Delbono, E. Stefani, Calcium transients in single mammalian skeletal muscle fibres., J. Physiol. 463 (1993) 689–707. http://www.ncbi.nlm.nih.gov/pubmed/8246201.

[216] A. Michelucci, M. García-Castañeda, S. Boncompagni, R.T. Dirksen, Role of STIM1/ORAI1-mediated store-operated Ca2+ entry in skeletal muscle physiology and disease, Cell Calcium. 76 (2018) 101–115. doi:10.1016/j.ceca.2018.10.004.

[217] N. Kurebayashi, Y. Ogawa, Depletion of Ca2+ in the sarcoplasmic reticulum

stimulates Ca2+ entry into mouse skeletal muscle fibres, J. Physiol. 533 (2001) 185–199. doi:10.1111/j.1469-7793.2001.0185b.x.

[218] G. Chen, P. Racay, S. Bichet, M.R. Celio, P. Eggli, B. Schwaller, Deficiency in parvalbumin, but not in calbindin D-28k upregulates mitochondrial volume and decreases smooth endoplasmic reticulum surface selectively in a peripheral, subplasmalemmal region in the soma of Purkinje cells, Neuroscience. 142 (2006) 97–105. doi:10.1016/j.neuroscience.2006.06.008.

[219] W. Maetzler, C. Nitsch, K. Bendfeldt, P. Racay, F. Vollenweider, B. Schwaller, Ectopic parvalbumin expression in mouse forebrain neurons increases excitotoxic injury provoked by ibotenic acid injection into the striatum, Exp. Neurol. 186 (2004) 78–88. doi:10.1016/j.expneurol.2003.10.014.

[220] L. Van Den Bosch, B. Schwaller, V. Vleminckx, B. Meijers, S. Stork, T. Ruehlicke, E. Van Houtte, H. Klaassen, M.R. Celio, L. Missiaen, W. Robberecht, M.W. Berchtold, Protective Effect of Parvalbumin on Excitotoxic Motor Neuron Death, Exp. Neurol. 174 (2002) 150–161. https://linkinghub.elsevier.com/retrieve/pii/S0014488601978586.

[221] L. Lichvarova, T. Henzi, D. Safiulina, A. Kaasik, B. Schwaller, Parvalbumin alters mitochondrial dynamics and affects cell morphology, Cell. Mol. Life Sci. (2018). doi:10.1007/s00018-018-2921-x.

[222] K. Palikaras, E. Lionaki, N. Tavernarakis, Balancing mitochondrial biogenesis and mitophagy to maintain energy metabolism homeostasis, Cell Death Differ. 22 (2015) 1399–1401. doi:10.1038/cdd.2015.86.

[223] I. Scott, R.J. Youle, Mitochondrial fission and fusion., Essays Biochem. 47 (2010) 85–98. doi:10.1042/bse0470085.

[224] T.S.M. and R.W.W. Martin J. Kushmerick, M.J. Kushmerick, T.S. Moerland, R.W. Wiseman, Mammalian Skeletal Muscle Fibers Distinguished by Contents of Phosphocreatine, ATP, and P i, (1992). doi:10.1073/pnas.89.16.7521.

[225] E. Zubrzycka-Gaarn, B. Korczak, H. Osinska, M.G. Sarzala, Studies on sarcoplasmic reticulum from slow-twitch muscle,]Ournal Muscle Res. Cell Motil. 3 (1982) 191–212. https://link.springer.com/content/pdf/10.1007%2FBF00711942.pdf.

[226] J.M. Sacheck, A. Ohtsuka, S.C. McLary, A.L. Goldberg, IGF-I stimulates muscle growth by suppressing protein breakdown and expression of atrophy-related ubiquitin ligases, atrogin-1 and MuRF1, Am. J. Physiol. Metab. 287 (2004) E591–E601. doi:10.1152/ajpendo.00073.2004.

[227] O. Delbono, Molecular mechanisms and therapeutics of the deficit in specific force in ageing skeletal muscle., Biogerontology. 3 (2002) 265–70. http://www.ncbi.nlm.nih.gov/pubmed/12237563.

[228] N. Weisleder, M. Brotto, S. Komazaki, Z. Pan, X. Zhao, T. Nosek, J. Parness, H. Takeshima, J. Ma, Muscle aging is associated with compromised Ca2+ spark signaling and segregated intracellular Ca2+ release., J. Cell Biol. 174 (2006) 639–45. doi:10.1083/jcb.200604166.

[229] F. De Backer, C. Vandebrouck, P. Gailly, J.M. Gillis, Long-term study of Ca(2+) homeostasis and of survival in collagenase-isolated muscle fibres from normal and mdx mice., J. Physiol. 542 (2002) 855–65. doi:10.1113/jphysiol.2002.020487.

[230] M. DiFranco, C.E. Woods, J. Capote, J.L. Vergara, Dystrophic skeletal muscle fibers display alterations at the level of calcium microdomains., Proc. Natl. Acad. Sci. U. S. A. 105 (2008) 14698–703. doi:10.1073/pnas.0802217105.

[231] N. Mallouk, V. Jacquemond, B. Allard, Elevated subsarcolemmal Ca2+ in mdx mouse skeletal muscle fibers detected with Ca2+-activated K+ channels., Proc. Natl. Acad. Sci. U. S. A. 97 (2000) 4950–5. doi:10.1073/pnas.97.9.4950.

[232] C. Vandebrouck, D. Martin, M. Colson-Van Schoor, H. Debaix, P. Gailly, Involvement of TRPC in the abnormal calcium influx observed in dystrophic (mdx) mouse skeletal muscle fibers., J. Cell Biol. 158 (2002) 1089–96.

doi:10.1083/jcb.200203091.

[233] X. Wang, N. Weisleder, C. Collet, J. Zhou, Y. Chu, Y. Hirata, X. Zhao, Z. Pan, M. Brotto, H. Cheng, J. Ma, Uncontrolled calcium sparks act as a dystrophic signal for mammalian skeletal muscle, Nat. Cell Biol. 7 (2005) 525–530. doi:10.1038/ncb1254.

[234] L. Pietrangelo, A. D'Incecco, A. Ainbinder, A. Michelucci, H. Kern, R.T. Dirksen, S. Boncompagni, F. Protasi, Age-dependent uncoupling of mitochondria from Ca²⁺ release units in skeletal muscle, Oncotarget. 6 (2015) 35358–71. doi:10.18632/oncotarget.6139.

[235] A. V. Loud, A quantitative stereological description of the ultrastructure of normal rat liver parenchymal cells, J. Cell Biol. 37 (1968) 27–46. doi:10.1083/jcb.37.1.27.

[236] B.A. Mobley, B.R. Eisenberg, Sizes of components in frog skeletal muscle measured by methods of stereology, J. Gen. Physiol. 66 (1975) 31–45. doi:10.1085/jgp.66.1.31.

[237] X. Rao, X. Huang, Z. Zhou, X. Lin, An improvement of the 2ˆ(-delta delta CT) method for quantitative real-time polymerase chain reaction data analysis., Biostat. Bioinforma. Biomath. 3 (2013) 71–85. http://www.ncbi.nlm.nih.gov/pubmed/25558171.

[238] J. Schindelin, I. Arganda-Carreras, E. Frise, V. Kaynig, M. Longair, T. Pietzsch, S. Preibisch, C. Rueden, S. Saalfeld, B. Schmid, J.-Y. Tinevez, D.J. White, V. Hartenstein, K. Eliceiri, P. Tomancak, A. Cardona, Fiji: an open-source platform for biological-image analysis, Nat. Methods. 9 (2012) 676–682. doi:10.1038/nmeth.2019.

[239] S.M. Müller, H. Galliardt, J. Schneider, B.G. Barisas, T. Seidel, Quantification of Förster resonance energy transfer by monitoring sensitized emission in living plant cells., Front. Plant Sci. 4 (2013) 413. doi:10.3389/fpls.2013.00413.

[240] P. Pinton, A. Rimessi, A. Romagnoli, A. Prandini, R. Rizzuto, Biosensors

for the Detection of Calcium and pH, Methods Cell Biol. 80 (2007) 297–325. doi:10.1016/S0091-679X(06)80015-4.

9. Appendices

In this section, the following items are present:

- Manuscript entitled “A MICU1 Splice Variant Confers High Sensitivity to the Mitochondrial Ca^{2+} Uptake Machinery of Skeletal Muscle”, published in Molecular Cell journal, vol. 64, no. 4, pp. 760–773, Nov. 2016
- Manuscript entitled “Crosstalk between Calcium and ROS in Pathophysiological Conditions,” published in Oxidative Medicine and Cellular Longevity journal, vol. 2019, pp. 1–18, Apr. 2019.

Article

Molecular Cell

A MICU1 Splice Variant Confers High Sensitivity to the Mitochondrial Ca^{2+} Uptake Machinery of Skeletal Muscle

Graphical Abstract

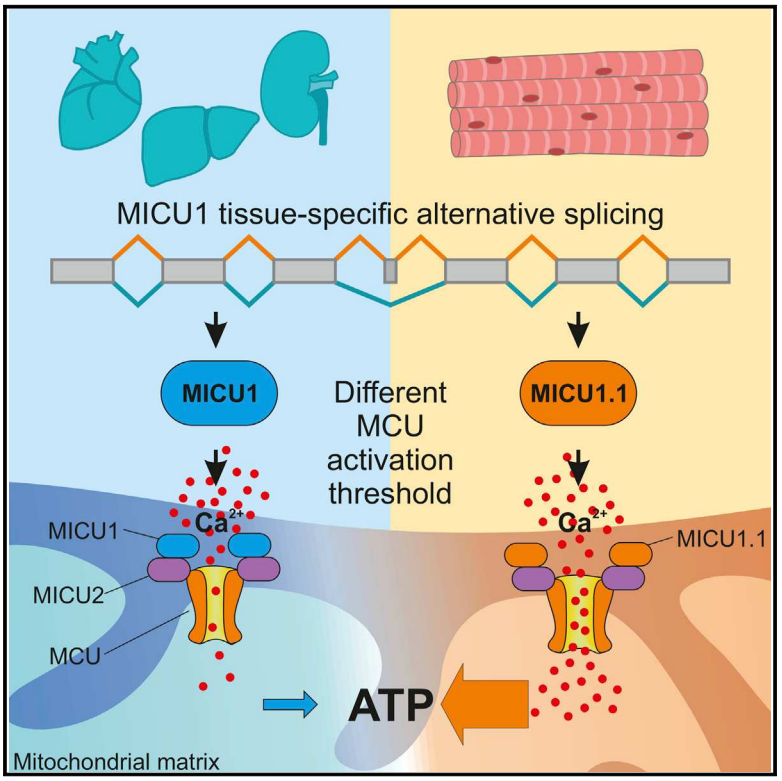

Authors

Denis Vecellio Reane, Francesca Vallese, Vanessa Checchetto, ..., Giuseppe Zanotti, Rosario Rizzuto, Anna Raffaello

Correspondence

rosario.rizzuto@unipd.it (R.R.), anna.raffaello@unipd.it (A.R.)

In Brief

Vecellio Reane et al. identify a unique skeletal muscle-specific mitochondrial Ca^{2+} uniporter complex containing an alternative splice isoform of MICU1, MICU1.1, that profoundly modifies the properties of mitochondrial Ca^{2+} uptake. MICU1.1 is required for providing sufficient levels of mitochondrial Ca^{2+} to sustain oxidative ATP production for resistance and strenuous exercise.

Highlights

- Skeletal muscle mitochondria express a unique MCU complex conserved in vertebrates
- The complex prevalently contains the alternative splice isoform of MICU1, MICU1.1
- MICU1.1-MICU2 heterodimers diminish the Ca^{2+} activation threshold of MCU
- In skeletal muscle, MICU1.1 is required to amplify ATP supply for contraction

Vecellio Reane et al., 2016, Molecular Cell *64*, 760–773
November 17, 2016
http://dx.doi.org/10.1016/j.molcel.2016.10.001

CellPress

CellPress

Molecular Cell
Article

A MICU1 Splice Variant Confers High Sensitivity to the Mitochondrial Ca^{2+} Uptake Machinery of Skeletal Muscle

Denis Vecellio Reane,[1] Francesca Vallese,[1] Vanessa Checchetto,[2] Laura Acquasaliente,[3] Gaia Butera,[1] Vincenzo De Filippis,[3] Ildikò Szabò,[2] Giuseppe Zanotti,[1] Rosario Rizzuto,[1,4,*] and Anna Raffaello[1,5,*]
[1]Department of Biomedical Sciences, University of Padua, 35122 Padua, Italy
[2]Department of Biology, University of Padua, 35122 Padua, Italy
[3]Laboratory of Protein Chemistry, Department of Pharmaceutical and Pharmacological Sciences, University of Padua, 35122 Padua, Italy
[4]CNR Institute of Neuroscience, National Council of Research, 35122 Padua, Italy
[5]Lead Contact
*Correspondence: rosario.rizzuto@unipd.it (R.R.), anna.raffaello@unipd.it (A.R.)
http://dx.doi.org/10.1016/j.molcel.2016.10.001

SUMMARY

Skeletal muscle is a dynamic organ, characterized by an incredible ability to rapidly increase its rate of energy consumption to sustain activity. Muscle mitochondria provide most of the ATP required for contraction via oxidative phosphorylation. Here we found that skeletal muscle mitochondria express a unique MCU complex containing an alternative splice isoform of MICU1, MICU1.1, characterized by the addition of a micro-exon that is sufficient to greatly modify the properties of the MCU. Indeed, MICU1.1 binds Ca^{2+} one order of magnitude more efficiently than MICU1 and, when heterodimerized with MICU2, activates MCU current at lower Ca^{2+} concentrations than MICU1-MICU2 heterodimers. In skeletal muscle in vivo, MICU1.1 is required for sustained mitochondrial Ca^{2+} uptake and ATP production. These results highlight a novel mechanism of the molecular plasticity of the MCU Ca^{2+} uptake machinery that allows skeletal muscle mitochondria to be highly responsive to sarcoplasmic $[Ca^{2+}]$ responses.

INTRODUCTION

Mitochondrial Ca^{2+} signaling triggers a vast repertoire of cellular functions such as oxidative metabolism, reactive oxygen species (ROS) production, and cell death (Rizzuto et al., 2012). Seminal discoveries in the last 5 years have identified the pore-forming and regulatory subunits of the mitochondrial Ca^{2+} uniporter (Mammucari et al., 2016). It is now clear that the intermembrane space proteins MICU1 and MICU2 sense cytosolic Ca^{2+} concentration ($[Ca^{2+}]_{cyt}$) through EF-hand Ca^{2+} binding sites and influence the activity of MCU (Csordás et al., 2013; Kamer and Mootha, 2014; Mallilankaraman et al., 2012; Patron et al., 2014; Wang et al., 2014). The emerging model is that the heterodimer formed by MICU1 and MICU2 cooperates in translating $[Ca^{2+}]_{cyt}$ in the sigmoidal response of mitochondrial Ca^{2+} uptake (Kamer and Mootha, 2014; Patron et al., 2014), although some discrepancies have not yet been resolved (Mammucari et al., 2016). We recently demonstrated that, during cell stimulation, MICU1 induces MCU activity, acting as the cooperative activator of the channel, whereas MICU2 acts as the genuine gatekeeper of MCU at low $[Ca^{2+}]_{cyt}$ (Patron et al., 2014), despite the huge driving force for matrix cation entry, thus preventing vicious cycling for Ca^{2+} accumulation (Rizzuto et al., 2012).

In skeletal muscle, contraction is initiated by the release of Ca^{2+} by the sarcoplasmic reticulum (SR), which induces an increase of Ca^{2+} concentration in the sarcoplasm. These waves are transmitted to mitochondria (Brini et al., 1997), which respond by activating Ca^{2+}-sensitive dehydrogenases that are key rate-controlling enzymes in tricarboxylic acid cycle flux to avoid a quick exhaustion of ATP during contraction (Glancy et al., 2013). The control of oxidative phosphorylation by Ca^{2+} is particularly crucial in skeletal muscle, one of the most ATP-consuming organs of the body. Indeed, oxygen consumption rates can increase over 100-fold from rest to maximal aerobic exercise (Madsen et al., 1996; Weibel and Hoppeler, 2005). It is thus not surprising that skeletal muscle mitochondria display the highest mitochondrial Ca^{2+} transients, as demonstrated by the measurement of the MCU current (I_{MCU}) by patch-clamp of mitoplasts from different tissues (Fieni et al., 2012).

Furthermore, skeletal muscle mitochondrial Ca^{2+} serves other specific functions. Indeed, we recently demonstrated that MCU controls muscle trophism by regulating the IGF1-AKT/PKB and PGC-1α4 pathways (Mammucari et al., 2015).

Given these crucial functions exerted by mitochondrial Ca^{2+} in skeletal muscle, we hypothesized the presence of a skeletal muscle-specific MCU complex. A detailed analysis of the MCU complex in skeletal muscle revealed a novel mechanism based on a muscle-specific alternative splice variant of MICU1, MICU1.1, characterized by the addition of a micro-exon coding for four amino acids that substantially modifies the properties of the MCU complex. Indeed, during cell stimulation, the dimer MICU1.1-MICU2 activates the channel, resulting in a higher

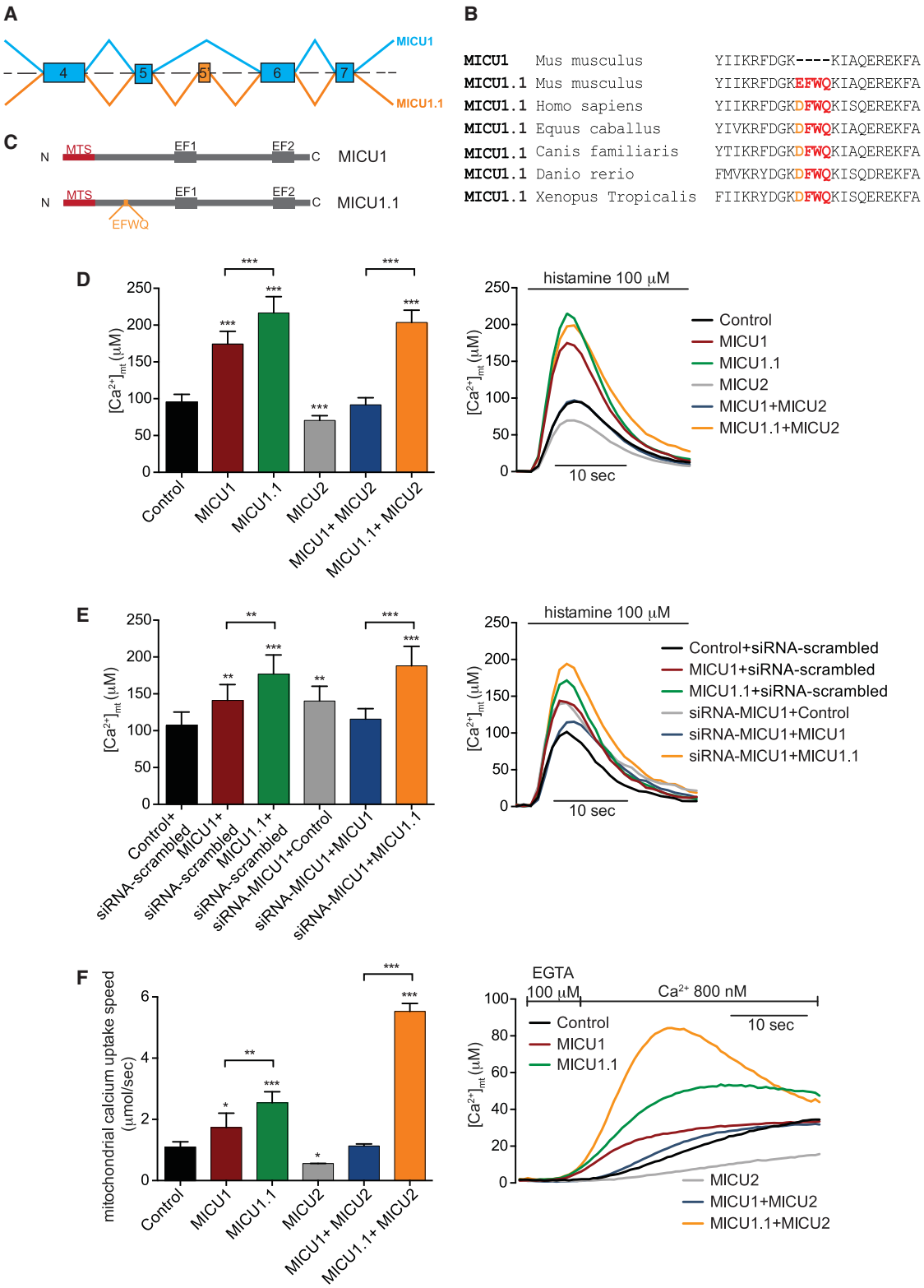

Figure 1. Identification of the Alternative Splice Variant of MICU1, MICU1.1, which Acts as a Strong MCU Activator in Stimulated Cells

(A) Partial schematic of the *Mus musculus* MICU1 genomic locus. In-frame inclusion of exon 5′ produces MICU1.1.

(B) Sequence alignment of conventional MICU1 and MICU1.1 of six vertebrate species. Conservative differences are marked in orange and sequence identities in red.

(legend continued on next page)

entry of Ca^{2+} into mitochondria than MICU1-MICU2, whereas, at low $[Ca^{2+}]_{cyt}$, the heterodimer MICU1.1-MICU2 acts as a gatekeeper of the channel. MICU1.1 interacts with the MCU complex components and heterodimerizes with MICU2 as conventional MICU1. As for the mechanism, the dimer MICU1.1-MICU2 shifts the threshold of activation of MCU to lower $[Ca^{2+}]$. This effect is accompanied by the higher Ca^{2+} binding affinity of the EF domains of MICU1.1 compared with those of MICU1. In skeletal muscle in vivo, acute and forced expression of MICU1 by antisense oligonucleotide-mediated exon skipping of the MICU1.1 micro-exon demonstrates that MICU1.1 is required to modulate mitochondrial metabolism.

These data reveal a muscle-specific unique mitochondrial Ca^{2+} uptake machinery that fully accounts for the high responsiveness of muscle mitochondria to sarcoplasmic Ca^{2+} signals.

RESULTS

Characterization of the Skeletal Muscle MCU Complex

By sequencing cDNAs derived from mouse skeletal muscle mRNA, we identified a splice variant of MICU1 that we named MICU1.1, characterized by the addition of a micro-exon, named exon 5′, coding for four amino acids (EFWQ) inserted after amino acid 181 of the MICU1 sequence (NM_144822) (Figure 1A). The sequence corresponding to this splice isoform is deposited in the NCBI database (NM_001291443). Intriguingly, exon 5′ of MICU1.1 is present and highly conserved in all vertebrates (Figure 1B). This additional micro-exon of MICU1.1 is localized far from the two EF-hand domains in the primary sequence (Figure 1C), and thus, a specific function cannot be immediately ascribed.

To unravel the role of this tissue-specific splicing variant of MICU1, we overexpressed MICU1.1 and MICU1 in HeLa cells that express only MICU1 (Figure S1A), and we measured mitochondrial Ca^{2+} uptake in intact cells (Figure 1D). Mitochondrial Ca^{2+} concentrations ($[Ca^{2+}]_{mt}$) measurements showed a 25% enhancement of the transient rise evoked by stimulation with the inositol 1,4,5-trisphosphate-generating agonist histamine (100 μM) in MICU1.1-overexpressing cells compared with MICU1-overexpressing ones (Figure 1D). Importantly, this response is not due to different levels of overexpression of the constructs (Figure S1B). The greater mitochondrial response of MICU1 and MICU1.1 overexpression is not secondary to alterations of the cytosolic response. Rather, a significant reduction in the $[Ca^{2+}]_{cyt}$ transient is observed, most likely because of increased Ca^{2+} clearance by mitochondria (Figure S1C). Furthermore, no significant change was detected in the driving force for Ca^{2+} accumulation upon MICU1.1 overexpression (mitochondrial membrane potential, $\Delta\Psi$) (Figure S1D).

We then overexpressed the genuine MCU gatekeeper MICU2 alone and together with MICU1 and MICU1.1 (Figure 1D). As expected, MICU2-overexpressing HeLa cells showed a significant reduction of the $[Ca^{2+}]_{mt}$ peak, and when MICU1 and MICU2 were both overexpressed, leading to an increase of the heterodimer, the MICU1-dependent potentiation of $[Ca^{2+}]_{mt}$ responses was almost abolished, as already shown (Figure 1D; Patron et al., 2014). Strikingly, MICU2 was unable to decrease MICU1.1-dependent potentiation of $[Ca^{2+}]_{mt}$ (Figure 1D), although the protein levels of the overexpressed proteins were comparable (Figure S1B).

Furthermore, we silenced endogenous human MICU1, and we rescued the knockdown by overexpressing mouse MICU1 or MICU1.1 (Figure 1E). The effect of MICU1 knockdown (Figure S1E) is efficiently rescued by MICU1 transfection in HeLa cells because, under this condition, the $[Ca^{2+}]_{mt}$ peak is undistinguishable from control cells. On the other hand, cells in which MICU1 was knocked down and rescued by MICU1.1 transfection (Figure S1F) display a $[Ca^{2+}]_{mt}$ peak significantly higher compared with control cells and, importantly, indistinguishable from MICU1.1-overexpressing cells (Figure 1E).

We also verified that these effects were not dependent on the model used, HeLa cells. Therefore, we analyzed $[Ca^{2+}]_{mt}$ responses under the same conditions as shown in Figure 1D in HEK293 cells stimulated with 100 μM ATP, obtaining comparable results (Figure S2A).

We also verified the effect of MICU1.1 in skeletal muscle in vivo by transfecting adult flexor digitorum brevis (FDB) mouse muscles with plasmids encoding a GFP-based Ca^{2+} probe targeted to mitochondria, mtGCaMP6f (Chen et al., 2013), in combination with a construct encoding pmCherry-P2A-N1 (control), MICU1-HA-P2A-pmCherry-N1 (MICU1), or MICU1.1-HA-P2A-pmCherry-N1 (MICU1.1). MICU1 and MICU1.1 sequences were linked to a self-cleaving P2A peptide to the mCherry red fluorescent protein (Kim et al., 2011) to visualize the transfected fibers and avoid mislocalization of MICU1 and MICU1.1 linked to mCherry. Eight days later, when FDB muscles expressed the proteins of interest (Figure S2B), real-time imaging experiments were performed on isolated single myofibers (Figure S2C), as already performed (Mammucari et al., 2015). Also, in skeletal muscle, MICU1.1 overexpression causes a significant increase in mitochondrial $[Ca^{2+}]$, evoked by discharging the SR pool with caffeine, compared with control (Figure S2C).

Because MICU1.1 is also present in humans (Figure 1B), we asked whether the human MICU1.1 also has the same effect on $[Ca^{2+}]_{mt}$. $[Ca^{2+}]_{mt}$ measurements on HeLa cells overexpressing *Homo sapiens* MICU1 (hs-MICU1), MICU1.1 (hs-MICU1.1),

(C) Domain structure of MICU1 and MICU1.1. N and C, N and C termini, respectively; MTS, mitochondrial targeting signal; EF1 and EF2, EF-hand domains; EFWQ, extra exon in the MICU1.1 primary structure.

(D and E) $[Ca^{2+}]_{mt}$ measurements in intact HeLa cells transfected with the indicated constructs (D) or constructs and siRNAs (E) and challenged with maximal histamine stimulation (n = 10).

(F) $[Ca^{2+}]_{mt}$ measurements in permeabilized HeLa cells transfected with the indicated constructs upon exposure to 800 nM $[Ca^{2+}]$. Right: representative traces of the experiment. Left: bar diagram representing the mean $[Ca^{2+}]_{mt}$ speed (n = 4).

Data are presented as mean ± SD. One-way ANOVA was used with post hoc Bonferroni tests for each sample. *$p < 0.05$, **$p < 0.01$, and ***$p < 0.005$ compared with the control unless specified otherwise. See also Figures S1 and S2.

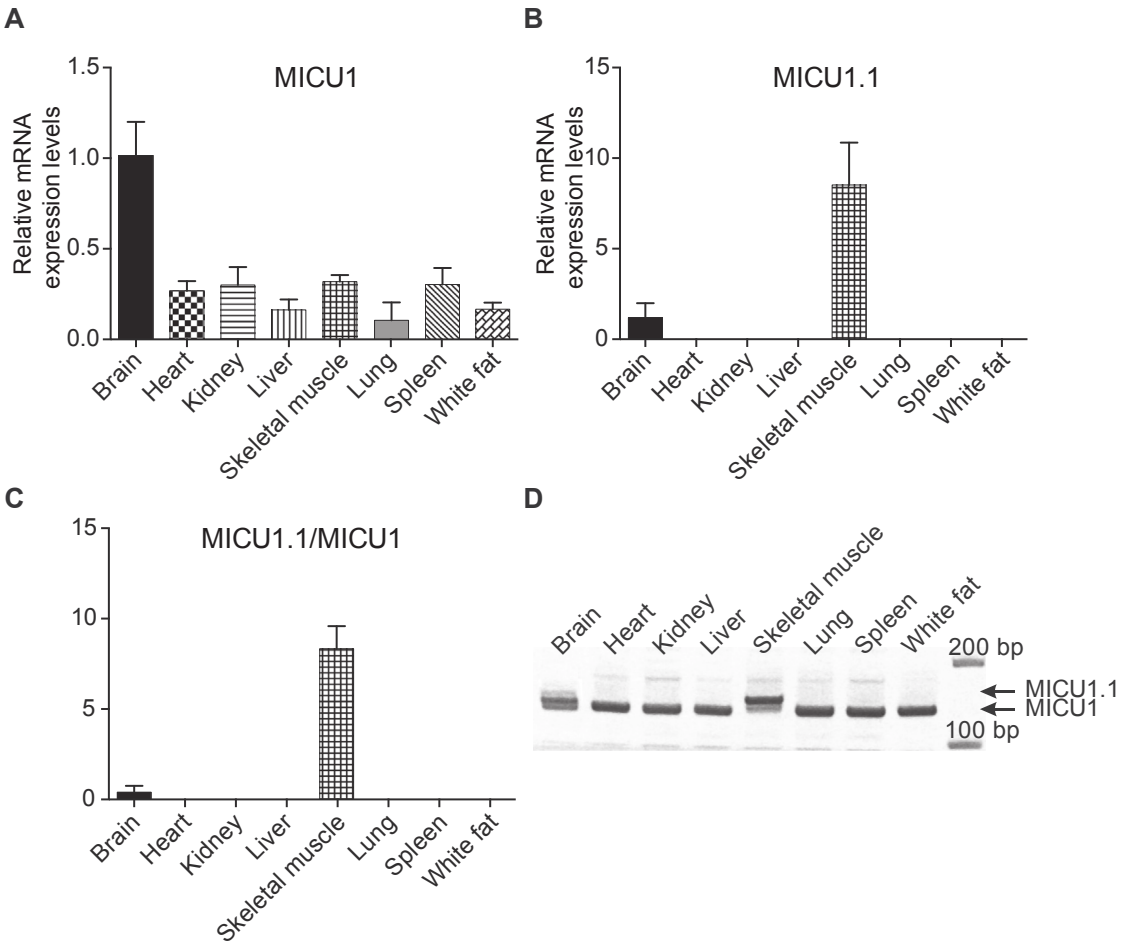

Figure 2. MICU1.1 Expression in Mouse Tissues

(A) MICU1 relative expression levels in mouse tissues measured by real-time PCR normalized for Thioredoxin 1 (TNX1). Expression levels are normalized to the brain and presented as mean ± SD (n = 4).

(B) MICU1.1 relative expression levels as in (A) (n = 4).

(C) MICU1.1/MICU1 expression ratio among different mouse tissues ($2^{-\Delta Ct}$ MICU1.1/ $2^{-\Delta Ct}$ MICU1).

(D) Representative acrylamide gel of PCR products using primers spanning the MICU1 extra exon of cDNA of different mouse tissues. MICU1.1 produces a band of 152 base pairs (bp) and MICU1 of 140 bp.

See also Figure S3.

showed a marked enhancement of the transient rise evoked by stimulation with histamine (100 μM) of hs-MICU1.1 compared with hs-MICU1 (Figure S2D), and, again, no reduction was observed upon overexpression of human MICU2 (hs-MICU2; Figure S2D).

To better define these unpredicted results, we analyzed the effect of MICU1.1 on mitochondrial Ca^{2+} uptake in permeabilized cells compared with the control (Figure 1F), as already performed (Patron et al., 2014). Overexpression of MICU1 increases the rate of Ca^{2+} accumulation, whereas MICU2 overexpression reduces it (Figure 1F, left). Overexpression of MICU1.1 causes a much greater enhancement of mitochondrial Ca^{2+} uptake than MICU1 (Figure 1F). Interestingly, co-expression of MICU2 with MICU1.1 not only reduces the rate of Ca^{2+} accumulation but, rather, further increases it (Figure 1F, left).

Tissue-Specific Expression and Subcellular Localization of MICU1.1

Next we analyzed the expression pattern of *Micu1.1* by real-time PCR in several mouse tissues. Different from *Micu1*, which is ubiquitously expressed (Figure 2A; Baughman et al., 2011; De Stefani et al., 2011; Plovanich et al., 2013), *Micu1.1* expression is restricted to skeletal muscle, and lower levels are found in the brain (Figure 2B). *Micu1 and Micu1.1* are co-expressed with an 1:1 *Micu1.1/Micu1* ratio in brain, whereas in skeletal muscle, *Micu1.1* is the predominant form with an 8:1 *Micu1.1/Micu1* ratio (Figure 2C). We also verified these data by conventional PCR using primers spanning exon 5′ and separating the PCR products in an acrylamide gel (Figure 2D). Furthermore, MICU1.1 localizes to mitochondria (Figure S3), as expected from the identity of the mitochondrial targeting sequence with MICU1.

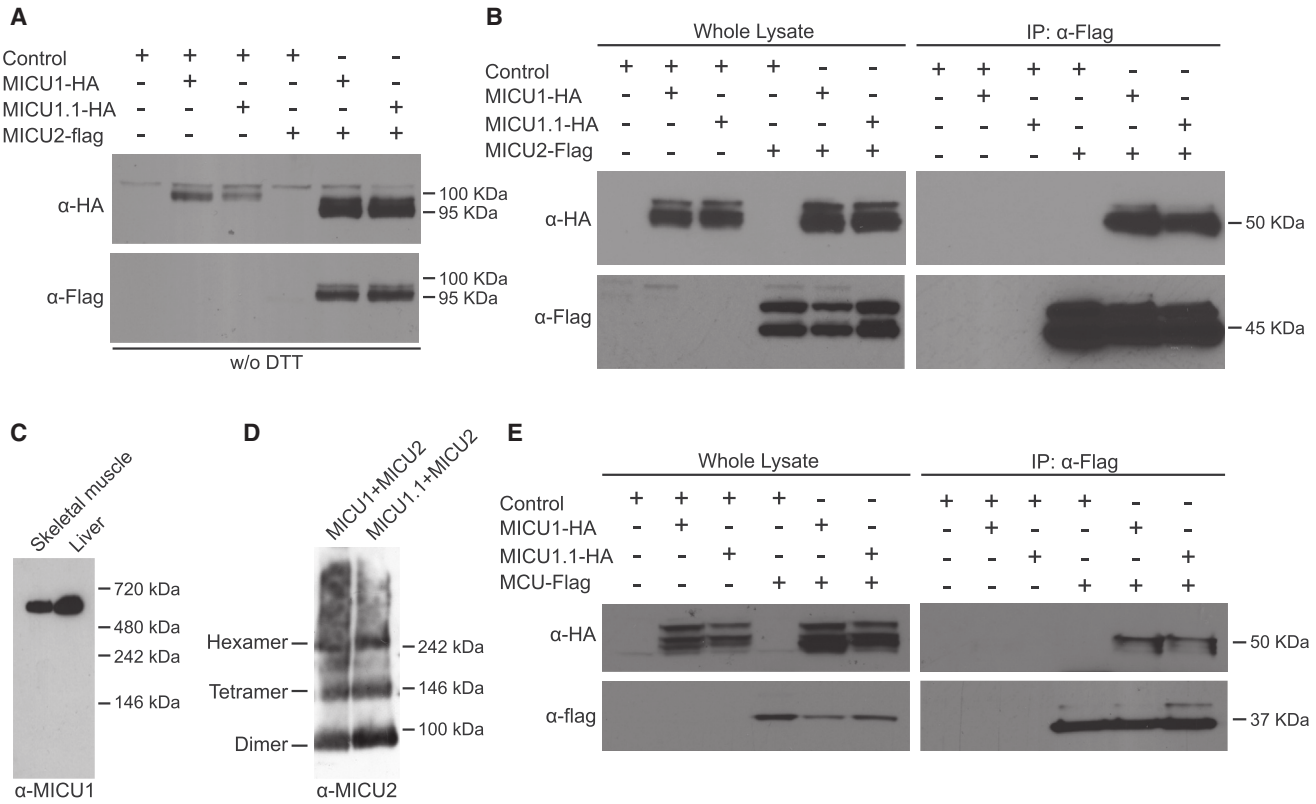

Figure 3. Biochemical Characterization of MICU1.1

(A) Homo- or heterodimer formation. HeLa cells were harvested after 24 hr of transfection with the indicated constructs, and total protein was extracted and subjected to western blotting analysis with α-FLAG and α-HA antibodies. SDS-PAGE was performed in the absence of DTT.

(B) Co-immunoprecipitation experiments. HeLa cells were transfected with the indicated constructs. FLAG-tagged MCU was immunoprecipitated from whole-cell lysate with a α-FLAG antibody. The precipitated proteins were immunoblotted with α-FLAG and α-HA antibodies.

(C) BN-PAGE of mitochondrial enriched fraction derived from mouse skeletal muscle and liver. The gel was immunoblotted with α-MICU1 antibody.

(D) BN-PAGE of MICU1-MICU2 and MICU1.1-MICU2 heterodimers purified through affinity chromatography from the insect cell line upon baculovirus infection and immunoblotted with α-MICU2 antibody. Based on the predicted molecular weight, the possible supercomplexes of dimers are indicated on the left.

(E) Co-immunoprecipitation experiments as in (B) with the indicated constructs.

See also Figure S4.

MICU1.1 Forms Homodimers and Heterodimers with MICU2 and Interacts with MCU as MICU1

We then asked whether the effects of MICU1.1 on mitochondrial Ca^{2+} homeostasis were due to changes in the MICU1.1 ability to homodimerize and to form high-molecular-weight complexes with MICU2. We carried out immunoblot analyses under non-reducing conditions because MICU1 can homodimerize and heterodimerize with MICU2 through a disulfide bond (Patron et al., 2014). Figure 3A shows that both MICU1 and MICU1.1 overexpression induces the formation of the 100-kDa homodimer and that they are equally able to form the 95-kDa heterodimer when MICU2 is overexpressed together with MICU1 and MICU1.1. We also revealed the in situ interaction between MICU1.1 and MICU2 by expressing, in HeLa cells, MICU1-HA, MICU1.1-HA and MICU2-FLAG. The α-FLAG antibody immunoprecipitated not only MICU1 but also MICU1.1 (Figure 3B).

In previous studies, it was demonstrated that MCU is present in high-molecular-weight complexes (Perocchi et al., 2010; Plovanich et al., 2013). To verify that MICU1.1 does not alter the composition and stoichiometry of the MCU complex, we purified mitochondria from mouse skeletal muscle, where MICU1.1 is the prevalent form, and from mouse liver, where MICU1 is the only isoform expressed, and the samples were loaded in a Blue Native (BN)-PAGE (Figure 3C). Incubation with an α-MICU1-specific antibody that can recognize both MICU1 and MICU1.1 demonstrates that the MCU complex present in skeletal muscle mitochondria does not differ from the liver complex (Figure 3C). To further confirm this result, we performed BN-PAGE of affinity-purified recombinant MICU1.1-MICU2 heterodimers. We could not produce functional heterodimers in *E. coli* because this system cannot ensure the formation of the disulfide bond between MICU1 and MICU2. Thus, we expressed MICU1 and MICU1.1 together with MICU2 in eukaryotic cells using a baculovirus/insect cells system that allows efficient production of recombinant proteins with the appropriated post-translational modifications. The purified heterodimers were loaded in a BN-PAGE and immunoblotted using an α-MICU2-specific antibody. We observed three different protein complexes that are compatible with the

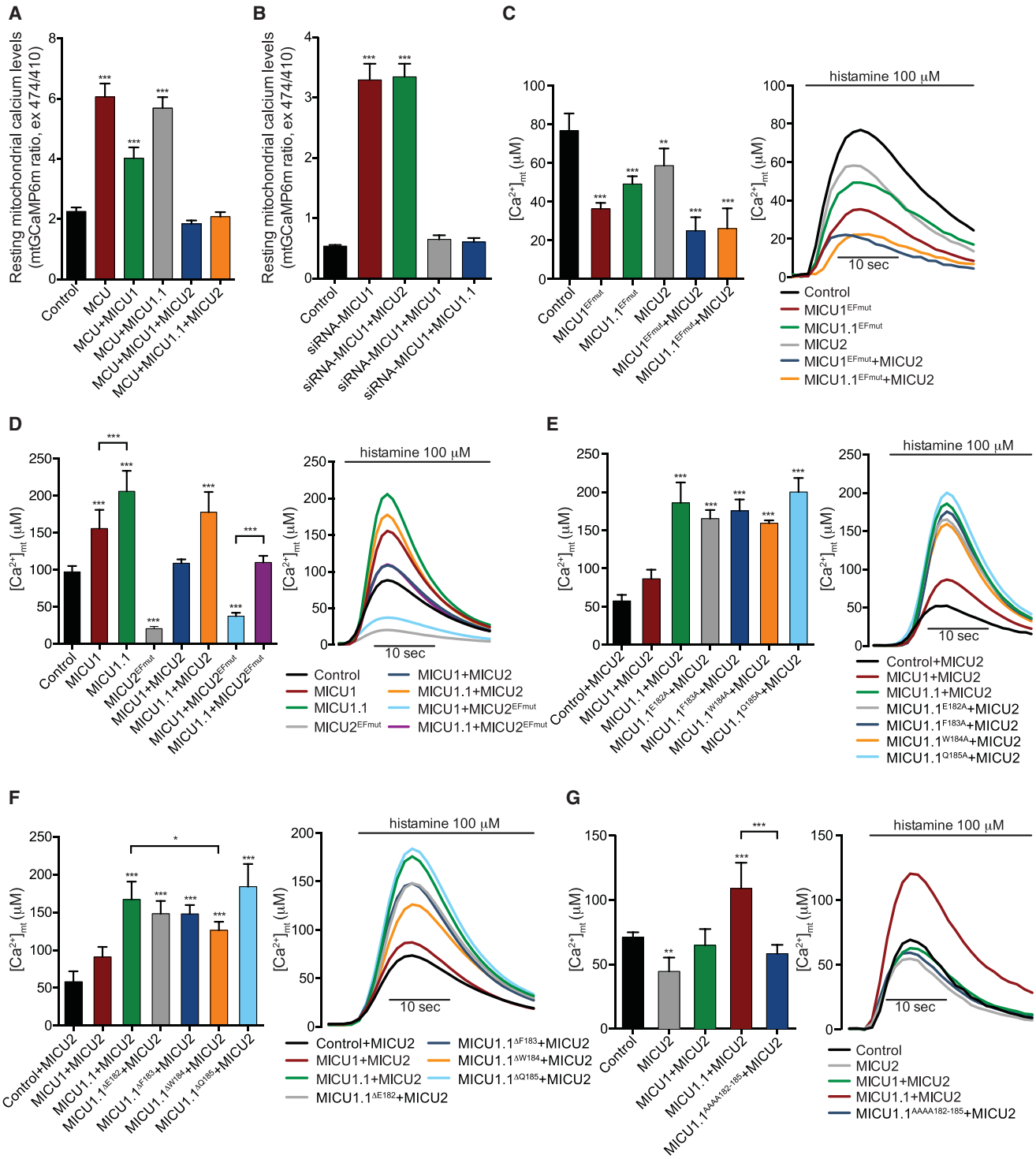

Figure 4. Ca^{2+}-Dependent Functional Effects of MICU1.1 and MICU2 and Mutagenesis Analysis of MICU1.1 Micro-exon Residues

(A) Resting mitochondrial Ca^{2+} levels in HeLa cells overexpressing the indicated constructs, evaluated through ratiometric imaging of the mitochondrial targeted GCaMP6m (n = 15).

(B) Resting mitochondrial Ca^{2+} levels in HeLa cells silenced for endogenous MICU1 and overexpressing MICU2, MICU1, or MICU1.1 performed as in (A) (n = 15).

(legend continued on next page)

dimeric, tetrameric, and hexameric forms of the MICU1-MICU2 complex (Figure 3D) on the basis of the predicted molecular weight of the MICU1-MICU2 heterodimer (95 kDa). Furthermore, we found that MICU1.1 interacts with MCU as well as MICU1 because MCU-FLAG can immunoprecipitate both MICU1 and MICU1.1 (Figure 3E).

Recently, affinity purification and quantitative proteomics of the MCU complex identified a 10-kDa, membrane-spanning, metazoan-specific protein called EMRE (essential MCU regulator) that was hypothesized to be required for the interaction of MCU with the heterodimer MICU1-MICU2 (Sancak et al., 2013). The binding properties of MCU/EMRE with MICU1 and MICU1.1 were investigated by surface plasmon resonance (SPR) analysis, which allowed us to quantitatively estimate the equilibrium dissociation constant, K_d, for the MICUs-MCU/EMRE complex. The sensograms in Figures S4A and S4B indicate that both MICU1 (Figure S4A, open dots) and MICU1.1 (Figure S4B, open dots) bind to immobilized MCU/EMRE. The binding data were analyzed in affinity mode within the framework of the one-site binding model and suggest that MICU1 and MICU1.1 interact with MCU/EMRE with identical affinities, yielding K_d values of 10.9 ± 2.1 μM and 8.1 ± 1.1 μM, respectively (Figure S4C). Control experiments carried out by immobilizing MCU alone on a carboxymethylated-dextran CM5 sensor chip demonstrated that, under these conditions, EMRE is not or only poorly involved in MCU-MICU1/MICU1.1 interaction (Figures S4A and S4B, solid dots). The K_d values derived from these sets of measurements (i.e., K_d = 14.0 ± 4.0 μM for MICU1/MCU and K_d = 19.2 ± 3.5 μM for MICU1.1/MCU; Figure S4C) are consistent with those estimated for the MCU/EMRE complex.

At Resting $[Ca^{2+}]_{cyt}$, MICU1.1 Acts as a Gatekeeper of the MCU Channel as MICU1

Although, at high $[Ca^{2+}]$, the stimulatory effect of MICU1 allows the prompt response of mitochondria to Ca^{2+} signals generated in the cytoplasm, at low $[Ca^{2+}]$, the dominant effect of MICU2 largely shuts down MCU activity (Patron et al., 2014). We thus asked whether MICU1.1 is able to act as a gatekeeper together with MICU2 under basal conditions by performing two assays of gatekeeper reconstitution in HeLa cells.

MCU-overexpressing cells showed higher resting $[Ca^{2+}]_{mt}$ values (Figure 4A; Patron et al., 2014) because of the imbalanced overexpression of the channel without its gatekeeper. In this configuration, coexpression of both MCU together with MICU1 or with MICU1.1 failed to recover normal resting $[Ca^{2+}]_{mt}$ (Figure 4A). On the contrary, the expression of MCU together with MICU1 and MICU2 or with MICU1.1 and MICU2, which substantially increased the formation of functional heterodimers (Figure 3A), efficiently rescued normal values of basal $[Ca^{2+}]_{mt}$, thus demonstrating that the heterodimer MICU1.1-MICU2 acts as a gatekeeper of the channel as well as MICU1-MICU2 at low $[Ca^{2+}]$ (Figure 4A).

To further verify these results, we silenced endogenous MICU1 using a specific small interfering RNA (siRNA) in HeLa cells. The loss of MICU1 is sufficient to destabilize MICU2 protein and leads MICU2 protein degradation (Kamer and Mootha, 2014; Patron et al., 2014; Plovanich et al., 2013). Consequently, by silencing endogenous MICU1, we obtained the loss of the channel gatekeeper and a 6-fold increase in basal mitochondrial Ca^{2+} levels (Figure 4B). We tried to rescue the $[Ca^{2+}]_{mt}$ by co-expressing MICU2 and either MICU1 or MICU1.1. MICU2, when overexpressed alone, is not able to rescue mitochondrial Ca^{2+} levels because the interaction of MICU2 with MCU relays on MICU1 (Kamer and Mootha, 2014; Figure 4B). On the contrary, we observed that the increase in mitochondrial Ca^{2+} levels is rescued by transfection of both MICU1 and MICU1.1 (Figure 4B).

Ca^{2+}-Dependent Functional Regulation of the MCU Complex

It has been shown that MICU1 and MICU2 are able to sense Ca^{2+} levels because of the two EF-hand domains present in their amino acid sequence. This is demonstrated by the functional behavior displayed by MICU1 and MICU2 mutants ($MICU1^{EFmut}$ and $MICU2^{EFmut}$, respectively) in which the EF-hand domains lose the capability to bind Ca^{2+} (Csordás et al., 2013; Mallilankaraman et al., 2012; Patron et al., 2014). Because MICU1 is activated upon Ca^{2+} binding, $MICU1^{EFmut}$ is locked in the "inactive state," thus losing the ability to cooperatively activate MCU (Patron et al., 2014). We thus decided to evaluate the effects of EF-hand domain mutations on MICU1.1 activity by creating $MICU1.1^{EFmut}$-hemagglutinin (HA) by mutating key residues of the two EF-hand domains (D237A, E248K, D427A, and E438K). As for $MICU1^{EFmut}$, $MICU1.1^{EFmut}$ acts as a dominant negative because its overexpression reduces $[Ca^{2+}]_{mt}$ peaks (Figure 4C). Furthermore, the heterodimer $MICU1.1^{EFmut}$-MICU2 dramatically reduces mitochondrial Ca^{2+} uptake exactly as the $MICU1^{EFmut}$-MICU2 dimer (Figure 4C). We also assessed the effect of $MICU2^{EFmut}$ (D372A) on MICU1.1 activity. As already shown, this mutant almost completely blunts mitochondrial Ca^{2+} uptake upon cell stimulation because Ca^{2+} is unable to relieve MICU2 inhibition of the uniporter regardless of Ca^{2+} concentration (Figure 4D; Kamer and Mootha, 2014; Patron et al., 2014). As expected, co-expression of $MICU2^{EFmut}$ together with MICU1 is not able to re-establish normal $[Ca^{2+}]_{mt}$ uptake, highlighting the inhibitory role of apo-MICU2 on MCU activity (Figure 4D). Surprisingly, cells co-transfected with $MICU2^{EFmut}$ and MICU1.1 display a $[Ca^{2+}]_{mt}$ peak comparable with the one in control cells (Figure 4D), suggesting that MICU1.1 activatory effect is less affected by MICU2 inhibition than conventional MICU1.

MICU1.1 Behavior Depends on the Residues that Compose the Extra Exon

We next wondered which amino acid that composes the extra exon is responsible for MICU1.1 striking behavior. We thus

(C–G) $[Ca^{2+}]_{mt}$ measurements in intact HeLa cells transfected with the indicated constructs or siRNAs and challenged with maximal histamine stimulation. (C) n = 5. (D) n = 5. (E) n = 4. (F) n = 5. (G) n = 6.

Data are presented as mean ± SEM in (A) and (B) and as mean ± SD in (C)–(G). One-way ANOVA was used with post hoc Bonferroni tests for each sample. *p < 0.05, **p < 0.01, ***p < 0.005 compared with the control unless specified otherwise. See also Figure S4.

created substitution and deletion MICU1.1 mutants of the extra exon residues. First, we substituted each residue with alanine (MICU1.1^{E182A}, MICU1.1^{F183A}, MICU1.1^{W184A}, and MICU1.1^{Q185A}), and we tested their effect when co-expressed with MICU2 because, under this condition, we observed the most dramatic effect of MICU1.1. All of these mutants behave indistinguishably from the MICU1.1 wild-type (Figure 4E). We carried out the same experiments with single deletion mutants of MICU1.1 extra exon residues (MICU1$^{\Delta E182}$, MICU1$^{\Delta F183}$, MICU1$^{\Delta W184}$, and MICU1$^{\Delta Q185}$). Only the deletion of tryptophan causes a statistically significant difference in mitochondrial Ca^{2+} uptake compared with MICU1.1, although the response is not comparable with that of MICU1 (Figure 4F).

Finally, we mutated all four residues of the extra exon in alanine (MICU1.1^{E182A,F183A,W184A,Q185A}, hereafter referred to as MICU1.1$^{AAAA182–185}$), and, as expected, this mutant, when expressed together with MICU2, evokes a mitochondrial Ca^{2+} uptake comparable with that observed in cells transfected with MICU1 together with MICU2 (Figure 4G).

We also performed circular dichroism (CD) of purified MICU1 and MICU1.1 (Figure S4D). Consistent with the MICU1 crystal structure (Wang et al., 2014), the far-UV CD spectrum of MICU1 is typical of a protein containing high α-helical secondary structure content characterized by two minima at 208 and 222 nm. Noteworthy, MICU1.1 shows a slight increase in both the CD signal at 222 nm and the 222-nm/208-nm intensity ratio, indicating a higher α-helix fraction content in the MICU1.1 variant compared with MICU1 (Figure S4D), suggesting that the insertion of the four amino acids encoded by the extra exon might have a significant effect on the domain structure.

Electrophysiological Characterization of the Effect of MICU1.1 on MCU Channel Activity

Next we performed electrophysiological experiments, comparing the activation of MCU activity by MICU1.1 and MICU1 in vitro in a medium containing 1 μM free Ca^{2+} to mimic the situation in intact cells. MICU1 and MICU1.1 were expressed and purified in *E. coli* (Figure S5A) and were used at the same concentration in all planar lipid bilayer experiments. We have reported previously that MICU1 is able to increase the open probability of MCU in the presence of Ca^{2+} (Patron et al., 2014). Here we confirm this result (Figure 5A) and further show that, although addition of MICU1 caused an approximately 2.5-fold increase in MCU activity, under the same conditions, MICU1.1 boosted MCU activity approximately 4-fold (Figure 5B). In both cases, addition of ruthenium red (RuR) inhibited the MICU1- and MICU1.1-activated MCU current (Figures S5C and S5D), proving that the observed increase in the overall current level was due to the opening of MCU channels and not due to unspecific leak current.

We then investigated how addition of the MICU1-MICU2 and MICU1.1-MICU2 dimers affects MCU activity. We expressed and purified heterodimers from insect cells (Figure S5B) as in Figure 3D. Under our experimental conditions, the former dimer caused only a slight increase in the mean open probability (Figure 5C; Figure S5E), whereas the latter substantially boosted MCU activity (Figure 5D; Figure S5F).

MICU1.1 Lowers the Activation Threshold of Mitochondrial Ca^{2+} Uptake and Shows a Higher Affinity for Ca^{2+} Binding Than MICU1

It has been demonstrated that MICU1 controls both the $[Ca^{2+}]_{cyt}$ threshold and cooperativity of the MCU complex, with the latter being dependent on Ca^{2+} binding to the EF-hand domains of MICU1 (Patron et al., 2014). Given that MICU1.1 induces mitochondrial Ca^{2+} uptake more efficiently than MICU1, we wondered whether this effect was mediated by changes in the threshold of initiation of mitochondrial Ca^{2+} uptake. To assess this, we measured mitochondrial Ca^{2+} uptake by perfusing permeabilized cells sequentially with solutions containing increasing free Ca^{2+} concentrations (from 400 nM to 1 μM) for the same period of time. The overexpression of MICU1.1 induces a faster response at each $[Ca^{2+}]$ compared with control cells and MICU1- and MICU1$^{AAAA182–185}$-overexpressing cells (Figure 6A).

On the contrary, as expected, MICU2 overexpression shows a negative modulation of the mitochondrial Ca^{2+} uptake speed response (Figure 6B). Furthermore, reconstitution of the MICU1-MICU2 heterodimer abrogates the faster and higher response caused by overexpression of MICU1 upon perfusion of 600 nM free $[Ca^{2+}]$ solution, and the same results were obtained when overexpressing MICU1.1$^{AAAA182–185}$ (Figure 6B). On the contrary, cells overexpressing the heterodimer MICU1.1-MICU2 display a sustained mitochondrial Ca^{2+} uptake at lower free $[Ca^{2+}]$ (at 400 nM free $[Ca^{2+}]$ solution), at which control cells and cells overexpressing MICU1 together with MICU2 do not initiate mitochondrial Ca^{2+} uptake (Figure 6B).

We asked whether the shift to the left of the mitochondrial Ca^{2+} response was due to the loss of the gatekeeper effect of MICU1.1-MICU2 on the MCU channel. Therefore, we measured mitochondrial Ca^{2+} uptake in permeabilized cells in which MICU1 was silenced by siRNA concomitantly with the overexpression of either MICU1 or MICU1.1 or the heterodimers MICU1-MICU2, MICU1.1-MICU2, or MICU1$^{AAAA182–185}$-MICU2 (Figure S6A; Figures 6C and 6D). It is clear from this experiment that MICU1.1, both when overexpressed alone (Figure 6C) and with MICU2 (Figure 6D), retains the gatekeeper function because the silencing of MICU1, which also causes the disappearance of MICU2 protein (Kamer and Mootha, 2014; Patron et al., 2014; Plovanich et al., 2013), induces a much higher and faster mitochondrial Ca^{2+} response (Figures 6C and 6D).

The affinity of MICU proteins for Ca^{2+} was quantitatively estimated by isothermal titration calorimetry (ITC). The titration profile was compatible with the presence of multiple binding sites for Ca^{2+} both in MICU1 (Figure S6B) and MICU1.1 (Figure 6E). In the case of MICU1, Wang et al. (2014) recently measured the Ca^{2+} binding affinity of individual MICU1 EF-hand domains by selectively switching off each Ca^{2+}-binding site by mutagenesis, thus reporting individual affinities of K_d = 21.4 μM and K_d = 15.8 μM, respectively. Our ITC data on MICU1, containing both Ca^{2+}-binding sites, did not allow to discriminate between the two affinity sites, and a cumulative K_d of 42 ± 10 μM for both sites was obtained (Figure S6B). At variance with MICU1, the ITC data reported in Figure 6E for MICU1.1 could be nicely fitted with a two-site binding model, yielding comparable but distinct affinities for the two binding sites; i.e., K^1_d = 56 ± 10 nM and K^2_d = 130 ± 15 nM—much higher than that determined for MICU1.

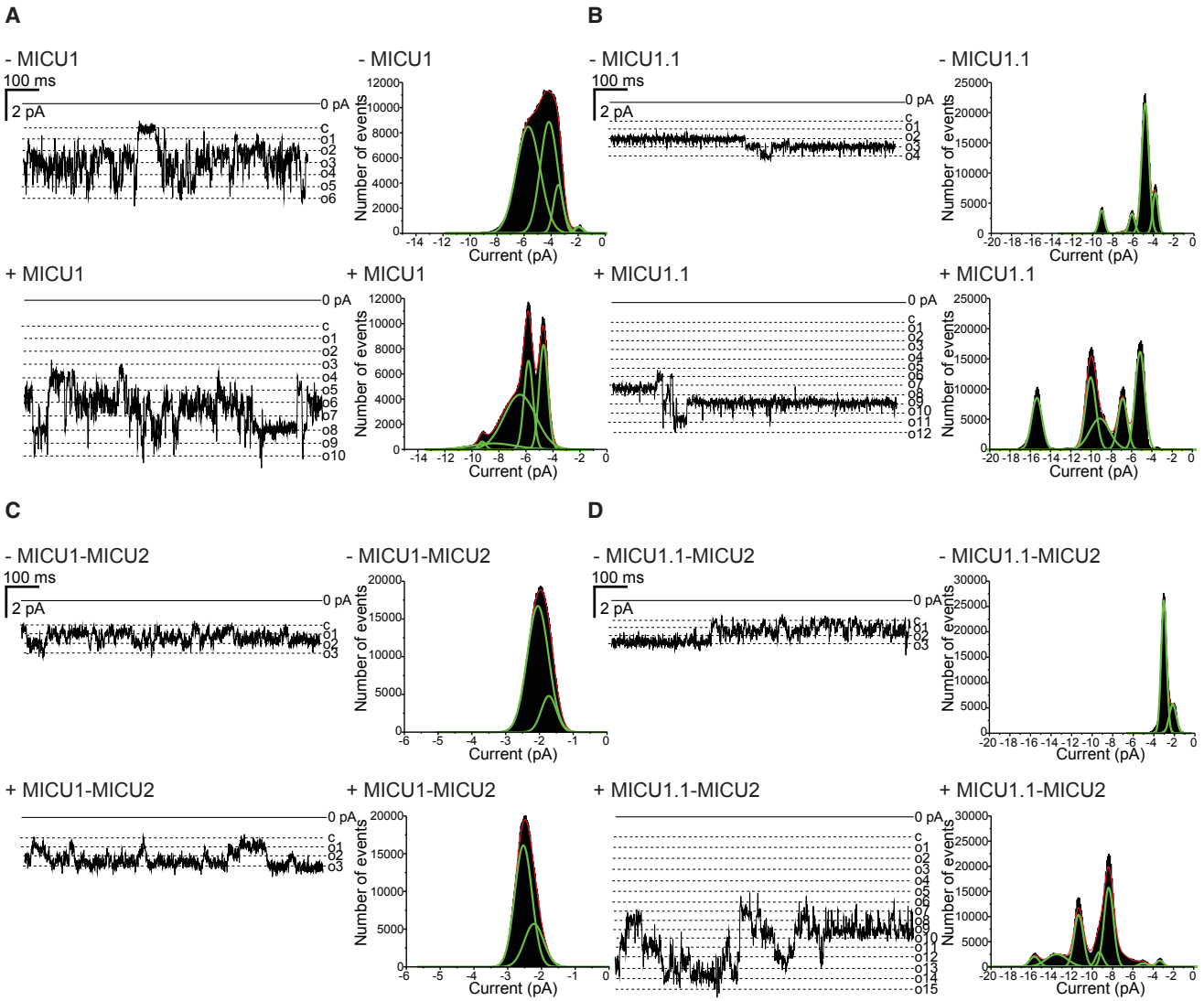

Figure 5. MICU1.1 Activates MCU More Efficiently Than MICU1, and the MICU1.1-MICU2 Heterodimer Activates MCU

(A–D) Representative 1-s-long current traces (left) and amplitude histograms obtained from 60-s-long traces (right) before (top) or after (bottom) addition of MICU1 (A), MICU1.1 (B), MICU1-MICU2 (C), and MICU1.1-MICU2 (D). Channel activity in the sodium gluconate and 1 μM free Ca^{2+} medium used here was detectable with much lower unitary current compared with the divalent cation-free medium containing sodium and 5 mM EDTA, yielding a conductance value of 17 ps, as reported previously (Kirichok et al., 2004; Patron et al., 2014). Gaussian fits of the multipeak histograms (red) and MCU current levels (green) were obtained using the Origin 7.5 program set. The shift of the amplitude histogram toward more negative values, in both cases, means activation. Mean open probability (Po): (A) 0.22 before and 0.58 after addition of MICU1; (B) 0.21 before and 0.82 after addition of MICU1.1. Similarly, a 2.5- to 3-fold increase in Po was observed in seven other experiments using MICU1, whereas a 3.9- to 4.8-fold increase was obtained in four further experiments with MICU1.1. (C) 0.42 before and 0.66 after addition of MICU1-MICU2; (D) 0.12 before and 0.61 for MICU1.1-MICU2. Similar results were obtained in six and seven other independent experiments, respectively. See Figures S5C–S5F for representative traces and amplitude histograms of the effect of the addition of 2 μM Ruthenium Red (RuR) to the same experiments. c, closed channel current level; o1, o2, etc.; and open channel levels. V_{cis} was −40 mV.
See also Figure S5.

MICU1.1 Is Required for Sustained Mitochondrial Ca^{2+} Uptake and Thus for Efficient ATP Production in Skeletal Muscle In Vivo

Finally, we asked what was the physiological relevance of MICU1.1 in skeletal muscle. For this purpose, we forced MICU1 expression in this tissue and concomitantly blunted MICU1.1 expression by using a specific antisense oligonucleotide (AON) that hides the MICU1.1 micro-exon from the splicing machinery. This technique has been used with success to induce exon skipping in vivo in humans (Arechavala-Gomeza et al., 2012; Veltrop and Aartsma-Rus, 2014). To achieve efficient levels of exon skipping in vivo, we used the Vivo-Morpholino chemistry (Morcos et al., 2008) and designed a sequence targeting the donor splicing site of the MICU1.1 micro-exon (MICU1.1-Mo), using as a control a non-targeting sequence (Control-Mo).

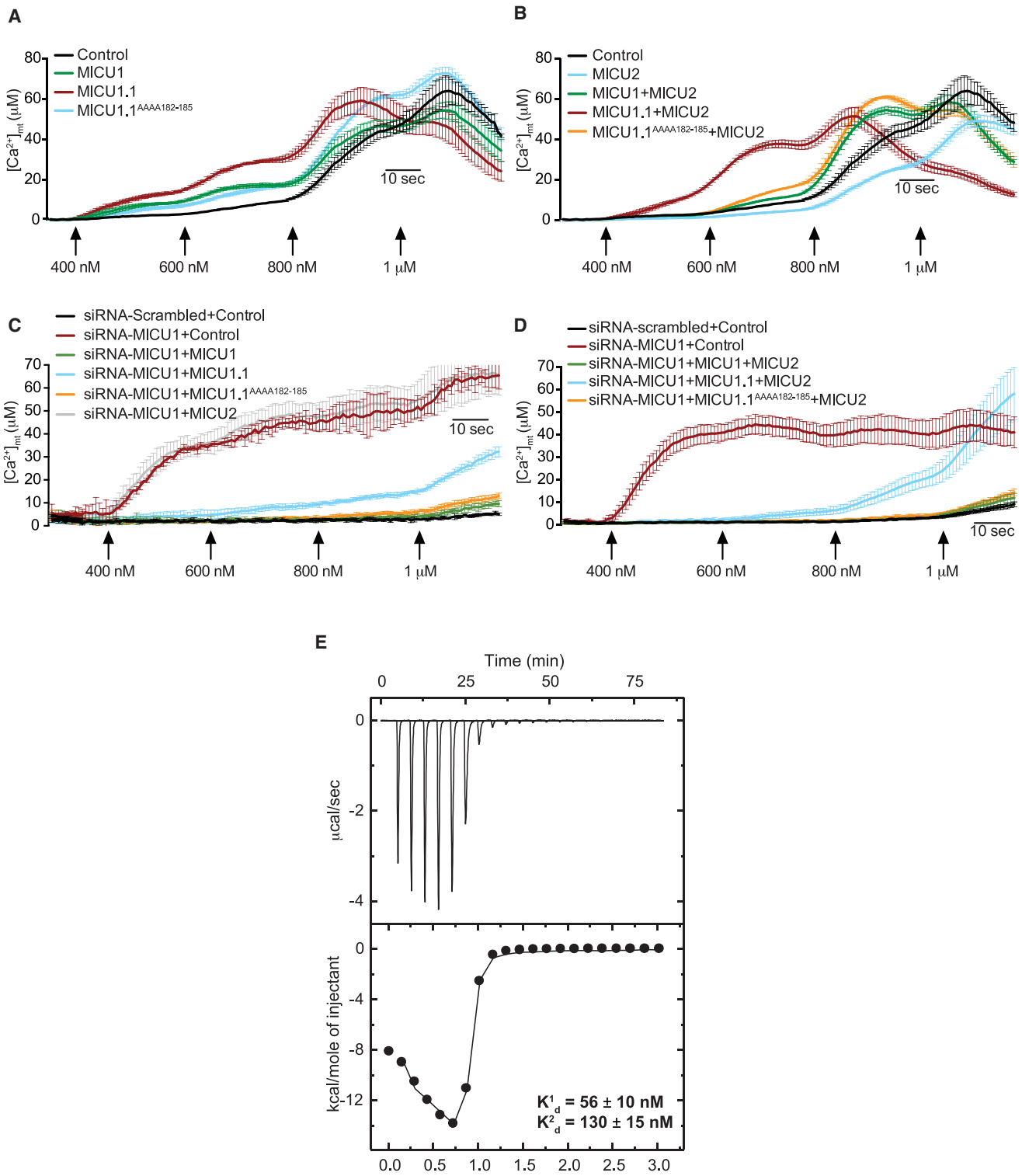

Figure 6. MICU1.1-Dependent Mitochondrial Ca^{2+} Uptake Kinetic at Different Ca^{2+} Concentrations and ITC Analysis of Ca^{2+} Binding to MICU1.1

(A–D) $[Ca^{2+}]_{mt}$ measurements in permeabilized HeLa cells overexpressing the indicated constructs (A and B) and constructs and siRNAs (C and D) upon sequential exposure to crescent $[Ca^{2+}]$. Data are presented as mean ± SD (n = 4).

(legend continued on next page)

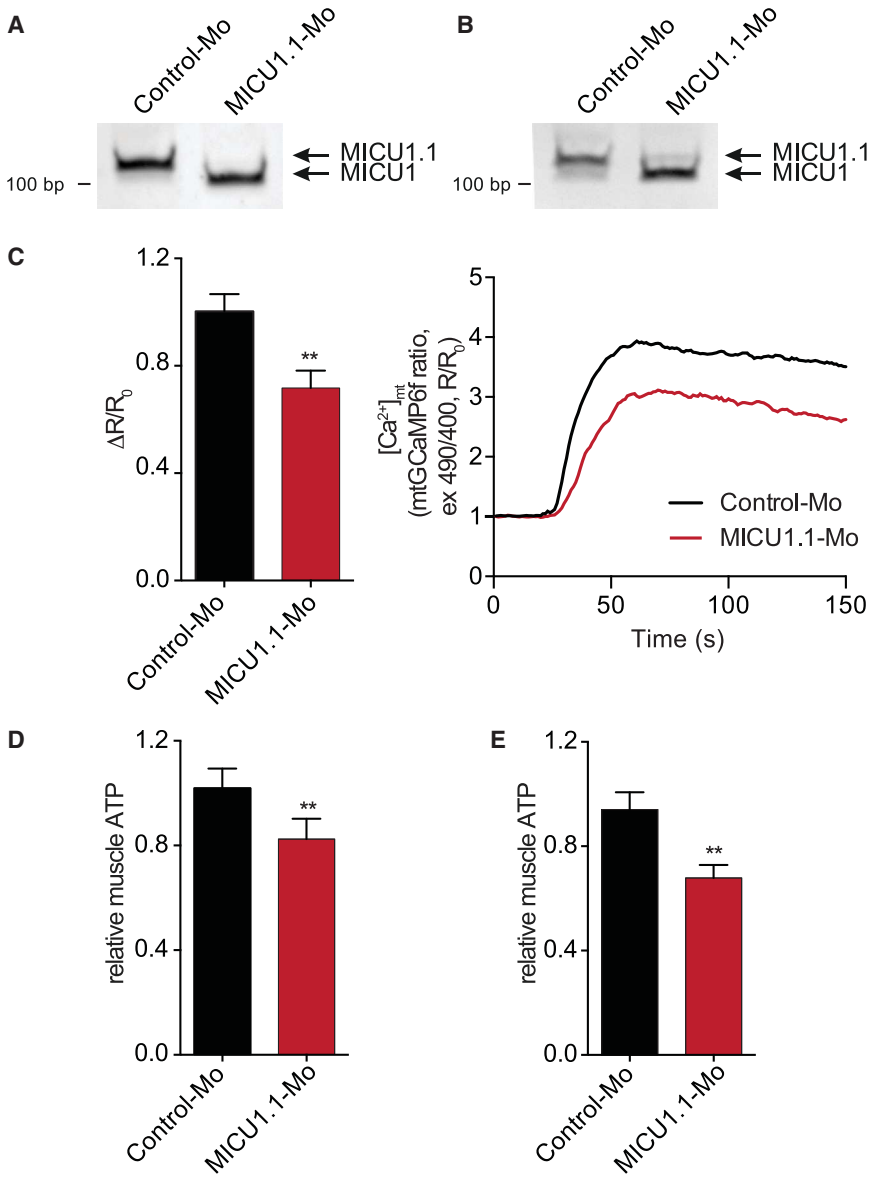

Figure 7. Mitochondrial Ca^{2+} Uptake and Total ATP Content in Skeletal Muscles Treated with Vivo-Morpholino Mediating MICU1.1 Micro-exon Skipping

(A and B) Representative acrylamide gel of PCR products using primers spanning the MICU1 extra exon of cDNA of TA (A) and FDB (B) mouse muscles treated with the indicated Vivo-Morpholino for 8 days. MICU1.1 produces a band of 152 bp and MICU1 of 140 bp.

(C) Right: representative traces of mitochondrial Ca^{2+} dynamics in FDB fibers treated with Vivo-Morpholino (Control-Mo) or MICU1.1 Vivo-Morpholino (MICU1.1-Mo) for 8 days upon caffeine stimulation, evaluated through ratiometric imaging of the mitochondrial targeted GCaMP6f. Left: normalized mitochondrial $[Ca^{2+}]$ increase (n = 25). (D and E) Relative skeletal muscle ATP levels in TA (D) and FDB (E) muscles treated as in (C) (n = 6). Data are presented as mean ± SEM in (C) and mean ± SD in (D) and (E). For pairwise comparison of means, t tests were used. **$p < 0.01$ compared with the control. See also Figure S7.

We transfected or injected adult mouse FDB and tibialis anterior (TA) muscles, respectively, as already performed (Koganti et al., 2015), and 8 days after, the *Micu1.1/Micu1* ratio was reverted, as demonstrated by PCR experiments on the injected muscles (Figures 7A and 7B). Importantly, the total amount of MICU1 was unchanged both at the mRNA and protein levels (Figures S7A and S7B, respectively), and no changes were detected in MICU2 and MCU protein levels (Figure S7B). Finally, H&E staining showed no sign of damage or inflammation in the treated muscles (Figure S7C).

We first evaluated mitochondrial Ca^{2+} uptake by transfecting FDB mouse muscles in vivo with Control-Mo or MICU1.1-Mo together with mtGCaMP6f, as already performed (Figure S2C; Mammucari et al., 2015). Eight days later, real-time imaging experiments were performed on isolated single myofibers (Figure 7C). After assessment of basal Ca^{2+} concentrations, a cytosolic and, hence, mitochondrial $[Ca^{2+}]$ rise was evoked with caffeine. In fibers treated with MICU1.1 Vivo-Morpholino, a significant reduction of about 30% on mitochondrial Ca^{2+} uptake was observed (Figure 7C). Considering the tight Ca^{2+}-dependent regulation of mitochondrial ATP production in skeletal muscle (Glancy et al., 2013), we analyzed total ATP both in FDB and TA muscles. The reduction in mitochondrial Ca^{2+} uptake in MICU1.1-Mo-treated muscles was accompanied by a significant reduction in total ATP both in FBD and TA muscles (Figures 7D and 7E).

DISCUSSION

Skeletal muscle is unique in its ability to maintain a moderate increase in energy consumption during prolonged periods of low-intensity contractions and to rapidly increase ATP production when explosive contractions are required (Sahlin et al., 1998).

(E) ITC analysis of Ca^{2+} binding to MICU1.1. Top: thermogram relative to the serial injection of a $CaCl_2$ stock solution (1 mM) into a MICU1.1 (40 μM) solution in the measured cell. Data are reported as microcalories per second versus time. Bottom: binding isotherm of Ca^{2+} binding to MICU1.1. Data are reported as the heat exchanged normalized per mole (kilocalories per mole) of injectant (i.e., $CaCl_2$) versus the Ca^{2+}/MICU1.1 molar ratio.
See also Figure S6.

When muscle is activated, the intracellular store of ATP is depleted within 2 s. Thus, anaerobic and aerobic pathways must be activated. The former dominate during high-intensity physical activity of short duration, whereas the latter predominate during prolonged submaximal exercise (Sahlin et al., 1998). Mitochondrial Ca^{2+} uptake has been shown to control the energy potential that is necessary to maintain energy homeostasis in contracting skeletal muscle (Glancy et al., 2013; McMillin and Madden, 1989). For this reason, compared with other tissues, skeletal muscle mitochondria display high Ca^{2+} conductance, as shown recently by experiments of direct patch-clamp recordings of I_{MCU} in mitoplasts (Fieni et al., 2012).

The molecular plasticity is achieved, at least in part, by the different expression of the components of the MCU complex in skeletal muscle (De Stefani et al., 2011; Kamer and Mootha, 2014; Perocchi et al., 2010; Plovanich et al., 2013; Raffaello et al., 2013) and by post-translational and post-transcriptional modifications of the complex components (Mammucari et al., 2016).

Here we identified an additional regulatory mechanism able to modulate mitochondrial Ca^{2+} uptake in skeletal muscle: alternative splicing. Indeed, we discovered an alternative splice isoform of MICU1 that we named MICU1.1, characterized by the addition of a micro-exon coding for four amino acids (EFWQ) between exon 5 and exon 6 (Figure 1A). Intriguingly, MICU1.1 is present in humans and conserved in all vertebrates (Figure 1B), and its expression is restricted to skeletal muscle, where it represents the predominant variant, and lower levels are found in the brain (Figures 2B–2D).

MICU1.1, when overexpressed in HeLa cells and skeletal muscle in vivo, causes a major increase of mitochondrial Ca^{2+} uptake upon stimulation that exceeds that induced by the overexpression of MICU1 both under intact and permeabilized conditions (Figures 1D and 1F; Figure S2C). This effect is specific because membrane potential is not perturbed by the overexpression of MICU1.1 (Figure S1D), and cytosolic Ca^{2+} is rather reduced (Figure S1C), most likely because of increased Ca^{2+} clearance by mitochondria, as already observed for the overexpression of MCU (De Stefani et al., 2011). This effect is not due to changes in the ability of MICU1.1 to interact with the other pore complex components. Indeed, we observed no differences in the ability of MICU1.1 to interact with MCU and MICU2 (Figures 3B and 3E; Figures S4A–S4C), to heterodimerize with MICU2 (Figure 3A), and to give rise to high-molecular-weight complexes of the same molecular weights as MICU1 (Figures 3C and 3D).

It has been proposed that, under physiological conditions, the heterodimer MICU1-MICU2 is the prevalent form (Patron et al., 2014). To mimic this condition, we overexpressed MICU1 and MICU1.1 together with MICU2 to shift the balance toward the MICU1-MICU2 and MICU1.1-MICU2 heterodimers. It has been demonstrated that MICU2 prevents the mitochondrial Ca^{2+} uptake increase upon MICU1 overexpression (Patron et al., 2014). Strikingly, MICU2 is not able to inhibit MICU1.1-induced mitochondrial Ca^{2+} uptake increase (Figure 1D). Moreover, in permeabilized cells, mitochondrial Ca^{2+} uptake speed is not decreased, as observed by overexpressing MICU1-MICU2 heterodimers; however, unexpectedly, it increases far more than in cells transfected only with MICU1.1 (Figure 1F). Together, these results suggest that the MICU1.1-MICU2 heterodimer is able to increase the ability of mitochondria to take up Ca^{2+} compared with the MICU1-MICU2 dimer. Electrophysiological characterization of MICU1 and MICU1.1 confirms that the latter is a stronger activator of MCU even in vitro and that the heterodimer MICU1.1-MICU2 strongly activates the MCU channel in the presence of Ca^{2+} (Figure 5; Figures S5C–S5F).

We have recently demonstrated that MICU2 is a genuine MCU gatekeeper that inhibits MCU activity at low $[Ca^{2+}]_{cyt}$, ensuring minimal Ca^{2+} accumulation in the presence of a huge driving force for cation accumulation, thus preventing the deleterious effects of matrix overload (Patron et al., 2014). We also demonstrated that the MICU1.1-MICU2 heterodimer is able to act as a gatekeeper of the channel under resting conditions and that the MICU1.1-MICU2 dimer causes minimal Ca^{2+} uptake at low $[Ca^{2+}]_{cyt}$ (Figures 4A and 4B). Experiments under permeabilized conditions in which mitochondria were subjected to increasing $[Ca^{2+}]$ demonstrated that mitochondria overexpressing MICU1.1 together with MICU2 take up Ca^{2+} at $[Ca^{2+}]$ at which mitochondria transfected with the MICU1-MICU2 heterodimer show only a mild uptake (Figures 6A–6D). These data strongly support the idea that the MICU1.1-MICU2 dimer activates mitochondrial Ca^{2+} uptake at lower $[Ca^{2+}]_{cyt}$, thus shifting to the left the $[Ca^{2+}]_{cyt}$ mitochondrial Ca^{2+} uptake curve. This effect can be explained by the measurement of the Ca^{2+} binding affinities of the two EF-hand domains of MICU1.1 that, strikingly, demonstrate that MICU1.1 binds Ca^{2+} one order of magnitude more efficiently than MICU1 (Figure 6E; Figure S6B). Furthermore, as already shown for MICU1 (Csordás et al., 2013; Kamer and Mootha, 2014; Patron et al., 2014), MICU1.1 activity relies on the binding of Ca^{2+} to its EF-hand domain because a MICU1.1 mutant ($MICU1.1^{EFmut}$), unable to bind Ca^{2+}, prevents MICU1-mediated enhancement of MCU opening (Figure 4C). However, MICU1.1 is less affected under conditions of high $[Ca^{2+}]_{cyt}$ by the dominant-negative effect of a MICU2 mutant whose EF hands are unable to bind Ca^{2+} ($MICU2^{EFmut}$) compared with MICU1 (Figure 4D), suggesting that MICU1.1 regulation of MCU activity is partially independent from MICU2.

We also asked whether one of the four additional residues was required for MICU1.1 activity. Our data demonstrate that neither the single substitution with alanine nor the deletion of single amino acids significantly influence the activity of MICU1.1 (Figures 4E and 4F). Only the substitution of all four amino acids of the extra exon with alanine is able to blunt MICU1.1 activity, recapitulating MICU1 function (Figure 4G). The crystal structure of conventional MICU1 (Wang et al., 2014) is of no help in understanding the role of this extra exon insertion because the loop region that contains the exon is flexible in MICU1 and not visible in the electron density map. Thus we cannot speculate how the MICU1.1 extra exon can modify the Ca^{2+} binding affinity of the EF-hand domains.

Furthermore, in vivo injection of Vivo-Morpholino oligos mediating exon skipping of the MICU1.1 extra exon, and thus forced expression of MICU1 (Figures 7A and 7B; Figures S7A and S7B), demonstrated that MICU1.1 is required for maintaining sufficient levels of mitochondrial Ca^{2+} uptake to provide the ATP needed for contraction (Figures 7C–7E), demonstrating that this alternative splice variant is an important mechanism in muscle where fast Ca^{2+} transients occur (Delbono and Stefani, 1993), allowing

a prompt response of mitochondrial metabolism and ensuring sustained ATP production needed for resistance and strenuous exercise.

Overall, the newly identified alternative splice variant of MICU1 represents a novel mechanism of regulation of mitochondrial Ca^{2+} uptake in skeletal muscle that contributes to unraveling the regulatory properties of MCU in this tissue and demonstrates a unique mitochondrial Ca^{2+} uptake machinery.

EXPERIMENTAL PROCEDURES

Cell Culture and Transfection

HeLa and HEK293 cells were cultured in DMEM (Thermo Fisher Scientific) supplemented with 10% FBS (Thermo Fisher Scientific) and containing penicillin (100 U/mL) and streptomycin (100 μg/mL). Cells were transfected with a standard Ca^{2+}-phosphate procedure as already performed (De Stefani et al., 2011; Raffaello et al., 2013). All experiments were carried out 24–36 hr after transfection. Mock vectors (i.e., pcDNA3.1 or pEGFP-N1) were used as controls in all overexpression experiments (referred to as the control condition). In parallel, a non-targeting siRNA (i.e., siRNA-scrambled) was used as a control in all silencing experiments.

Aequorin Ca^{2+} Measurements

HeLa cells grown on 13-mm round glass coverslips at 60% confluence in a 24-well plate were transfected with the indicated constructs and siRNAs and with the cytosolic (cytAEQ) or the low-affinity mitochondrial (mtAEQmut) probe with the Ca^{2+}-phosphate procedure with the appropriate mix of DNA (in an aequorin/total DNA ratio of 1:4), as described previously (Pinton et al., 2007). Ca^{2+} measurements were performed as described previously (Patron et al., 2014). Output data were analyzed and calibrated with a custom-made macro-enabled Excel workbook.

The experiments with permeabilized cells were performed as described previously (Patron et al., 2014). Mitochondrial Ca^{2+} uptake speed was calculated as the first derivative by using the SLOPE Excel function and smoothed for three time points. The higher value reached during Ca^{2+} addition represents the maximal Ca^{2+} uptake speed. All materials were from Sigma-Aldrich unless specified otherwise.

Vivo-Morpholino Treatment of FDB and TA Mouse Muscles

For all experiments, adult male CD1 mice (25–30 g) were used. Vivo-Morpholinos were provided by Gene Tools. For FDB treatment, 500 ng of Vivo-Morpholino was injected concomitantly with mtGCaMP6f DNA, and the transfection was carried out as reported previously (Mammucari et al., 2015). TA muscles were treated with 2.5 μg of Vivo-Morpholino that was administered through intramuscular injection in TA muscle, as reported previously (Koganti et al., 2015). 8 days after treatment, muscles were collected and analyzed. See Supplemental Experimental Procedures for details.

Vivo-Morpholino Injection and DNA Transfection

In vivo experiments were performed in accordance with the Italian law D. L.vo n°26/2014.

Statistical Analysis of Data

All data were analyzed for statistical significance using GraphPad Prism software. All data are expressed as mean ± SD unless otherwise specified. For comparison between two independent groups, unpaired t tests were used. For comparison between three or more independent groups, one-way ANOVA was used with post hoc Bonferroni tests for each sample. Adjusted $^{*}p < 0.05$, $^{**}p < 0.01$, and $^{**}p < 0.01$.

SUPPLEMENTAL INFORMATION

Supplemental Information includes Supplemental Experimental Procedures and seven figures and can be found with this article online at http://dx.doi.org/10.1016/j.molcel.2016.10.001.

AUTHOR CONTRIBUTIONS

Conceptualization, A.R. and R.R.; Methodology, D.V.R. and A.R.; Investigation, D.V.R., F.V., V.C., L.A., and G.B.; Writing – Original Draft, A.R. and R.R.; Writing – Review & Editing, A.R. and R.R.; Funding Acquisition, A.R. and R.R.; Resources, V.D.F., I.S., G.Z., A.R., and R.R.; Supervision, V.D.F., I.S., and G.Z.

ACKNOWLEDGMENTS

We thank Sebastiano Pasqualato, Nicoletta Caridi, and Silvia Monzani at the European Institute of Oncology for the preparation of proteins from insect cells. We thank Dr. Lele Wang for advice regarding the purification of MICU1. We thank Prof. Francesco Muntoni and Dr. Haiyan Zhou for help with designing the AONs. We thank Prof. Tullio Pozzan, Prof. Leonardo Salviati, Dr. Eva Trevisson, Dr. Diego De Stefani, Dr. Emy Basso, and Prof. Chiara Romualdi for helpful discussions. This research was supported by grants from the European Research Council (ERC mitoCalcium no. 294777 to R.R.); the Italian Telethon Foundation (GPP10005A to R.R.); the Italian Ministry of Health (Ricerca Finalizzata RF-2009-15-26404 to R.R.); the Italian Ministry of Education, University, and Research (FIRB RBAP11X42L to R.R.); the NIH (1P01AG025532-01A1 to R.R.); the Cariparo Foundation (2012-0646 to R.R.); the Cariplo Foundation (to R.R.); the Italian Association for Cancer Research (10016 to R.R.); and the French Muscular Dystrophy Association (19471 to A.R.).

Received: June 8, 2016
Revised: September 6, 2016
Accepted: September 30, 2016
Published: November 3, 2016

REFERENCES

Arechavala-Gomeza, V., Anthony, K., Morgan, J., and Muntoni, F. (2012). Antisense oligonucleotide-mediated exon skipping for Duchenne muscular dystrophy: progress and challenges. Curr. Gene Ther. *12*, 152–160.

Baughman, J.M., Perocchi, F., Girgis, H.S., Plovanich, M., Belcher-Timme, C.A., Sancak, Y., Bao, X.R., Strittmatter, L., Goldberger, O., Bogorad, R.L., et al. (2011). Integrative genomics identifies MCU as an essential component of the mitochondrial calcium uniporter. Nature *476*, 341–345.

Brini, M., De Giorgi, F., Murgia, M., Marsault, R., Massimino, M.L., Cantini, M., Rizzuto, R., and Pozzan, T. (1997). Subcellular analysis of Ca2+ homeostasis in primary cultures of skeletal muscle myotubes. Mol. Biol. Cell *8*, 129–143.

Chen, T.-W., Wardill, T.J., Sun, Y., Pulver, S.R., Renninger, S.L., Baohan, A., Schreiter, E.R., Kerr, R.A., Orger, M.B., Jayaraman, V., et al. (2013). Ultrasensitive fluorescent proteins for imaging neuronal activity. Nature *499*, 295–300.

Csordás, G., Golenár, T., Seifert, E.L., Kamer, K.J., Sancak, Y., Perocchi, F., Moffat, C., Weaver, D., de la Fuente Perez, S., Bogorad, R., et al. (2013). MICU1 controls both the threshold and cooperative activation of the mitochondrial Ca^{2+}uniporter. Cell Metab. *17*, 976–987.

De Stefani, D., Raffaello, A., Teardo, E., Szabò, I., and Rizzuto, R. (2011). A forty-kilodalton protein of the inner membrane is the mitochondrial calcium uniporter. Nature *476*, 336–340.

Delbono, O., and Stefani, E. (1993). Calcium transients in single mammalian skeletal muscle fibres. J. Physiol. *463*, 689–707.

Fieni, F., Lee, S.B., Jan, Y.N., and Kirichok, Y. (2012). Activity of the mitochondrial calcium uniporter varies greatly between tissues. Nat. Commun. *3*, 1317.

Glancy, B., Willis, W.T., Chess, D.J., and Balaban, R.S. (2013). Effect of calcium on the oxidative phosphorylation cascade in skeletal muscle mitochondria. Biochemistry *52*, 2793–2809.

Kamer, K.J., and Mootha, V.K. (2014). MICU1 and MICU2 play nonredundant roles in the regulation of the mitochondrial calcium uniporter. EMBO Rep. *15*, 299–307.

Kim, J.H., Lee, S.-R., Li, L.-H., Park, H.-J., Park, J.-H., Lee, K.Y., Kim, M.-K., Shin, B.A., and Choi, S.-Y. (2011). High cleavage efficiency of a 2A peptide derived from porcine teschovirus-1 in human cell lines, zebrafish and mice. PLoS ONE *6*, e18556.

Kirichok, Y., Krapivinsky, G., and Clapham, D.E. (2004). The mitochondrial calcium uniporter is a highly selective ion channel. Nature *427*, 360–364.

Koganti, S.R.K., Zhu, Z., Subbotina, E., Gao, Z., Sierra, A., Proenza, M., Yang, L., Alekseev, A., Hodgson-Zingman, D., and Zingman, L. (2015). Disruption of KATP channel expression in skeletal muscle by targeted oligonucleotide delivery promotes activity-linked thermogenesis. Mol. Ther. *23*, 707–716.

Madsen, K., Ertbjerg, P., Djurhuus, M.S., and Pedersen, P.K. (1996). Calcium content and respiratory control index of skeletal muscle mitochondria during exercise and recovery. Am. J. Physiol. *271*, E1044–E1050.

Mallilankaraman, K., Doonan, P., Cárdenas, C., Chandramoorthy, H.C., Müller, M., Miller, R., Hoffman, N.E., Gandhirajan, R.K., Molgó, J., Birnbaum, M.J., et al. (2012). MICU1 is an essential gatekeeper for MCU-mediated mitochondrial Ca(2+) uptake that regulates cell survival. Cell *151*, 630–644.

Mammucari, C., Gherardi, G., Zamparo, I., Raffaello, A., Boncompagni, S., Chemello, F., Cagnin, S., Braga, A., Zanin, S., Pallafacchina, G., et al. (2015). The mitochondrial calcium uniporter controls skeletal muscle trophism in vivo. Cell Rep. *10*, 1269–1279.

Mammucari, C., Raffaello, A., Vecellio Reane, D., and Rizzuto, R. (2016). Molecular structure and pathophysiological roles of the Mitochondrial Calcium Uniporter. Biochim. Biophys. Acta *1863*, 2457–2464.

McMillin, J.B., and Madden, M.C. (1989). The role of calcium in the control of respiration by muscle mitochondria. Med. Sci. Sports Exerc. *21*, 406–410.

Morcos, P.A., Li, Y., and Jiang, S. (2008). Vivo-Morpholinos: a non-peptide transporter delivers Morpholinos into a wide array of mouse tissues. Biotechniques *45*, 613–614, 616, 618 passim.

Patron, M., Checchetto, V., Raffaello, A., Teardo, E., Vecellio Reane, D., Mantoan, M., Granatiero, V., Szabò, I., De Stefani, D., and Rizzuto, R. (2014). MICU1 and MICU2 finely tune the mitochondrial Ca2+ uniporter by exerting opposite effects on MCU activity. Mol. Cell *53*, 726–737.

Perocchi, F., Gohil, V.M., Girgis, H.S., Bao, X.R., McCombs, J.E., Palmer, A.E., and Mootha, V.K. (2010). MICU1 encodes a mitochondrial EF hand protein required for Ca(2+) uptake. Nature *467*, 291–296.

Pinton, P., Rimessi, A., Romagnoli, A., Prandini, A., and Rizzuto, R. (2007). Biosensors for the detection of calcium and pH. Methods Cell Biol. *80*, 297–325.

Plovanich, M., Bogorad, R.L., Sancak, Y., Kamer, K.J., Strittmatter, L., Li, A.A., Girgis, H.S., Kuchimanchi, S., De Groot, J., Speciner, L., et al. (2013). MICU2, a paralog of MICU1, resides within the mitochondrial uniporter complex to regulate calcium handling. PLoS ONE *8*, e55785.

Raffaello, A., De Stefani, D., Sabbadin, D., Teardo, E., Merli, G., Picard, A., Checchetto, V., Moro, S., Szabò, I., and Rizzuto, R. (2013). The mitochondrial calcium uniporter is a multimer that can include a dominant-negative pore-forming subunit. EMBO J. *32*, 2362–2376.

Rizzuto, R., De Stefani, D., Raffaello, A., and Mammucari, C. (2012). Mitochondria as sensors and regulators of calcium signalling. Nat. Rev. Mol. Cell Biol. *13*, 566–578.

Sahlin, K., Tonkonogi, M., and Söderlund, K. (1998). Energy supply and muscle fatigue in humans. Acta Physiol. Scand. *162*, 261–266.

Sancak, Y., Markhard, A.L., Kitami, T., Kovacs-Bogdan, E., Kamer, K.J., Udeshi, N.D., Carr, S.A., Chaudhuri, D., Clapham, D.E., Li, A.A., et al. (2013). EMRE is an Essential Component of the Mitochondrial Calcium Uniporter Complex. Science *30*, 1143–1148.

Veltrop, M., and Aartsma-Rus, A. (2014). Antisense-mediated exon skipping: taking advantage of a trick from Mother Nature to treat rare genetic diseases. Exp. Cell Res. *325*, 50–55.

Wang, L., Yang, X., Li, S., Wang, Z., Liu, Y., Feng, J., Zhu, Y., and Shen, Y. (2014). Structural and mechanistic insights into MICU1 regulation of mitochondrial calcium uptake. EMBO J. *33*, 594–604.

Weibel, E.R., and Hoppeler, H. (2005). Exercise-induced maximal metabolic rate scales with muscle aerobic capacity. J. Exp. Biol. *208*, 1635–1644.

Hindawi
Oxidative Medicine and Cellular Longevity
Volume 2019, Article ID 9324018, 18 pages
https://doi.org/10.1155/2019/9324018

Review Article

Crosstalk between Calcium and ROS in Pathophysiological Conditions

Simona Feno, Gaia Butera, Denis Vecellio Reane, Rosario Rizzuto, and Anna Raffaello

Department of Biomedical Sciences, University of Padova, via U. Bassi 58/b, 35131 Padova, Italy

Correspondence should be addressed to Rosario Rizzuto; rosario.rizzuto@unipd.it and Anna Raffaello; anna.raffaello@unipd.it

Received 24 January 2019; Accepted 1 April 2019; Published 24 April 2019

Guest Editor: Ulrike Hendgen-Cotta

Calcium ions are highly versatile intracellular signals that regulate many cellular processes. The key to achieving this pleiotropic role is the spatiotemporal control of calcium concentration evoked by an extensive molecular repertoire of signalling components. Among these, reactive oxygen species (ROS) signalling, together with calcium signalling, plays a crucial role in controlling several physiopathological events. Although initially considered detrimental by-products of aerobic metabolism, it is now widely accepted that ROS, in subtoxic levels, act as signalling molecules. However, dysfunctions in the mechanisms controlling the physiological ROS concentration affect cellular homeostasis, leading to the pathogenesis of various disorders.

1. Calcium Homeostasis

Calcium ions (Ca^{2+}) are one of the most crucial intracellular second messengers, involved in a plethora of cellular functions including cell survival and death, muscle contraction, regulation of metabolism, and gene expression [1]. To control these highly specialized functions, cells have developed sophisticated mechanisms to decode frequency-encoded Ca^{2+} signals [1].

The spatiotemporal regulation of cytosolic Ca^{2+} concentration ($[Ca^{2+}]_{cyt}$) relies on two key requirements. The first is the cooperation of two different sources of Ca^{2+} in the generation of $[Ca^{2+}]_{cyt}$ fluctuations: the extracellular medium, a virtually unlimited reservoir with a $[Ca^{2+}]$ of ~1 mM [2], and the intracellular stores which are endowed with a $[Ca^{2+}] > 100\,\mu M$, which allow rapid release of Ca^{2+} through store-resident channels [2]. The second requirement is the existence of a broad range of molecules that generate and decode $[Ca^{2+}]_{cyt}$ variations, such as pumps, channels, Ca^{2+}-binding signalling molecules, enzymes, and buffering proteins [2].

Once having entered the cytosol, Ca^{2+} exerts its allosteric regulatory effects on many enzymes and proteins, impacting nearly every aspect of cellular life [3]. This is corroborated by the amount of energy that cells invest to maintain this strictly regulated $[Ca^{2+}]$. Importantly, while complex molecules can be chemically altered, the only mechanism that exerts control over Ca^{2+} are chelation, subcellular compartmentalization and cell extrusion. The consequence is a very steep $[Ca^{2+}]$ gradient across the plasma membrane and the intracellular stores [3]. In resting cells, $[Ca^{2+}]_{cyt}$ are maintained within very low values of ~100 nM, while the extracellular space generally presents a $[Ca^{2+}]$ of over 1 mM [2]. Different channels in the plasma membrane regulate Ca^{2+} entry from the extracellular space. Among these are the voltage-operated calcium channels (VOCCs), the receptor-operated calcium channels (ROCCs), the store-operated calcium channels (SOCCs), and the second messenger-operated calcium channels (SMOCs) that, according to the stimuli evoking channel activation, allow Ca^{2+} entry through the plasma membrane [3].

As mentioned above, Ca^{2+} is also efficiently stored in intracellular compartments that serve as the main sources of releasable Ca^{2+} for eliciting crucial cellular functions [3]. The most important intracellular store is the endoplasmic reticulum (ER) and its specialized counterpart in muscle

cells, the sarcoplasmic reticulum (SR). In these compartments, $[Ca^{2+}]$ can reach ~0.8 mM, depending on the cell type. Rapid release of Ca^{2+} from these compartments ensures $[Ca^{2+}]_{cyt}$ rises required for specific cellular functions [3] and is controlled by two large families of channels: the inositol 1,4,5-trisphosphate receptor (InsP3R) and ryanodine receptor (RYR) families [4].

The agonist of IP3R is generated by the phospholipase C (PLC) enzymatic activity. This enzyme usually undergoes a receptor-promoted activation, and it hydrolyses its substrate phosphatidylinositol 4,5-bisphosphate (PIP2) in diacylglycerol (DAG) and inositol 1,4,5-trisphosphate (InsP3) [5]. The interaction of InsP3 with its receptors (InsP3Rs) induces Ca^{2+} release to the cytosol [6]. Ca^{2+} itself regulates the InsP3Rs' open probability, activating InsP3Rs at increasing $[Ca^{2+}]$ up to a specific $[Ca^{2+}]$ threshold, above which further increases in $[Ca^{2+}]$ play an inhibitory function [2]. The InsP3R family displays a broad tissue distribution and comprises three isoforms, InsP3R1, InsP3R2, and InsP3R3, which show different expression profiles among different tissues. Of note, InsP3R1 is most abundant in the central nervous system (CNS) and InsP3R2 is ubiquitously expressed among tissues and is the most abundant isoform in cardiac muscle [7]. InsP3Rs form heterotetramers, whose activity displays unique properties and responsiveness to ATP, Ca^{2+}, and InsP3 [8].

RyRs are structurally and functionally analogous to InsP3Rs, although they have approximately twice the conductance and molecular mass of InsP3Rs. RyRs are transmembrane proteins located in the ER/SR membrane, activated by the alkaloid ryanodine and by Ca^{2+} itself. Although Ca^{2+} is a major triggering ligand, several other players modulate RyRs' activity, such as the dihydropyridine receptor (DHPR; also known as L-type Ca^{2+} channel, $Ca_V1.1/1.2$), protein kinase A (PKA), calmodulin (CaM), Ca^{2+}/calmodulin-dependent protein kinase II (CaMKII), calsequestrin (CSQ), and the FK506-binding protein (FKBP12) [9]. Similarly to InsP3Rs, RyRs include three isoforms (RyR1-3), but, unlike the InsP3Rs that are widely expressed among tissues, RyR1-3 are almost exclusively expressed in excitable cell types. In detail, RyR1 is particularly enriched in skeletal muscle, RyR2 in cardiac muscle, and RyR3 is expressed more widely, although higher levels are found in the brain [6].

Once Ca^{2+} has carried out its signalling functions, it has to be rapidly removed from the cytosol by extrusion to the extracellular space or by compartmentalization to intracellular stores. This is achieved thanks to the activity of various pumps and exchangers, allowing intracellular $[Ca^{2+}]$ to return to its resting condition [3]. ATPase pumps compartmentalize Ca^{2+} into the ER/SR stores via the activity of ER/SR Ca^{2+} ATPase pumps (SERCAs) or extrude Ca^{2+} in the extracellular milieu via plasma membrane Ca^{2+} ATPases (PMCA pumps) by exploiting ATP-derived energy. A second mechanism utilizes the electrochemical gradient of Na^+ across the plasma membrane to provide the energy to transport Ca^{2+} to the extracellular space through the Na^+/Ca^{2+} (NCX) and Na^+/Ca^{2+}-K^+ exchangers (NCKX) [3].

In addition, many studies have highlighted a role in regulation of $[Ca^{2+}]_{cyt}$ also for other membrane-bound compartments such as the Golgi apparatus, endolysosomes, and mitochondria [6]. Among these organelles, mitochondria are recognized as crucial regulators of cellular Ca^{2+} homeostasis. Indeed, mitochondrial Ca^{2+} uptake regulates many cellular processes, controlling the delicate balance between cell survival and death [2]. Moreover, mitochondrial Ca^{2+} buffering is involved in the control of Ca^{2+} gradient in defined cellular domains [2]. This is possible thanks to a strategic localization of mitochondria to the Ca^{2+} release units of the ER/SR that contributes to shape both the amplitude and the spatiotemporal patterns of cellular Ca^{2+} responses [3].

1.1. Mitochondrial Ca^{2+} Signalling. Over the past 60 years, intense research has defined the basic properties of mitochondria in Ca^{2+} handling. These studies have highlighted the role of mitochondria in decoding the cytosolic Ca^{2+} oscillations and in the regulation of cellular Ca^{2+} homeostasis [3]. The first evidence that mitochondria can take up Ca^{2+} dates back to the 60s, when pioneering studies demonstrated that energized mitochondria can rapidly and efficiently accumulate Ca^{2+} [10, 11]. The formulation of the chemiosmotic theory, together with the measurement of the mitochondrial membrane potential ($\Delta\Psi_m$), led to the concept of an energetically favourable Ca^{2+} uptake mechanism [12, 13]. The generation of an internal negative electrochemical gradient by the mitochondrial respiratory chain, indeed, provides the thermodynamic basis for cation accumulation into the organelle matrix [13]. However, further characterizations of the mitochondrial Ca^{2+} uptake demonstrated that, despite the high selectivity of the mitochondrial Ca^{2+} uniporter (MCU) for Ca^{2+}, measured by direct mitoplast patch-clamp of mitoplasts (dissociation constant $(Kd) \leq 2$ nM) [14], the apparent mitochondrial affinity for Ca^{2+} was very low at physiological $[Ca^{2+}]$ [15]. Since cytosolic $[Ca^{2+}]$ is about 10-100 nM in resting conditions and reaches values of 2-3 μM during cell stimulation, the role of mitochondria in Ca^{2+} homeostasis was considered marginal. Therefore, the plasma membrane and the ER became the major players in the Ca^{2+} signalling scene [15]. The situation reversed when tools to perform reliable measurement of $[Ca^{2+}]$ in intact living cells were developed, allowing to uncover the role of mitochondria in Ca^{2+} handling [16, 17]. Indeed, while $[Ca^{2+}]_{mit}$ in basal resting condition is very low, comparable to the cytosolic one (10-100 nM), upon cell stimulation, mitochondria are able to rapidly and efficiently accumulate Ca^{2+} at levels that exceed that of the bulk cytosol that, in some cell lines, can reach also $[Ca^{2+}]$ of 100 μM [16]. The discrepancy between the low affinity of mitochondrial Ca^{2+} uptake and the prompt response of mitochondria to $[Ca^{2+}]$ increases was later solved by the demonstration that mitochondria are located in close proximity to the Ca^{2+} channels that elicit the rise in $[Ca^{2+}]_{cyt}$, the InsP3Rs, and the RYRs on the ER and SR [18, 19]. Indeed, these quasi-synaptic junctions with the ER/SR membranes allow mitochondria to directly sense local high $[Ca^{2+}]$ compatible with the low affinity of the MCU and that dissipates rapidly, thus preventing mitochondrial Ca^{2+} overload or vicious Ca^{2+} cycling across the mitochondrial membrane [18, 19].

Although the process of mitochondrial calcium uptake is prevalently studied at the level of the solutes impermeable inner mitochondrial membrane (IMM), the ability of Ca^{2+} to cross the outer mitochondrial membrane (OMM) plays a crucial role. The OMM permeability to solutes is prevalently due to the high expression of the voltage-dependent ion channels (VDACs), permeable to solutes smaller than 5 kDa and, thus, also Ca^{2+} [20]. Three different VDAC isoforms, VDAC1, VDAC2, and VDAC3, have been identified. VDAC1, the best characterized isoform [21], acts as a mitochondrial gatekeeper, controlling the metabolic and energy crosstalk between the mitochondria and the rest of the cell [21]. Furthermore, it has been also shown that VDACs' expression levels can limit calcium accumulation inside the matrix. It was demonstrated, indeed, that VDAC overexpression augments agonist-dependent rises in $[Ca^{2+}]_{mit}$, whereas VDAC downregulation has the opposite effect [22, 23].

1.2. The Mitochondrial Ca^{2+} Uniporter Complex: Structural and Functional Complexity. The molecular identity of the protein responsible for mitochondrial Ca^{2+} uptake, MCU, was uncovered only in 2011 by two different groups [24, 25], marking a turning point in the study of the pathophysiological roles of mitochondrial Ca^{2+} uptake. The characterization of the MCU revealed that this channel is a high-molecular-weight complex composed of both pore-forming and regulatory subunits [1].

From the primary amino acidic sequence analysis, MCU consists of two transmembrane domains spanning the IMM (Figure 1 and [1]). Soon after its discovery, it was clear that the MCU was part of a macromolecular complex since it lacks classical Ca^{2+}-binding domains and the loop region that faces the intermembrane space (IMS) appears to be too small to contain regulatory elements [1]. This was confirmed by blue native gel separation experiments of purified mitochondria that display a high-molecular-weight complex containing MCU with an apparent molecular weight of about 450 kDa, suggesting that many other proteins are part of the channel [24, 26–28].

Recently, the MCU protein structure was solved by different laboratories. First, MCU was shown to be a pentamer of the MCU homolog from *Caenorhabditis elegans* deleted of the N-terminal domain, which was defined by using nuclear magnetic resonance (NMR) and negative-stain electron microscopy [29]. Recently, four independent groups characterized the structure full-length *Fungi* homologs of MCU by Cryo-EM and/or X-ray diffraction approaches [30–33]. Unlike the previous study, they found a tetrameric architecture. Since these *Fungi* MCU homologs share only about 40% of similarity with metazoan MCU, prevalently conserved in the transmembrane regions and in the coiled-coil domains, Baradaran and coworkers performed Cryo-EM studies also on zebrafish MCU homolog, which displays a higher similarity with human MCU (91%). Although the resolution obtained is lower (8.5 Å), the overall structure is similar to that of *Fungi* MCU and also displays a tetrameric architecture [30]. Interestingly, the conserved DIME motif that connects the two transmembrane domains appears to be part of the second transmembrane domain and seems to confer Ca^{2+} selectivity to the MCU. The N-terminal domain is poorly conserved in these MCU homologs, but the human NTD of MCU was previously crystallized [34].

After the discovery of MCU, we have witnessed an explosion of studies aimed at clarifying the composition of the channel and the regulation of its activity. These studies demonstrated that three proteins compose the protein structure that spans the IMM: MCU, MCUb, and EMRE. Furthermore, three regulatory subunits were identified (MICU1, MICU2, and MICU3).

EMRE ("essential MCU regulator") is a 10 kDa, metazoan-specific protein with a single transmembrane domain that spans the IMM with a highly acidic carboxyl terminus (Figure 1 and [28]). This protein has been proposed to play a dual function in the regulation of MCU activity. First, it seems required for MCU channel activity since its silencing abrogates mitochondrial Ca^{2+} uptake [28], although experiments in the planar lipid bilayer demonstrated that mouse MCU alone is sufficient to give rise to Ca^{2+} currents [25]. Second, EMRE seems fundamental in mediating the interaction between MCU and the regulatory subunits MICU1 and MICU2 [28], although it has also been observed that MICU1 is sufficient to induce MCU channel activity [26]. In addition, in yeast cells that do not present mitochondrial Ca^{2+} uptake, the *Dictyostelium discoideum* MCU homolog conducts Ca^{2+} in the absence of an EMRE homolog while human MCU requires the presence of EMRE to act as a functional channel [35]. Very recently, it was shown that the acidic C-terminal domain functions as a matrix Ca^{2+} sensor that regulates the MCU activity. In this model, EMRE acts, together with MICU1, as a regulatory complex able to sense $[Ca^{2+}]$ at both sides of IMM [36]. Nevertheless, these data were questioned by a study showing that EMRE displays a different topology across the IMM [37]. Future experiments will clarify the role of EMRE in the regulation of MCU channel activity.

MCUb is a MCU isoform conserved in most vertebrates and in many plants but absent in other organisms where the MCU is present (Figure 1 and [38]). MCU and MCUb share 50% sequence similarity, and each possesses two transmembrane domains separated by a short loop almost identical between the two [38]. Despite the huge sequence similarity in the transmembrane domains, MCUb displays altered ion permeation, given to two conserved amino acid substitutions in close proximity of the conserved DIME motif that drastically reduces the conductivity of the channel [38]. Specifically, the Arg 251 and Glu 256 residues are mutated in Trp and Val, respectively (R251W and E256V). These substitutions drastically reduce conductivity of the channel reducing $[Ca^{2+}]_{mit}$uptake [38]. According to this evidence, in living cells, the overexpression of MCUb reduces the amplitude of $[Ca^{2+}]_{mit}$ transients evoked by agonist stimulation and MCUb silencing elicits the opposite effect, suggesting that this protein acts as a dominant-negative subunit that incorporates into the channel and reduces its activity [38]. Interestingly, MCU and MCUb expression profiles widely differ among tissues, possibly providing an intrinsic regulatory mechanism to set the mitochondrial responsiveness to Ca^{2+}-mediated signals in a defined cell type [38]. Consistently, tissues characterized by low mitochondrial

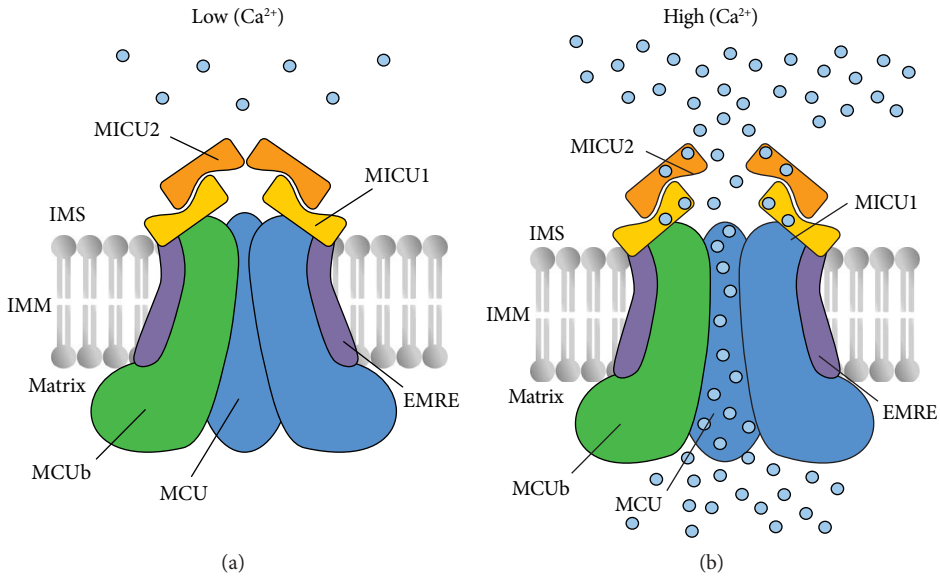

Figure 1: Schematic representation of the mitochondrial Ca^{2+} uniporter (MCU) complex. The MCU complex is composed by pore-forming subunits (that comprise the channel subunits MCU, the dominant-negative subunits MCUb, and the transmembrane regulator EMRE) and regulatory subunits (MICU1 and MICU2). MICU1 and MICU2 sense, through EF-hand domains, the increase of Ca^{2+} levels in the intermembrane space (IMS). In resting conditions (on the left), MICU1-MICU2 heterodimers act as gatekeeper of the channel, thus preventing Ca^{2+} vicious cycling and mitochondrial matrix overload. Increases in calcium concentration as a result of cell stimulation (on the right) not only release the inhibitory function of the MICU1-MICU2 heterodimers but also further stimulate MCU channel opening, ensuring the prompt response of mitochondrial metabolism to cell stimulation.

Ca^{2+} transients, such as the heart, exhibit a low MCU/MCUb ratio, while others, such as skeletal muscle, display a higher ratio and high mitochondrial Ca^{2+} uptake levels [38].

1.3. MCU-Associated Regulators. One of the key features of mitochondrial Ca^{2+} uptake is its sigmoidal response to extra-mitochondrial $[Ca^{2+}]$. At resting $[Ca^{2+}]_{cyt}$, mitochondrial Ca^{2+} uptake is inhibited, despite the steep $\Delta\Psi_m$ [3]. This property prevents matrix Ca^{2+} overload and the dissipation of the $\Delta\Psi_m$, leading to deleterious effects of Ca^{2+} cycling and matrix overload. At higher $[Ca^{2+}]_{cyt}$, when cells are stimulated, mitochondria have to respond promptly, increasing the Ca^{2+}-carrying capacity [3]. The lack of Ca^{2+}-sensing domains in the MCU protein sequence, as mentioned above, suggested the existence of a highly sophisticated gatekeeping mechanism, including both negative modulators, acting at low $[Ca^{2+}]$, and activators able to induce Ca^{2+} uptake during cell stimulation. Accordingly, it was shown that the regulation of the MCU complex activity is possible thanks to the MICU (mitochondrial calcium uptake) family of intermembrane space (IMS) proteins, composed by MICU1, MICU2, and MICU3 [39]. These three regulators share common features: they are localized to mitochondria, they display EF-hand Ca^{2+}-binding domains in their protein sequence, and they interact with MCU (Figure 1) [39].

MICU1 (mitochondrial calcium uptake 1) was identified even before the identification of MCU as a critical modulator of mitochondrial Ca^{2+} uptake (Figure 1 and [40]). MICU1 was initially proposed to be required for mitochondrial Ca^{2+} uptake, since its silencing was sufficient to abolish mitochondrial Ca^{2+} entry in intact and permeabilized cells [40]. This evidence was questioned by other laboratories that showed that MICU1 silencing is sufficient to induce mitochondrial Ca^{2+} overload, suggesting that MICU1 could play a gatekeeping role in preventing mitochondrial Ca^{2+} uptake at low $[Ca^{2+}]_{cyt}$, while playing a minor role at higher $[Ca^{2+}]_{cyt}$ [41]. The identification of MICU1 loss-of-function mutations in patients affected by a disease characterized by proximal myopathy, learning difficulties, a progressive extrapyramidal movement disorder, and increased mitochondrial Ca^{2+} load supported this hypothesis [42]. The gatekeeper role of MICU1 was confirmed by Csordás and coworkers [43]. They also showed that silencing of MICU1 highly affects the cooperativity of mitochondrial Ca^{2+} uptake, thus hypothesizing that MICU1 could play a dual function depending on $[Ca^{2+}]_{cyt}$.

Very recently, Csordás et al.s' group dissected the mechanism that allows MICU1 to interact with MCU, to regulate mitochondrial Ca^{2+} entry and the sensitivity to ruthenium red/Ru360 (RuRed/Ru360), a compound that inhibits the activity of the uniporter [44]. Indeed, a structural and functional interaction of the DIME motif of MCU was reported, identified as the selectivity filter, with a domain of MICU1, named DID, as the DIME-interacting domain. The interaction between these two domains appears to be fundamental for ensuring both the threshold and cooperative activation of the MCU complex-mediated Ca^{2+} uptake and thus to avoid mitochondrial Ca^{2+} overload [44]. Furthermore, the DID motif limits the access of RuRed/Ru360 to its target site in the DIME domain of MCU since MICU1 removal can sensitize mitochondria to inhibition by this compound, thus

predicting a different RuRed/Ru360 sensitivity of the MCU complex in various tissues, in light of recent data on tissue-specific differences in MICU1 abundance relative to MCU [45].

In addition to MICU1, other MCU complex components have also been discovered. Two paralogs of MICU1, originating from a gene duplication event prior to vertebrate evolution, were identified: MICU2 (Figure 1 and [27]), which displays a tissue expression pattern similar to that of MICU1, and MICU3, whose expression is restricted to the nervous system (NS) and, at lower levels, to the skeletal muscle [27].

MICU2 discovery [27] helped to clarify the mechanism responsible for the sigmoidal response of the MCU to extramitochondrial [Ca^{2+}] that allows on the one hand minimal Ca^{2+} uptake in the presence of a very large driving force for cation accumulation thus preventing mitochondrial Ca^{2+} overload and on the other hand ensures rapid Ca^{2+} accumulation during cell stimulation. Importantly, MICU2 protein stability depends on that of MICU1 [26, 27, 46], since MICU1 silencing induces MICU2 protein degradation, suggesting that the effect of MICU1 silencing on mitochondrial Ca^{2+} uptake could be due also to the concomitant disappearance of MICU2 protein. Notably, MICU1 and MICU2 have been shown to form an obligate heterodimer through the formation of a disulphide bond [26], which is regulated by the mitochondrial oxidoreductase Mia40 [47].

MICU2 was demonstrated to act as the genuine gatekeeper of the MCU at low $[Ca^{2+}]_{cyt}$ [26]. As soon as extramitochondrial [Ca^{2+}] increases, Ca^{2+}-dependent MICU2 inhibition and MICU1 activation guarantee the prompt response of rapid mitochondrial Ca^{2+} accumulation (Figure 1 and [26]).

Recently, an alternative splice variant of MICU1, named MICU1.1, was identified and characterized [48]. It has been shown that the expression of this splice variant varies greatly among tissues. Indeed, MICU1.1 is present only in skeletal muscle, where it is the predominant isoform, and lower levels are found in the brain, suggesting tissue-specific functions. MICU1.1 is characterized by the addition of a micro-exon coding for four amino acids (EFWQ) far from the EF-hand domains, which greatly modifies the properties of the protein. In detail, MICU1.1 can bind Ca^{2+} one order of magnitude more efficiently than MICU1 and, when heterodimerized with MICU2, activates MCU current at lower [Ca^{2+}] than MICU1-MICU2 heterodimers [48].

How the MICU1.1 extra exon impact on MICU1 structure and modifies the Ca^{2+}-binding affinity of the EF-hand domains remains unaccounted. In this regard, the domain that contains the extra exon was not resolved in the MICU1 crystal structure, suggesting that it is part of a highly flexible region [49]. This can suggest a putative role of this protein domain in protein-protein interactions, which can modify the MICU1 modulatory properties.

It was hypothesized that the inclusion of this splice variant in the MCU complex could represent an important mechanism in excitable tissues, where fast Ca^{2+} transients occur. Indeed, in skeletal muscle, the prevalent expression of MICU1.1 allows a prompter response of mitochondria metabolism to [Ca^{2+}] [48], ensuring a sustained ATP production during contraction, since mitochondrial Ca^{2+} positively regulates the activity of three key dehydrogenases of the tricarboxylic acid (TCA) cycle: pyruvate, isocitrate, and α-ketoglutarate dehydrogenases [50].

MICU3 shares a mitochondrial targeting sequence (MTS) at the amino terminus and two canonical Ca^{2+}-binding EF-hand domains with MICU1 and MICU2 [27]. MICU3, unlike MICU1 and MICU2 that present a ubiquitous and strongly correlated expression pattern among tissues, is expressed only in the CNS and, at low levels, in skeletal muscle [27]. Recently, it was shown that MICU3 exists in a disulfide bond-mediated dimer only with MICU1 but not with itself or MICU2 and acts as a highly potent stimulator of MCU activity, with no gatekeeping function [51]. In this regard, it was shown that neurons simultaneously express both MICU1-MICU2 and MICU1-MICU3 heterodimers. The first avoids low vicious Ca^{2+} cycling in resting conditions; the latter anticipates MCU opening, activating organelle Ca^{2+} uptake even in the presence of small and rapid cytosolic Ca^{2+} signals. Thus, MICU3 in neurons allows enhancing MCU opening in order to guarantee organelle Ca^{2+} uptake also in response to small and fast increases of $[Ca^{2+}]_{cyt}$ [51].

Finally, MCUR1, an IMM-integral protein, was initially reported to function as a regulator of the MCU complex [52], although this protein was not among the MCU interactors [28]. Furthermore, MCUR1 has a homolog in *Saccharomyces cerevisiae*, an organism that lacks mitochondrial Ca^{2+} uptake. Its role in MCU complex regulation is highly debated, since it has been shown, both in yeast and mammalian cells, that it is involved in complex IV assembly [53]. Furthermore, it has been reported that MCUR1 silencing causes a consistent drop of $\Delta\Psi_m$, with consequent reduction of mitochondrial Ca^{2+} uptake [53].

Moreover, recently, Chaudhuri and coworkers found discordant results. Indeed, they found no significant changes in $\Delta\Psi_m$ and no changes in mitochondrial Ca^{2+} uptake rates after manipulating MCUR1 expression, but they demonstrated that MCUR1 regulates the amount of Ca^{2+} required to induce the permeability transition [54].

Therefore, whether this protein controls directly the activity of MCU or whether it affects mitochondrial Ca^{2+} uptake by indirectly impinging on mitochondrial bioenergetics is still highly debated.

2. Ca^{2+} and ROS as a Mutual Interplay

The understanding of the role of mitochondria as integration points of different cellular signals, and the mechanisms through which mitochondria translate these stimuli in biological responses, represents a new challenge in biomedical research. As discussed above, the ability of mitochondria to accumulate Ca^{2+} is fundamental for tissue homeostasis [1]. However, mitochondrial Ca^{2+} overload leads to reduced ATP production and sustained opening of the mPTP, a high conductance channel, whose opening enables the release of proapoptotic mitochondrial components [55].

Matrix Ca^{2+}, beyond a certain threshold, together with other causal factors, most notably oxidative stress, high

Figure 2: ROS production and scavenging systems. In physiological conditions, the balance between ROS generation and ROS scavenging is highly controlled. The energy production pathways (TCA cycle and OXPHOS), enzymatic reactions, by-products of metabolic pathways, and physical or chemical agents can lead to ROS production. As for the ROS-scavenging mechanisms, enzymatic defences and antioxidant scavengers neutralize the free radical reactions. When an imbalance between ROS production and ROS scavenging occurs, cells undergo oxidative stress, leading to severe cellular damage, cell death, and consequently whole organ and organism failure.

phosphate concentrations, and low adenine nucleotide concentration, is an essential permissive factor for mPTP opening [55]. This event triggers the so-called mitochondrial permeability transition that is characterized by a dramatic increase in the mitochondrial membrane permeability to any molecule smaller than 1.5 kDa. The consequent dissipation of the mitochondrial $\Delta\Psi_m$ leads to membrane depolarization and mitochondrial swelling, increased mitochondrial reactive oxygen species (mROS) generation, cytochrome c release, and apoptosis [55].

The molecular identity of the mPTP is still debated. It was proposed that the adenosine nucleotide translocase (ANT), VDAC, and the translocator protein (TSPO) are essential components of the mPTP [54]. However, biochemical characterization to knockout models of these proteins suggests that they are dispensable for mPTP activity [56]. It has been recently proposed that mPTP is generated at the interface of two adjacent monomers of the F-ATP synthase through a strictly Ca^{2+}-dependent mechanism, since gel-excised dimers of F-ATP synthase rapidly give rise to mPTP-like channels in lipid bilayers [57, 58]. Nevertheless, the mechanism of PTP formation and activation is still debated. Detailed discussion of this aspect is beyond the scope of this review, and readers are referred to specific contributions on this topic [59–65].

2.1. Mitochondrial ROS Production and Regulation. Mitochondria, through the respiratory chain, especially complexes I and III, are considered the main source of physiological ROS [66]. mROS are generated in both physiological and pathological conditions [66]. Indeed, on the one hand moderate levels of ROS are involved in cell signalling by affecting the redox state of signalling proteins, but on the other hand, when in excess, mROS are among the major determinants of toxicity in cells and organisms [66].

During respiration, superoxide (O_2^-) is produced by partial reduction of molecular oxygen. Subsequently, hydrogen peroxide (H_2O_2) is formed by the action of matrix antioxidant defence enzymes as superoxide dismutase (SOD) [66]. H_2O_2 is transformed in water by glutathione peroxidase (GPX), peroxiredoxin (PRX), and catalases [66]. The regulation of the activity and the expression levels of these antioxidant enzymes are controlled by a plethora of mechanisms [66]. Under physiological conditions, the balance between ROS generation and ROS scavenging is highly controlled (Figure 2). Physiological ROS levels initiate a wide array of cellular responses, ranging from triggering signalling pathways, activation of mitochondrial fission and autophagy, adaptation to hypoxic condition, and differentiation to regulation of aging-related processes [67]. In these specific conditions, ROS production is induced in response to a stress and it functions as an intermediate signalling to facilitate cellular adaptation [68].

ROS production, when not compensated by ROS scavenging, results in oxidative stress leading to severe cellular damage and cell death [67]. In this condition, ROS become causative of several pathological states by the direct modification of cellular macromolecules, leading to alterations of the redox state of factors involved in signal transduction, inducing either hyper- or hypofunctionality of several signalling pathways [67, 68]. Oxidative stress has been shown to be at the basis of aging and many pathological disorders. Indeed, ROS are responsible of cell death in pathological conditions such as myocardial infarct or stroke [67].

In physiological conditions and in a tissue-specific manner, mitochondrial Ca^{2+} uptake, by impinging on Krebs cycle enzymes and electron transport chain (ETC) activity, generates a ROS signals [69]. This signalling axis operates within a physiological window of $[Ca^{2+}]$. Therefore, when $[Ca^{2+}]$ overcomes this threshold, mROS production becomes detrimental and compromises mitochondrial bioenergetics and cell functions [70, 71]. Mitochondrial Ca^{2+} may promote mROS formation both directly, by stimulating mROS-generating enzymes, like glycerol phosphate

and α-ketoglutarate dehydrogenase, and indirectly, as in the case of nitric oxide synthase (NOS) activation that, by forming NO, blocks complex IV, leading to excessive mROS formation [70].

Finally, mitochondrial Ca^{2+} overload triggers mPTP opening. Indeed, $[Ca^{2+}]_{cyt}$ increases beyond a certain value and induces mitochondrial Ca^{2+} overload, triggering the mitochondrial "permeability transition." In this condition, the mitochondrial membrane becomes permeable to any molecule less than 1.5 kDa in size. Consequent dissipation of $\Delta\Psi_m$ leads to a permanent membrane depolarization, decreased ATP production, and eventually cell apoptosis. Moreover, mitochondrial membrane depolarization leads to crista unfolding, uncoupling of oxidative phosphorylation, and the reverse electron transport (RET). RET is evoked when electrons from ubiquinol are transferred back to respiratory complex I, reducing NAD^+ to NADH. This process generates a significant amount of ROS [56].

Since mitochondrial Ca^{2+} plays a key role in ROS production, the cellular redox state can also significantly modulate Ca^{2+} signalling [70, 71]. Indeed, it has been clearly demonstrated that redox equilibrium controls a variety of receptors, proteins, and other signalling molecules that, in turn, might directly or indirectly modify components of Ca^{2+} signalling pathways, thus altering Ca^{2+} homeostasis and reshaping local and global Ca^{2+} signals [70]. When the redox equilibrium is disturbed, due to the excessive accumulation or clearance of ROS, many cellular signalling pathways are influenced, leading to cellular dysfunction and subsequently to the development of various pathologies, including neurodegenerative disorders, cancer, diabetes, atherosclerosis, and ischemia/reperfusion (I/R) injury. Therefore, both mROS and mitochondrial Ca^{2+} signalling are two functional entities that strictly cooperate in order to contribute to the maintenance of cellular homeostasis [71].

Intriguingly, Dong and coworkers analysed the crosstalk between intracellular ROS levels and $[Ca^{2+}]_{mit}$, suggesting that oxidative stress, and thus ROS accumulation, plays a positive feedback role in modulating MCU activity [72]. Indeed, they observed that MCU activity increases in cells exposed to endotoxin-mediated oxidative stress, leading to augmented $[Ca^{2+}]_{mit}$ at resting $[Ca^{2+}]_{cyt}$. In detail, they identified a conserved cysteine in metazoan at position 97 (Cys-97) in the NTD of the MCU protein sequence to be the only reactive thiol in human MCU that undergoes redox modification (S-glutathionylation). The Cys-97 residue is surface-exposed and primed for an oxidative posttranslational modification that induces a conformational change of MCU that promotes the clustering of MCU channels and their persistent activation [72]. These data suggest that, in condition of oxidative stress, mROS overproduction in the mitochondrial matrix perturbs mitochondrial antioxidant activity resulting in S-glutathionylation of MCU Cys-97. The conjugation of glutathione causes a conformation change within the N-terminal domain that appears to promote MCU channel activity in resting condition. The increased MCU activity, in turn, enhances the production of mROS in the mitochondrial matrix in a positive feedback mechanism, thus leading to perturbation of mitochondrial bioenergetics and cell functions [72]. Overall, these data strongly suggest that ROS and mitochondrial Ca^{2+} signals are intimately interconnected, leading to a specific and adaptive response to given stimuli.

Excessive ROS are recognized as one of the causative factors in the development of a diverse array of diseases including cardiovascular, skeletal muscle, and neurodegenerative diseases and cancer progression (Figure 3 and [67, 71]). This review is aimed at describing some pathological conditions characterized by a dysregulation of mitochondrial Ca^{2+} uptake associated with an excessive ROS production.

3. Crosstalk of Mitochondrial Ca^{2+} Uptake and Mitochondrial Redox State in Physiopathology

3.1. Heart. Most of the ATP necessary for cardiac excitation and contraction is synthesized within mitochondria via oxidative phosphorylation which, as described above, is a process modulated by Ca^{2+} [1]. Furthermore, mitochondria are the major source of ROS that represent by-products of oxidative phosphorylation [73]. In living cells, and in particular in cardiac myocytes, ROS are also produced by extra-mitochondrial sources including NADPH oxidase, uncoupled NOS, xanthine oxidase, and monoamine oxidase [74]. In physiological conditions, ROS concentration is tightly regulated by antioxidants keeping them in a picomolar range. Low concentrations of ROS allow them to act as second messengers in signal transduction for vascular homeostasis and cell signalling [73]. In detail, the activity of redox-sensitive proteins, including Ca^{2+}-handling proteins, contractile proteins, and proteins involved in various signalling pathways and in transcriptional activities, can be modulated by ROS [73].

Redox modulation of calcium-handling proteins directly affects cardiac contraction by altering intracellular calcium concentration [75]. In detail, ROS can oxidase and directly enhance the activity of Ca^{2+}/calmodulin-dependent kinase II (CaMKII) that in turn phosphorylates and activates several Ca^{2+}-handling proteins such as the cardiac ryanodine receptor RyR2 or cardiac SERCA [76]. Cardiac RyR2 mediates Ca^{2+} release to the cytosolic compartment from SR during excitation-contraction coupling (ECC) and is itself subject to oxidation that increases RyR2 open probability but may lead to irreversible activation and Ca^{2+} leak [77]. Similarly to RyR2, cardiac SERCA, which transfers Ca^{2+} from the cytosol to the SR at the expense of ATP hydrolysis during diastole, might be also directly regulated by oxidation. In particular, low oxidation levels reversibly increase SERCA activity whereas higher levels cause irreversible inactivation [77].

When the equilibrium between ROS production and scavenging is altered, ROS can cause damage to lipids, proteins, and DNA by contributing to the development and progression of cardiovascular diseases such as atherosclerosis, I/R injury, chronic ischemic heart disease, cardiomyopathy, heart failure, and arrhythmias [73]. As already discussed in the previous paragraph, excessive ROS levels is caused not

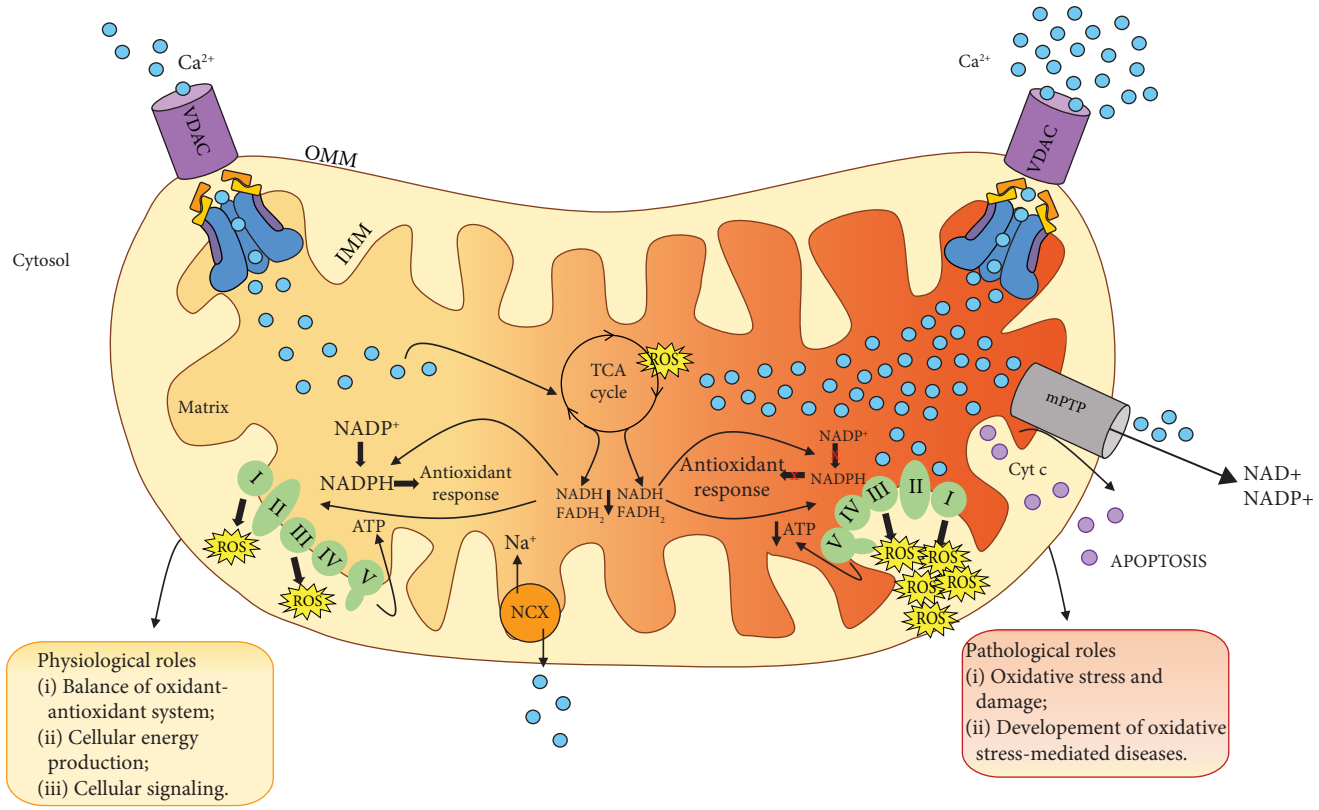

FIGURE 3: Regulation of mitochondrial Ca^{2+} uptake controls energy metabolism, mtROS production, and cell death. mtROS represent a by-product of oxidative phosphorylation and exert a beneficial or detrimental effect depending on their concentration and on the biological contest. In physiological conditions, mitochondrial Ca^{2+} uptake stimulates the TCA cycle and ATP production (left part). At physiological $[Ca^{2+}]_{mit}$, the amount of ROS is counteracted by the activity of the antioxidant system (left part). In pathological conditions, excessive Ca^{2+} accumulation by mitochondria (right part) increases mtROS production which, in turn, affects antioxidant response. Altogether, this leads to the increase in the mPTP open probability, leading to irreversible collapse of the mitochondrial membrane potential, swelling of mitochondria, and thus release of cytochrome c, culminating in cell death.

only by defective ROS scavenging mechanisms but also by excessive ROS production.

Since cardiac mitochondria are the major producers of ROS through oxidative phosphorylation and Ca^{2+} plays a key role in promoting aerobic metabolism, dysregulation of mitochondrial Ca^{2+} homeostasis translates also in oxidative stress [73].

During myofibril contraction, ATP is hydrolysed to adenosine diphosphate (ADP) which moves into mitochondria through the adenine nucleotide transporter (ANT) and activates the F_1F_0-ATPase to regenerate ATP [78]. The increase in mitochondrial ADP content accelerates electron flux along the ETC and induces the oxidation of the reduced NADH and $FADH_2$ which act as electron donors to sustain oxidative phosphorylation [78]. At the same time, Ca^{2+} is accumulated into the mitochondrial matrix through the MCU, where it stimulates the activity of the Krebs cycle to replenish the reduced pyridine nucleotides as NADH and $FADH_2$ which act as electron donors and sustain oxidative phosphorylation [78]. Therefore, Ca^{2+} plays a dual role since it both increases electron flux along the ETC and regenerates energy by increasing the electron flow from the Krebs cycle to the ETC [79, 80].

The ability of mitochondria to cope the increase in energy demand, occurring during increased cardiac workload or hormonal stimulation, is due to the close apposition of mitochondria and the SR [3, 81, 82]. It was hypothesized that Ca^{2+} released from the SR will elevate local Ca^{2+} to high levels resulting in a large mitochondrial Ca^{2+} influx [81]. Nevertheless, direct patch clamp recordings demonstrated that cardiac mitochondria's MCU current (I_{MCU}) is substantially smaller than that of other tissues, such as skeletal muscle, where I_{MCU} is 30 times bigger [83]. Notably, these two tissues present different mitochondrial volume fractions. Indeed, cardiac myocytes show one of the highest mitochondrial volume fractions in mammalian cells (37%), while in skeletal muscle this fraction is much lower (5%) [83]. Furthermore, also the MCU complex component stoichiometry is different between these two tissues. For example, in the heart, the expression of the dominant-negative subunit MCUb is higher than that in the skeletal muscle, inversely correlating with mitochondrial Ca^{2+} current [38]. In addition, mitochondrial Ca^{2+} uptake in the heart is controlled by a low MICU1/MCU ratio, thus lowering the threshold and cooperativity of the MCU complex [45]. It has been proposed that both the low Ca^{2+} conductivity of the MCU and the

complexity of its regulatory components could represent protective mechanisms by which cardiac mitochondria regulate $[Ca^{2+}]_{mit}$ by preventing Ca^{2+} overload [83]. Indeed, an excessive mitochondrial Ca^{2+} uptake associated with an increase in ROS accumulation leads to the opening of the PTP, irreversible collapse of mitochondrial membrane-potential, swelling of mitochondria, and thus release of cytochrome c resulting in necrotic cardiomyocyte cell death, a common scenario observed in the ischemic/reperfused myocardium [55].

In chronic heart failure (HF), perturbations of ECC cause contractile dysfunction [84] which is the result of decreased systolic Ca^{2+} transients, caused by at least three mechanisms that altogether contribute to reduce $[Ca^{2+}]_{mit}$ by affecting the activation of the Krebs cycle during increased workload [85]. The first mechanism is associated with a decreased Ca^{2+} load of the SR, with consequent reduction of cytosolic Ca^{2+} transients. The reduction in SR Ca^{2+} load is due both to a lower activity of the SERCA and to leaky RyR2 [84]. During relaxation, Ca^{2+} removal is mainly due to SERCA and the sarcolemmal NCX. Interestingly, in HF, SERCA activity is reduced and, concomitantly, NCX activity increases. As a consequence, more Ca^{2+} is extruded from the cell and less is taken up by SERCA, thus decreasing the SR Ca^{2+} available to be released during subsequent ECC [86, 87]. The second mechanism, associated with contractile dysfunction in failing cardiomyocytes, is the huge increase in cytosolic Na^+ levels ($[Na^+]_{cyt}$), which accelerates mitochondrial Ca^{2+} efflux via the mitochondrial Na^+/Ca^{2+} exchanger (mNCX) [88, 89]. This hampers the activation of Krebs cycle dehydrogenases by Ca^{2+}, and it results in pronounced oxidation of NADH to NAD^+ during transitions of workload [90]. The higher $[Na^+]_{cyt}$ could be explained by lower Na^+/K^+ pump activity, consistent with a decreased Na^+/K^+ pump expression in some models of HF [91, 92]. However, this finding was questioned by a more recent study performed in HF rabbit ventricular myocytes demonstrating that the higher $[Na^+]_{cyt}$ is due to elevated diastolic Na^+ influx rather than altered Na^+/K^+ pump activity [93]. The huge increase in $[Na^+]_{cyt}$ modifies the direction of the sarcoplasmic NCX transport by inducing the increase in cytosolic Ca^{2+} that partially compensates the decreased SR Ca^{2+} load and release in failing myocytes [89]. On the contrary, no compensatory effects have been detected on mitochondrial Ca^{2+} uptake since the rather slow NCX-mediated Ca^{2+} influx shows less impact on mitochondrial Ca^{2+} uptake [94]. The third mechanism involves changes in the activity of the MCU. Indeed, Michels and colleagues demonstrated that in human cardiac mitochondria from patients affected by HF, the open probability of MCU is decreased [94]. This affects both the energy supply and demand matching and thus the oxidative capacity. This evidence was also observed in isolated cardiomyocytes from a guinea pig model of systolic HF characterized by decreased NADH and NADPH levels and thus in the amount of reducing equivalents necessary for ATP production accompanied by an increase in ROS levels [95].

ROS directly act on cellular structures and activate signalling molecules involved in myocardial remodelling and failure. Indeed, on the one hand low levels of ROS are associated with the activation of the mitogen-activated protein kinase (MAPK) and protein synthesis; on the other hand, high levels of ROS affect ECC in cardiac myocytes [96]. The latter can cause arrhythmias, activate prohypertrophic signalling, and induce apoptotic and/or necrotic cell death through the activation of the mPTP [78]. In addition, mitochondrial ROS play a key role in the development and progression of HF in response to different stimuli such as I/R, pressure overload, and angiotensin II [97]. It has also been demonstrated that oxidative stress stimulates the activity of myocardial metalloproteinases (MMP), a family of proteolytic enzymes that regulates extracellular matrix turnover and that is implicated in the cardiac remodelling after myocardial infarction [98].

The concept that ROS production by cardiac mitochondria is dynamically regulated by Ca^{2+} and ADP and controlled by the redox state of mitochondrial pyridine nucleotides gave rise to the finding that an imbalance between decreased mitochondrial Ca^{2+} uptake and increased cardiac workload triggers oxidative stress [78]. As already discussed above, mitochondrial Ca^{2+} uptake plays a key role in matching ATP production to demand and has a great impact on the redox state of pyridine nucleotides [78]. Therefore, the regulation of mitochondrial Ca^{2+} uptake mediated by the MCU complex in the pathophysiology of heart failure has been extensively investigated in the past years. Indeed, after the characterization of the MCU complex, three different mouse models have been generated: a mouse model with a constitutive global MCU knockout (KO) [99, 100], a conditional cardiac myocyte-specific MCU KO [101, 102], and a transgenic mouse overexpressing a dominant-negative form of MCU (DN-MCU) [103, 104].

Surprisingly, total body knockout of MCU mice is viable and exhibits a very mild phenotype, with slightly smaller body mass than those of wild-type littermates and a slight decrease in skeletal muscle strength and performance [99]. As for the heart, no differences between MCU KO heart and WT littermates were observed [99]. As expected, MCU knockout cardiac mitochondria seem incapable of any rapid mitochondrial calcium uptake and showed alterations in Ca^{2+}-dependent oxygen consumption although basal ATP levels were unaltered, suggesting that MCU depletion does not affect basal mitochondrial metabolism [100]. These results can be partially explained by the observation that resting free $[Ca^{2+}]$ in knockout mitochondria is only partially reduced [99]. Altogether, these results suggest the existence of alternative mechanisms for Ca^{2+} accumulation in basal conditions, although MCU KO mitochondria were not able to take up Ca^{2+} during cell stimulation [99], fundamental phenomena for responding to variation in energy demands during cell activation. Furthermore, MCU deletion is viable in the outbred CD1 strain, while it results in embryonic lethality in the inbred C57BL/6 strain, suggesting the existence of compensatory mechanisms that allow animal viability only in the mixed background [105]. Another puzzling result is the lack of protection from cell death in the hearts lacking MCU. Indeed, in isolated mitochondria from KO hearts, the addition of large amounts of extramitochondrial

calcium did not lead to mPTP activation. Surprisingly following global I/R injury, infarct size was indistinguishable between WT hearts and hearts from MCU KO mice [99], but cyclosporine A, an inhibitor of mPTP, was able to reduce infarct size only in hearts of WT hearts.

As regards the heart-specific MCU KO mice and the transgenic mice overexpressing DN-MCU, a common feature is that, although mitochondria isolated from the heart of these mice are unable to accumulate Ca^{2+}, cardiomyocyte function is altered only after β adrenergic receptor (β-AR) stimulation. This highlights the importance of MCU-mediated mitochondrial Ca^{2+} uptake in sustaining cardiac function during physiological increases in workload. In addition, in DN-MCU mice, it was observed that $[Ca^{2+}]_{cyt}$ increases after the positive inotropic and chronotropic responses to β-AR stimulation [103, 104]. This finding, corroborated by a study performed on neonatal cardiomyocytes in which MCU was silenced, suggests that MCU may contribute to cytosolic Ca^{2+} buffering in the heart [81, 104].

The genetic ablation of MCU in the heart affects reducing equivalent productions. Since the redox state of NADH is closely linked to NADPH through the activity of a key antioxidant enzyme, the mitochondrial membrane-bound nicotinamide nucleotide transhydrogenase (Nnt), which normally regenerates NADPH from NADH, reduced mitochondrial Ca^{2+} uptake in failing myocytes which increases ROS production [56, 85, 106]. Oxidative stress, in turn, increases $[Na^{+}]_{cyt}$ [107] and enhances NCX-mediated Ca^{2+} influx [108], thus generating a vicious cycle of defective ECC, reduced mitochondrial Ca^{2+} uptake, energetic deficit, and oxidative stress, a common scenario observed in HF. Overall, these findings suggest that, in HF, a mismatch of workload and mitochondrial Ca^{2+} uptake causes oxidation of pyridine nucleotides by inducing energy deprivation and oxidative stress [78].

Both the global constitutive MCU KO and DN-MCU mouse models are characterized by a constitutive modulation of MCU activity that may not exclude adaptations to embryonic long-term loss of mitochondrial Ca^{2+} uptake [99, 100, 103, 104]. Phenomena of adaptation have been excluded with the generation of a conditional cardiac MCU KO. Surprisingly, the heart phenotype observed in this mouse was quite similar to constitutive mouse models [101, 102]. However, deletion of MCU in adult cardiomyocytes leads to protection from cell death induced by I/R injury [104]. Furthermore, Ca^{2+}/calmodulin-dependent protein kinase II (CaMKII) has been proposed to induce mPTP opening-dependent myocardial death by increasing I_{MCU} [109]. CAMKII directly interacts and increases I_{MCU}. Coherently, transgenic mice with myocardial expression of CaMKIIN, a CaMKII inhibitor, targeted to mitochondria, were protected against I/R injury and showed reduced mitochondrial Ca^{2+} uptake and decreased I_{MCU}. Nevertheless, these findings have been questioned since the I_{MCU} recorded was two orders of magnitude greater than the one previously measured and characterized by high fluctuations incompatible with the low single-channel conductance of MCU [110].

Altogether, these findings demonstrated that the MCU-mediated regulation of mitochondrial Ca^{2+} uptake plays a key role in the onset and progression of HF and thus may be useful for the development of novel treatments targeting mitochondria to ameliorate the progression of the disease.

3.2. Skeletal Muscle. Mitochondria play a crucial role in skeletal muscle function by providing ATP largely consumed by actomyosin contraction and SERCA activity. As in the heart, skeletal muscle mitochondria are commonly considered as the predominant source of ROS [111]. Indeed, during exercise, the intense skeletal muscle contractile activity enhances mitochondrial oxidative phosphorylation that increases the oxygen consumption rate and thus ROS production [111]. In detail, it has been demonstrated that O_2^{-} generation in skeletal muscle increases to about 50- or 100-fold during aerobic contraction [112]. Although ROS have been considered as deleterious species for skeletal muscle tissue, several evidences indicate that they might also play a positive role in physiological processes occurring in muscle cells [111]. Whether a beneficial or detrimental effect prevails depends on several variables among which the most relevant are the duration of ROS flow, the site of ROS production, and the antioxidant status of the cells [111]. In line with this, recently the redox-optimized ROS balance theory has been postulated that assumes that ROS levels depend on the redox state of a cell [113, 114]. In detail, ROS production increases both at high electron fluxes along the ETC, because the ROS production overwhelms the scavenging systems, and when the cellular metabolic state is reduced since reducing equivalents to sustain the antioxidant defences are lacking. Thus, ROS emission from mitochondria is minimal at an intermediate redox state with low ROS production at the ETC, but with sufficient levels of reduced NADPH to neutralize ROS [114]. Although the threshold of physiological ROS concentration above which ROS exert their negative effects has not been yet characterized, different pathways induced or affected by ROS in skeletal muscle has been intensively studied [111]. In particular, low levels of ROS activate signalling molecules such as PGC1-α, AMPK, and MAPK that control mechanisms of muscle adaptation such as oxidative metabolism and mitochondrial biogenesis [111]. Importantly, they also exert a self-control mechanism by regulating the activity of antioxidant enzymes. On the contrary, high levels of ROS induce functional oxidative damage of proteins, lipids, nucleic acids, and cell components, a huge increase in intracellular $[Ca^{2+}]$ leading to apoptosis and necrosis [111]. Furthermore, several studies demonstrated that dysregulation in ROS production has been considered as causal factors in various muscular pathologies [115–118]. In particular, oxidative stress appears to trigger the myopathic phenotype of malignant hyperthermia susceptibility (MHS) and central core disease (CCD) [119]. MHS is a pharmacogenetic disorder characterized by life-threatening episodes after treatment with depolarizing muscle relaxants while CCD represents one of the most common congenital myopathies [120]. Mutations of the RyR1 gene account for the majority of cases of MHS and CCD [120]. Initial treatment for MHS includes the administration of the RyR antagonist dantrolene, a

hydantoin derivate that inhibits the release of Ca^{2+} from SR without stimulating its reuptake [121]. However, since dantrolene suppresses Ca^{2+} release and Ca^{2+} entry, it is not surprising that it could affect protein involved in ECC [122]. Nevertheless, dantrolene is currently the only available pharmacological treatment of MH [121]. Importantly, in several models of these pathologies, it has been observed that the treatment with antioxidant agents ameliorates the muscular phenotype [123]. Indeed, it has been demonstrated that enhanced Ca^{2+} leak from mutant RyR1 increases oxidative/-nitrosative stress in the RyR^{Y522S} knock-in mice. This oxidative stress leads to S-nitrosylation of RyR1 which further enhances Ca^{2+} leak from this channel and increases susceptibility to heat-induced sudden death [124].

Dysregulation of $[Ca^{2+}]_{mit}$ associated with an increase in ROS production has been proposed as a possible mechanism for skeletal muscle fiber death in Duchenne muscular dystrophy (DMD) [125]. DMD is caused by loss-of-function mutations in the dystrophin gene located in chromosome X [125]. Loss of dystrophin protein increases muscle membrane permeability by inducing a huge increase in $[Ca^{2+}]_{cyt}$ that, in turn, induces mitochondrial Ca^{2+} overload [125]. This causes dysfunction of several oxidative phosphorylation enzymes and is accompanied by decreased ATP-synthase activity by influencing both ROS and ATP production in DMD muscles [125]. Increased mitochondrial Ca^{2+} load, occurring in DMD muscles, impairs the ability of mitochondria to reduce free radicals [125] and leads to the onset of apoptotic pathways that culminate in muscle atrophy [125]. This evidence places mitochondria as central participants in the aetiology of DMD, describing the relationship between increased intracellular $[Ca^{2+}]$, mitochondrial permeability, and dysfunction culminating in muscle loss [125].

Among the mechanisms that induce the increase in ROS production, the regulation of mitochondrial Ca^{2+} uptake is one of the most relevant. As already mentioned above, the MCU complex plays a key role in regulating Ca^{2+} entry into mitochondria and therefore it might be implicated in the development and progression of different muscular diseases [1]. In particular, the skeletal muscle of total MCU KO mice represents the most affected tissue [99], probably because it shows a much higher I_{MCU} compared to the heart (see previous paragraph and [83]). Interestingly, it has also been demonstrated that loss-of-function mutations of the MICU1 gene in humans causes dysfunctional Ca^{2+} uptake and results in clinical and pathological features that usually characterize mitochondrial myopathies, congenital core myopathies, and muscular dystrophies [42]. In particular, muscle biopsies from affected individuals clearly show a myopathic phenotype, characterized by a diffuse variation in fiber size, increased frequency of internal and central nuclei, and clusters of regenerating fibers, without pronounced fibrosis or fat infiltration. Surprisingly, two different MICU1 KO mice display perinatal mortality. One of these models displays an incomplete penetrance, and the KO animals that survive exhibit marked ataxia and muscle weakness, which progressively ameliorate during growth [126]. The physiological relevance of the MCU complex components, and thus the regulation of mitochondrial Ca^{2+} uptake in the onset and progression of muscular diseases, identifies the MCU complex as a potential target for the development of specific pharmacological therapies aimed at both improving the quality of life and increasing the life span of patients.

3.3. Neurons. The regulation of mitochondrial shape, volume, number, and distribution within the cells influences mitochondrial function especially in the CNS, where mitochondria show a strategic intracellular distribution, according to local energy demand [127]. Indeed, neurons require extremely precise spatiotemporal control of Ca^{2+}-dependent processes, since they regulate vital functions such as transmission of depolarizing signals, synaptic plasticity, and metabolism [1]. For this reason, neurons are extremely sensitive to variations of $[Ca^{2+}]$, and even small defects in Ca^{2+} homeostasis, hallmark of aging and neurodegenerative diseases, are able to impair neuronal activity [128, 129]. $[Ca^{2+}]_{cyt}$ increases in neurons principally occur through Ca^{2+} entry from the plasma membrane through ligand-gated glutamate receptors, such as the N-methyl-d-aspartate receptor (NMDAR) or various voltage-dependent Ca^{2+} channels (VDCCs), as well as from the release of Ca^{2+} from intracellular stores [130]. The contribution of these sources to intracellular Ca^{2+} in neurons depends on their size, transmitter system, and location in neural circuits (excitatory or inhibitory) [130]. In addition, in presynaptic neurons, Ca^{2+} entry through voltage-operated Ca^{2+} channels promotes the release of neurotransmitters into the synaptic cleft that, in turn, activates receptors located in the postsynaptic plasma membrane by initiating signal transmission [129]. This event generates Ca^{2+} signals that induce specific responses according to the type of receptors that have been activated [129]. Beyond its importance in synaptic transmission, mitochondrial Ca^{2+} uptake guarantees activity-dependent regulation of cellular energy metabolism [131]. Neurons use mitochondrial oxidative phosphorylation to generate ATP, required for cellular metabolism. The major by-product of this process is O_2^- which is dismutated to H_2O_2 by the mitochondrial enzyme superoxide dismutase 2 (SOD2) [132]. Since neurons show an extremely high metabolic rate, they produce elevated amounts of ROS in comparison to other organs [132].

In physiological conditions, ROS play active roles in many cellular processes. In particular, in the nervous system, ROS production regulates neuronal development, differentiation, and axon formation [132]. In particular, angiotensin II (Ang-II), brain-derived neurotrophic factor (BDNF), and vascular cell adhesion molecule-1 (VCAM-1) modulate cellular ROS production to regulate neural precursor proliferation and differentiation [133, 134]. Furthermore, it has also been demonstrated that ROS participate in synaptic plasticity as second messengers in several areas of the CNS, including the hippocampus, cerebral cortex, spinal cord, hypothalamus, and amygdala [135–139]. In this regard, it has been shown that repetitive stimuli, by inducing high Ca^{2+} influx, cause an increase in mitochondrial superoxide production. The latter induces the activation of CaMKII and PKA, two kinases involved in synaptic potentiation [132]. Furthermore, it has been demonstrated that increased mitochondrial

Ca^{2+} uptake and the consequent stimulation of ROS production plays a key role for the induction of the long-term potentiation (LTP), the principal form of synaptic plasticity in the mammalian brain, thought to endure experience-dependent enhancement of synaptic transmission [132]. In detail, inhibition of MCU blocks potentiation despite the increase in cytosolic Ca^{2+} levels produced after NMDA receptor activation [140]. Mitochondrial ROS, mainly superoxide, activate downstream signalling cascades involving PKA, PKC, and ERK which in turns results in synaptic plasticity of the dorsal horn neurons [140].

Mitochondria-derived ROS levels are regulated by intracellular Ca^{2+} levels. Indeed, ROS increase when mitochondria are exposed to high $[Ca^{2+}]$ and $[Na^{+}]$, for example, after having sustained NMDA receptor activation [141, 142]. Ca^{2+} influx from N-methyl-d-aspartate (NMDA) receptors triggers mitochondrial activation of caspase 3 which stimulates the synthesis of the myocyte enhancer factor 2 (MEF2) that regulates the transcription of the mitochondrial gene NADH dehydrogenase 6 (ND6), which encodes an essential component of complex I [143]. The MEF2-dependent expression of ND6 reduces cellular levels of the antioxidant enzymes superoxide dismutase and hydrogen peroxidase by increasing oxidative stress [143]. Therefore, dysregulation of mitochondrial Ca^{2+} uptake, and thus a decrease in the rate of ATP production, may influence mitochondrial metabolism and function, thus affecting neuronal activity [131]. In particular, excessive mitochondrial Ca^{2+} accumulation induces an overproduction of ROS that has detrimental effects on neurons [144]. Although mitochondria produce the largest amount of cellular ROS, other sources contribute to the generation of ROS in neurons such as the enzyme neural NOS and the NADPH oxidase. The huge increase in ROS levels induces cellular damage, impairment of the DNA repair system, and mitochondrial dysfunction, all of which are recognized as major determinants of aging and of neurodegenerative disorder development [132].

A recent study highlighted the importance of MCU in controlling excitotoxicity and its implication in NMDA receptor-mediated cell death [145]. In this study, Qiu and coworkers demonstrated that the overexpression of MCU in hippocampal and cortical neurons of newborn mice causes an NMDA-mediated increase in the $[Ca^{2+}]_{mit}$ [145]. This increase, in concert with NO production and activation of poly (ADP-ribose) polymerase-1 (PARP-1), leads to the loss of mitochondrial membrane potential which in turn energetically compromises neurons and leads to ROS generation [145]. In addition, knockdown of MCU in neurons causes a decrease in NMDA-mediated mitochondrial Ca^{2+} levels, thus preventing the loss of the mitochondrial membrane potential and excitotoxic cell death [145]. These findings suggest that MCU, and thus mitochondrial Ca^{2+}, plays an essential role in neuronal excitotoxicity, although more studies are required to confirm the function of MCU *in vivo*.

3.4. Cancer. Tumor formation and progresssion are directly related to mitochondrial dysfunction [146]. Furthermore, reprogramming of mitochondrial metabolism and an aberrant Ca^{2+} homeostasis are considered hallmarks of cancer cells [146]. Multiple lines of evidence highlighted the key role of Ca^{2+} homeostasis deregulation in tumor cell proliferation, apoptosis resistance, tumor development, and metastasis [147]. Although mitochondria exert a key role in cancer progression and Ca^{2+} signalling is altered in a wide variety of tumors, the mechanisms that connect mitochondrial Ca^{2+} homeostasis with malignant tumor formation and growth have not been characterized yet. Recently, Marchi et al. demonstrated that prostate and colon cancers overexpress an MCU-targeting microRNA that, by reducing mitochondrial Ca^{2+} uptake, allows cancer cell resistance to apoptotic stimuli thus increasing tumor cell survival [148]. However, a correlation between MCU overexpression and poor prognosis in breast cancer patients was also recently hypothesized [149]. This study demonstrated that in the MDA-MB-231 cell line, a triple-negative breast cancer model (TNBC), MCU expression correlates with breast tumor size and lymph node infiltration [149]. Coherently, MCU silencing causes a significant decline in $[Ca^{2+}]_{mit}$, metastatic cell motility, and matrix invasiveness. Most importantly, in MDA-MB-231 xenografts, deletion of MCU greatly reduces tumor growth and metastasis formation and this is associated with a decrease in mitochondrial ROS production, suggesting that mitochondrial ROS might play a crucial role in cell malignancy regulation by mitochondrial Ca^{2+} uptake [149]. In addition, MCU silencing in TNBC cells downregulates hypoxia-inducible factor 1-alpha (HIF1-α) expression, thus negatively affecting the expression of HIF1-α target genes involved in cancer progression [149]. Elevated levels of ROS have been detected in almost all cancers including Akt-positive tumors [150]. Akt or more commonly known as protein kinase B (PKB) is a cytosolic protein kinase that regulates cellular energy metabolism and apoptosis through mechanisms that converge on mitochondria or via the phosphorylation of key proteins like the Bcl-2-associated death promoter (BAD) protein. BAD is a proapoptotic member of the Bcl-2 gene family which is involved in initiating apoptosis. Marchi and coworkers demonstrated that Akt phosphorylates MICU1 at the N-terminal domain by affecting MICU1 proteolytic maturation and stability, thus altering mitochondrial Ca^{2+} uptake homeostasis [151]. Akt-mediated phosphorylation of the MCU complex regulator MICU1 may sustain cancer progression by increasing the basal mitochondrial Ca^{2+} level and ROS production [151]. In addition, mitochondrial Ca^{2+} uptake not only represents a fundamental mechanism to regulate cell survival and metabolism but also plays a pivotal role in the regulation of autophagy that plays both a negative and a positive role in cancer [152, 153]. In particular, mitophagy is an essential process that maintains mitochondrial quality and number by the removal of damaged or unnecessary mitochondria using autophagic machinery, thus limiting cellular degeneration [154]. Increasing evidence from different studies supports the concept that dysregulation of mitophagy is an etiologic factor in tumorigenesis [155]. Even though tumorigenesis relies on inhibition of mitophagy, tumor progression likely relies on the presence of functional mitophagy [156–160].

It is important to underline that dysregulation of mitophagy represents a scenario that characterizes not only cancer

but also different spectra of diseases including neurodegenerative diseases, motor neuron disorders, autosomal dominant optic atrophy, I/R injury, diabetes, aging, and cancer [161]. The discussion of this aspect is beyond the scope of this review and has been reviewed in greater detail elsewhere.

Altogether, these data reveal the importance of the association between aberrant mitochondrial Ca^{2+} levels and tumor development and strongly suggest that alteration in the activity of the MCU complex components represents a critical checkpoint of metastatic behaviour and thus a potential pharmacological target to combat aggressive cancers.

4. Conclusions

Mitochondria are key intracellular organelles that play a fundamental role in energy production and control many cellular processes from signalling to cell death. The function of the mitochondrial electron transport chain, the major source of ATP in the cell, is coupled with the production of ROS that are maintained at physiological levels by highly efficient mitochondrial antioxidant systems. Moreover, these antioxidant defences rely on mitochondrial metabolism that supplies the reducing equivalents needed for their activity.

In the last years, several studies demonstrated that quick changes in ROS levels, coupled with essential cellular functions, are fundamental participants of physiological signalling. Importantly, mitochondrial calcium, by impinging on aerobic metabolism, plays a crucial role in this process, since it joins the cellular activation stimuli and ROS production. This phenomenon plays a crucial role in the maintenance of cellular homeostasis in several tissues, as discussed above.

When the balance between ROS production and clearance is altered by either overproduction of mROS or impairment of the antioxidant defence, mitochondrial dysfunction occurs, leading to the induction of the cell death cascade. Indeed, the overproduction of mROS and the change in mitochondrial redox homeostasis have been shown to be involved in several pathological conditions, which often are associated with mitochondrial Ca^{2+} overload. For these reasons, the physiopathological role of mitochondrial Ca^{2+} uptake and mROS production has been extensively studied in the past years.

The molecular and functional characterization of the MCU complex components highlights the importance of the dynamic regulation of mitochondrial Ca^{2+} in organ physiology. In particular, in this review, we highlighted the contribution of the MCU complex activity, and thus the regulation of mitochondrial Ca^{2+} uptake, in cardiovascular, skeletal muscle, and neurodegenerative diseases and cancer. Although after the discovery of the molecular identity of the MCU complex many studies have confirmed the crucial role of mitochondrial Ca^{2+} signals in the regulation of cell survival, metabolism, and autophagy, many findings are controversial, and many questions are still open. In this regard, the characterization of the mechanisms responsible for the survival of the total MCU KO mouse only in the outbred strain and the analysis of the mechanisms underlying the different phenotypes of the MICU1 KO mice will be fundamental important to finely dissect the physiological role of mitochondrial Ca^{2+}. Furthermore, the structural and functional complexity of the MCU complex needs to be clarified. Thus, the study of the physiological role of the different MCU complex components might be useful to better characterize the regulation of mitochondrial Ca^{2+} uptake in different physiopathological conditions thus resulting in the identification of novel therapeutic strategies to cure pathologies characterized by dysregulation of mitochondrial Ca^{2+} homeostasis. In line with this, the discovery of drugs that modulate the activity of the MCU complex shall be extremely relevant for the future development of MCU-targeting therapies.

Conflicts of Interest

The authors declare that there is no conflict of interest regarding the publication of this paper.

Authors' Contributions

Simona Feno and Gaia Butera contributed equally to this work.

Acknowledgments

Research was supported by funding from the Italian Ministry of Education, the Fondazione Telethon (GGP16029 to R.R. and GGP16026 to A.R.), the Italian Association for Cancer Research (IG 18633 to R.R.), the French Muscular Dystrophy Association (19471 to A.R.), and the Italian Ministries of Health (Ricerca Finalizzata) (GR-2016-02362779 to A.R.).

References

[1] C. Mammucari, A. Raffaello, D. Vecellio Reane, G. Gherardi, A. De Mario, and R. Rizzuto, "Mitochondrial calcium uptake in organ physiology: from molecular mechanism to animal models," *Pflügers Archiv - European Journal of Physiology*, vol. 470, no. 8, pp. 1165–1179, 2018.

[2] R. Rizzuto, D. De Stefani, A. Raffaello, and C. Mammucari, "Mitochondria as sensors and regulators of calcium signalling," *Nature Reviews Molecular Cell Biology*, vol. 13, no. 9, pp. 566–578, 2012.

[3] D. De Stefani, R. Rizzuto, and T. Pozzan, "Enjoy the trip: calcium in mitochondria back and forth," *Annual Review of Biochemistry*, vol. 85, no. 1, pp. 161–192, 2016.

[4] R. Rizzuto, S. Marchi, M. Bonora et al., "Ca^{2+} transfer from the ER to mitochondria: when, how and why," *Biochimica et Biophysica Acta (BBA) - Bioenergetics*, vol. 1787, no. 11, pp. 1342–1351, 2009.

[5] M. Schmidt, P. A. Oude Weernink, F. vom Dorp, M. B. Stope, and K. H. Jakobs, "Mammalian phospholipase C," *Advances in Molecular and Cell Biology*, vol. 33, pp. 431–450, 2004.

[6] A. Raffaello, C. Mammucari, G. Gherardi, and R. Rizzuto, "Calcium at the center of cell signaling: interplay between endoplasmic reticulum, mitochondria, and lysosomes," *Trends in Biochemical Sciences*, vol. 41, no. 12, pp. 1035–1049, 2016.

[7] R. Chandrasekhar, K. J. Alzayady, and D. I. Yule, "Using concatenated subunits to investigate the functional consequences of heterotetrameric inositol 1,4,5-trisphosphate

receptors," *Biochemical Society Transactions*, vol. 43, no. 3, pp. 364–370, 2015.

[8] R. Chandrasekhar, K. J. Alzayady, L. E. Wagner, and D. I. Yule, "Unique regulatory properties of heterotetrameric inositol 1,4,5-trisphosphate receptors revealed by studying concatenated receptor constructs," *Journal of Biological Chemistry*, vol. 291, no. 10, pp. 4846–4860, 2016.

[9] J. T. Lanner, D. K. Georgiou, A. D. Joshi, and S. L. Hamilton, "Ryanodine receptors: structure, expression, molecular details, and function in calcium release," *Cold Spring Harbor Perspectives in Biology*, vol. 2, no. 11, article a003996, 2010.

[10] H. F. Deluca and G. W. Engstrom, "Calcium uptake by rat kidney mitochondria," *Proceedings of the National Academy of Sciences of the United States of America*, vol. 47, no. 11, pp. 1744–1750, 1961.

[11] F. D. Vasington and J. V. Murphy, "Ca^{++} uptake by rat kidney mitochondria and its dependence on respiration and phosphorylation," *Journal of Biological Chemistry*, vol. 237, pp. 2670–2677, 1962.

[12] P. Mitchell, "Chemiosmotic coupling in oxidative and photosynthetic phosphorylation," *Biological Reviews*, vol. 41, no. 3, pp. 445–501, 1966.

[13] H. Rottenberg and A. Scarpa, "Calcium uptake and membrane potential in mitochondria," *Biochemistry*, vol. 13, no. 23, pp. 4811–4817, 1974.

[14] Y. Kirichok, G. Krapivinsky, and D. E. Clapham, "The mitochondrial calcium uniporter is a highly selective ion channel," *Nature*, vol. 427, no. 6972, pp. 360–364, 2004.

[15] C. Mammucari, A. Raffaello, D. Vecellio Reane, and R. Rizzuto, "Molecular structure and pathophysiological roles of the mitochondrial calcium uniporter," *Biochimica et Biophysica Acta*, vol. 1863, no. 10, pp. 2457–2464, 2016.

[16] R. Rizzuto, A. W. Simpson, M. Brini, and T. Pozzan, "Rapid changes of mitochondrial Ca^{2+} revealed by specifically targeted recombinant aequorin," *Nature*, vol. 358, no. 6384, pp. 325–327, 1992.

[17] R. Rizzuto, M. Brini, P. Pizzo, M. Murgia, and T. Pozzan, "Chimeric green fluorescent protein as a tool for visualizing subcellular organelles in living cells," *Current Biology*, vol. 5, no. 6, pp. 635–642, 1995.

[18] R. Rizzuto, P. Pinton, W. Carrington et al., "Close contacts with the endoplasmic reticulum as determinants of mitochondrial Ca^{2+} responses," *Science*, vol. 280, no. 5370, pp. 1763–1766, 1998.

[19] G. Csordás, A. P. Thomas, and G. Hajnóczky, "Quasi-synaptic calcium signal transmission between endoplasmic reticulum and mitochondria," *The EMBO Journal*, vol. 18, no. 1, pp. 96–108, 1999.

[20] S. P. Mathupala and P. L. Pedersen, "Voltage dependent anion channel-1 (VDAC-1) as an anti-cancer target," *Cancer Biology & Therapy*, vol. 9, no. 12, pp. 1053–1056, 2010.

[21] V. Shoshan-Barmatz, S. De, and A. Meir, "The mitochondrial voltage-dependent anion channel 1, Ca^{2+} transport, apoptosis, and their regulation," *Frontiers in Oncology*, vol. 7, pp. 1–12, 2017.

[22] M. Madesh and G. Hajnoczky, "VDAC-dependent permeabilization of the outer mitochondrial membrane by superoxide induces rapid and massive cytochrome c release," *The Journal of Cell Biology*, vol. 155, no. 6, pp. 1003–1016, 2001.

[23] E. Rapizzi, P. Pinton, G. Szabadkai et al., "Recombinant expression of the voltage-dependent anion channel enhances the transfer of Ca^{2+} microdomains to mitochondria," *The Journal of Cell Biology*, vol. 159, no. 4, pp. 613–624, 2002.

[24] J. M. Baughman, F. Perocchi, H. S. Girgis et al., "Integrative genomics identifies MCU as an essential component of the mitochondrial calcium uniporter," *Nature*, vol. 476, no. 7360, pp. 341–345, 2011.

[25] D. De Stefani, A. Raffaello, E. Teardo, I. Szabò, and R. Rizzuto, "A forty-kilodalton protein of the inner membrane is the mitochondrial calcium uniporter," *Nature*, vol. 476, no. 7360, pp. 336–340, 2011.

[26] M. Patron, V. Checchetto, A. Raffaello et al., "MICU1 and MICU2 finely tune the mitochondrial Ca^{2+} uniporter by exerting opposite effects on MCU activity," *Molecular Cell*, vol. 53, no. 5, pp. 726–737, 2014.

[27] M. Plovanich, R. L. Bogorad, Y. Sancak et al., "MICU2, a paralog of MICU1, resides within the mitochondrial uniporter complex to regulate calcium handling," *PLoS One*, vol. 8, no. 2, article e55785, 2013.

[28] Y. Sancak, A. L. Markhard, T. Kitami et al., "EMRE is an essential component of the mitochondrial calcium uniporter complex," *Science*, vol. 342, no. 6164, pp. 1379–1382, 2013.

[29] K. Oxenoid, Y. Dong, C. Cao et al., "Architecture of the mitochondrial calcium uniporter," *Nature*, vol. 533, no. 7602, pp. 269–273, 2016.

[30] R. Baradaran, C. Wang, A. Francis Siliciano, S. Barstow long, R. Baradaran, and C. Wang, "Cryo-EM structures of fungal and metazoan mitochondrial calcium uniporters," *Nature*, vol. 559, no. 7715, pp. 580–584, 2018.

[31] J. Yoo, M. Wu, Y. Yin, M. A. Herzik, G. C. Lander, and S.-Y. Lee, "Cryo-EM structure of a mitochondrial calcium uniporter," *Science*, vol. 361, no. 6401, pp. 506–511, 2018.

[32] C. Fan, M. Fan, B. J. Orlando et al., "X-ray and cryo-EM structures of the mitochondrial calcium uniporter," *Nature*, vol. 559, no. 7715, pp. 575–579, 2018.

[33] N. X. X. Nguyen, J. P. P. Armache, C. Lee et al., "Cryo-EM structure of a fungal mitochondrial calcium uniporter," *Nature*, vol. 559, no. 7715, pp. 570–574, 2018.

[34] Y. Lee, C. K. Min, T. G. Kim et al., "Structure and function of the N-terminal domain of the human mitochondrial calcium uniporter," *EMBO Reports*, vol. 16, no. 10, pp. 1318–1333, 2015.

[35] E. Kovacs-Bogdan, Y. Sancak, K. J. Kamer et al., "Reconstitution of the mitochondrial calcium uniporter in yeast," *Proceedings of the National Academy of Sciences*, vol. 111, no. 24, pp. 8985–8990, 2014.

[36] H. Vais, K. Mallilankaraman, D. O. D. Mak et al., "EMRE is a matrix Ca^{2+} sensor that governs gatekeeping of the mitochondrial Ca^{2+} uniporter," *Cell Reports*, vol. 14, no. 3, pp. 403–410, 2016.

[37] T. Yamamoto, R. Yamagoshi, K. Harada et al., "Analysis of the structure and function of EMRE in a yeast expression system," *Biochimica et Biophysica Acta (BBA) - Bioenergetics*, vol. 1857, no. 6, pp. 831–839, 2016.

[38] A. Raffaello, D. De Stefani, D. Sabbadin et al., "The mitochondrial calcium uniporter is a multimer that can include a dominant-negative pore-forming subunit," *The EMBO Journal*, vol. 32, no. 17, pp. 2362–2376, 2013.

[39] K. J. Kamer and V. K. Mootha, "The molecular era of the mitochondrial calcium uniporter," *Nature Reviews. Molecular Cell Biology*, vol. 16, no. 9, pp. 545–553, 2015.

[40] F. Perocchi, V. M. Gohil, H. S. Girgis et al., "*MICU1* encodes a mitochondrial EF hand protein required for $Ca2^{+}$ uptake," *Nature*, vol. 467, no. 7313, pp. 291–296, 2010.

[41] K. Mallilankaraman, P. Doonan, C. Cárdenas et al., "MICU1 is an essential gatekeeper for MCU-mediated mitochondrial Ca(2+) uptake that regulates cell survival," *Cell*, vol. 151, no. 3, pp. 630–644, 2012.

[42] C. V. Logan, G. Szabadkai, J. A. Sharpe et al., "Loss-of-function mutations in *MICU1* cause a brain and muscle disorder linked to primary alterations in mitochondrial calcium signaling," *Nature Genetics*, vol. 46, no. 2, pp. 188–193, 2013.

[43] G. Csordás, T. Golenár, E. L. Seifert et al., "MICU1 controls both the threshold and cooperative activation of the mitochondrial Ca^{2+} uniporter," *Cell Metabolism*, vol. 17, no. 6, pp. 976–987, 2013.

[44] M. Paillard, G. Csordás, K.-T. Huang, P. Várnai, S. K. Joseph, and G. Hajnóczky, "MICU1 interacts with the D-ring of the MCU pore to control its Ca^{2+} flux and sensitivity to Ru360," *Molecular Cell*, vol. 72, no. 4, pp. 778–785.e3, 2018.

[45] M. Paillard, G. Csordás, G. Szanda et al., "Tissue-specific mitochondrial decoding of cytoplasmic Ca^{2+} signals is controlled by the stoichiometry of MICU1/2 and MCU," *Cell Reports*, vol. 18, no. 10, pp. 2291–2300, 2017.

[46] K. J. Kamer and V. K. Mootha, "MICU1 and MICU2 play nonredundant roles in the regulation of the mitochondrial calcium uniporter," *EMBO Reports*, vol. 15, no. 3, pp. 299–307, 2014.

[47] C. Petrungaro, K. M. Zimmermann, V. Küttner et al., "The Ca^{2+}-dependent release of the Mia40-induced MICU1-MICU2 dimer from MCU regulates mitochondrial Ca^{2+} uptake," *Cell Metabolism*, vol. 22, no. 4, pp. 721–733, 2015.

[48] D. Vecellio Reane, F. Vallese, V. Checchetto et al., "A MICU1 splice variant confers high sensitivity to the mitochondrial Ca^{2+} uptake machinery of skeletal muscle," *Molecular Cell*, vol. 64, no. 4, pp. 760–773, 2016.

[49] L. Wang, X. Yang, S. Li et al., "Structural and mechanistic insights into MICU1 regulation of mitochondrial calcium uptake," *The EMBO Journal*, vol. 33, no. 6, pp. 594–604, 2014.

[50] J. G. McCormack, A. P. Halestrap, and R. M. Denton, "Role of calcium ions in regulation of mammalian intramitochondrial metabolism," *Physiological Reviews*, vol. 70, no. 2, pp. 391–425, 1990.

[51] M. Patron, V. Granatiero, and J. Espino, "MICU3 is a tissue-specific enhancer of mitochondrial calcium uptake," *Cell Death & Differentiation*, vol. 26, no. 1, pp. 179–195, 2018.

[52] K. Mallilankaraman, C. Cárdenas, P. J. Doonan et al., "*MCUR1* is an essential component of mitochondrial Ca^{2+} uptake that regulates cellular metabolism," *Nature Cell Biology*, vol. 14, no. 12, pp. 1336–1343, 2012.

[53] V. Paupe, J. Prudent, E. P. Dassa, O. Z. Rendon, and E. A. Shoubridge, "CCDC90A (MCUR1) is a cytochrome c oxidase assembly factor and not a regulator of the mitochondrial calcium uniporter," *Cell Metabolism*, vol. 21, no. 1, pp. 109–116, 2015.

[54] D. Chaudhuri, D. J. Artiga, S. A. Abiria, and D. E. Clapham, "Mitochondrial calcium uniporter regulator 1 (MCUR1) regulates the calcium threshold for the mitochondrial permeability transition," *Proceedings of the National Academy of Sciences*, vol. 113, no. 13, pp. E1872–E1880, 2016.

[55] F. Di Lisa and P. Bernardi, "A CaPful of mechanisms regulating the mitochondrial permeability transition," *Journal of Molecular and Cellular Cardiology*, vol. 46, no. 6, pp. 775–780, 2009.

[56] L. Biasutto, M. Azzolini, I. Szabò, and M. Zoratti, "The mitochondrial permeability transition pore in AD 2016: an update," *Biochim. Biophys. Acta - Mol. Cell Res.*, vol. 1863, no. 10, pp. 2515–2530, 2016.

[57] V. Giorgio, S. von Stockum, M. Antoniel et al., "Dimers of mitochondrial ATP synthase form the permeability transition pore," *Proceedings of the National Academy of Sciences*, vol. 110, no. 15, pp. 5887–5892, 2013.

[58] V. Giorgio, V. Burchell, M. Schiavone et al., "Ca^{2+} binding to F-ATP synthase β subunit triggers the mitochondrial permeability transition," *EMBO Reports*, vol. 18, no. 7, pp. 1065–1076, 2017.

[59] P. Bernardi, A. Rasola, M. Forte, and G. Lippe, "The mitochondrial permeability transition pore: channel formation by F-ATP synthase, integration in signal transduction, and role in pathophysiology," *Physiological Reviews*, vol. 95, no. 4, pp. 1111–1155, 2015.

[60] M. Bonora, C. Morganti, G. Morciano et al., "Mitochondrial permeability transition involves dissociation of F_1F_O ATP synthase dimers and C-ring conformation," *EMBO Reports*, vol. 18, no. 7, pp. 1077–1089, 2017.

[61] J. He, H. C. Ford, J. Carroll, S. Ding, I. M. Fearnley, and J. E. Walker, "Persistence of the mitochondrial permeability transition in the absence of subunit c of human ATP synthase," *Proceedings of the National Academy of Sciences*, vol. 114, no. 13, pp. 3409–3414, 2017.

[62] J. He, J. Carroll, S. Ding, I. M. Fearnley, and J. E. Walker, "Permeability transition in human mitochondria persists in the absence of peripheral stalk subunits of ATP synthase," *Proceedings of the National Academy of Sciences*, vol. 114, no. 34, pp. 9086–9091, 2017.

[63] G. Morciano, C. Giorgi, M. Bonora et al., "Molecular identity of the mitochondrial permeability transition pore and its role in ischemia-reperfusion injury," *Journal of Molecular and Cellular Cardiology*, vol. 78, pp. 142–153, 2015.

[64] V. Giorgio, F. Fogolari, G. Lippe, and P. Bernardi, "OSCP subunit of mitochondrial ATP synthase: role in regulation of enzyme function and of its transition to a pore," *British Journal of Pharmacology*, 2018.

[65] M. Carraro, V. Giorgio, J. Sileikyte et al., "Channel formation by yeast F-ATP synthase and the role of dimerization in the mitochondrial permeability transition," *The Journal of Biological Chemistry*, vol. 289, no. 23, pp. 15980–15985, 2014.

[66] A. Nickel, M. Kohlhaas, and C. Maack, "Mitochondrial reactive oxygen species production and elimination," *Journal of Molecular and Cellular Cardiology*, vol. 73, pp. 26–33, 2014.

[67] D. B. Zorov, M. Juhaszova, and S. J. Sollott, "Mitochondrial reactive oxygen species (ROS) and ROS-induced ROS release," *Physiological Reviews*, vol. 94, no. 3, pp. 909–950, 2014.

[68] L. A. Sena and N. S. Chandel, "Physiological roles of mitochondrial reactive oxygen species," *Molecular Cell*, vol. 48, no. 2, pp. 158–167, 2012.

[69] J. F. Turrens, "Mitochondrial formation of reactive oxygen species," *The Journal of Physiology*, vol. 552, no. 2, pp. 335–344, 2003.

[70] A. Görlach, K. Bertram, S. Hudecova, and O. Krizanova, "Calcium and ROS: a mutual interplay," *Redox Biology*, vol. 6, pp. 260–271, 2015.

[71] P. S. Brookes, Y. Yoon, J. L. Robotham, M. W. Anders, and S.-S. Sheu, "Calcium, ATP, and ROS: a mitochondrial love-hate triangle," *American Journal of Physiology. Cell Physiology*, vol. 287, no. 4, pp. C817–C833, 2004.

[72] Z. Dong, S. Shanmughapriya, D. Tomar et al., "Mitochondrial Ca^{2+} uniporter is a mitochondrial luminal redox sensor that augments MCU channel activity," *Molecular Cell*, vol. 65, no. 6, pp. 1014–1028.e7, 2017.

[73] Y. J. H. J. Taverne, A. J. J. C. Bogers, D. J. Duncker, and D. Merkus, "Reactive oxygen species and the cardiovascular system," *Oxidative Medicine and Cellular Longevity*, vol. 2013, Article ID 862423, 15 pages, 2013.

[74] S. Dey, A. Sidor, and B. O'Rourke, "Compartment-specific control of reactive oxygen species scavenging by antioxidant pathway enzymes," *Journal of Biological Chemistry*, vol. 291, no. 21, pp. 11185–11197, 2016.

[75] S. F. Steinberg, "Oxidative stress and sarcomeric proteins," *Circulation Research*, vol. 112, no. 2, pp. 393–405, 2013.

[76] J. R. Erickson, M. A. Joiner, X. Guan et al., "A dynamic pathway for calcium-independent activation of CaMKII by methionine oxidation," *Cell*, vol. 133, no. 3, pp. 462–474, 2008.

[77] A. Zima and L. Blatter, "Redox regulation of cardiac calcium channels and transporters," *Cardiovascular Research*, vol. 71, no. 2, pp. 310–321, 2006.

[78] M. Kohlhaas, A. G. G. Nickel, and C. Maack, "Mitochondrial energetics and calcium coupling in the heart," *The Journal of Physiology*, vol. 595, no. 12, pp. 3753–3763, 2017.

[79] S. Cortassa, M. A. A. Aon, B. O. Rourke et al., "A computational model integrating electrophysiology, contraction, and mitochondrial bioenergetics in the ventricular myocyte," *Biophysical Journal*, vol. 91, no. 4, pp. 1564–1589, 2006.

[80] R. S. Balaban, "Cardiac energy metabolism homeostasis: role of cytosolic calcium," *Journal of Molecular and Cellular Cardiology*, vol. 34, no. 10, pp. 1259–1271, 2002.

[81] I. Drago, D. De Stefani, R. Rizzuto, and T. Pozzan, "Mitochondrial Ca^{2+} uptake contributes to buffering cytoplasmic Ca^{2+} peaks in cardiomyocytes," *Proceedings of the National Academy of Sciences of the United States of America*, vol. 109, no. 32, pp. 12986–12991, 2012.

[82] M. Giacomello, I. Drago, M. Bortolozzi et al., "Ca^{2+} hot spots on the mitochondrial surface are generated by Ca^{2+} mobilization from stores, but not by activation of store-operated Ca^{2+} channels," *Molecular Cell*, vol. 38, no. 2, pp. 280–290, 2010.

[83] F. Fieni, S. B. B. Lee, Y. N. N. Jan, and Y. Kirichok, "Activity of the mitochondrial calcium uniporter varies greatly between tissues," *Nature Communications*, vol. 3, no. 1, pp. 1317–1317, 2012.

[84] D. M. M. Bers, "Altered cardiac myocyte ca regulation in heart failure," *Physiology*, vol. 21, no. 6, pp. 380–387, 2006.

[85] C. Maack, S. Cortassa, M. A. Aon, A. N. Ganesan, T. Liu, and O. Rourke, "Elevated cytosolic Na^+ decreases mitochondrial Ca^{2+} uptake during excitation-contraction coupling and impairs energetic adaptation in cardiac myocytes," *Circulation Research*, vol. 99, no. 2, pp. 172–182, 2009.

[86] S. M. Pogwizd, J. P. McKenzie, and M. E. Cain, "Mechanisms underlying spontaneous and induced ventricular arrhythmias in patients with idiopathic dilated cardiomyopathy," *Circulation*, vol. 98, no. 22, pp. 2404–2414, 1998.

[87] S. M. Pogwizd, M. Qi, W. Yuan, A. M. Samarel, and D. M. Bers, "Upregulation of Na^+/Ca^{2+} exchanger expression and function in an arrhythmogenic rabbit model of heart failure," *Circulation Research*, vol. 85, no. 11, pp. 1009–1019, 1999.

[88] C. R. Weber, V. Piacentino, S. R. Houser, and D. M. Bers, "Dynamic regulation of sodium/calcium exchange function in human heart failure," *Circulation*, vol. 108, no. 18, pp. 2224–2229, 2003.

[89] A. A. Armoundas, I. A. Hobai, G. F. Tomaselli, R. L. Winslow, and B. O'Rourke, "Role of sodium-calcium exchanger in modulating the action potential of ventricular myocytes from normal and failing hearts," *Circulation Research*, vol. 93, no. 1, pp. 46–53, 2003.

[90] E. Bertero and C. Maack, "Calcium signaling and reactive oxygen species in mitochondria," *Circulation Research*, vol. 122, no. 10, pp. 1460–1478, 2018.

[91] R. H. Schwinger, J. Wang, K. Frank et al., "Reduced sodium pump α_1, α_3, and β_1-isoform protein levels and Na^+,K^+-ATPase activity but unchanged Na^+-Ca^{2+} exchanger protein levels in human heart failure," *Circulation*, vol. 99, no. 16, pp. 2105–2112, 1999.

[92] O. I. Shamraj, I. L. Grupp, G. Grupp et al., "Characterisation of Na/K-ATPase, its isoforms, and the inotropic response to ouabain in isolated failing human hearts," *Cardiovascular Research*, vol. 27, no. 12, pp. 2229–2237, 1993.

[93] S. Despa, M. A. Islam, C. R. Weber, S. M. Pogwizd, and D. M. Bers, "Intracellular Na^+ concentration is elevated in heart failure but Na/K pump function is unchanged," *Circulation*, vol. 105, no. 21, pp. 2543–2548, 2002.

[94] G. Michels, I. F. F. Khan, J. Endres-Becker et al., "Regulation of the human cardiac mitochondrial Ca^{2+} uptake by 2 different voltage-gated Ca^{2+} channels," *Circulation*, vol. 119, no. 18, pp. 2435–2443, 2009.

[95] M. Kohlhaas and C. Maack, "Adverse bioenergetic consequences of Na^+-Ca^{2+} exchanger–mediated Ca^{2+} influx in cardiac myocytes," *Circulation*, vol. 122, no. 22, pp. 2273–2280, 2010.

[96] M. Schieber and N. S. Chandel, "ROS function in redox signaling and oxidative stress," *Current Biology*, vol. 24, no. 10, pp. R453–R462, 2014.

[97] D. N. Granger and P. R. Kvietys, "Reperfusion injury and reactive oxygen species: the evolution of a concept," *Redox Biology*, vol. 6, pp. 524–551, 2015.

[98] G. C. Koenig, R. G. Rowe, S. M. Day et al., "MT1-MMP–dependent remodeling of cardiac extracellular matrix structure and function following myocardial infarction," *The American Journal of Pathology*, vol. 180, no. 5, pp. 1863–1878, 2012.

[99] X. Pan, J. Liu, T. Nguyen et al., "The physiological role of mitochondrial calcium revealed by mice lacking the mitochondrial calcium uniporter," *Nature Cell Biology*, vol. 15, no. 12, pp. 1464–1472, 2013.

[100] K. M. Holmström, X. Pan, J. C. Liu et al., "Assessment of cardiac function in mice lacking the mitochondrial calcium uniporter," *Journal of Molecular and Cellular Cardiology*, vol. 85, pp. 178–182, 2016.

[101] J. Q. Kwong, X. Lu, R. N. Correll et al., "The mitochondrial calcium uniporter selectively matches metabolic output to

acute contractile stress in the Heart," *Cell Reports*, vol. 12, no. 1, pp. 15–22, 2015.

[102] T. S. Luongo, J. P. Lambert, A. Yuan et al., "The mitochondrial calcium uniporter matches energetic supply with cardiac workload during stress and modulates permeability transition," *Cell Reports*, vol. 12, no. 1, pp. 23–34, 2015.

[103] Y. Wu, T. P. Rasmussen, O. M. Koval et al., "The mitochondrial uniporter controls fight or flight heart rate increases," *Nature Communications*, vol. 6, no. 1, p. 6081, 2015.

[104] T. P. Rasmussen, Y. Wu, M. A. Joiner et al., "Inhibition of MCU forces extramitochondrial adaptations governing physiological and pathological stress responses in heart," *Proceedings of the National Academy of Sciences of the United States of America*, vol. 112, no. 29, pp. 9129–9134, 2015.

[105] E. Murphy, X. Pan, T. Nguyen, J. Liu, K. M. Holmström, and T. Finkel, "Unresolved questions from the analysis of mice lacking MCU expression," *Biochemical and Biophysical Research Communications*, vol. 449, no. 4, pp. 384-385, 2014.

[106] T. Liu and B. O'Rourke, "Enhancing mitochondrial Ca^{2+} uptake in myocytes from failing hearts restores energy supply and demand matching," *Circulation Research*, vol. 103, no. 3, pp. 279–288, 2008.

[107] Y. Song, J. C. Shryock, S. Wagner, L. S. Maier, and L. Belardinelli, "Blocking late sodium current reduces hydrogen peroxide-induced arrhythmogenic activity and contractile dysfunction," *The Journal of Pharmacology and Experimental Therapeutics*, vol. 318, no. 1, pp. 214–222, 2006.

[108] O. Zeitz, A. E. Maass, P. Van Nguyen et al., "Hydroxyl radical-induced acute diastolic dysfunction is due to calcium overload via reverse-mode Na(+)-Ca(2+) exchange," *Circulation Research*, vol. 90, no. 9, pp. 988–995, 2002.

[109] M.-L. A. Joiner, O. M. Koval, J. Li et al., "CaMKII determines mitochondrial stress responses in heart," *Nature*, vol. 491, no. 7423, pp. 269–273, 2012.

[110] F. Fieni, D. E. Johnson, A. Hudmon, and Y. Kirichok, "Mitochondrial Ca^{2+} uniporter and CaMKII in heart," *Nature*, vol. 513, no. 7519, pp. E1–E2, 2014.

[111] E. Barbieri and P. Sestili, "Reactive oxygen species in skeletal muscle signaling," *Journal of Signal Transduction*, vol. 2012, Article ID 982794, 17 pages, 2012.

[112] M. L. Urso and P. M. Clarkson, "Oxidative stress, exercise, and antioxidant supplementation," *Toxicology*, vol. 189, no. 1-2, pp. 41–54, 2003.

[113] S. Cortassa, B. O'Rourke, and M. A. Aon, "Redox-optimized ROS balance and the relationship between mitochondrial respiration and ROS," *Biochimica et Biophysica Acta (BBA) - Bioenergetics*, vol. 1837, no. 2, pp. 287–295, 2014.

[114] M. A. Aon, S. Cortassa, and B. O'Rourke, "Redox-optimized ROS balance: a unifying hypothesis," *Biochimica et Biophysica Acta (BBA) - Bioenergetics*, vol. 1797, no. 6-7, pp. 865–877, 2010.

[115] S. Messina, D. Altavilla, M. Aguennouz et al., "Lipid peroxidation inhibition blunts nuclear factor-κB activation, reduces skeletal muscle degeneration, and enhances muscle function in *mdx* mice," *The American Journal of Pathology*, vol. 168, no. 3, pp. 918–926, 2006.

[116] A. Toscano, S. Messina, G. M. Campo et al., "Oxidative stress in myotonic dystrophy type 1," *Free Radical Research*, vol. 39, no. 7, pp. 771–776, 2005.

[117] S. Fulle, F. Protasi, G. Di Tano et al., "The contribution of reactive oxygen species to sarcopenia and muscle ageing," *Experimental Gerontology*, vol. 39, no. 1, pp. 17–24, 2004.

[118] M. Buck and M. Chojkier, "Muscle wasting and dedifferentiation induced by oxidative stress in a murine model of cachexia is prevented by inhibitors of nitric oxide synthesis and antioxidants," *The EMBO Journal*, vol. 15, no. 8, pp. 1753–1765, 1996.

[119] J. S. Moylan and M. B. Reid, "Oxidative stress, chronic disease, and muscle wasting," *Muscle & Nerve*, vol. 35, no. 4, pp. 411–429, 2007.

[120] R. Robinson, D. Carpenter, M.-A. Shaw, J. Halsall, and P. Hopkins, "Mutations in RYR1 in malignant hyperthermia and central core disease," *Human Mutation*, vol. 27, no. 10, pp. 977–989, 2006.

[121] D. Schneiderbanger, S. Johannsen, N. Roewer, and F. Schuster, "Management of malignant hyperthermia: diagnosis and treatment," *Therapeutics and Clinical Risk Management*, vol. 10, pp. 355–362, 2014.

[122] P. Szentesi, C. Collet, S. Sárközi et al., "Effects of dantrolene on steps of excitation-contraction coupling in mammalian skeletal muscle fibers," *The Journal of General Physiology*, vol. 118, no. 4, pp. 355–376, 2001.

[123] A. Michelucci, A. De Marco, F. A. Guarnier, F. Protasi, and S. Boncompagni, "Antioxidant treatment reduces formation of structural cores and improves muscle function in $RYR1^{Y522S/WT}$ mice," *Oxidative Medicine and Cellular Longevity*, vol. 2017, Article ID 6792694, 15 pages, 2017.

[124] W. J. Durham, P. Aracena-Parks, C. Long et al., "RyR1 S-nitrosylation underlies environmental heat stroke and sudden death in Y522S RyR1 knockin mice," *Cell*, vol. 133, no. 1, pp. 53–65, 2008.

[125] M. Kelly-Worden and E. Thomas, "Mitochondrial dysfunction in Duchenne muscular dystrophy," *Open Journal of Endocrine and Metabolic Diseases*, vol. 4, no. 8, pp. 211–218, 2014.

[126] J. C. Liu, J. Liu, K. M. Holmström et al., "MICU1 serves as a molecular gatekeeper to prevent in vivo mitochondrial calcium overload," *Cell Reports*, vol. 16, no. 6, pp. 1561–1573, 2016.

[127] T. Calì, D. Ottolini, and M. Brini, "Mitochondrial Ca^{2+} and neurodegeneration," *Cell Calcium*, vol. 52, no. 1, pp. 73–85, 2012.

[128] A. Kumar, K. Bodhinathan, and T. C. Foster, "Susceptibility to calcium dysregulation during brain aging," *Frontiers in Aging Neuroscience*, vol. 1, p. 2, 2009.

[129] M. Brini, T. Calì, D. Ottolini, and E. Carafoli, "Neuronal calcium signaling: function and dysfunction," *Cellular and Molecular Life Sciences*, vol. 71, no. 15, pp. 2787–2814, 2014.

[130] M. J. Berridge, "Neuronal calcium signaling," *Neuron*, vol. 21, no. 1, pp. 13–26, 1998.

[131] I. Llorente-Folch, C. B. Rueda, B. Pardo, G. Szabadkai, M. R. Duchen, and J. Satrustegui, "The regulation of neuronal mitochondrial metabolism by calcium," *The Journal of Physiology*, vol. 593, no. 16, pp. 3447–3462, 2015.

[132] T. F. Beckhauser, J. Francis-Oliveira, and R. De Pasquale, "Reactive oxygen species: physiological and physiopathological effects on synaptic plasticity," *Journal of Experimental Neuroscience*, vol. 10s1, 2016.

[133] J. Chao, L. Yang, S. Buch, and L. Gao, "Angiotensin II increased neuronal stem cell proliferation: role of AT2R," *PLoS One*, vol. 8, no. 5, article e63488, 2013.

[134] E. Topchiy, E. Panzhinskiy, W. S. T. Griffin, S. W. Barger, M. Das, and W. M. Zawada, "Nox4-generated superoxide drives angiotensin II-induced neural stem cell proliferation," *Developmental Neuroscience*, vol. 35, no. 4, pp. 293–305, 2013.

[135] C. Hidalgo and A. Arias-Cavieres, "Calcium, reactive oxygen species, and synaptic plasticity," *Physiology*, vol. 31, no. 3, pp. 201–215, 2016.

[136] C. A. Massaad and E. Klann, "Reactive oxygen species in the regulation of synaptic plasticity and memory," *Antioxidants & Redox Signaling*, vol. 14, no. 10, pp. 2013–2054, 2011.

[137] Z. Li, G. Ji, and V. Neugebauer, "Mitochondrial reactive oxygen species are activated by mGluR5 through IP3 and activate ERK and PKA to increase excitability of amygdala neurons and pain behavior," *The Journal of Neuroscience*, vol. 31, no. 3, pp. 1114–1127, 2011.

[138] R. De Pasquale, T. F. Beckhauser, M. S. Hernandes, and L. R. Giorgetti Britto, "LTP and LTD in the visual cortex require the activation of NOX2," *The Journal of Neuroscience*, vol. 34, no. 38, pp. 12778–12787, 2014.

[139] H. Fujii and T. Hirano, "Calcineurin regulates induction of late phase of cerebellar long-term depression in rat cultured Purkinje neurons," *The European Journal of Neuroscience*, vol. 16, no. 9, pp. 1777–1788, 2002.

[140] H. Y. Kim, K. Y. Lee, Y. Lu et al., "Mitochondrial Ca^{2+} uptake is essential for synaptic plasticity in pain," *The Journal of Neuroscience*, vol. 31, no. 36, pp. 12982–12991, 2011.

[141] J. A. Dykens, "Isolated cerebral and cerebellar mitochondria produce free radicals when exposed to elevated Ca^{2+} and Na^{+}: implications for neurodegeneration," *Journal of Neurochemistry*, vol. 63, no. 2, pp. 584–591, 1994.

[142] I. J. Reynolds and T. G. Hastings, "Glutamate induces the production of reactive oxygen species in cultured forebrain neurons following NMDA receptor activation," *The Journal of Neuroscience*, vol. 15, no. 5, pp. 3318–3327, 1995.

[143] H. She, Q. Yang, K. Shepherd et al., "Direct regulation of complex I by mitochondrial MEF2D is disrupted in a mouse model of Parkinson disease and in human patients," *The Journal of Clinical Investigation*, vol. 121, no. 3, pp. 930–940, 2011.

[144] G. H. Kim, J. E. Kim, S. J. Rhie, and S. Yoon, "The role of oxidative stress in neurodegenerative diseases," *Experimental Neurobiology*, vol. 24, no. 4, pp. 325–340, 2015.

[145] J. Qiu, Y.-W. Tan, A. M. Hagenston et al., "Mitochondrial calcium uniporter Mcu controls excitotoxicity and is transcriptionally repressed by neuroprotective nuclear calcium signals," *Nature Communications*, vol. 4, no. 1, p. 2034, 2013.

[146] N. N. Pavlova and C. B. Thompson, "The emerging hallmarks of cancer metabolism," *Cell Metabolism*, vol. 23, no. 1, pp. 27–47, 2016.

[147] S. Marchi and P. Pinton, "Alterations of calcium homeostasis in cancer cells," *Current Opinion in Pharmacology*, vol. 29, pp. 1–6, 2016.

[148] S. Marchi, L. Lupini, S. Patergnani et al., "Downregulation of the mitochondrial calcium uniporter by cancer-related miR-25," *Current Biology*, vol. 23, no. 1, pp. 58–63, 2013.

[149] A. Tosatto, R. Sommaggio, C. Kummerow et al., "The mitochondrial calcium uniporter regulates breast cancer progression via HIF-1α," *EMBO Molecular Medicine*, vol. 8, no. 5, pp. 569–585, 2016.

[150] G.-Y. Liou and P. Storz, "Reactive oxygen species in cancer," *Free Radical Research*, vol. 44, no. 5, pp. 479–496, 2010.

[151] S. Marchi, M. Corricelli, A. Branchini et al., "Akt-mediated phosphorylation of MICU1 regulates mitochondrial Ca^{2+} levels and tumor growth," *The EMBO Journal*, vol. 38, no. 2, article e99435, 2019.

[152] A. Gastaldello, H. Callaghan, P. Gami, and M. Campanella, "Ca^{2+} -dependent autophagy is enhanced by the pharmacological agent PK11195," *Autophagy*, vol. 6, no. 5, pp. 607–613, 2010.

[153] J. M. Vicencio, C. Ortiz, A. Criollo et al., "The inositol 1,4,5-trisphosphate receptor regulates autophagy through its interaction with Beclin 1," *Cell Death and Differentiation*, vol. 16, no. 7, pp. 1006–1017, 2009.

[154] A. Rimessi, M. Bonora, S. Marchi et al., "Perturbed mitochondrial Ca^{2+} signals as causes or consequences of mitophagy induction," *Autophagy*, vol. 9, no. 11, pp. 1677–1686, 2013.

[155] J. P. Bernardini, M. Lazarou, and G. Dewson, "Parkin and mitophagy in cancer," *Oncogene*, vol. 36, no. 10, pp. 1315–1327, 2017.

[156] M. C. Picchio, E. S. Martin, R. Cesari et al., "Alterations of the tumor suppressor gene Parkin in non-small cell lung cancer," *Clinical Cancer Research*, vol. 10, no. 8, pp. 2720–2724, 2004.

[157] F.-M. Kong, M. S. Anscher, M. K. Washington, J. K. Killian, and R. L. Jirtle, "M6P/IGF2R is mutated in squamous cell carcinoma of the lung," *Oncogene*, vol. 19, no. 12, pp. 1572–1578, 2000.

[158] S. R. Denison, F. Wang, N. A. Becker et al., "Alterations in the common fragile site gene Parkin in ovarian and other cancers," *Oncogene*, vol. 22, no. 51, pp. 8370–8378, 2003.

[159] S. Saito, S. Sirahama, M. Matsushima et al., "Definition of a commonly deleted region in ovarian cancers to a 300-kb segment of chromosome 6q27," vol. 56, no. 24, pp. 5586–5589, 1996.

[160] H. Alder, M. Shimizu, A. Drusco et al., "Parkin, a gene implicated in autosomal recessive juvenile parkinsonism, is a candidate tumor suppressor gene on chromosome 6q25-q27," *Proceedings of the National Academy of Sciences*, vol. 100, no. 10, pp. 5956–5961, 2003.

[161] C. Giorgi, C. Agnoletto, A. Bononi et al., "Mitochondrial calcium homeostasis as potential target for mitochondrial medicine," *Mitochondrion*, vol. 12, no. 1, pp. 77–85, 2012.